NASA/TM—2017-219405

Lessons Learned: Mechanical Component and Tribology Activities in Support of Return to Flight

Robert F. Handschuh and Erwin V. Zaretsky
Glenn Research Center, Cleveland, Ohio

March 2017

NASA STI Program . . . in Profile

Since its founding, NASA has been dedicated to the advancement of aeronautics and space science. The NASA Scientific and Technical Information (STI) Program plays a key part in helping NASA maintain this important role.

The NASA STI Program operates under the auspices of the Agency Chief Information Officer. It collects, organizes, provides for archiving, and disseminates NASA's STI. The NASA STI Program provides access to the NASA Technical Report Server—Registered (NTRS Reg) and NASA Technical Report Server—Public (NTRS) thus providing one of the largest collections of aeronautical and space science STI in the world. Results are published in both non-NASA channels and by NASA in the NASA STI Report Series, which includes the following report types:

- TECHNICAL PUBLICATION. Reports of completed research or a major significant phase of research that present the results of NASA programs and include extensive data or theoretical analysis. Includes compilations of significant scientific and technical data and information deemed to be of continuing reference value. NASA counter-part of peer-reviewed formal professional papers, but has less stringent limitations on manuscript length and extent of graphic presentations.

- TECHNICAL MEMORANDUM. Scientific and technical findings that are preliminary or of specialized interest, e.g., "quick-release" reports, working papers, and bibliographies that contain minimal annotation. Does not contain extensive analysis.

- CONTRACTOR REPORT. Scientific and technical findings by NASA-sponsored contractors and grantees.

- CONFERENCE PUBLICATION. Collected papers from scientific and technical conferences, symposia, seminars, or other meetings sponsored or co-sponsored by NASA.

- SPECIAL PUBLICATION. Scientific, technical, or historical information from NASA programs, projects, and missions, often concerned with subjects having substantial public interest.

- TECHNICAL TRANSLATION. English-language translations of foreign scientific and technical material pertinent to NASA's mission.

For more information about the NASA STI program, see the following:

- Access the NASA STI program home page at http://www.sti.nasa.gov

- E-mail your question to help@sti.nasa.gov

- Fax your question to the NASA STI Information Desk at 757-864-6500

- Telephone the NASA STI Information Desk at 757-864-9658

- Write to:
  NASA STI Program
  Mail Stop 148
  NASA Langley Research Center
  Hampton, VA 23681-2199

NASA/TM—2017-219405

Lessons Learned: Mechanical Component and Tribology Activities in Support of Return to Flight

Robert F. Handschuh and Erwin V. Zaretsky
Glenn Research Center, Cleveland, Ohio

National Aeronautics and
Space Administration

Glenn Research Center
Cleveland, Ohio 44135

March 2017

Acknowledgments

Along with the editors of this report, the following individuals are thanked for their dedicated work toward conducting research efforts in support of return to flight of the NASA space shuttle: Christopher Burke, Timothy Jett, Bradley Lerch, Wilfredo Morales, Fred Oswald, Roamer Predmore, Margaret Proctor, Michael Savage, and Kenneth Street, Jr.

Level of Review: This material has been technically reviewed by technical management.

Available from

NASA STI Program
Mail Stop 148
NASA Langley Research Center
Hampton, VA 23681-2199

National Technical Information Service
5285 Port Royal Road
Springfield, VA 22161
703-605-6000

This report is available in electronic form at http://www.sti.nasa.gov/ and http://ntrs.nasa.gov/

Return to Flight—Space Shuttle Body Flap Actuators and Rudder/Speed Brake Actuators: An Engineering Analysis and Lessons Learned

Preface

On February 1, 2003, the crew of the *Columbia* Space Shuttle STS–107 was lost during entry into the Earth's atmosphere over east Texas. At the time of the *Columbia* tragedy, I was assigned as a backup crewmember for the then Expedition 8 crew and was training in Russia with my fellow crewmates: Leroy Chiao, Bill McArthur, and Mike Foale. There was a total of about seven astronauts, flight doctors, and support personnel huddled together in one of the NASA cottages in Star City, Russia, as we all watched the television in horror and learned of the terrible tragedy which had befallen our dear friends and colleagues, the crew of STS–107. The details were slowly coming in and it was becoming apparent that a probable cause of the accident was a piece of bi-pod foam debris, which had liberated during launch from the external tank and possibly struck the ceramic thermal protection system tiles on the underside of the orbiter, critically damaging the vehicle.

We stayed up late that evening trying to garner as much information as we could from back home. I remember contacting several of my prior colleagues from NASA's Langley Research Center, some of whom had since retired and had to be reached at home, to try to locate some of the old technical papers regarding testing that was done on the thermal protection system tiles during the development of the space shuttle in the 1970s. I am sure I must have seemed like a man possessed as I contacted my friends and colleagues across the United States from Russia, but I am equally sure that there were many others, like myself, who were desperately trying to help and offer support in any way they could. I would find when I returned to the United States that this was indeed the case.

Our crew remained in Russia 1 week after the accident to complete training before returning back to the United States to join our friends and colleagues in the Astronaut Office. I believed it would take several years to understand what caused the accident, to fix the problem, and to ensure subsequent shuttle flights would be safe to fly. I also knew that I could best serve my Office and the Agency not as an Expedition Crewmember but as an engineer. The Head of the Astronaut Office, Captain Kent V. Rominger ("Rommel"), thankfully allowed me the opportunity to work directly with researchers across the country, who I knew personally, to help solve some of the complex problems to understand what caused the accident and to help develop technologies that would ensure a safe and continued return to space.

I immediately began calling up key contacts within and without NASA with expertise in several areas/disciplines, which would be crucial for the investigation. Having had worked multiple inter-Center programs within NASA and Joint programs with other agencies like the Air Force, Department of Defense (DOD), Defense Advanced Research Projects Agency (DARPA), etc., I was very lucky to have a long list of very capable researchers and engineers from which to call for help. In addition, the tragedy so galvanized the technical community throughout the country that I have little doubt we would have gotten support from anyone we needed. I also began to monitor the progress of the Space Shuttle Program and several of the key teams that were being formed to address the cause of the accident and what would be necessary for return to flight.

On July 7, 2003, Jay E. Bennett of the NASA Johnson Space Flight Center contacted Erwin V. Zaretsky of the NASA Glenn Research Center (GRC) regarding body flap actuators (BFAs) removed from the space shuttle fleet. NASA had examined one outboard and two inboard BFAs from the OV–104 Space Shuttle *Atlantis*. Zaretsky was then the Chief Engineer of the NASA GRC Structures and Acoustics Division. He together with Fred Dolan of the NASA Marshall Space Flight Center had played a key role in discovering and preventing a turbopump bearing failure that would have resulted in another space shuttle loss after the Jan. 28, 1986, *Challenger* Space Shuttle STS–51–L disaster.

On July 17, 2003, Zaretsky sent to Bennett a memorandum, subject, OV–104 Body Flap Actuator. In this memorandum, Zaretsky states:

> *The actuator had a design life of "10 years." However, you had no information at the time of our conversation on how the 10-year life estimate was determined. All of the mechanisms on all of the Space Shuttles have been in service for "20 years" or more during which time they have never been serviced nor inspected except for the three mentioned above. You had no information on the number of bearings or type in the system nor the resultant loading that the system and its components experience over the flight operation envelope. The gears were manufactured from AISI 9310 steel. The entire actuator mechanism is lubricated by Braycote grease. Except for the initial grease in the mechanism, there has been no grease added nor have any of the actuators been regreased during their 20 years of operation.*
>
> *Examination of the photographs sent to me by email confirmed the presence of corrosion products and cracking of the gear component. It appears that the gear may have been cleaned before being photographed since there were no visible signs of grease being present. There was a pit on what appears from the schematic to be the mating surface for contacting seals of the one-piece machined integral sun gear shaft.*
>
> *While I realize that it is difficult and expensive to access and inspect the actuators now in service in the Shuttle Fleet, it is my opinion that there is a high probability that one or more of the actuators can experience a seizure with the current lubrication condition and corrosion being present. I would recommend that all actuators now in service be cleaned, inspected and regreased, and, if necessary, be refurbished. Depending on the condition of the remaining actuators, a substitute grease should be considered.*

In response to the *Columbia* Accident Investigation Board (CAIB) report on the *Columbia* tragedy, NASA formed in 2003 the NASA Engineering and Safety Center (NESC). "The NESC performs value-added independent testing, analysis, and assessments of NASA's high-risk projects to ensure safety and mission success." The GRC under the auspices of the NESC organized a team to investigate and analyze the concerns enumerated by their Chief Engineer for Structures and Acoustics Erwin Zaretsky in his July 17, 2003, memorandum to Jay Bennett regarding both BFAs and rudder/speed brake (RSB) actuators**.** The team members besides those staff members of GRC included staff members of the NASA Marshall Space Flight Center (MSFC).

The NESC/GRC Shuttle Actuator Team recommended to the Space Shuttle Program Offices (SSPO) together with their contractor United Space Alliance (USA) that all the actuators on the space shuttles be removed and inspected per Zaretsky's July 13, 2003, letter. There was disagreement between the Shuttle Program Offices and USA (SSPO/USA) and the NESC/GRC Team regarding the necessity to inspect the actuators or, if in fact, there was even an issue or problem with the actuators.

The SSPO/USA did not want to incur the cost and delay the shuttle's return to flight by removing and opening up these actuators for inspection. They wanted to keep them in situ on their respective shuttles until the end of the Space Shuttle Program. However, after continued insistence by the NESC/GRC Team, the SSPO/USA agreed as a compromise to remove one BFA from a shuttle and, without opening it up, to x-ray it to determine if there was any visible damage. The results of this x-ray inspection reverberated throughout the SSPO. The actuator had been assembled incorrectly and was not fit for its intended purpose. The fact that it did not jam or malfunction during shuttle flight causing a shuttle loss was in itself astounding and nothing short of a miracle.

Visible inspection of two partially dissembled RSB actuators from the Space Shuttle *Discovery* was made on September 16, 2003. Pitted gears and discolored grease were observed inside. The grease-lubricated ball bearing and gears making up the actuators exhibited various degrees of wear. As a result of these observations, the NESC/GRC Shuttle Actuator Team undertook several research efforts to

determine the causes of grease degradation, damage, and wear to estimate the future life and reliability of the shuttle actuators and to investigate design improvements for future heavily loaded space mechanisms. These works, which are reported and archived in this publication include

1. Analysis of the condition of the grease in two actuators after 39 flights
2. Probabilistic analysis of the life and reliability BFA bearings
3. Wear analysis of spur gears lubricated by perfluoropolyalkyl ether grease
4. Characterization of gear scuffing damage observed in the RSB actuators
5. Determine the probability that a tooth breaking off from a planetary gear can jam the actuator
6. Perform a probabilistic fatigue life and reliability and analysis of the RSB actuators

Based on the results of the testing and analysis of the NESC/GRC Shuttle Actuator Team, it was agreed to on May 18, 2005, during a NESC telecon, that the space shuttle actuators be limited to 12 flights or 6 years (whichever comes first). The combined reliability for the entire BFA assembly and the RSB assembly for 12 missions on a single space shuttle was 86.2 percent. This yields a 13.8 percent probability that a bearing and/or gear failure will occur on either a BFA or RSB actuator. While this probability of failure was considered high by the team it was also their consensus that a single bearing or gear failure short of a tooth breakage would not immediately render the actuator inoperable within the entire time constraints of the 12 missions.

As a result of the work of the NESC/GRC Team, the BFAs on all remaining space shuttles were limited to 12 flights each before refurbishment. The remaining two RSB actuators were removed from the Space Shuttle *Discovery*. All four of the removed RSB actuators were replaced with four actuators that had been subjected to three flights and had been removed from a sister space shuttle.

On July 26, 2005, the *Discovery* returned to flight on a mission to the International Space Station (ISS), the first space shuttle to fly since the Space Shuttle *Columbia* disaster on February 1, 2003. This was the 31st mission and flight of the *Discovery*. On July 4, 2006, the 32nd flight of the *Discovery* occurred on a mission to the ISS. This was the second consecutive return to flight since the *Columbia* disaster. The *Discovery* was flown seven more times to the ISS without incident for a total of 39 flights. After the 39th mission on March 9, 2011, the Space Shuttle *Discovery* was retired from service and was placed on permanent display in the Smithsonian Air and Space Museum, Washington, DC.

The BFAs and the RSB actuators functioned as intended without incident. The RSB actuators in the *Discovery* at the time of its retirement had a total of 12 flights, 9 flights from those in the *Discovery,* and 3 previous flights before being removed from the Space Shuttle *Endeavor*. I cannot say with reasonable certainty that the NESC\GRC Team saved a space shuttle or, in fact, the Space Shuttle Program. However, what I can say with absolute certainty is that they made the space shuttle safer.

The rudder speed brake story is one of many such stories where “research engineers” like Dr. Zaretsky were able to identify key anomalies post *Columbia* tragedy and use their highly skilled expertise, honed by over 30 years of dedicated research, to understand and successfully fix critical flaws on an “experimental” vehicle that was incorrectly deemed “operational”!

Dr. Charles Camarda
Astronaut STS–114
Senior Advisor for Engineering Development
NASA’s Langley Research Center

Contents

Executive Summary

On February 1, 2003, the Space Shuttle *Columbia* broke up upon reentry into the atmosphere over the southwestern United States. The Report of the Columbia Accident Investigation Board (CAIB) published in August 2003 declared that a breach of the wing leading edge thermal protection system was damaged upon launch and was the reason why *Columbia* broke up during reentry. The loss of the crew and the second space shuttle resulted in the NASA Management to revisit every critical system onboard this very complex, reusable space vehicle in an effort to return to flight (RTF) as soon as possible. Efforts were also initiated to determine how on-orbit repairs could be made of the insulating tile on the wing leading edges and bottom of the aircraft. Inspection techniques from the space station or robot arm for examination were developed. All these initial efforts centered on ice intrusion through the fragile wing leading edges during liftoff.

Many months after the disaster and publishing of the CAIB report, an initial phone contact between NASA Johnson Space Center and NASA Glenn Research Center evolved into an in-depth assessment of the actuator drive systems for the Rudder Speed Brake and Body Flap Systems. The initial contact was with respect to a crack found in one of the shafts that drives the rudder speed brake actuators. The actuators are CRIT 1–1 systems. This means that failure of any of the actuators could result in loss of crew and loss of vehicle.

The question posed to the staff at NASA Glenn was the following: is a cracked shaft of concern in this system? The answer received back at Johnson Space Center was that the shaft should be replaced and the system that is driven by this shaft should be inspected. This meant that the rudder speed brake actuator would need to be removed from the shuttle under inspection. Also it was to be disassembled at the contractor's facility for further evaluation. Upon complete disassembly many other issues were found. These included: some gears with fretted surfaces, discolored space lubricant (grease), gear teeth with cracks, and worn gear surfaces to mention a few of the issues.

These actuation systems were suppose to last 100 missions or 10 years of use. The shuttle was supposed to be a highly reliable and reusable space vehicle that could land back at the launch site like an airplane. The initial shuttle use rate was to be 10 flights per year. The use rate never came close to the 10 missions per year and the length of time of these components were installed without maintenance typically was in excess of 10 years.

Qualification of these highly loaded actuators was done as a system. The requirement for the testing was to run a scripted set of assumed mission loads to simulate 400 missions. These missions were run concurrently. If the system tested passed this phase of the actuator design, then it was deemed qualified to conduct 100 missions having a 4X period of performance validated for flight. Unfortunately, the scripted flights did not have some of the extreme loads and other operational conditions that were imposed during actual shuttle processing and flight.

However, some of the loads that were applied during the qualification testing were very severe in comparison to that used for aerospace applications requiring long operational life times. Stress levels were so extreme that specialized gear tooth geometry (crowning and tip relief) was excessive but necessary to permit operation through the very high loads portion of the qualification testing. After accessing the level of loads and the various problem areas that were found led the NASA Glenn Mechanical Components Branch to look into areas that could support the RTF effort.

The NASA Glenn Team worked in the following areas: (i) fretting—dither damage of space grease-lubricated gears; (ii) space grease degradation; (iii) low-cycle fatigue of aerospace gear steels used; (iv) wear rates of dither damaged gearing; (v) power drive unit (PDU) gear tooth scuffing due to backdriving of the power system; (vi) fretting—pitting effect on stress/reuse of components; and (vii) misground root-fillet of gear components stress effects. The data generated in all of these tests are contained in this document in the chapters that follow.

Lessons Learned

The following lists of topics are items that were learned through the research process contributing to the RTF efforts. This list is intended to serve as items that need to be considered when mechanical systems are designed for future space-related systems.

(1) To the best of the design team's ability, properly note all loads that a system will be subjected to in quantity and level. Flight loads are not the only loads on many space vehicle components.
(2) Include ground operations on the mechanical system fatigue, wear, etc.
(3) Validation of a system via the 4X the actual intended use does not necessarily equal a system that will survive the intended life of the mechanical system. Also, same systems are not necessarily the same with respect to life of the system.
(4) Lowest life of an individual component is not the expected life of a complex mechanical system.
(5) Extreme loads and operating conditions require adequate (component) testing to prove successful operation of each component of a system. Life assessment can be made due to these extreme loads when a statistically significant number of tests have been conducted.
(6) Double check assembly of systems. Like geometries can allow mis-assembly of a system and result in subsequent failure due to overload.
(7) Do not use damaged components in a rebuilt system. Any types of surface irregularity, cracks, or other defects on components need to be replaced.
(8) Grease has a useful life and needs to be serviced at an interval similar to that of commercial airlines. Just because the device has not been used, does not mean that the grease originally supplied is still good.

Lessons Learned: Mechanical Component and Tribology Activities in Support of Return to Flight

Robert F. Handschuh and Erwin V. Zaretsky[1]
National Aeronautics and Space Administration
Glenn Research Center
Cleveland, Ohio 44135

Abstract

The February 2003 loss of the Space Shuttle *Columbia* resulted in NASA Management revisiting every critical system onboard this very complex, reusable space vehicle in an effort to return to flight. Many months after the disaster, contact between NASA Johnson Space Center and NASA Glenn Research Center evolved into an in-depth assessment of the actuator drive systems for the Rudder Speed Brake and Body Flap Systems. The actuators are CRIT 1–1 systems that classifies them as failure of any of the actuators could result in loss of crew and vehicle. Upon further evaluation of these actuator systems and the resulting issues uncovered, several research activities were initiated, conducted, and reported to the NASA Space Shuttle Program Management. The papers contained in this document are the contributions of many researchers from NASA Glenn Research Center and Marshall Space Flight Center as part of a "Lessons Learned" on mechanical actuation systems as used in space applications. Many of the findings contained in this document were used as a basis to safely return to flight for the remaining space shuttle fleet until their retirement.

[1]Distinguished Research Associate

Chapter 1: A Study of Spur Gears Lubricated With Grease—Observations From Seven Experiments

Timothy L. Krantz and Robert F. Handschuh
U.S. Army Research Laboratory
Glenn Research Center
Cleveland, Ohio 44135

Abstract

To improve understanding of gears operating with a perfluoro type space-qualified grease, seven spur gear experiments were performed. Test conditions were selected to study the influences of torque, lubricant type, and atmosphere. Two testing torques provided nominal pitch-line Hertz stresses greater and lesser than the contact stress limit as recommended by the grease manufacturer. As was expected, all tests resulted in some gear tooth wear. Discoloration of the perfluoro type grease occurred for all tests. Tests in dry nitrogen produced some dark-grey colored perfluoro type grease. Testing in either ambient or dry air produced red debris after short test duration, and for tests of longer duration large amounts of red debris, red grease, and wear were evident. Tests using higher torques produced more debris. The first indications of discoloration occurred more quickly with higher test torques. Total amounts of wear were quite significant, up to four times the profile tolerance for AGMA (American Gear Manufacturers Association) class 10 gears.

Introduction

Perfluoro type greases are in use for many space applications including the rudder speed brake actuator gearboxes for space shuttle orbiters. Discussions in support of orbiter actuator gearbox maintenance have highlighted the need for data to better understand the behavior of mechanical components operated using a perfluoro type grease. To develop some needed data and understanding, seven spur gear experiments were completed. The purposes of the experiments were to (1) develop a test protocol for testing of grease-lubricated gears and (2) to record and document observations to support decisions concerning the maintenance of actuator gearboxes.

Test Rig

The experiments were conducted using the NASA Glenn Research Center Spur Gear Fatigue Test Rigs. These test rigs have been used for more than 30 years to test oil-lubricated spur gears, with emphasis on studying contact fatigue (spalling, pitting, and micropitting). The test rig as shown in Figure 1.1(a) uses the four-square (torque-regenerative) principle of applying test loads, and thus the motor needs to overcome only the frictional losses in the system. The test rig is belt driven using a variable speed electric motor with a belt and pulley system. A schematic of the loading apparatus is shown in Figure 1.1(b). Hydraulic oil pressure and leakage replacement flow is supplied to the load vanes through a shaft seal. As the oil pressure is increased on the load vanes located inside one of the slave gears, torque is applied to its shaft. This torque is transmitted through the test gears and back to the slave gears. In this way power is circulated, and the desired load and corresponding stress level on the test gear teeth may be obtained by adjusting the hydraulic pressure.

Figure 1.1 depicts the spur gear rig as has been used for tests operated at 10,000 rpm for the purpose of evaluating the fatigue lives of oil-lubricated gears. The test setup as used for the grease tests reported herein differed from the depiction of Figure 1.1 in two important ways. Figure 1.1 illustrates the test gears operating with faces offset. The face-offset condition is used to concentrate the Hertz contact stress as is desired for accelerated life testing of high cycle fatigue. For the grease-lubricated gear testing, the gears

were operated with zero offset (full faces in contact with each other). Also, Figure 1.1 depicts pressurized labyrinth seals on the two shafts. For the grease testing reported herein, lip seals were used on the two shafts to prevent leakage of the slave gear lubricating oil to the grease-lubricated test gear section. The lip seals have been used with much success on these rigs to maintain zero-leakage even for speeds of 10,000 rpm. Testing reported herein was done at speeds no greater than 705 rpm.

Test Gears and Lubricants

The test gears used for these experiments were a set of spur gears made from case-carburized AISI 9310 steel. By chemical analysis, the proper alloy content was verified. The gear geometry is 8 pitch, 20° pressure angle, 28 teeth, standard tooth proportion, a 3.5 in. pitch diameter, and AGMA class 11 tolerances. The measured tooth profiles are pure involutes (no designed tip relief), and the teeth have lead crowning of about 0.0005 in. height across the nominal 0.250 in. face width. The primary test lubricant used was from a single cartridge of grade 2 perfluoro type grease. One test was completed using a hydrocarbon-based grade 2 grease. One test was completed with no lubricant on the test gears.

Test Procedures and Operating Conditions

The test gears were cleaned prior to installation of the test rig. The cleaning procedure for all gears was ultrasonic cleaning using alcohol for 5 min minimum, immediate blow dry with air, installation on the test rig, and application of the test grease. For tests 3 to 6, the test gears were first subjected to a mild glass bead cleaning (cleaning equipment set to 20 psi supply pressure) just prior to ultrasonic cleaning in alcohol.

Table 1.1 provides the operating conditions for the seven tests. Note, for example, that test 1 and test 2 made use of the same pair of gears. The “setup” column of Table 1.2 documents whether the gears were installed with etched serial numbers facing the back (A) or front (B) of the test rig. Each test began with new tooth surfaces (using both sides of the teeth). For the case of gears used for more than one test, the gears were cleaned using the ultrasonic cleaning procedure after the first and before the second test.

Tests 1, 2, 6, and 7 were conducted with a cover attached, and ports were open to ambient air. Tests 3 and 4 were conducted with a cover attached and a flow of dry nitrogen into the test chamber. Test 5 was conducted with a flow of dry air into the test chamber. Nitrogen and air flows were supplied by a central laboratory supply. The gas flowed through a desiccant before entering the chamber to ensure a dry atmosphere. The air supply was filtered using a new 45 μm rated filter element. The gas flow entered the test chamber by a tube directed at the gear teeth. Gas flow leaving the test chamber flowed through a beaker containing water, and the bubbling of the water in the beaker provided visual indication of positive gas flow for the duration of the test. The gas flowed for 30 min minimum to purge the test chamber of ambient air and moisture before operating the gears.

All testing was done at a constant load and speed for the duration of a particular test. However, speeds and loads varied from test to test (per Table 1.1) since test protocol and procedures were being developed as part of the testing objectives. Test speed and loads were selected to provide tribological conditions similar to the rudder speed brake actuator gearing, but further analysis is required to understand how closely these test conditions relate to actual actuator operation.

Test Results and Observations

Testing results will be presented in a manner to facilitate understanding, and the order is not necessarily the chronological order of testing. Five gear tests were completed using perfluoro type grease, one test was completed using a hydrocarbon-based grease, and one test was completed using no lubricant. Two test conditions were adjusted to investigate the effects of the operating condition: (1) the testing torque (a low torque level and a high torque level) and (2) the atmosphere in the test chamber (ambient

air, dry nitrogen flow, or dry air flow). The maximum Hertz contact stress pressure on the gear teeth surfaces corresponding to the two test torques were estimated using a nominal 0.0005- in. lead crown and considering gears operating at the pitch-point position. Using this approximation as a load index, the lower test torque of 2 ft-lb resulted in a peak pitch-line Hertz stress index of about 90 ksi. The higher test torque of 5 ft-lb resulted in a peak pitch-line Hertz stress index of about 120 ksi. The manufacturer of the perfluoro type grease suggests limiting the use of this grease to applications having less than 100 ksi Hertz stress.

The first grease test was conducted at 5 ft-lb of torque, ambient air, and a speed of 515 rpm. Red colored debris was present after 1 hr of operation. Figure 1.2 documents the appearance of the test hardware after 3 hr of operation. Significant wear was observed, and the grease and contact areas of the gears have a red color. The test was then run an additional 26 hr unattended. The total test duration in terms of shaft revolutions was 927,000. At the completion of the test, a significant amount of red "dust" covered the test chamber, shafts, and gear teeth sides (Fig. 1.3). The grease was discolored, including some red colored grease. It is not known at this time if the red grease samples contain red colored wear debris or if the red color also indicates some chemical breakdown of the grease. Grease samples were collected and stored for post-test evaluations.

Profilometer inspections of a gear tooth made in the profile direction both before and after test number 1 revealed significant wear of the tooth surface (Fig. 1.4(a)). By overlaying the tooth traces to match up the profiles in noncontacting areas and then subtracting the tested profile from the new profile, wear as a function of position along the tooth profile was determined (Fig. 1.4(b)). Maximum wear depths occurred in the dedendum (root region) below the pitch line, and wear depth amounts were on the order of 50 μm (0.002 in.). The measured wear depth is quite significant, about four times the tolerance for the profile for an AGMA class 10 gear of this size.

Profilometer inspections of gear teeth were also made in the lead direction (across the tooth face). Before testing, gear tooth surfaces were all of a crowned, convex shape in the lead direction (Fig. 1.5(a)). Measurements of mating gear teeth after testing revealed that the convex shape of the mating gear's tooth tip region has worn a concave shape into the root region of the driving gear (Fig. 1.5(b)). It is also of significance that the worn surfaces are much rougher than the original ground gear surfaces. The increased roughness will promote higher wear rates and will tend to increase vibration.

The second perfluoro type grease-lubricated gear test was conducted at 2 ft-lb of torque (less torque than test number 1) and in ambient air. The test was run with a shaft speed of 200 rpm. To provide a more complete evaluation of test progression, the testing was temporarily stopped after 15, 30, and 60 min of cumulative testing time. When the test was stopped temporarily, the cover was removed for close inspections of the working tooth surfaces. Inspections after the 15 and 30 min test durations revealed only the appearance of the expected contact patterns. No discolored debris or grease was observed. However, at the completion of 60 min total test duration, the centers of contact patterns of the working surfaces of some teeth had some red colored areas. Most of the grease still had the original white color at that time. The test was then restarted and run for an additional 15 hr unattended. At completion of 194,000 shaft revolutions, the test was stopped. A significant amount of red debris and red colored grease was present at the end of the test (Fig. 1.6).

The two tests conducted using perfluoro type grease and ambient air environment suggests that wear debris is created rather quickly even for mild load conditions. It is probable that the red colored dust is oxidized wear debris that was introduced to the air. The colored grease might be due either to the oxidized wear debris becoming trapped in the grease, or due to a breakdown of the grease itself producing by-products, or due to both events. Post-test evaluations of collected grease samples should clarify the end-of-test condition.

The third perfluoro type grease-lubricated gear test was conducted to closely match the speed and torque of grease test number 2 (the test described above). However, for this test the chamber contained a dry nitrogen atmosphere. The "Test Procedure and Operating Conditions" section of this report describes the manner for introducing flows of dry gas. The test was not stopped for close inspections of the teeth to avoid introducing air and moisture into the test chamber. Neither red colored wear debris, nor red colored

grease was generated during this third test. The duration of the test was 18.5 hr and comprised 238,000 shaft revolutions, somewhat longer than the equivalent test done in ambient air. The gear contact patterns reveal that, as expected, some wear occurred during this test number 3 (Fig. 1.7). Some grey grease streaks were observed on the tips of some of the gear teeth after completion of the tests. The composition of the grey streaks is not known at this time.

The fourth perfluoro type grease-lubricated gear test was conducted to closely match the speed and torque of grease test number 1. However, for this test the chamber contained a dry nitrogen atmosphere. The test torque was the higher of the two test torques (5 ft-lb). Once again, the test was not stopped for occasional close inspection of the teeth to avoid introducing air and moisture into the test chamber. The total test duration was 16 hr and comprised 205,000 shaft revolutions. At the end of the test there was a mixture of original white and dark-grey colored grease (Fig. 1.8). The grey colored grease tended to be collected in the roots of the driven gear and towards the tips of the driving gear, suggesting that the dark color is due to wear debris that has been pushed to the end of tooth contact. At this time, it is not known if the discoloration is only due to wear debris, chemical degradation of the grease, physical separation of oil and grease base, or some combination of these phenomena.

The fifth perfluoro type grease-lubricated gear test was conducted to closely match the speed and torque of grease test number 4 (the test just described in preceding text). The test torque was the higher of the two test torques (5 ft-lb). For this test the chamber contained a dry air atmosphere while for the previous test the chamber contained a dry nitrogen atmosphere. The "Test Procedure and Operating Conditions" section of this report describes the manner for introducing flows of dry gas. The test chamber cover was not removed for the duration of the test to avoid introducing moisture into the test atmosphere. The front cover of the test chamber was a clear plate that permitted observation of the gear teeth. The test was stopped temporarily after 2 hr of cumulative testing time, and red deposits were observed on the working surfaces of the teeth. After the completion of 16 hr (210,000 shaft revolutions) the gears had a significant amount of discolored grease including red deposits and red grease (Fig. 1.9). At this time, it is not known if the discoloration is only due to wear debris, chemical degradation of the grease, physical separation of oil and grease base, or some combination of these phenomena.

To provide a baseline for comparison, one gear test was conducted using a hydrocarbon-based grease. The grease was grade 2 (selected to match the grade of the perfluoro type grease) and described as appropriate for wheel bearings. The test chamber atmosphere was ambient air, and the test load and speed were chosen to provide direct comparison to grease test number 2. A test duration of 1 hr was selected since red coloring within the tooth contact patterns was observed after 1 hr of testing with the perfluoro type grease. After the 1 hr test comprising 13,000 shaft revolutions, red deposits were found on all of the gear teeth contact areas (Fig. 1.10). Any differences in wear rates or composition of wear debris (as compared to operation with perfluoro type grease) will require further inspections and analysis.

To provide another baseline for comparison, one gear test was conducted using no lubricant on the test gears. The atmosphere was ambient air. The running speed was somewhat higher than for the other testing. The test was conducted for 1 hr comprising 42,000 shaft revolutions. As was expected, wear of the teeth occurred, and red colored wear debris was present at the end of the test (Fig. 1.11).

Summary

Seven grease-lubricated gear tests were completed using spur gears. Tests were done using two testing torque levels, with differing atmosphere (ambient air, dry nitrogen flow, and dry air flow), and with differing lubricant types (perfluoro type grade 2 grease, hydrocarbon-based grade 2 grease, and no lubricant). The two testing torque levels (2 and 5 ft-lb) provided nominal pitch-line Hertz stresses somewhat above and somewhat below the limit for the grease as recommended by the manufacturer. Further post-test analysis is needed to determine the composition of discolored grease. Further analysis is also needed to quantify any differences in wear rates, wear debris characteristics, or grease breakdown phenomena owing to differing operating conditions. The following observations were made:

(1) Some wear occurred, as expected, during all testing.
(2) Testing done using perfluoro type grease in ambient air produced red colored debris. Red debris was observed after 1 hr of testing at 2 ft-lb of torque and 200 rpm shaft speed (12,000 shaft revolutions). Large amounts of red debris were produced during tests of extended duration (30 hr). Profilometry traces reveal significant wear of the gear teeth.
(3) Testing done using perfluoro type grease in dry nitrogen and 2 ft-lb of torque did not produce any red colored debris or red colored grease even after extended test duration. Some dark-grey streaks of grease were found on the tips of some teeth. The composition of the grey streaks is not yet known.
(4) Testing done using perfluoro type grease in dry nitrogen and 5 ft-lb of torque produced some dark-grey colored grease.
(5) Testing done using perfluoro type grease in a dry air atmosphere produced red colored deposits.
(6) Testing done using a hydrocarbon-based grease in ambient air produced some red colored deposits and wear debris after short test duration.
(7) Testing done using no lubricant in ambient air produced some red colored deposits and debris after short test duration.

TABLE 1.1.—TESTING CONDITIONS AND DOCUMENTATION

TEST	GEAR PAIR	SETUP	LUBE	TORQUE (FT-LB)	SPEED (RPM)	TOTAL SHAFT REVOLUTIONS	OPERATING GEARS EXPOSED TO
1	1	A	PERFLU ORO	5	515	927,000	AMBIENT AIR
2	1	B	PERFLU ORO	2	200	194,000	AMBIENT AIR
3	3	A	PERFLU ORO	2	214	238,000	DRY NITROGEN
4	4	A	PERFLU ORO	5	214	205,000	DRY NITROGEN
5	5	B	PERFLU ORO	5	219	210,000	DRY AIR
6	2	A	NO LUBE	2	705	42,000	AMBIENT AIR
7	2	B	HYROCARBON	2	214	13,000	AMBIENT AIR

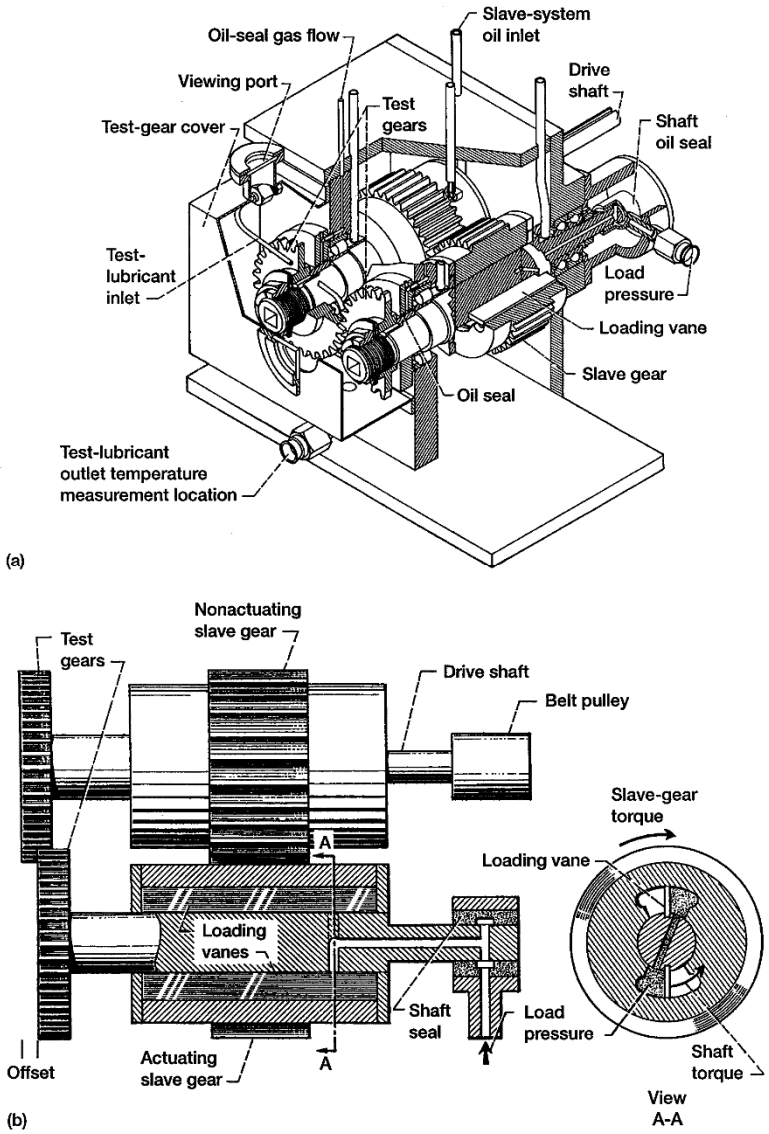

Figure 1.1.—NASA Glenn Research Center gear fatigue test apparatus. (a) Cutaway view. (b) Schematic view.

Figure 1.2.—Condition of the test gears after 3 hr of operation for test number 1 having test conditions of perfluoro type grease, 515 rpm shaft speed, 5 ft-lb torque, and ambient air atmosphere.

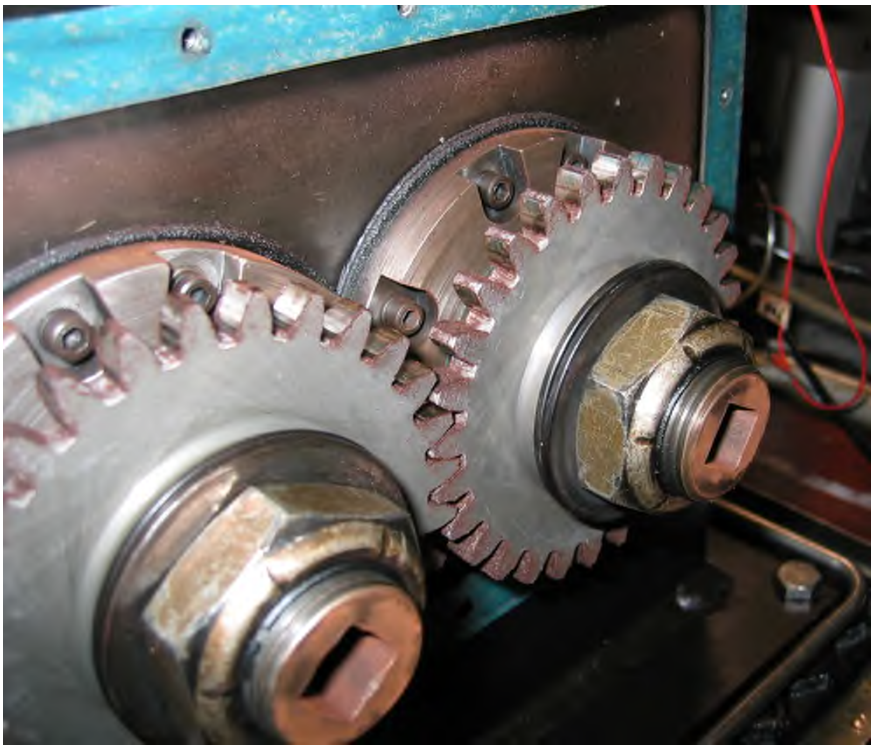

Figure 1.3.—Condition of the test gears after 30 hr of operation for test number 1 having test conditions of perfluoro type grease, 515 rpm shaft speed, 5 ft-lb torque, and ambient air atmosphere.

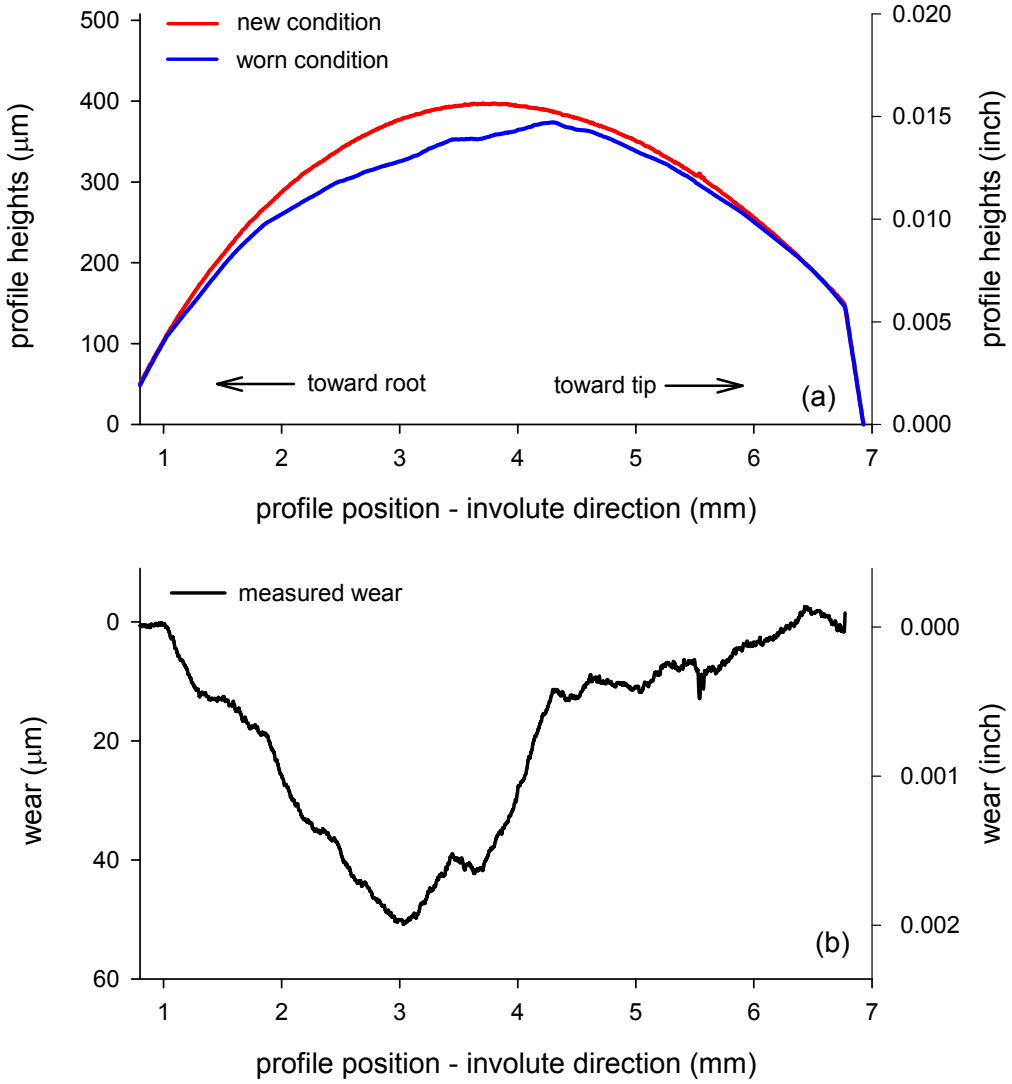

Figure 1.4.—Analysis of profilometry traces of a gear tooth in the profile direction reveal significant wear during test number 1. (a) Profile traces of tooth number 1 on gear 6–28–2A (the driving gear) at approximately the middle of the tooth face width measured before and after testing. (b) Wear depths determined as the difference of the new and worn profiles.

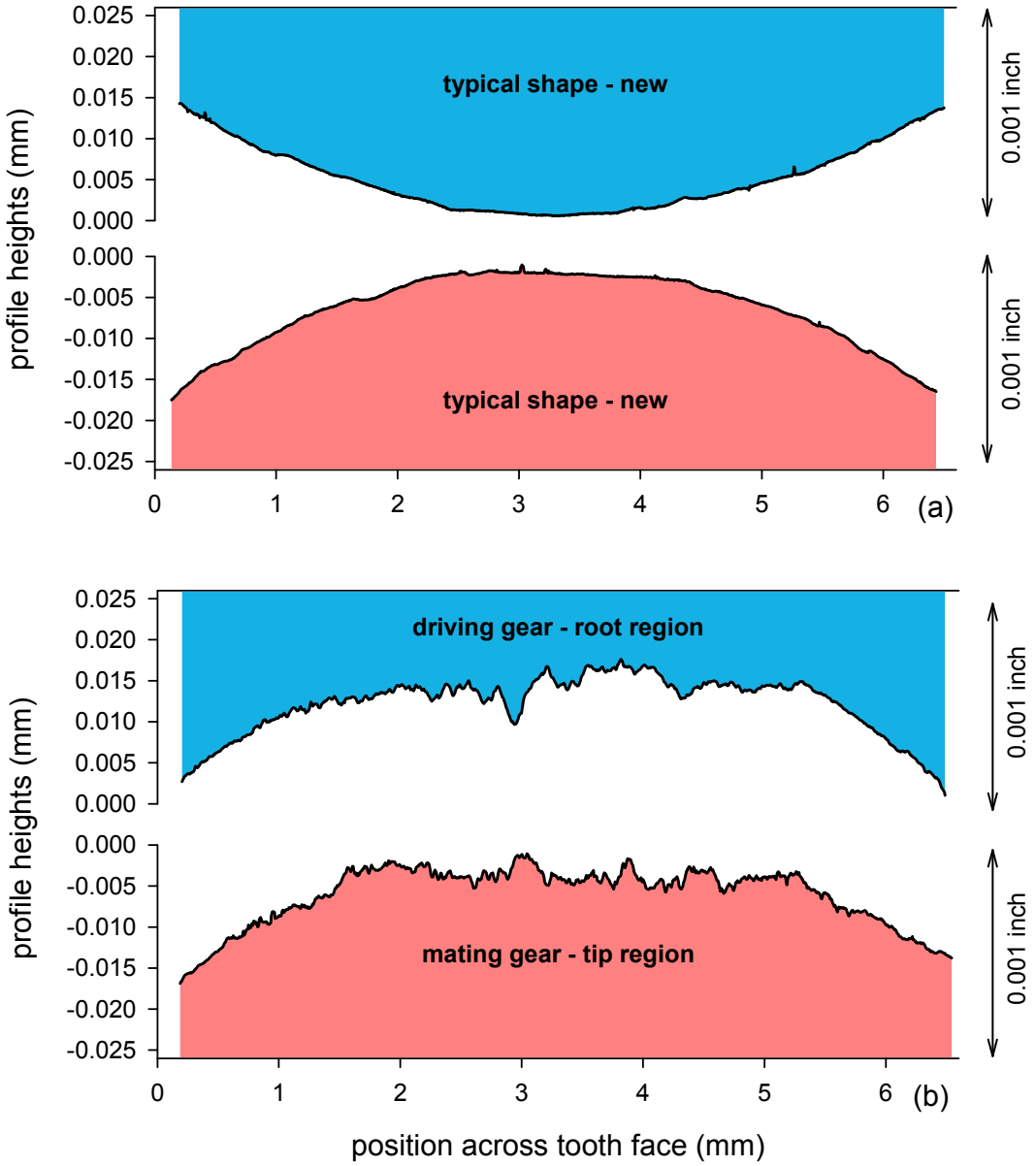

Figure 1.5.—Profilometry traces of gear teeth in the lead direction reveal that the original crowned geometry is significantly changed with increase of roughness due to wear during test number 1. (a) Typical measurements of gear teeth before running shows crowned lead geometry. (b) Measurements of mating teeth after running show that the crowned geometry of the mating gear's tip region has been worn into the driving gear's root region.

Figure 1.6.—Condition of the driven gear after 15 hr of testing for test number 2 having test conditions of perfluoro type grease, 200 rpm shaft speed, 2 ft-lb torque, and ambient air atmosphere. A mixture of original white and red colored grease is evident along with wear patterns.

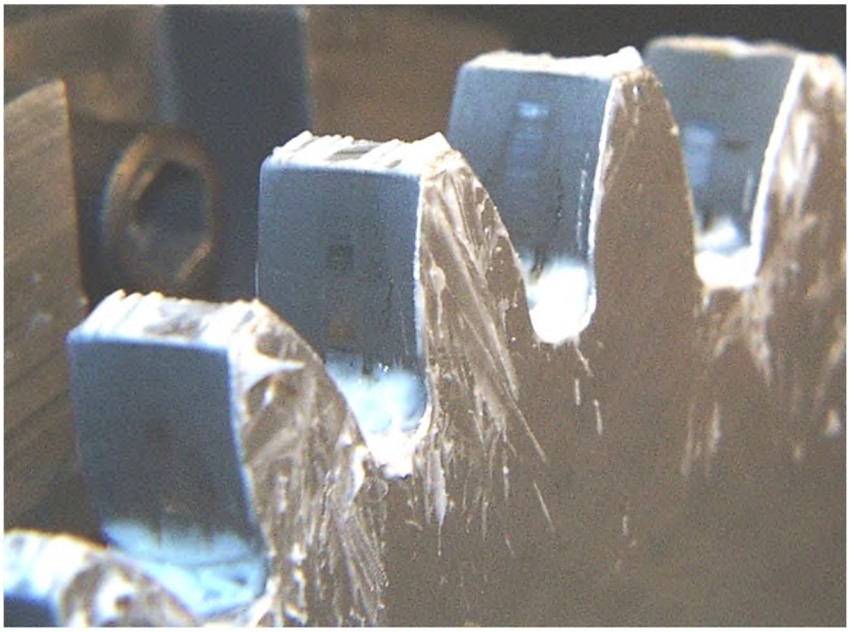

Figure 1.7.—Condition of the driven gear after 18.5 hr of testing for test number 3 having test conditions of perfluoro type grease, 214 rpm shaft speed, 2 ft-lb torque, and dry nitrogen atmosphere.

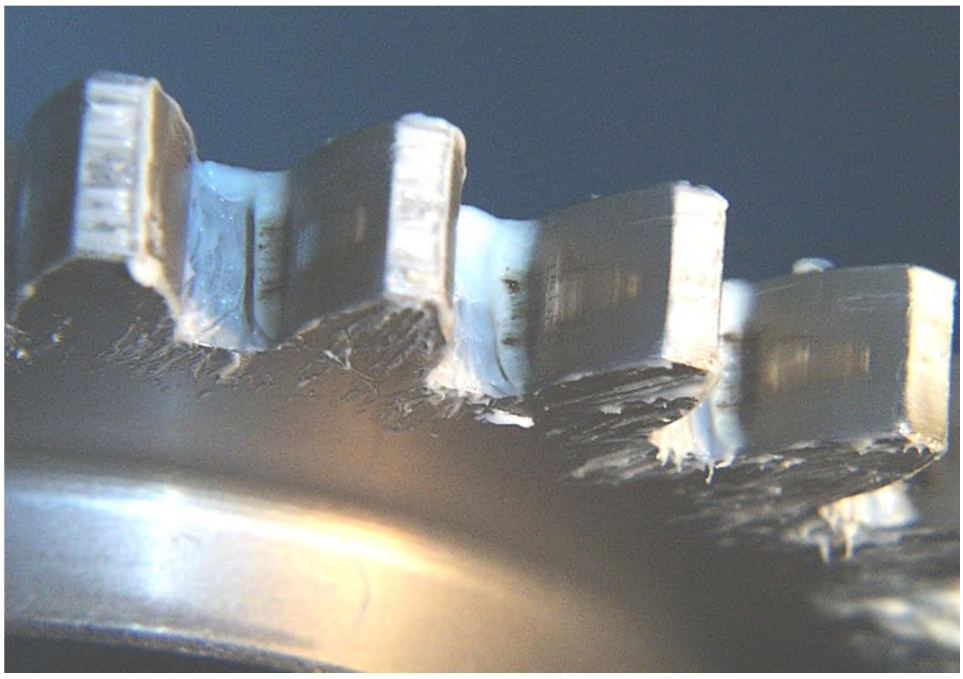

Figure 1.8.—Condition of the driven gear after 16 hr of testing for test number 4 having test conditions of perfluoro type grease, 214 rpm shaft speed, 5 ft-lb torque, and dry nitrogen atmosphere.

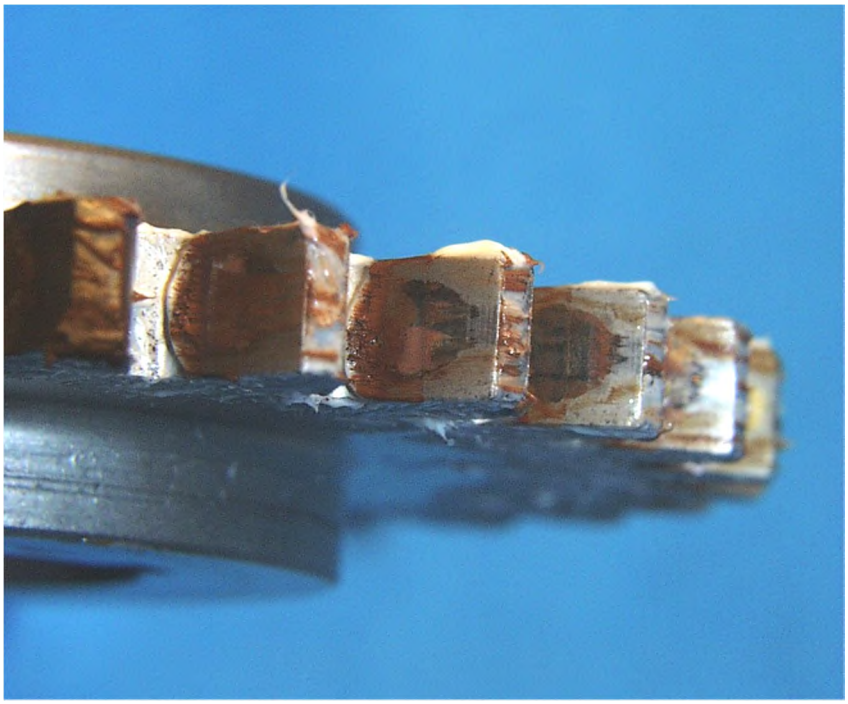

Figure 1.9.—Condition of the driven gear after 16 hr of testing for test number 5 having test conditions of perfluoro type grease, 214 rpm shaft speed, 5 ft-lb torque, and dry air atmosphere.

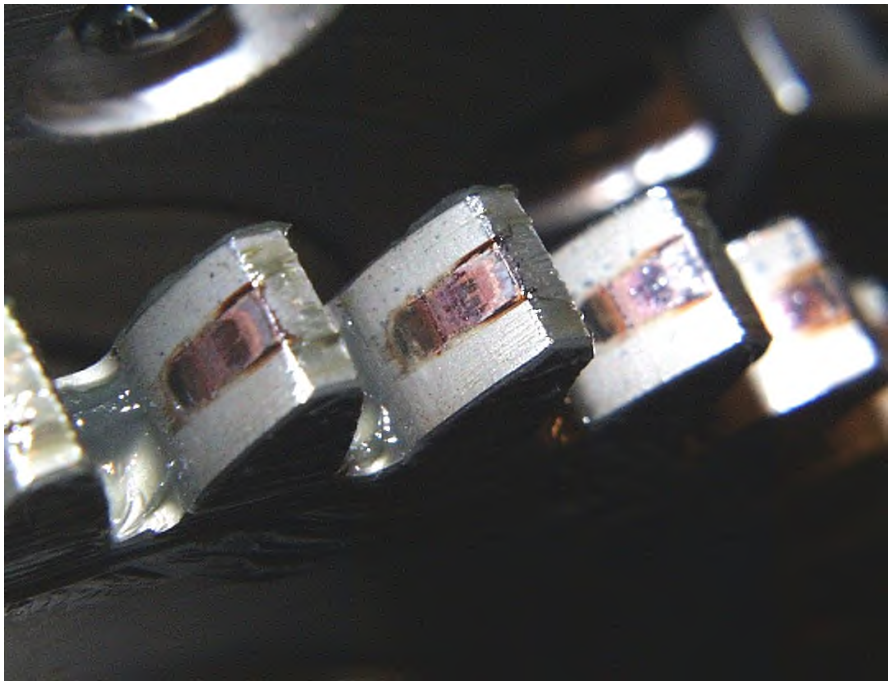

Figure 1.10.—Condition of the driven gear after 1 hr of testing for test number 6 having test conditions of hydrocarbon-based grade 2 grease, 214 rpm shaft speed, 2 ft-lb torque, and ambient air atmosphere.

Figure 1.11.—Condition of the driven gear after 1 hr of testing for test number 7 having test conditions of no lubricant, 705 rpm shaft speed, 2 ft-lb torque, and ambient air atmosphere.

Chapter 2: Investigation of Low-Cycle Bending Fatigue of AISI 9310 Steel Spur Gears

Robert F. Handschuh and Timothy L. Krantz
U.S. Army Research Laboratory
Glenn Research Center
Cleveland, Ohio 44135

Bradley A. Lerch
National Aeronautics and Space Administration
Glenn Research Center
Cleveland, Ohio 44135

Christopher S. Burke
QSS Group, Inc.
Cleveland, Ohio 44135

Abstract

An investigation of the low-cycle bending fatigue of spur gears made from 9310 gear steel was completed. Tests were conducted using the single-tooth bending method to achieve crack initiation and propagation. Tests were conducted on spur gears in a tensile test machine using a dedicated gear test fixture. Test loads were applied at the highest point of single-tooth contact. Gear bending stresses for a given testing load was calculated using a linear-elastic finite element model. Test data was accumulated from ¼ cycle to several thousand cycles depending on the test stress. The relationship of stress and cycles for crack initiation was found to be semi-logarithmic. The relationship of stress and cycles for crack propagation was found to be linear.

Introduction

In certain space applications the level of loading applied to the gear mesh members can be large enough to cause a great deal of the gear's life to be used in a short number of cycles. The American Gear Manufacturers Association (AGMA) standard for evaluating fatigue of gears (Ref. 2.1) that states: "The use of this standard at bending stress levels above those permissible for 10^4 cycles requires careful analysis." In the AGMA standard, the stress-life relationship for the cycle regime comprising 100 to 1000 cycles is depicted as a single value for the allowed bending stress. Thus, the problem is how to properly account for severe loads to estimate the fatigue lives of gear teeth. The standard's analysis techniques calculate a life at a given stress for 99 percent reliability at the component level. This means that a large population of components designed using the allowable stress values should experience crack initiation at a rate no greater than 1 per 100 for the given cycle count. To provide a credible estimate of fatigue life at 99 percent reliability, extensive experimental data is required to establish the load-life relationship in the low-cycle fatigue ($< 10^4$) regime.

Published experimental data for the fatigue of case-carburized gears for loads sufficient to fail the gear in the range of hundreds to several thousand cycles is sparse (Refs. 2.2 and 2.3). At gear loads that can fail a gear within several thousand cycles a certain degree on nonlinear material response is taking place since the bending stress calculated at the fillet radius—root region of the tooth exceeds the material yield strength. Therefore, linear-elastic-based gear stress analyses should be considered as providing stress-based indices of loading intensity rather than as representing the true stress condition of the material.

The objective of this work is to assess experimentally the low-cycle bending fatigue of spur gears made to aerospace quality from AISI 9310 material. Tests were conducted using a commercially available tensile test machine with a special fixture specifically designed to load the test gear tooth at the highest point of single-tooth contact.

Test Specimens and Material

The test gears used for this work were manufactured from consumable-electrode vacuum-melted AISI 9310 steel. The nominal chemical composition of the AISI 9310 material is given in Table 2.1. The gears were case carburized and heat treated according to Table 2.2. The nominal properties of the carburized gears were a case hardness of Rockwell C60, a case depth of 0.038 in., and a core hardness of Rockwell C38. The dimensions for the test gears are given in Table 2.3. The gear pitch diameter was 3.5 in. and the tooth form was a 20° pressure angle involute profile modified to provide a tip relief of 0.0005 in. starting at the highest point of single-tooth contact. The gears have zero lead crowning but do have a nominal 0.0005-in. radius edge break at the tips and sides of the teeth. The gear tooth surface finish after final grinding was specified as a maximum of 16 μin. rms. Tolerances for the gear geometries were specified to meet AGMA (American Gear Manufacturers Association) quality-level class 11. Gears manufactured to these specifications have been used at the Army Research Laboratory and the NASA Glenn Research Center for gear experiments including contact fatigue (Refs. 2.4 to 2.6), gear wear (Ref. 2.7), loss-of-lubricant performance (Ref. 2.8), gear crack propagation paths (Ref. 2.9), and health and usage monitoring (Ref. 2.10).

Note that the gears used for testing were of the same alloy and were manufactured to specifications similar to gears used for actuators on space shuttle orbiters. However, there exists some differences between the actuator gears and the test gears. The actuator gears are protuberance-hobbed and shot-peened in the area of the gear teeth fillets to improve the fatigue strength. Also, the actuator gears are provided a manganese-phosphate treatment. The test specimens were standard-hobbed, were not shot-peened, and were not provided a manganese-phosphate treatment.

Test Fixture

The fatigue test machine used for this investigation was an MTS 810 servo-hydraulic test system with 20,000 lb load capacity. With the exception of the gear test assembly, the test system was in standard configuration for fatigue testing smooth shank, cylindrical specimens. The load train features an alignment fixture that can be used for closely controlled positional and angular adjustments. The 20,000 lb load cell is positioned between the alignment fixture and the top grip. The output from the load cell can be used for control purposes and/or simply monitored as required by the test program. The gear test assembly (Fig. 2.1) is mounted in the load frame using a support arm that is attached to the two-post load frame. The bottom grip is attached to the actuator that serves to power the system using 3000 psi oil supplied by a central hydraulic system. An AC type linear variable differential transformer (LVDT) is attached to the base of the load frame and used to measure actuator displacement or stroke. As in the case of load, stroke output can be used for test system control and/or simply monitored as required by programmatic needs.

Key details of the gear test assembly are shown in Figures 2.2 and 2.3. The gear test specimen is positioned on a shaft that is a press fit in the fixture's casing. The test assembly was designed to conduct tests on gear teeth in sets of three. This approach was adopted in part to provide the necessary clearance for the two load rods. To permit access to the gear tooth to be tested several teeth nearby needed to be removed. Teeth were removed using the Electrode Discharge Machining (EDM) process. The upper load rod bears on the reaction gear tooth toward the base of the tooth. In contrast, the lower load rod bears on the test gear tooth at the highest point of single-tooth contact. Adopting this approach, highest bending stresses are introduced into the test gear tooth and the location of fatigue failure is predetermined with a

high degree of confidence. The rotational orientation of the test gear is precisely established using setup tooling. The rod that loads the test tooth at the highest point of single-tooth contact is representative of a rack gear (flat profile or infinite radius of curvature) contacting the test tooth. The various stages of fatigue crack growth can readily be observed through the viewing port provided Figure 2.3 shows the test arrangement ready for operation.

During installation of the gear test assembly, extreme care was taken to ensure that the load rods were in exact alignment with the load line of the test system. Furthermore, the test fixture was designed such that the load line of the test system is tangent to the nominal involute base circle. Use was made of the clearances between the various bolts and bolt holes to make the necessary positional and angular adjustments. When proper alignment was achieved, both load rods moved freely in their respective bushings and exhibited minimum friction.

A check on the performance of the fixture alignment was made by "bluing" the gears prior to testing. The contact patterns created by the load rod contact areas gave a clear indication that uniform load distributions on both gear teeth had been achieved. The contact pattern procedure was followed in all tests with excellent results, and the contact pattern data were recorded photographically and stored for quality assurance purposes.

Test Operation

The single-tooth bending tests conducted for this study were conducted using unidirectional loading. Testing was done using load control. The gear was positioned to provide load on the test tooth at the theoretical highest point of single-tooth contact for the case of the test gear mating with an identical gear at the standard center distance. The load is cycled from a small minimum load to the maximum load desired for the given fatigue test. The load range was maintained a constant value throughout the test. Loading was cycled at 0.5 Hz using a sinusoidal waveform. Typical loading is shown in Figure 2.4.

For the testing conducted in this study crack initiation was assumed to occur when the loading rod stroke increased approximately 2 percent relative to the stroke for the new gear tooth. At this point a crack had initiated with a size on the order of the case depth. The gear was cycled until the test termination point when the rod stroke was 0.010 in. greater relative to that achieved on the new gear tooth. At this time the gear tooth would have a visible crack on the order of 30 to 50 percent across the tooth thickness as seen on the side of tooth. To determine the extent of the crack face at the middle location across the face width would require post-test removal of the tooth. An example of one of the test specimens is shown in Figure 2.5 at the test termination cycle limit.

Finite Element Gear Model

In order to relate the normal load applied to the fillet—root stresses that the loading would induce, a finite element model of two identical gears as documented in Table 2.3 operating at a standard center distance was analyzed via a specialty code developed for gears (Ref. 2.11). The FEA modeling requires selection of the radius of the tip of the hob that made the gear. In this work, a hob tip radius of 0.040 in. was used to provide a gear root radius of nominal print dimensions. The largest possible hob tip that could properly make this gear has a tip radius of 0.051 in. Assuming linear-elastic material response, the gear bending stress scales linearly with applied load. Therefore, the analysis was done for one load case only and stresses for any load case found by proportional scaling. However, for the loads used in this study some plasticity that must have occurred on a local level where stresses exceed the yield strength of the material. Therefore, the stresses reported should be considered as stress-based indices of load severity. An example of the predicted distribution of maximum principal stress for the test specimen is shown in Figure 2.6. A 4000 lb normal force produces a 379 ksi bending stress maximum at the fillet-root region.

Test Results

A total of 29 fatigue and crack propagation tests were run. The data from these tests are shown in Tables 2.4 and 2.5. In Table 2.4, normal loads for the fatigue tests are listed. The fatigue tests loads ranged from approximately 3000 to 5000 lbf. In Table 2.5, a single load of increasing amount was applied using stroke control until the gear failed. The single 1/4 cycle load to failure ranged from approximately 5850 to 6900 lbf.

Table 2.4 provides the initial stroke (total deflection of load rods, gear test, and reaction teeth), the crack initiation cycles, and the number of cycles to test termination. The bending stress values shown from each test was based on proportional scaling of the maximum applied load to the load applied in the finite element model results mentioned earlier.

Table 2.5 provides data for three tests conducted for single load to failure (1/4 cycle). These tests were conducted on previously untested gear teeth. The maximum bending stress is shown in the table (calculated as previously described) along with an equivalent load capacity of load per inch of face width. The bending stress ranged from 554 to 654 ksi and the load per inch of face width ranged from approximately 23,000 to 27,000 lbf per inch of face width.

For the data of Table 2.4, five of the tests were on gears that had been previously tested for another potential failure mode known as dithering. Dithering is small relative motion between meshing gears that can exhaust the contact of lubricant and cause fretting wear and fretting fatigue at the contact locations. Dynamic (rotating) testing was done on test specimens having dithering-induced damage for millions of stress cycles (at a low level of bending stress, in the range of 30 ksi). Five teeth with dithering-induced damage were tested during this research using the single-tooth bending method. These five tests showed that the bending fatigue strength was not compromised due to the fretting on the gear flank surface. The gear teeth failed at the usual site in the root and fillet region and not at the location of the dithering-induced damage on the active flank of the tooth. This indicated, based on the relatively low number of tests conducted, that a bending failure would not occur from a dither-damaged surface. One of the teeth tested had both fretting damage and contact-fatigue pitting damage present prior to single-tooth bending testing. Testing of that gear resulted in fatigue cracks through the case in both the root-fillet region and on active flank where pitting was present. For that tooth, the cracks in the fillet region were larger than the crack in the pitting region. For purposes of the present research, it was assumed that the dynamic testing done at low levels of load on teeth with dither-induced damage did not represent any significant fatigue damage. That is, the low-load cycles were not included in the cycle-counting for purposes of reporting the data.

All the data generated in this study for bending fatigue are shown in Figure 2.7. Remember that the testing was unidirectional and that the bending stress values are stress-based indices of load intensity based on linear-elastic material response. Test termination data is plotted in Figure 2.8. For the range of 200 to 20,000 cycles, the relationships of stress to cycles for crack initiation and to cycles for test termination were found to be semi-logarithmic. The relationship of load intensity to crack propagation cycles (defined as the difference of crack initiation cycles and test termination cycles) is shown in Figure 2.9. There is a linear relationship between level of stress and the cycles for crack propagation.

Summary

A series of single-tooth bending tests have been conducted on aerospace quality, AISI 9310 spur gears. Tests were conducted from 1/4 cycle to thousands of cycles. The bending stresses reported were calculated using a linear-elastic finite element model. The reported values for bending stress exceeded the known yield properties of the material for a small volume of material in the root-fillet region. Testing produced cycle-load relationships for crack initiation and crack propagation. When tests were terminated, the crack size as visible on the tooth side face was approximately 30 to 50 percent of the tooth thickness. For the range of 200 to 20,000 cycles, the relationship of stress to crack initiation and to test termination was found to be semi-logarithmic (linear trend of stress versus log(cycles)). The relationship of stress to

crack propagation cycles was found to be linear. The crack initiation data could be used to validate methodology for fatigue life evaluations. The crack propagation data could be used to validate methodology for damage-tolerance evaluations.

Five fatigue tests were done using gear teeth having dithering-induced surface damage on the active tooth profile. The fatigue crack location was at the usual position in the root and fillet, not at the dithering-induced damage location. For these five tests, the dithering-induced damage did not reduce that bending fatigue capability of the gear tooth.

References

2.1. Fundamental Rating Factors and Calculation Methods for Involute Spur and Helical Gear Teeth. ANSI/AGMA 2001–C95, 1995.

2.2. Malott, R.C.; and McIntire, W.L: Advancement of Spur Gear Design Technology Final Report, 29 Jun. 1965–Jul. 1966. USAAVLABS–TR–66–85, 1966.

2.3. Heath, Gregory F.; and Bossler, Jr., Robert B.: Advanced Rotorcraft Transmission (ART) Program. NASA CR–191057 (ARL–CR–14), 1993. http://ntrs.nasa.gov

2.4. Townsend, D.P.; Chevalier, J.L.; and Zaretsky, E.V.: Pitting Fatigue Characteristics of AISI M–50 and Super Nitralloy Spur Gears. NASA TN–D–7261, 1973. http://ntrs.nasa.gov

2.5. Townsend, D.P.: Surface Fatigue Life and Failure Characteristics of EX–53, CBS 1000M, and AISI 9310 Gear Materials. NASA TP–2513, 1985. http://ntrs.nasa.gov

2.6. Krantz, Timothy: The Influence of Roughness on Gear Surface Fatigue. NASA/TM—2005-213958, (ARL–TR–3134), 2005. http://ntrs.nasa.gov

2.7. Krantz, Timothy; and Kahraman, Ahmet: An Experimental Investigation of the Influence of the Lubricant Viscosity and Additives on Gear Wear. NASA/TM—2005-213956 (ARL–TR–3126), 2005. http://ntrs.nasa.gov

2.8. Handschuh, Robert; and Morales, Wilfredo: Lubrication System Failure Baseline Testing on an Aerospace Quality Gear Mesh. NASA/TM—2000-209954 (ARL–TR–2214), 2000. http://ntrs.nasa.gov

2.9. Lewicki, David G.: Crack Propagation Studies To Determine Benign or Catastrophic Failure Modes For Aerospace Thin-Rim Gears. NASA TM–107170 (ARL–TR–971), 1996. http://ntrs.nasa.gov

2.10. Dempsey, Paula J.: Integrating Oil Debris and Vibration Measurements for Intelligent Machine Health Monitoring. Ph.D. Dissertation, Univ. of Toledo (NASA/TM—2003-211307), 2002. http://ntrs.nasa.gov

2.11. Vijayakar, Sandeep; Abad, Samir; and Gunda, Rajendra: Multi-Body Dynamic Contact Analysis. Tool for Transmission Design SBIR Phase II Final Report. ARL–CR–487, 2003.

TABLE 2.1.—NOMINAL CHEMICAL COMPOSITION OF AISI 9310 GEAR MATERIAL

Element	Wt%
Carbon	0.10
Nickel	3.22
Chromium	1.21
Molybdenum	0.12
Copper	0.13
Manganese	0.63
Silicon	0.27
Sulfur	0.005
Phosphorous	0.005
Iron	Balance

TABLE 2.2.—HEAT TREATMENT FOR AISI 9310 GEARS

Step	Process	Temperature		Time, hr
		K	°F	
1	Preheat in air	-------	-------	----------
2	Carburize	1,172	1,650	8
3	Air cool to room temperature	-------	-------	-------
4	Copper plate all over	-------	-------	-------
5	Reheat	922	1,200	2.5
6	Air cool to room temperature	-------	-------	-------
7	Austentize	1,117	1,550	2.5
8	Oil quench	-------	-------	-------
9	Subzero cool	180	–120	3.5
10	Double temper	450	350	2 each
11	Finish grind	-------	-------	-------
12	Stress relieve	450	350	2

TABLE 2.3.—TEST GEAR DESIGN PARAMETERS

Number of teeth	28
Module, mm	3.175
Diametral pitch (1/in.)	8
Circular pitch, mm (in.)	9.975 (0.3927)
Whole depth, mm (in.)	7.62 (0.300)
Addendum, mm (in.)	3.18 (.125)
Chordal tooth thickness ref. mm (in.)	4.85 (0.191)
Pressure angle, deg.	20
Pitch diameter, mm (in.)	88.90 (3.500)
Outside diameter, mm (in.)	95.25 (3.750)
Root fillet, mm (in.)	1.02 to 1.52 (0.04 to 0.06)
Measurement over pins, mm (in.)	96.03 to 96.30 (3.7807 to 3.7915)
Pin diameter, mm (in.)	5.49 (0.216)
Backlash reference, mm (in.)	0.254 (0.010)
Tip relief, mm (in.)	0.010 to 0.015 (0.0004 to 0.0006)
Note: Gear tolerances are per AGMA class 11.	

TABLE 2.4.—LOW-CYCLE BENDING FATIGUE DATA

Specimen number	Maximum load (lbs)	Minimum load (lbs)	Bending stress (ksi) finite element model	Stroke (in.)	Crack initiation (cycles)	Test termination (cycles)
GT0014-1A	–3500	–50	331	0.0141	4721	6413
GT0014-2A	–3511	–115	332	0.0134	6679	7921
GT0014-4A	–4105	–42	389	0.0159	855	1611
GT0014-3A	–4081	–20	386	0.0159	1208	1999
GT0014-5A	–3762	–25	356	0.0148	2181	3261
GT0050-C *	–3494	–79	331	0.0134	2235	3675
GT0050-D *	–3486	–77	330	0.0140	2108	3746
GT0021-1	–3687	–71	349	0.0143	4524	5820
GT0021-2	–3675	–61	348	0.0143	4170	5178
GT0021-3	–3680	–70	348	0.0142	3426	4578
GT0021-4A	–3987	–62	377	0.0153	2151	3159
GT0021-5	–3984	–54	377	0.0154	1163	2315
GT0062-D *	–3717	–37	352	0.0150	1095	2049
GT0062-C *	–3715	–47	352	0.0145	2000	3024
GT0062-B *	–3716	–39	352	0.0145	1638	3060
GT0062-NT **	–3750	–49	355	0.0144	1752	------
GT0053-A	–4194	–30	397	0.0165	1900	2599
GT0053-B	–4199	–43	397	0.0169	1242	1667
GT0018-A	–4242	–99	402	0.0165	462	1378
GT0018-B	–4250	–100	402	0.0168	348	1034
GT0050-E	–4714	–70	446	0.0190	190	668
GT0045-A	–4750	–59	450	0.0189	638	858
GT0045-B	–5015	–119	475	0.0200	460	755
GT0045-C	–5002	–73	473	0.0201	498	725
GT0045-D	–2994	–42	283	0.0123	14800	16167
GT0045-E	–3004	–40	284	0.0122	16400	18315

*Test tooth had dithering-induced surface damage and had experienced low-load-level dynamic testing.
**Test tooth was only tested to crack initiation.

TABLE 2.5.—SINGLE LOAD TO FAILURE TEST DATA

Specimen number	Fracture maximum load (lbs)	Load per in. of face width (lb/in.)	Bending stress ksi at fracture load, finite element value
GT0053-C	–6914	27656	654
GT0053-PF2	–6750	27000	639
GT0062-A	–5848	23392	554

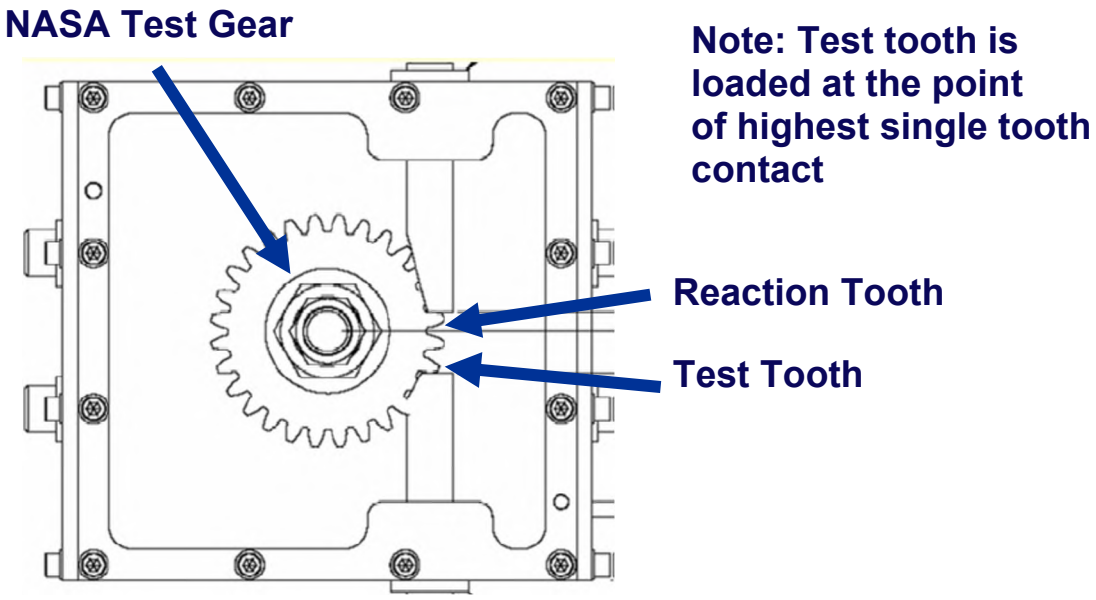

Figure 2.1.—Schematic of test fixture for low-cycle bending fatigue of spur gears.

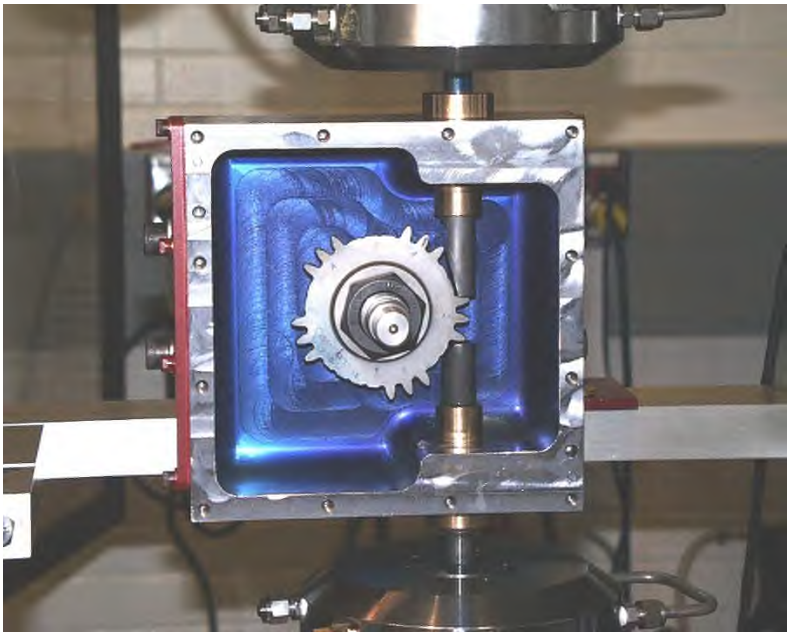

Figure 2.2.—Test gear modified and installed in test fixture.

Figure 2.3.—Test fixture in tensile test machine.

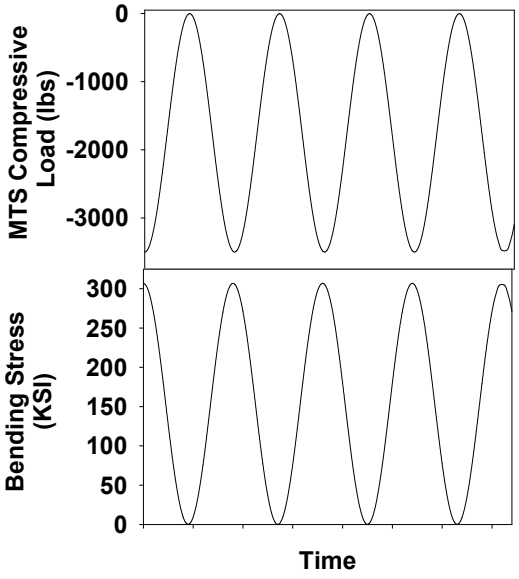

Figure 2.4.—Loading and stress as a function of time.

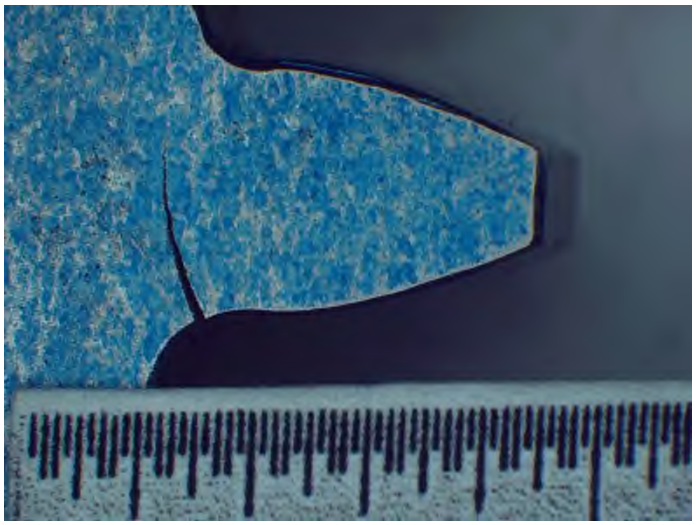

Figure 2.5.—Single-tooth bending failure at test termination.

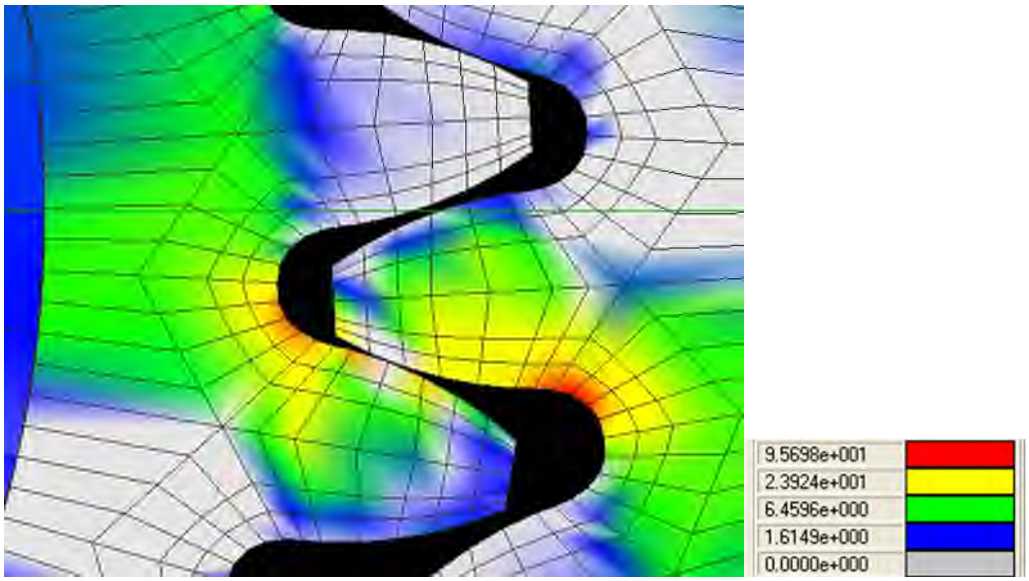

Figure 2.6.—Finite element analysis result showing distribution of maximum principal tensile stresses for a unit load at the highest point of single-tooth contact. The color key has units of psi.

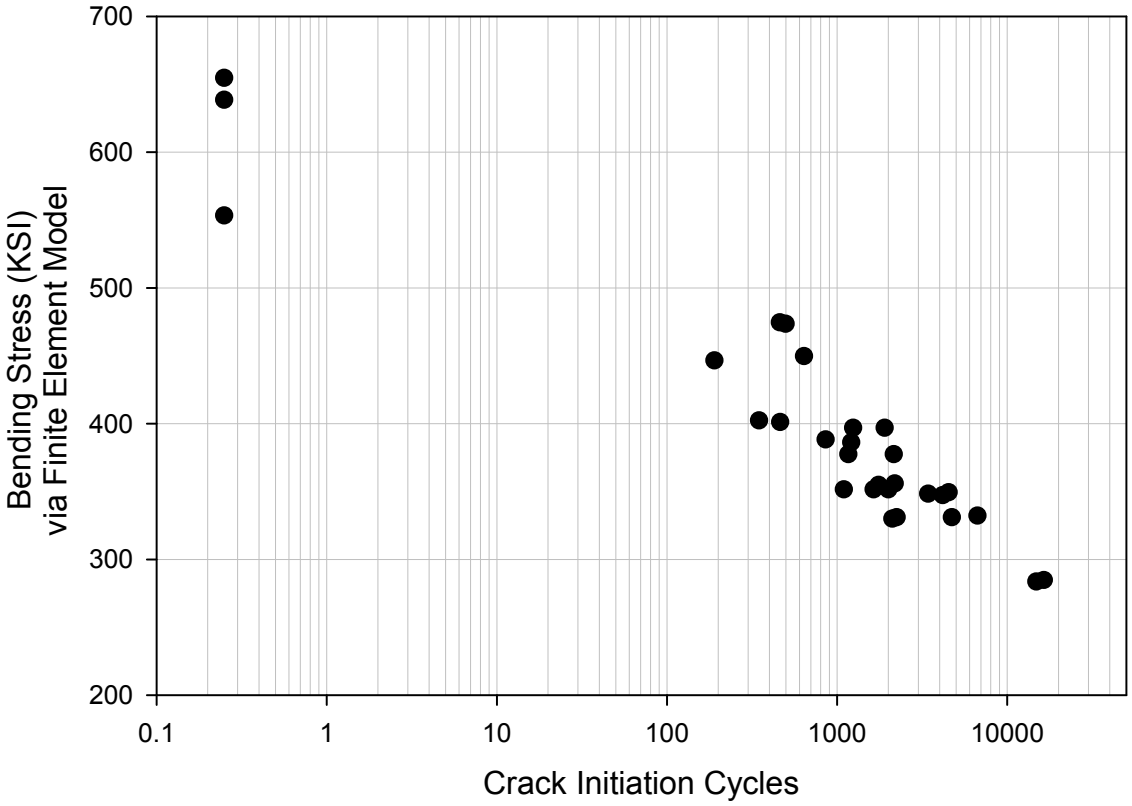

Figure 2.7.—Single-tooth bending data, crack initiation.

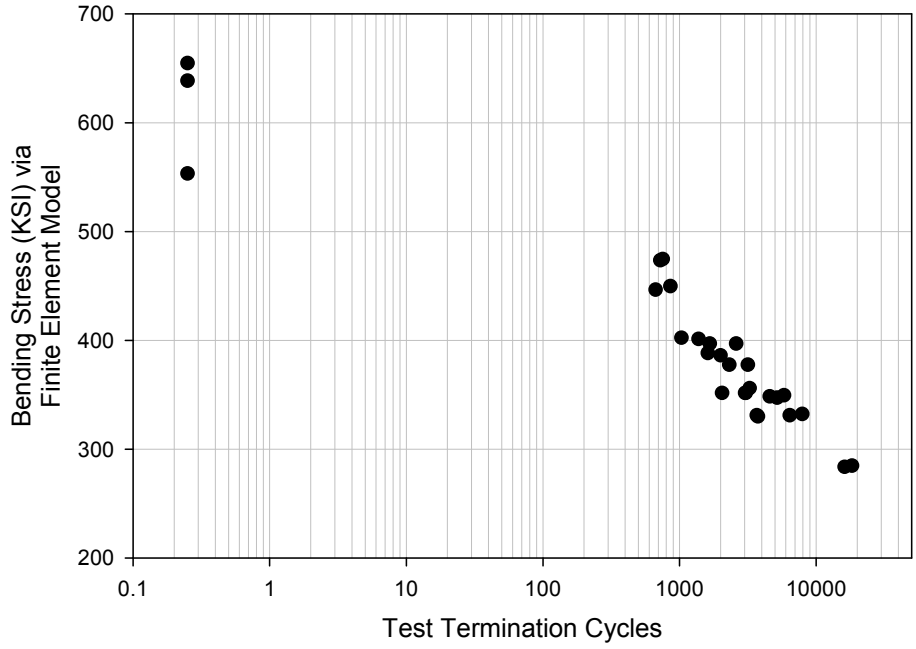

Figure 2.8.—Single-tooth bending data, test termination.

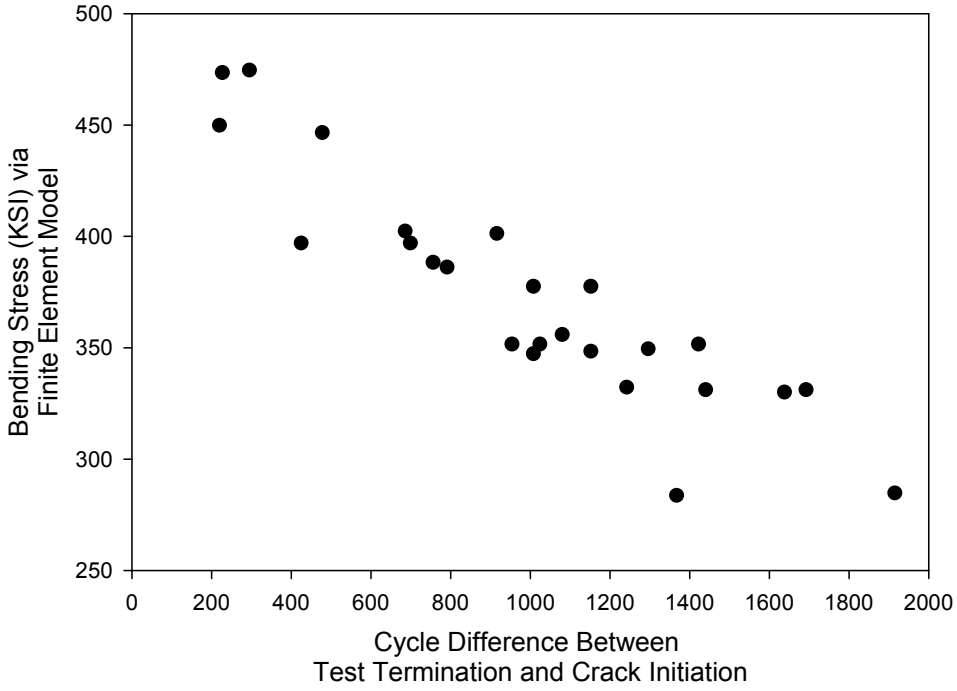

Figure 2.9.—Crack propagation cycles (difference between test termination and crack initiation) as a function of linear-elastic-based tooth bending stress.

Chapter 3: Shuttle Rudder/Speed Brake Power Drive Unit (PDU) Gear Scuffing Tests With Flight Gears

Margaret P. Proctor and Fred B. Oswald
National Aeronautics and Space Administration
Glenn Research Center
Cleveland, Ohio 44135

Timothy L. Krantz
U.S. Army Research Laboratory
Glenn Research Center
Cleveland, Ohio 44135

Abstract

Scuffing-like damage has been found on the tooth surfaces of gears 5 and 6 of the NASA space shuttle rudder/speed brake power drive unit (PDU) number 2 after the occurrence of a transient backdriving event in flight. Tests were conducted using a pair of unused spare flight gears in a bench test at operating conditions up to 2866 rpm and 1144 in.-lb at the input ring gear and 14,000 rpm and 234 in.-lb at the output pinion gear, corresponding to a power level of 52 hp. This test condition exceeds the maximum estimated conditions expected in a backdriving event thought to produce the scuffing damage. Some wear marks were produced, but they were much less severe than the scuffing damage produced during shuttle flight. Failure to produce scuff damage like that found on the shuttle may be due to geometrical variations between the scuffed gears and the gears tested herein, more severe operating conditions during the flight that produced the scuff than estimated, the order of the test procedures, the use of new hydraulic oil, differences between the dynamic response of the flight gearbox and the bench-test gearbox, or a combination of these. This report documents the test gears, apparatus, and procedures, summarizes the test results, and includes a discussion of the findings, conclusions, and recommendations.

Executive Summary

Scuffing-like damage has been found on the tooth surfaces of gears 5 and 6 of the NASA space shuttle rudder/speed brake power drive unit (PDU) number 2 after the occurrence of a transient backdriving event in flight. Experiments were conducted at NASA Glenn Research Center (GRC) using a pair of unused spare flight gears for PDU serial number 0405 in a bench test setup to achieve the following objectives:

(1) Recreate scuffing damage similar to that found on the flight gears at conditions expected during backdriving and document conditions that induce scuffing.
(2) Demonstrate that scuffed PDU flight gears can be operated long enough to complete a shuttle mission.
(3) Quantify the scuffing and tooth wear.

Tests were conducted up to 2866 rpm and 1144 in.-lb at the input ring gear and 14,000 rpm and 234 in.-lb at the output pinion gear, that corresponds to a power level of 52 hp. This test condition exceeded the maximum estimated condition of the backdriving event that produced scuffing-like damage in flight.

The scuffing tests performed did not produce scuff marks similar to that produced during shuttle flight. Wear marks were produced on the pinion teeth near the tips and on the ring gear teeth faces during the test Back-3c, which was conducted at an input speed, torque, and power of 2402 rpm, 664 in.-lb, and

25.3 hp. Very light wear marks were generated on side-2 of the pinion gear during the test Score-1 conducted at input speed, torque, and power of 2865 rpm, 1167 in.-lb, and 53 hp.

Failure to produce scuff damage like that found on the shuttle gears may be due to geometrical variations between the scuffed gears and the gears tested herein, more severe operating conditions during the flight that produced the scuff than estimated, the order of the test procedures, the use of new hydraulic oil, differences between the dynamic response of the flight gearbox and the bench-test gearbox, or a combination of these.

Options to consider for resolving the scuffing issue include, but are not limited to

- Analyze the shuttle PDU to determine the inertial loads and transient conditions expected during backdrive.
- Examine inspection reports and possibly re-inspect the pinion and ring gears to assess variations in tooth profile, particularly at the edge break at the tips of the teeth and their possible contributions towards scuffing.
- Change the test procedure to attain the most severe test conditions early on in the test matrix.
- Conduct transient scuffing tests.

Also, if a future shuttle flight includes a backdriving event that produces gear scuffing, the GRC bench-test rig could be used to assess the remaining life capability of gears that were scuffed in flight. Such an approach provides the most direct assessment method short of system-level testing. However, it does require removal of the PDU unit from service for replacement of the scuffed gears.

Introduction

Gears used in the NASA space shuttle rudder/speed brake power drive units (PDUs) have been damaged during transient events termed “backdriving.” The damage occurs to the working surface of the gear teeth. The damage is termed “scuffing.” Scuffing was observed on gears 5 and 6, on one side of the gear teeth, in the tooth-tooth contact area. The damage can be seen in Figure 3.1 (from Ref. 3.1). During backdrive, the outer teeth of the ring gear (gear 6) drive the smaller pinion gear (gear 5). In normal operation the pinion gear drives the ring gear. Motion of the PDU gears is produced by hydraulic motors, and so the backdriving event is torque limited. The maximum speed and power for gear 5, the pinion, during backdriving is estimated to be 50 hp at 14,000 rpm.

Gear scuffing is considered as a failure mode for many applications. The term “scuffing” refers to surfaced distress (material removal) that can occur when load-carrying surfaces are in intimate contact and have some amount of relative sliding. Scuffing is of concern for mechanical components such as cams, bearings, and gears. Scuffing refers to a wear mode associated with a complete breakdown of lubrication. Wear rates are high, and a scuffed surface shows scoring-like marks in the direction of sliding. Scuffing is usually associated with some amount of solid-phase welding of asperity-scale features of the surfaces that is accompanied by tearing, material transfer, and galling of the sliding surfaces.

Gear technologists sometimes differentiate between cold-scuffing and hot-scuffing. During hot-scuffing, thermal energy within the lubricated contact assists the breakdown of both lubricant films and chemical boundary lubricating films. The onset of hot-scuffing has been postulated to be a type of thermal stability problem. “Flash temperature” limits were established for concentrated mechanical contacts lubricated with nonreactive mineral oils by classical experiments of Blok (Ref. 3.2). Flash temperature approaches are also commonly used for other types of lubricants.

Scuffing can also occur without the “thermal-instability” phenomena as described above, and such scuffing is usually referred to as “cold-scuffing.” Calculation methods to predict the probability of scuffing have been developed. The scuffing prediction analyses provide guidance for product design and development, but highly reliable predictions for the onset of scuffing for any particular gear application has remained elusive. Predictions are difficult because many interdependent factors influence the onset of

scuffing including geometric accuracy of tooth profile, dynamic load effects, rolling and sliding speeds, surface finish and microtopography, oil physical properties, and the chemical interactions of the metal alloy and lubricating oil.

Previous to the research reported herein, research was done by Wedeven Associates and GRC to better understand the root cause, the severity of damage, and the capability of the gears to continue to operate safely after scuffing damage occurs and the backdriving event is concluded. The following was learned from the previous research (Refs. 3.1 and 3.3):

- The damage observed on flight gears and bench test specimens are consistent with a cold-scuffing mode. There is no evidence to suggest that hot-scuffing of the gears is likely. These facts are important since cold-scuffing tends to be a self-relieving event while hot-scuffing can cause extensive damage and weaken the gear teeth by tempering the case-carburized gear teeth.
- The damage observed on flight gears and bench test specimens is consistent with gears having insufficient tip relief for the operating torque. The evidence suggests that during backdriving the transient torque was sufficiently high to cause gouging of the tips of the meshing gear teeth.

Although the previous research provided insight concerning the scuffing damage, it was desired to better understand the conditions (temperature, speed, torque, and rate of change for speed and torque) that produced scuffing during a backdriving event. It was also desired to study the capability of scuffed gears to operate safely and successfully for the remainder of a mission and, perhaps, for multiple missions. Should the scuffed gears fail to carry torque, then proper positioning of the rudder and speedbrake panels for safely controlled flight would not be possible. To better understand the scuffing phenomena and any potential safety implications, experiments were conducted at GRC using a pair of flight gears in a bench test setup to achieve the following objectives:

(1) Recreate scuffing damage similar to that found on the flight gears at conditions expected during backdriving and document conditions that induced scuffing.

(2) Demonstrate that scuffed PDU flight gears can be operated long enough to complete a shuttle mission.

(3) Quantify the scuffing and tooth wear.

Previous research results and technical discussions were used to develop the test protocols. The Mechanical Components Branch conducted the tests in the Gear Noise Facility with support from the Engineering and Technical Services Directorate to design and fabricate the test gearbox. Testing began on June 1, 2005, with the bulk of the data obtained prior to launch of STS–114 on July 26, 2005. The final test was conducted on Aug. 9, 2005. This report documents the test gears, apparatus, and test procedures, summarizes the test results, and includes a discussion of the findings, conclusions, and recommendations.

Test Gears

The test gears were unused spares from the Rudder Speed Brake Power Drive Unit (RSB PDU), number 2, S/N 0405. Table 3.1 shows their part and serial numbers and key design parameters. Both of these spur gears are made of AMS 6265 (AISI 9310), a standard aerospace gear steel. For these tests the outer teeth of the ring gear drove the pinion gear. The distance between the test gear centerlines is approximately 3.3125 in.

To mount the ring and pinion gears to their test shafts some modifications were required. These modifications included removing the inner teeth of the ring gear and cutting off the internal spline of the pinion gear.

Apparatus

Test gearbox

A test gearbox was designed and fabricated specifically for these tests (Fig. 3.2). Design decisions were driven by an extremely tight schedule that initially required both the design and fabrication to be completed in just 5-1/2 weeks.

The welded test gearbox is made of 1/2-in.-thick mild steel plate. Endplates that support the ends of the shafts were bolted to the gearbox and location pins installed to assure precision assembly. The ring gear is bolted on a steel hub (Fig. 3.3), which is mounted on a 3/4-in. ground and hardened shaft. The shaft drives the hub with two 1/8-in. rectangular keys. The maximum speed of the input shaft is 2,864 rpm.

The pinion gear is also mounted on a 3/4-in. ground and hardened shaft, which drives the pinion through two 1/8-in. rectangular keys. The maximum speed of this output shaft is 14,000 rpm. The shafts are supported by steel ball bearings rated for a maximum speed of 19,000 rpm. The pinion and ring gears are mounted with collars and/or sleeves to maintain their axial position on the shaft. Once the gears were mounted to the shafts, the shafts were balanced.

Lip seals are used at the shaft ends to contain the hydraulic fluid lubricant. Polymer spacers, metal shims, and e-clips are used at each shaft end to hold the axial positions of the shafts so that the gears have a centered engagement. A lid is bolted on to the top of the gearbox to contain the lubricant. The lid has handles for easy removal for visual inspections of the test gears. The lid is vented to atmosphere with a tube connected to a plastic bottle to capture any lubricant mist.

There were a total of three builds of the test gearbox. In the order tested, they are referred to as "side-1, build-1; side-2, build-1; and side-1, build-2." Side refers to the loading side of the gear teeth. Most of the testing was conducted on side-1. Side-2 is the opposite teeth sides of side-1. Testing on side-2 was performed by removing the shafts and flipping the shafts end-for-end with the gears still on them and then reinstalling the shafts in the gearbox.

Lubricant

The test gearbox was filled to the shaft centerlines (Fig. 3.4), with Brayco Micronic 882 hydraulic fluid to splash lubricate the gears and the bearings. New hydraulic fluid was used for each build of the gearbox and the fluid is from the same batch used on the shuttle.

Test Facility

The test gearbox was installed in the Gear Noise Test Facility (Fig. 3.5). A 200-hp DC motor powers a pulley-belt system to drive the input shaft. A torque meter on the input shaft measures both the speed and torque of the input ring gear. The maximum input shaft speed was 2864 rpm. The output shaft or pinion gear shaft has a maximum speed of 14,000 rpm and is connected to a 5 to 1 speed reduction gearbox. The speed reduction gearbox, which can be seen in Figure 3.2, is connected to an absorption dynamometer rated for 175 hp and 6000 rpm. This eddy current dynamometer provides load torque for the system.

To accommodate the test gearbox and the speed reduction gearbox, a shorter shaft was made to connect the torque meter to the input shaft to the test gearbox. Also, a pedestal was added to support the speed reduction gearbox. The Gear Noise/Dynamics Rig (with a different test gearbox) is described in more detail in Reference 3.4.

Research Measurements

Type K thermocouples were used to measure the bath temperature of the hydraulic fluid at the bottom of the gearbox and the oil fling-off temperature at approximately 1/2 in. above the gear mesh. Accelerometers were installed on the drive-side endplate of the test gearbox under each shaft bearing (Fig. 3.6), to measure the vertical vibration in each shaft. It was anticipated that either the fling-off temperature of the hydraulic fluid or the vibration would give some indication if a scuffing event had occurred.

A speed transducer was used to measure the input shaft speed. The torque meter on the input shaft was used to measure the input shaft torque to an accuracy of ±2 rpm. The output torque at the dynamometer was also measured. Note that the dynamometer torque reflects power losses in both the test gearbox and the speed reduction gearbox. These measurements along with the rms vibration level, date and time of test initiation, and the accumulated time of the test were recorded using a data acquisition system on a personal computer. These data were recorded typically once every second during testing.

Approximately once every 50 sec, a vibration time record was recorded for spectral analysis. Each vibration record consisted of 8192 readings for each of the two channels. The sample rate was approximately 60,000 samples per second per channel. Alias protection was provided by 26 kHz low-pass filters.

Test Procedures

Pre-test Measurements

A profilometer was used to measure the tooth surface roughness of the pinion gear teeth. The ring gear teeth surface roughness was not measured, because the profilometer stylus is too big to get between the teeth. The pre-test profile was measured using a stylus profilometer having a 2 μm radius, and the data was filtered using a 0.25 mm cutoff and 100:1 bandwidth. The roughness average (Ra) of the surface was 0.25 μm (10 μin.). A typical micro-topography of a pinion gear tooth is shown in Figure 3.7.

Once the test gearbox was assembled, the backlash between the gears was measured at four positions approximately one-quarter turn of the ring gear apart. Backlash is the amount by which the width of a tooth space exceeds the thickness of the engaging tooth measured on the pitch circles (Ref. 3.5). The backlash measurements are shown in Table 3.2. The backlash checks verified that the test gears were suitably mounted to the test gearbox shafts and had appropriately small runout.

A rubber mold of three teeth on each of the pinion and ring gears was made prior to any testing. A second set of rubber molds was made on 6/23/05 as a post-test mold for side-1, build-1 and pre-test mold for side-2, build-1. The product Repliset F5 was used and set up in about 20 min at room temperature. It was easily peeled off of the gear teeth. An acid pen mark on the ring gear mounting hub was easily observed in the rubber mold indicating that surface wear marks could be transferred to the rubber mold. A two-part epoxy (80 percent epoxy and 20 percent catalyst), Durelco 4525, was then poured into the rubber mold used to make a hard model of two pinion teeth. The epoxy, which cures in 24 hr at room temperature or in 20 min at 160 °F, was oven cured at 120 °F for 1 hr since the rubber mold material has a 150 °F temperature limit. The black rubber mold easily separated from the hard epoxy model of the tooth. The intent was to develop a process to transfer any wear marks to the hard epoxy tooth. If this process worked then it would be a way to examine the ring gear teeth, since the epoxy teeth could be cut apart so they could be measured with the profilometer. No profilometer measurements were made of the hard epoxy teeth to verify the usefulness of this process. This may be worth pursuing if further work is desired. The pre-test rubber mold of the pinion and ring gear teeth and the hard epoxy replications of the pinion teeth are shown in Figure 3.8.

A digital camera with +1, +2, and +4 diopter closeup lenses was used to photograph the pinion and ring gear teeth in the gearbox to document their condition throughout the testing. Pre-test photos of the pinion and ring gear teeth are shown in Figures 3.9 and 3.10, respectively.

Tests Conducted

The tests conducted are summarized in Tables 3.3 to 3.5 for side-1, build-1; side-2, build-1; and side-1, build-2, respectively.

First, with side-1, build-1, a short checkout test to verify operation of the rig and the data system was conducted at an input speed of 500 rpm and torque of 162 in.-lb. Next a speed survey was conducted at a low input torque of approximately 75 to100 in.-lb and the input speed was incrementally increased and decreased between 500 to 1429 rpm. After the speed survey, the test gearbox lid was removed to make a visual inspection and take photographs.

The Run-in test was then conducted at an input speed of approximately 800 rpm while the input torque was increased from 100 to 500 by 100 in.-lb increments. After each steady-state test condition was held for approximately 10 min, the rig was shut down, the lid removed, and the gears visually inspected.

Three backdrive simulations were made. The first, "Back-1," was conducted at 500 in.-lb of input torque and shaft speeds of 1000, 1250, and 1431 rpm. Each condition was held for approximately 5 min before the rig was shut down and the gears visually inspected and photographed. The second, "Back-2," was conducted at an input shaft speed of 1432 rpm and the input gear torque set to 500, 700, 900, and 1040 in.-lb. Again each test condition was held for approximately 5 min before the test was terminated and gears visually inspected and photographed. The third backdrive simulation, "Back-3," was intended to be conducted at 1040 in.-lb and speeds of 1432, 1900, 2400, and 2863 rpm, but these conditions could not be obtained due to dynamic instability of the test rig. The actual conditions obtained are shown in Table 3.3. Each test condition was held for approximately 5 min before the test was terminated and gears visually inspected and photographed.

To improve control of the drive train, a soft rubber coupling between the drive motor and the torquemeter was replaced with a hard gear coupling. Then tests "Back-3x" and "Back-3y" were conducted. Removing the rubber coupling improved but did not eliminate the instability problem; therefore, the desired test conditions of "Back-3" could not be fully attained.

Next, the high-speed pulley on the test rig was changed to reduce the speed up ratio of the pulley system from 4.3:1 to 3:1. Also, a heat gun and a heat lamp were used to heat up the hydraulic fluid in the test gearbox. Then "Back-3z" tests were conducted attaining the test conditions indicated in Table 3.3. Modifications to the motor control circuit were made and several stability tests ("Stab-test-1" through "Stability-9") were conducted at the conditions shown in Table 3.3.

It was then decided to test on the unused face of the gear teeth. The test conditions attained for this side-2, build-1 configuration are shown in Table 3.4. In these tests the rig was brought up to low speed (~200 rpm) and then the full the torque was set. Then the speed was rapidly increased to the test point conditions and held for 5 sec. Then the test was stopped to inspect and photograph the gears. Unfortunately, in the last test, an e-clip that restrained the high-speed (14,000 rpm) shaft flung off, allowing the gears to move axially out of mesh. This event damaged side-2 of the gear teeth, as well as the spacers and shims that set the axial positions of the gears. Rough burrs were hand filed off of the teeth to allow the gears to be further tested on side-1.

A final set of tests was conducted on the first side of the teeth. See Table 3.5 for the test conditions for side-1, build-2. The intent of this sequence of tests was to see if higher torques would cause scuffing. At a low speed the desired torque was set and then the speed increased to the test condition. The test condition was held for approximately 5 min. Then the test rig was shut down and a visual inspection and photography were performed. During test Final-5 the belts from the drive motor to pulley broke before steady conditions were obtained and testing ended.

Test Results

The only tests that generated any damage beyond normal polishing wear of the gear teeth were Back-3c, Score-1, and Score-2. The Back-3c test was conducted at an input speed, torque, and power of 2402 rpm, 664 in.-lb, and 25.3 hp. A plot of the time history of the speed, input torque, oil fling temperatures, and the pinion vibration levels for Back-3c is shown in Figure 3.11.

It is interesting to note the fling temperature shows a sudden increase at approximately 300 sec. Just prior to this there is a spike in both the pinion and ring gear vibration and an instability in the input torque and speed measurements. This may indicate the time when the wear marks were created.

Visual inspection after the Back-3c test found half-moon-shaped wear marks near the tip of the driven side of all pinion gear teeth (Fig. 3.12). These wear marks were slightly offset from the tooth center towards the drive motor. There were corresponding marks on the driving side of the ring gear teeth near the root (Fig. 3.13). While the wear pattern is similar to the scuffing found on the shuttle flight gears, it is much less severe. The mark had no depth perceptible to touch.

Frequency spectra of the accelerometer located near the pinion shaft taken at 250 and 550 sec are shown in Figure 3.14(a) and (b), respectively. The spectra show the vibration frequencies for the first four harmonics of gear mesh frequency. If we speculate that the tooth damage observed after this test occurred at 300 sec, when the oil temperature increased, we might expect to see a difference in these vibration traces because of this damage. However, the traces do not show any indirect evidence of a change to the tooth surfaces.

Small wear marks near the tips of the driven side of the pinion teeth (Fig. 3.15), were generated during the Score-1 test on side-2, build-1 conducted at input speed, torque, and power of 2865 rpm, 1167 in.-lb, and 53 hp. No corresponding wear was observed on the ring gear teeth as shown in Figure 3.16. The time histories of input speed, input torque, oil fling temperature, and pinion vibration are shown in Figure 3.17. There is no distinct corroboration of vibration rise and fling temperature rise as in the Back-3c test. There are some high vibration levels in the test however. The drop in oil fling temperature is likely due to turning off the heat gun and heat lamp prior to rotation and some initial cooling due to flinging the oil to cooler surfaces above the oil bath.

As mentioned previously, during the Score-2 test on side-2, build-1 the gear mesh disengaged at high speed. The resulting damage to the pinion and ring gear teeth is shown in Figures 3.18 and 3.19, respectively. Note that cloth fibers are visible in these photos. The fibers were created by rough burrs on the damaged gears when the teeth were wiped for photographs.

The condition of the pinion and ring gear teeth at the completion of testing (after the Final-5 test) is shown in Figures 3.20 and 3.21, respectively. The tooth surfaces, including the mild damage created earlier, appear to have been polished.

Discussion

The tests conducted did not create scuff marks similar to those found on the shuttle PDU. Possible reasons for this are

- Geometrical differences between the flight gears that scuffed and the gears used for these tests may be sufficient to cause or prevent scuffing. Even small differences within gear blueprint tolerances provide a plausible explanation.
- The operating conditions during a backdrive event, when it is thought that scuffing occurs on the shuttle, may be more severe than estimated.
- The procedure of testing used may have gradually worn away the sharp edge at the gear teeth tips, which may be responsible for the scuffing, prior to testing at operating conditions that would produce scuffing if the tips were new.

- The oil used in the shuttle PDUs was several years old. Thus, the additives in this oil may have been used up. In contrast, these tests were conducted with new oil.
- The flight gear unit and the bench test arrangement have different dynamic responses that could give rise to very different dynamic gear tooth forces and motions.

To help assess the capability of a scuffed gear to operate safely, it may be helpful to note that 18.96 min of operation at pinion speed of 7000 rpm and pinion torque of approximately 212 in.-lb were accumulated on side-1, build-1 of the gears. Of this, 7.29 min were accumulated after the wear mark was generated in the Back-3c test. Further, 30.8 min of operation at input power of at least 23 hp, with a pinion speed 7000 rpm or greater were accumulated after the wear mark was generated in the test Back-3c on side-1, build-1. An additional 14.4 min of operation at input power of 37 hp or higher at pinion speed at least 7000 rpm, and pinion torque at least 237 in.-lb were obtained on side-1, build-2.

The maximum torque applied occurred in the Final-5 test and was 2212 in.-lb at 1660 rpm on the ring gear and 452 in.-lb and 8115 rpm on the pinion gear. This condition was obtained just prior to failure of the belts on the pulleys and was sustained for about 1 sec.

Options to consider for resolving the scuffing issue include, but are not limited to

- Analyze the shuttle PDU to determine the inertial loads and transient conditions expected during backdrive.
- Examine inspection reports and possibly re-inspect the pinion and ring gears to assess variations in tooth profile, particularly at the edge break at the tips of the teeth and their possible contributions towards scuffing.
- Change the test procedure to attain the most severe test conditions early on in the test matrix.
- Conduct transient scuffing tests.

Also, if a future shuttle flight includes a backdriving event that produces gear scuffing, the GRC bench-test rig could be used to assess the remaining life capability of gears that were scuffed in flight. Such an approach provides the most direct assessment method short of system-level testing. However, it does require removal of the PDU unit from service for replacement of the scuffed gears.

Conclusions

The scuffing tests performed did not produce scuff marks similar to that produced during shuttle flight. Wear marks were produced on the pinion teeth near the tips and on the ring gear teeth faces during the test Back-3c, which was conducted at an input speed, torque, and power of 2402 rpm, 664 in.-lb, and 25.3 hp. Very light wear marks were generated on side-2 of the pinion gear during the test Score-1 conducted at input speed, torque, and power of 2865 rpm, 1167 in.-lb, and 53 hp.

Failure to produce scuff damage like that found on the shuttle may be due to geometrical variations between the scuffed gears and the gears tested herein, more severe operating conditions during the flight that produced the scuff than estimated, the order of the test procedures, the use of new hydraulic oil, differences between the dynamic response of the flight gearbox and the bench-test gearbox, or a combination of these.

References

3.1. Wedeven, L.D., et al.: Space Shuttle Power Drive Unit Gear Scuffing Simulation and Analysis. NESC Contract No. NNL04AM36P, 2005.

3.2. Blok, H.: The Postulate About the Constancy of Scoring Temperature. Interdisciplinary Approach to the Condition of Concentrated Contacts, P.M. Ku, ed., NASA SP–237, 1969, pp. 153–248. http://ntrs.nasa.gov

3.3. Krantz, T.L.: GRC Gear Bench Testing of PDU Gear Scuffing—Final Report. NASA Technical Memorandum, to be published.

3.4. Oswald, Fred B.: Mechanical Components Branch Test Facilities and Capabilities. NASA/TM—2004-212722, 2004. http://ntrs.nasa.gov

3.5. Shigley, Joseph Edward, Mechanical Engineering Design. Third Ed., McGraw-Hill, New York, NY, 1977, p. 400.

TABLE 3.1.—IDENTIFICATION AND KEY DESIGN PARAMETERS OF TEST GEARS

Test gear	Part number	Serial number	Number of teeth	Diametral pitch	Pitch diameter, in.	Tooth width, in.	Pressure angle
Ring (no. 6)	5001513	D5K001	88	16	5.5	0.188	25°
Pinion (no. 5)	5001517	D5G009	18	16	1.125	0.265	25°

TABLE 3.2.—MEASURED BACKLASH OF RING AND PINION GEARS IN THE TEST GEARBOX

Position	Side-1, build-1 5/23/05 in.	Side-2, build-1 6/24/05 in.
1	0.010	0.008
2	.012	.010
3	.010	.010
4	.011	.009
Average	.011	.009

TABLE 3.3.—SUMMARY OF SHUTTLE GEAR SCUFFING TESTS CONDUCTED ON SIDE-1, BUILD-1

Test name	Date	Ring gear input			Pinion output		Oil bath temperature		Oil fling temperature		Time at condition	Total time of rotation	No. of cycles at condition		Visual assessment	
		Speed (rpm)	Torque (in.-lb)	Power (hp)	Speed (rpm)	Torque (in.-lb)	Initial (°F)	Final (°F)	Initial (°F)	Final (°F)	(sec)	(sec)	Ring gear	Pinion gear	Ring gear	Pinion gear
Checkout	06/01/2005	500.0	162.4	1.3	2444.4	33.2	69.3	69.5	68.6	68.9	78.0	98.0	650.0	3177.8	n/a	n/a
SpdSurvey	06/01/2005	498.0	98.8	0.8	2434.7	20.2	63.6	63.8	62.9	63.2	48.0		398.4	1947.7		
		714.0	91.5	1.0	3490.7	18.7	63.8	64.0	63.2	63.4	76.0		904.4	4421.5		
		1000.0	96.7	1.5	4888.9	19.8	64.1	64.4	63.5	63.8	48.0		800.0	3911.1		
		1250.0	95.3	1.9	6111.1	19.5	64.4	65.1	63.9	64.6	64.0		1333.3	6518.5		
		1429.0	92.9	2.1	6986.2	19.0	65.2	67.0	64.8	66.6	154.0		3667.8	17931		
		1248.5	82.7	1.6	6103.8	16.9	67.0	67.9	66.7	67.5	112.0		2330.5	11394		
		998.5	76.9	1.2	4881.6	15.7	68.0	68.6	67.6	68.1	104.0		1730.7	8461.4		
		714.0	98.1	1.1	3490.7	20.1	69.6	69.7	68.9	69.0	64.0		761.6	3723.4		
		495.0	101.0	0.8	2420.0	20.7	69.6	69.7	69.0	69.0	178.0	1256.0	1468.5	7179.3	okay	okay
Run-In-1	06/01/2005	799.0	98.1	1.2	3906.2	20.1	70.1	73.2	69.7	72.7	624.0	850.0	8309.6	40625	okay	okay
Run-In-2	06/02/2005	799.4	198.8	2.5	3908.2	40.7	77.7	81.5	77.2	80.9	657.5	780.0	8760.1	42827	okay	okay
Run-In-3	06/02/2005	798.9	298.9	3.8	3905.7	61.1	79.4	83.2	78.9	82.8	692.0	720.0	9214.0	45046	okay	okay
Run-In-4	06/02/2005	798.8	399.0	5.1	3905.2	81.6	82.8	86.3	82.3	85.8	638.0	702.0	8493.9	41526	okay	okay
Run-In-5	06/02/2005	801.7	497.0	6.3	3919.4	101.7	83.7	84.8	83.4	84.3	142.0	212.0	1897.4	9276		
Run-In-5a	06/02/2005	800.6	497.9	6.3	3914.0	101.8	84.8	88.5	84.4	88.0	698.0	728.0	9313.6	45533	okay	okay
Back-1b	06/02/2005	1000.1	498.0	7.9	4889.4	101.9	87.1	88.9	86.7	88.7	304.0	334.0	5067.2	24773	okay	okay
Back-1c	06/02/2005	1250.0	495.3	9.8	6111.1	101.3	87.7	91.0	87.3	90.8	333.0	371.0	6937.5	33917	okay	okay
Back-1d	06/02/2005	1431.0	500.1	11.4	6996.0	102.3	89.1	92.8	88.8	92.6	332.0	371.0	7918.2	38711	okay	okay
Back-2a	06/03/2005	1432.0	497.2	11.3	7000.9	101.7	80.2	84.9	79.8	84.5	353.0	386.0	8424.9	41189	okay	okay
Back-2b	06/03/2005	1432.0	699.0	15.9	7000.9	143.0	82.8	87.4	82.7	87.2	331.0	384.0	7899.9	38622	okay	okay
Back-2c	06/03/2005	1432.0	898.6	20.4	7000.9	183.8	86.3	91.9	n/a	n/a	317.0	344.0	7565.7	36988	okay	okay
Back-2d	06/03/2005	1431.7	1040.6	23.6	6999.4	212.9	90.4	95.4	90.3	95.4	328.0	365.0	7826.6	38264	okay	okay
Back-3a	06/03/2005	1430.5	1035.6	23.5	6993.6	211.8	89.2	95.4	89.0	95.4	372.0	457.0	8869.1	43360		
Back-3b	06/03/2005	1896.0	905.7	27.2	9269.3	185.3	99.9	107.0	100.1	107.1	370.0	632.0	11692.0	57161	okay	okay
Back-3c	06/03/2005	2401.7	664.5	25.3	11741.6	135.9	109.1	116.8	109.4	117.1	332.0	665.0	13289.4	64970	wear at mid-tooth	thumbnail wear mark at tip on all teeth
Back-3d	06/03/2005	2864.6	390.0	17.7	14004.7	79.8	114.5	125.0	114.8	125.4	416.0	740.0	19861.2	97099	Similar to Back-3c	Similar to Back-3c
Back-3xb	06/07/2005	1898.0	1032.8	31.1	9279.1	211.3	81.1	83.8	80.9	83.5	122.5	355.5	3875.1	18945	no change	no change
Back-3xc	06/07/2005	2393.8	900.0	34.2	11703.0	184.1	72.0	74.5	72.3	74.9	62.0	232.0	2473.6	12093	no change	no change
Back-3yc	06/07/2005	2400.6	920.0	35.0	11736.3	188.2	78.2	88.4	78.3	88.6	337.0	510.0	13483.4	65919	no change	no change[a]
Back-3za	06/08/2005	1433.7	1037.9	23.6	7009.2	212.3	167.9	169.5	168.0	169.4	343.0	443.0	8196.0	40069	no change	no change[b]
Back-3zb	06/08/2005	1900.4	1039.1	31.3	9290.8	212.5	161.9	164.4	161.8	164.5	320.0	431.0	10135.5	49551	no change	no change[c]

TABLE 3.3.—SUMMARY OF SHUTTLE GEAR SCUFFING TESTS CONDUCTED ON SIDE-1, BUILD-1 (Continued)

Test name	Date	Ring gear input			Pinion output		Oil bath temperature		Oil fling temperature		Time at condition	Total time of rotation	No. of cycles at condition		Visual assessment	
		Speed (rpm)	Torque (in.-lb)	Power (hp)	Speed (rpm)	Torque (in.-lb)	Initial (°F)	Final (°F)	Initial (°F)	Final (°F)	(sec)	(sec)	Ring gear	Pinion gear	Ring gear	Pinion gear
Back-3zc	06/08/2005	2397.7	965.2	36.7	11722.1	197.4	161.8	162.9	162.0	163.2	58.0	456.4	2317.8	11331	no change	no change[d]
Stab-test-1	06/17/2005	925.2	245.9	3.6	4523.2	50.3	74.1	75.4	73.5	74.8	143.5		2212.8	10818	n/a	n/a
	06/17/2005	2403.4	1038.9	39.6	11750.0	212.5	80.2	82.5	80.3	82.6	55.5		2223.1	10869	n/a	n/a
	06/17/2005	2857.1	1033.4	46.8	13968.0	211.4	85.4	88.5	85.8	88.8	72.0	516.8	3428.5	16762	n/a	n/a
Stab-test-2	06/17/2005	2633.8	261.9	10.9	12876.4	53.6	83.9	84.6	83.9	84.6	14.4		632.1	3090.3	n/a	n/a
	06/17/2005	2872.1	267.2	12.2	14041.4	54.7	85.0	86.5	85.0	86.6	33.0	77.5	1579.7	7722.8	n/a	n/a
Stab-test-3	06/17/2005	2676.3	573.2	24.3	13084.3	117.2	86.5	86.6	86.3	86.7	6.0	34.0	267.6	1308.4	n/a	n/a[e]
Stab-test-4	06/17/2005	2628.0	270.6	11.3	12847.8	55.4	86.2	87.0	86.2	87.0	18.5		810.3	3961.4	n/a	n/a
	06/17/2005	2856.6	278.1	12.6	13965.6	56.9	87.1	88.0	87.1	88.1	23.0		1095.0	5353.5	n/a	n/a
	06/17/2005	2875.0	473.5	21.6	14055.7	96.9	88.3	88.9	88.5	89.0	11.0	93.5	527.1	2576.9	n/a	n/a
Stab-test-5	06/17/2005	2861.4	698.7	31.7	13989.3	142.9	90.2	90.8	90.5	91.1	11.5		548.4	2681.3	n/a	n/a
	06/17/2005	2833.1	933.1	41.9	13850.6	190.9	95.3	95.8	95.7	96.2	12.0	307.5	566.6	2770.1	n/a	n/a
Stab-test-6	06/17/2005	2382.2	1041.3	39.4	11646.4	213.0	96.7	100.2	96.9	100.5	109.0	238.0	4327.7	21158	n/a	n/a
Stab-test-7	06/17/2005	2417.5	960.2	36.8	11819.0	196.4	101.4	101.8	101.5	101.8	11.0	181.5	443.2	2166.8	okay	okay
Stability-1	06/20/2005	2864.4	1041.4	47.3	14003.9	213.0	87.8	89.5	88.0	89.8	17.8	233.7	849.8	4154.5	n/a	n/a
Stability-2*	06/20/2005			0.0	0.0	0.0						~20	0.0	0	n/a	n/a[f]
Stability-2	06/20/2005	2855.9	965.3	43.7	13961.9	197.5	96.3	97.4	96.5	97.7	29.6	297.0	1408.9	6887.9	okay	okay
Stability-3	06/20/2005	1430.5	1039.0	23.6	6993.6	212.5	91.2	92.1	90.9	91.8	39.7	132.4	946.5	4627.4	n/a	n/a
Stability-4	06/20/2005	1432.5	1048.1	23.8	7003.3	214.4	91.9	92.8	91.4	92.1	30.8	92.9	735.4	3595	n/a	n/a
Stability-5	06/20/2005	1439.6	1040.9	23.8	7038.1	212.9	92.1	92.5	91.8	92.1	15.4	74.9	369.5	1806.5	n/a	n/a
Stability-6	06/20/2005	1436.2	1045.8	23.8	7021.2	213.9	92.7	92.8	92.3	92.5	8.8	79.7	210.6	1029.8	okay	okay
Stability-7	06/22/2005	2864.6	1146.4	52.1	14004.5	234.5	88.0	90.2	88.3	80.4	44.3	391.4	2115.0	10340	n/a	n/a
Stability-8	06/22/2005	2547.3	1140.7	46.1	12453.5	233.3	90.2	95.6	90.4	95.9	129.2	257.8	5485.2	26817	n/a	n/a[g]
Stability-9	06/22/2005	2409.8	1141.2	43.6	11781.3	233.4	95.8	96.5	96.0	96.7	15.0	122.4	602.5	2945.3	okay	okay[h]

[a]"±85 on input torque"

[b]shaft rotating when file ends

[c]shaft rotating when file ends

[d]See time history

[e]not very stable. Max input torque 1073 in.-lb at 2736 rpm

[f]File deleted

[g]Not very stable.

[h]Max torq 3387 in.-lb at 181.3 rpm

TABLE 3.4.—SUMMARY OF SHUTTLE GEAR SCUFFING TESTS CONDUCTED ON SIDE-2, BUILD-1

Test name	Date	Ring gear input			Pinion output		Oil bath temperature		Oil fling temperature		Time at condition	Total time of rotation	No. of cycles at condition		Visual assessment	
		Speed	Torque	Power	Speed	Torque	Initial	Final	Initial	Final			Ring gear	Pinion gear	Ring gear	Pinion
		(rpm)	(in.-lb)	(hp)	(rpm)	(in.-lb)	(°F)	(°F)	(°F)	(°F)	(sec)	(sec)				
Score-1	6/24/2005	2866.5	1143.9	52.0	14014.0	234.0	162.5	162.8	162.9	163.1	6.0	175.5	286.7	1401.4		small scuff
Score-2	6/24/2005	2865.2	1167.0	53.1	14007.5	238.7	162.4	164.8	162.9	165.2	37.5	189.0	1790.7	8754.7	Damaged due to disengagement	Damaged due to disengagement

TABLE 3.5.—SUMMARY OF SHUTTLE GEAR SCUFFING TESTS CONDUCTED ON SIDE-1, BUILD-2

Test name	Date	Ring gear input			Pinion output		Oil bath temperature		Oil fling temperature		Time at condition	Total time of rotation	No. of cycles at condition		Visual assessment	
		Speed	Torque	Power	Speed	Torque	Initial	Final	Initial	Final			Ring gear	Pinion gear	Ring gear	Pinion
		(rpm)	(in.-lb)	(hp)	(rpm)	(in.-lb)	(°F)	(°F)	(°F)	(°F)	(sec)	(sec)				
Final-1	8/9/2005	2048.1	1162.1	37.8	10012.8	237.7	80.1	88.9	78.0	87.0	314.0	462.0	10718.2	52400.1	No scuff	No scuff
Final-2	8/9/2005	1981.7	1502.6	47.2	9688.4	307.4	86.1	95.1	84.4	93.4	295.5	442.5	9760.0	47715.6	No scuff	No scuff
Final-3	8/9/2005	1497.6	1796.1	42.7	7321.5	367.4	93.5	98.3	91.7	96.5	256.5	514.0	6402.2	31299.4	No scuff	No scuff
Final-4	8/9/2005	1316.3	2001.1	41.8	6435.2	409.3	96.0	101.4	94.1	99.6	298.5	504.5	6548.6	32015.2	No scuff	No scuff
Final-5	8/9/2005	1055.2	2212.2	37.0	5158.7	452.5	90.7	93.6	88.4	91.9	164.5	270.5	2893.0	14143.5	No scuff	No scuff[a]

[a]Speed is average while being ramped up. Std dev =326 rpm for input speed.

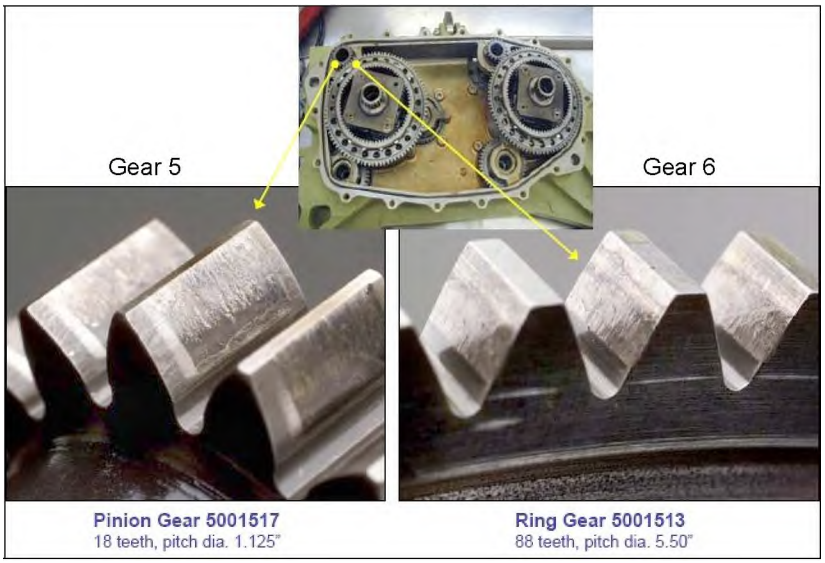

Figure 3.1.—Damaged gear teeth from shuttle power drive unit 2.

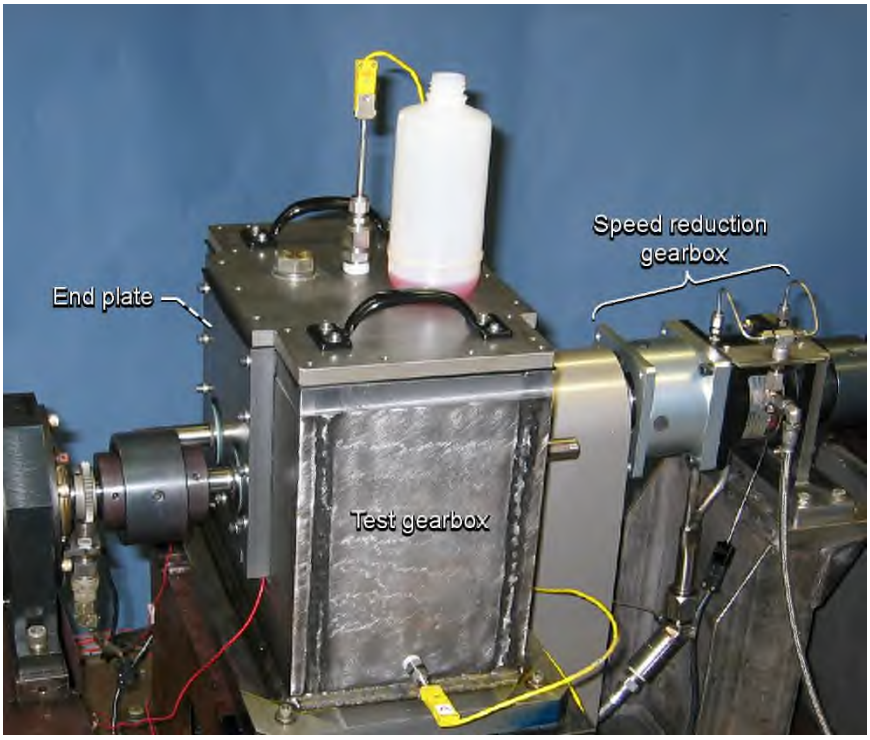

Figure 3.2.—Test gearbox.

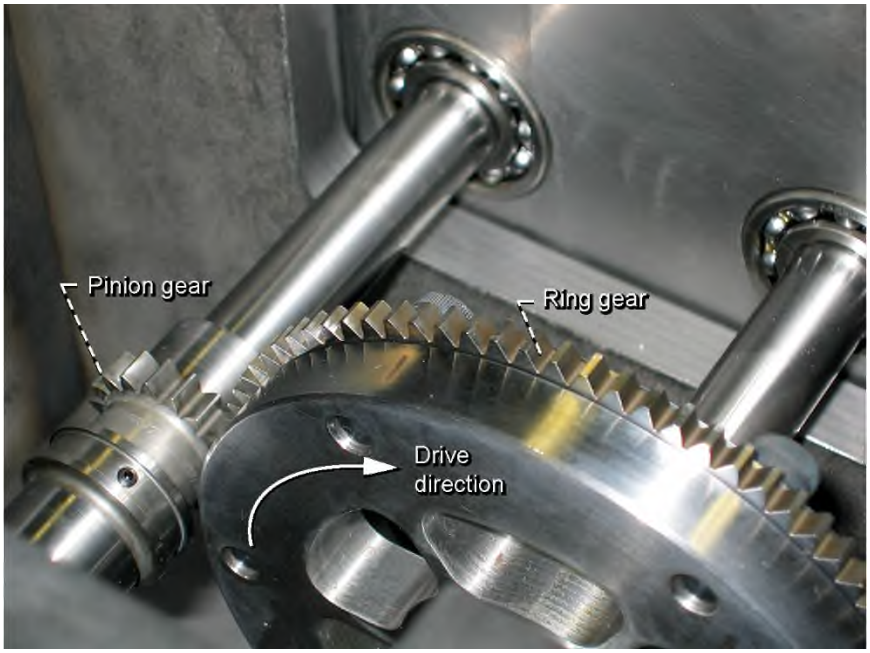

Figure 3.3—Pre-test photo of ring and pinion gears installed in the test gearbox for side-1, build-1.

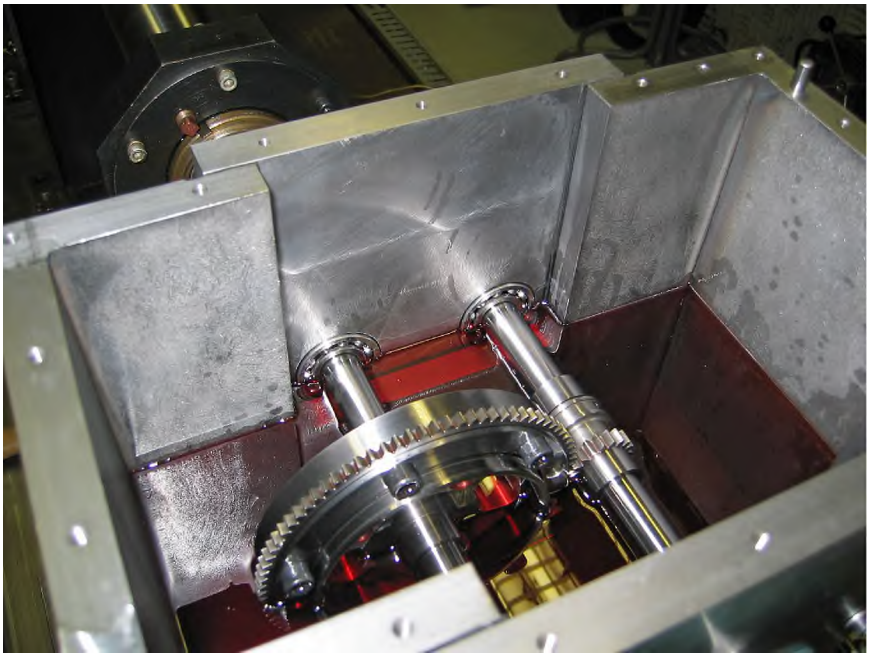
Figure 3.4.—Test gearbox as assembled for side-1, build-1 is filled to centerline with Brayco Micronic 882 hydraulic fluid.

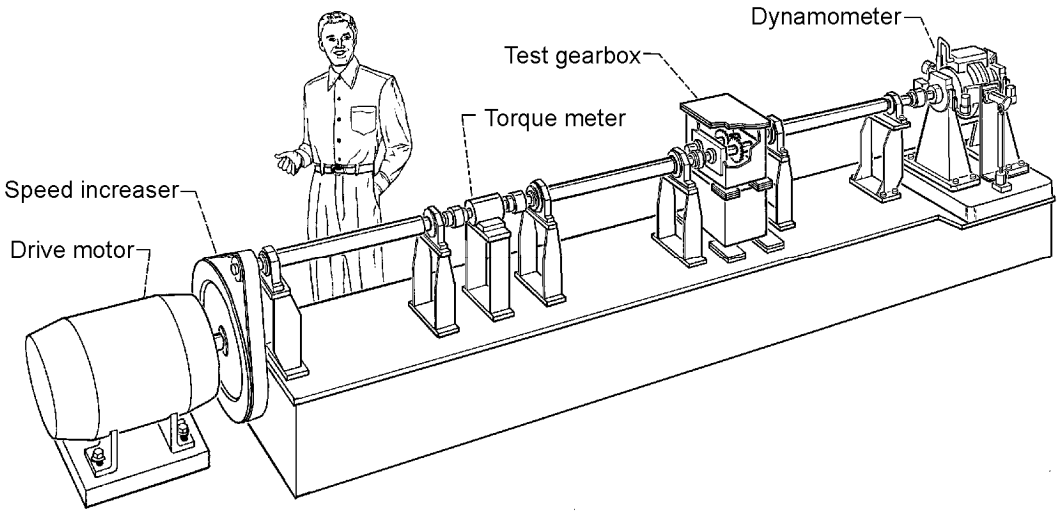

Figure 3.5.—Gear noise test facility as configured before modifications for gear scuffing experiments.

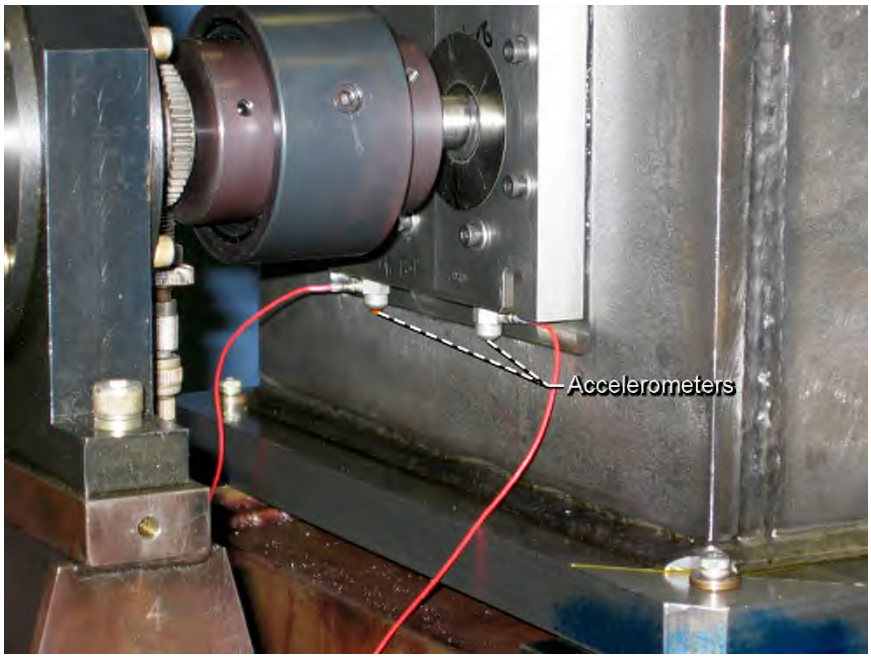

Figure 3.6.—Accelerometers mounted to input endplate underneath the input and output shafts.

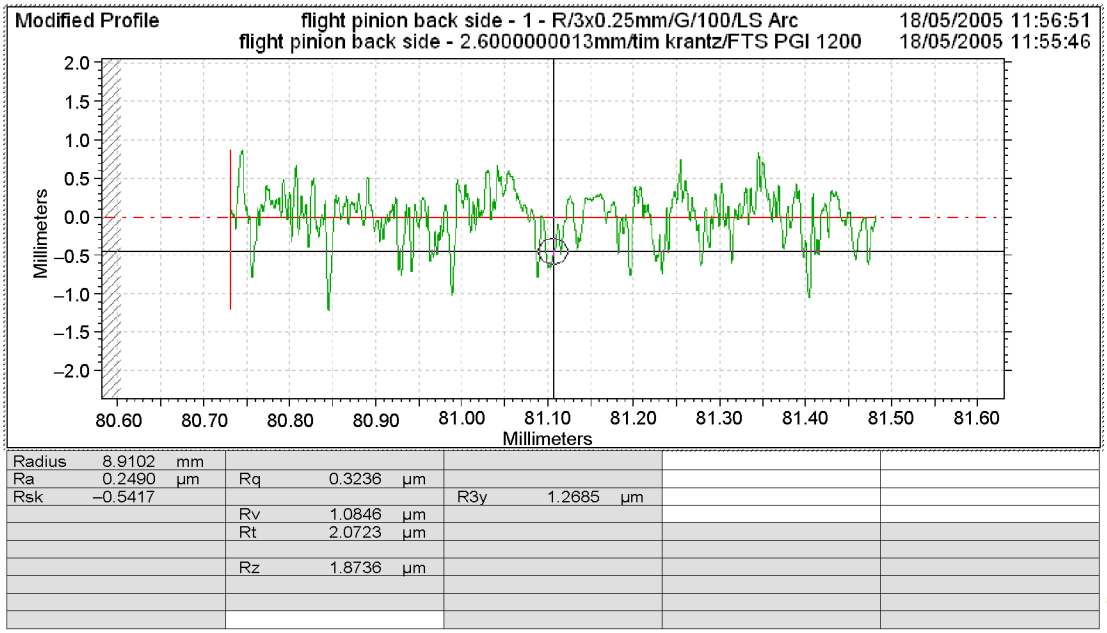

Figure 3.7.—Typical microtopography of the pinion gear teeth.

Figure 3.8.—Pre-test rubber mold of the pinion and ring gear teeth and the hard epoxy replication of the pinion teeth.

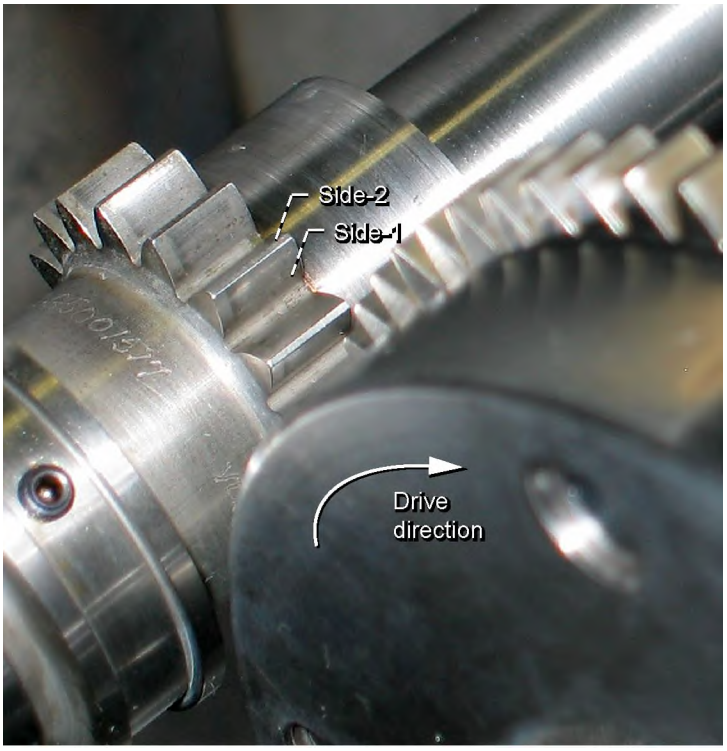

Figure 3.9.—Pre-test photo of pinion teeth.

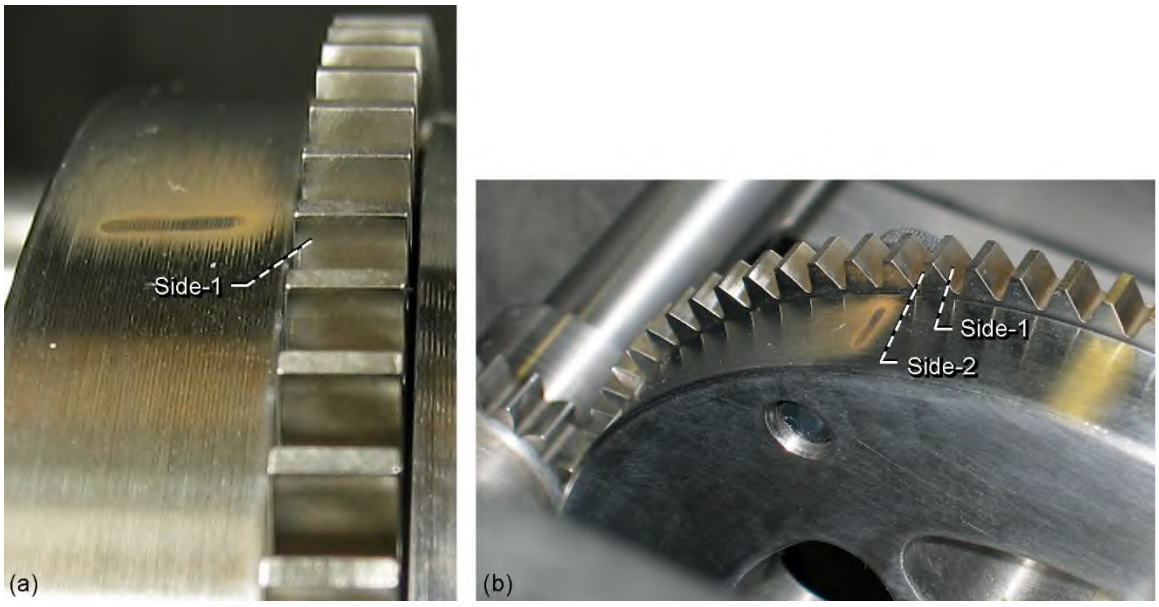

Figure 3.10.—(a) Pre-test photo of ring gear teeth showing side-1. (b) Pre-test photo showing another view of ring gear teeth, side-1 and side-2.

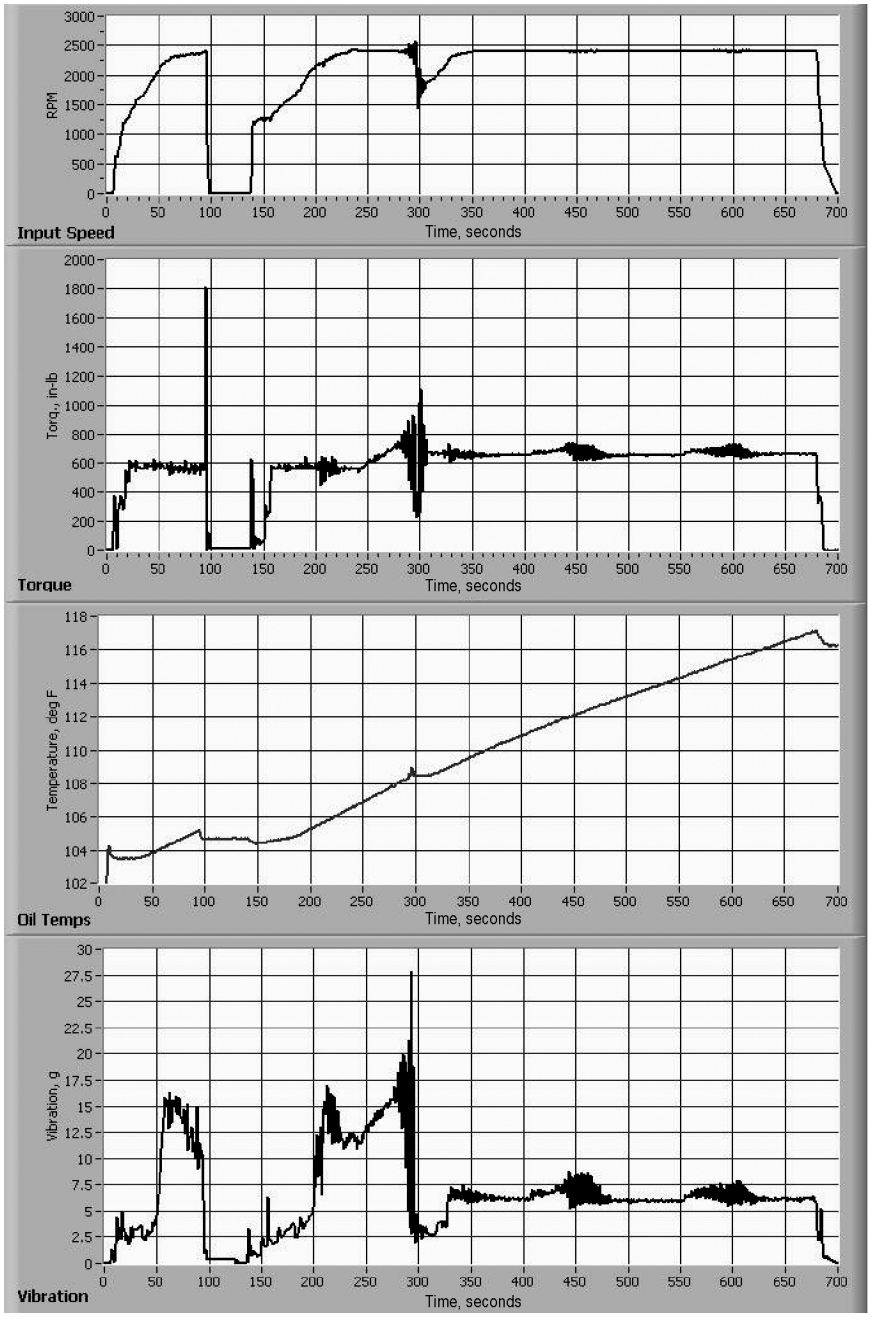

Figure 3.11.—Time history of test Back-3c with side-1, build-1 showing input ring gear speed and torque, oil fling temperature and vibration data from the accelerometer near the pinion shaft.

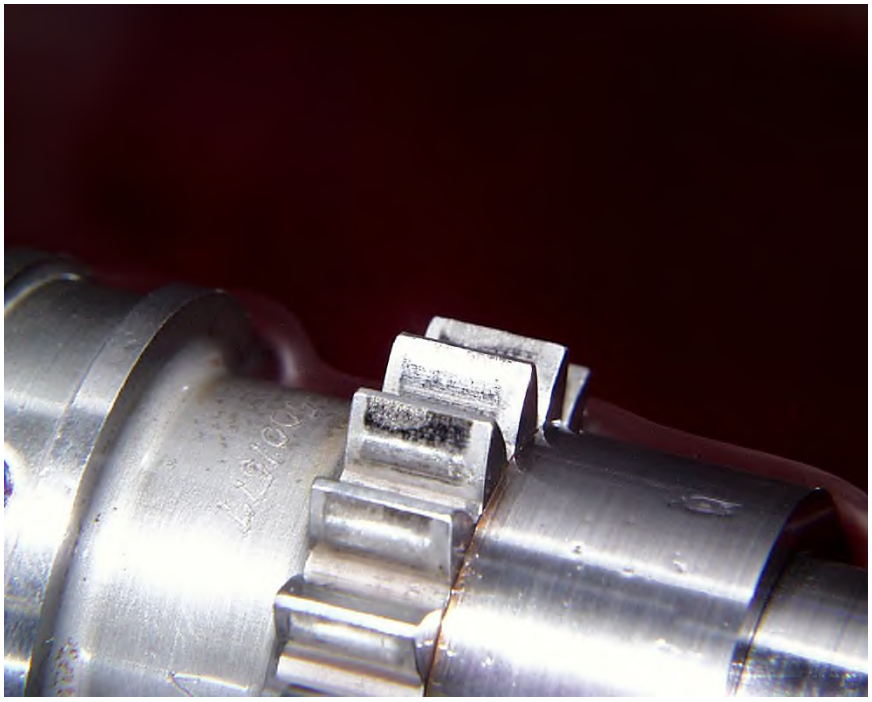

Figure 3.12.—Wear marks on driven side of pinion gear teeth after Back-3c.

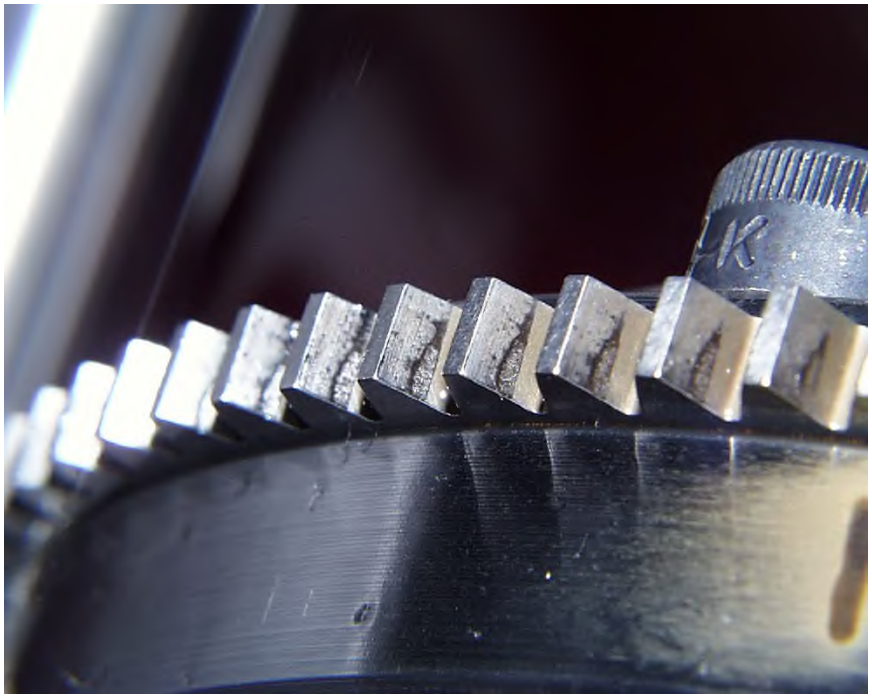

Figure 3.13.—Wear marks on driving side of ring gear teeth after Back-3c.

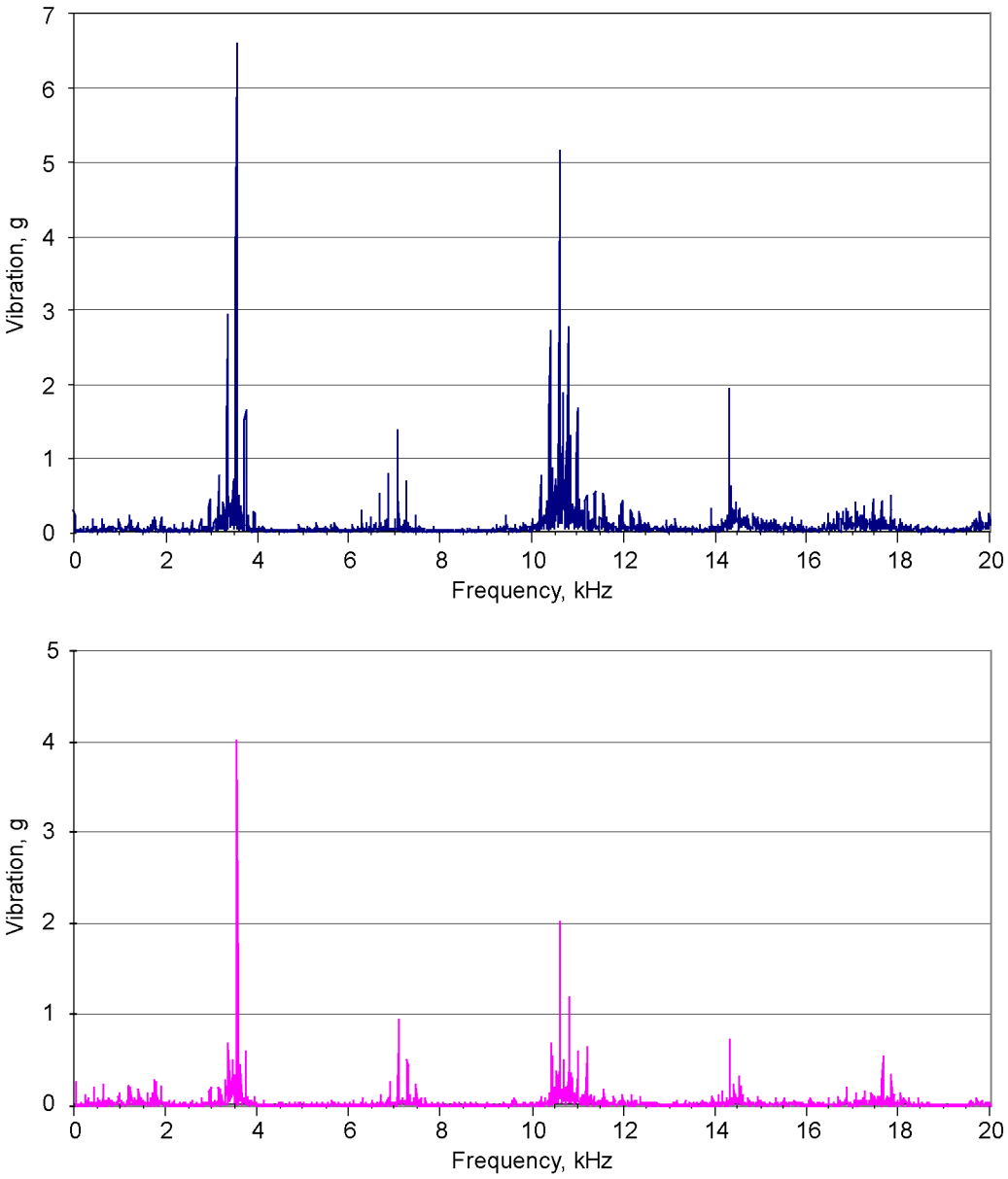

Figure 3.14.—Frequency spectra from test Back-3c at 250 sec (top) and 550 sec (bottom). The first harmonic of gear mesh frequency occurs at 3523 Hz (2402 rpm × 88 teeth/60 sec/min).

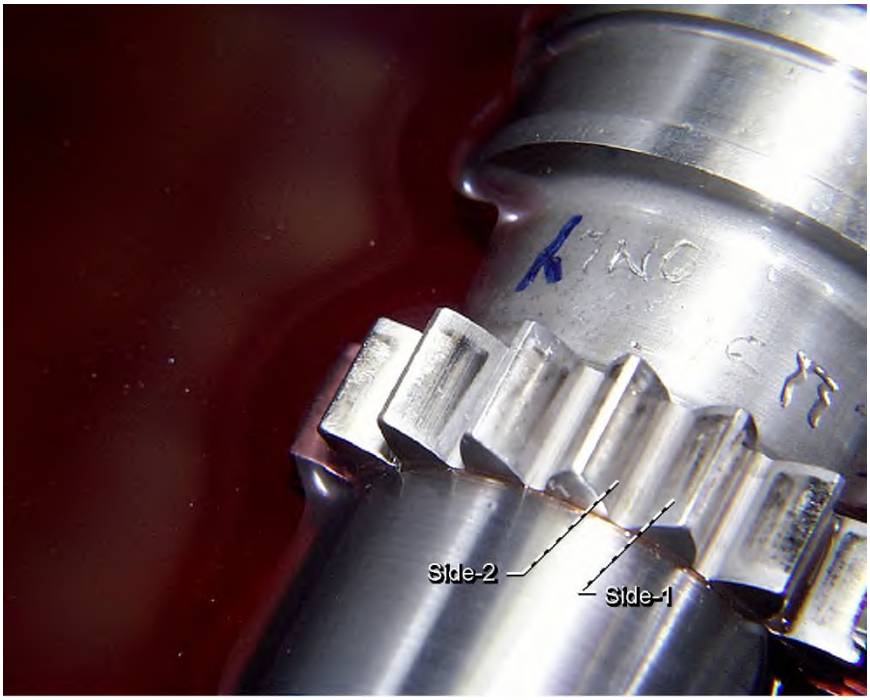

Figure 3.15.—Wear marks on driven side of pinion gear teeth after Score-1 test on side-2, build-1.

Figure 3.16.—No visible damage on driving side of ring gear teeth after Score-1 test on side-2, build-1.

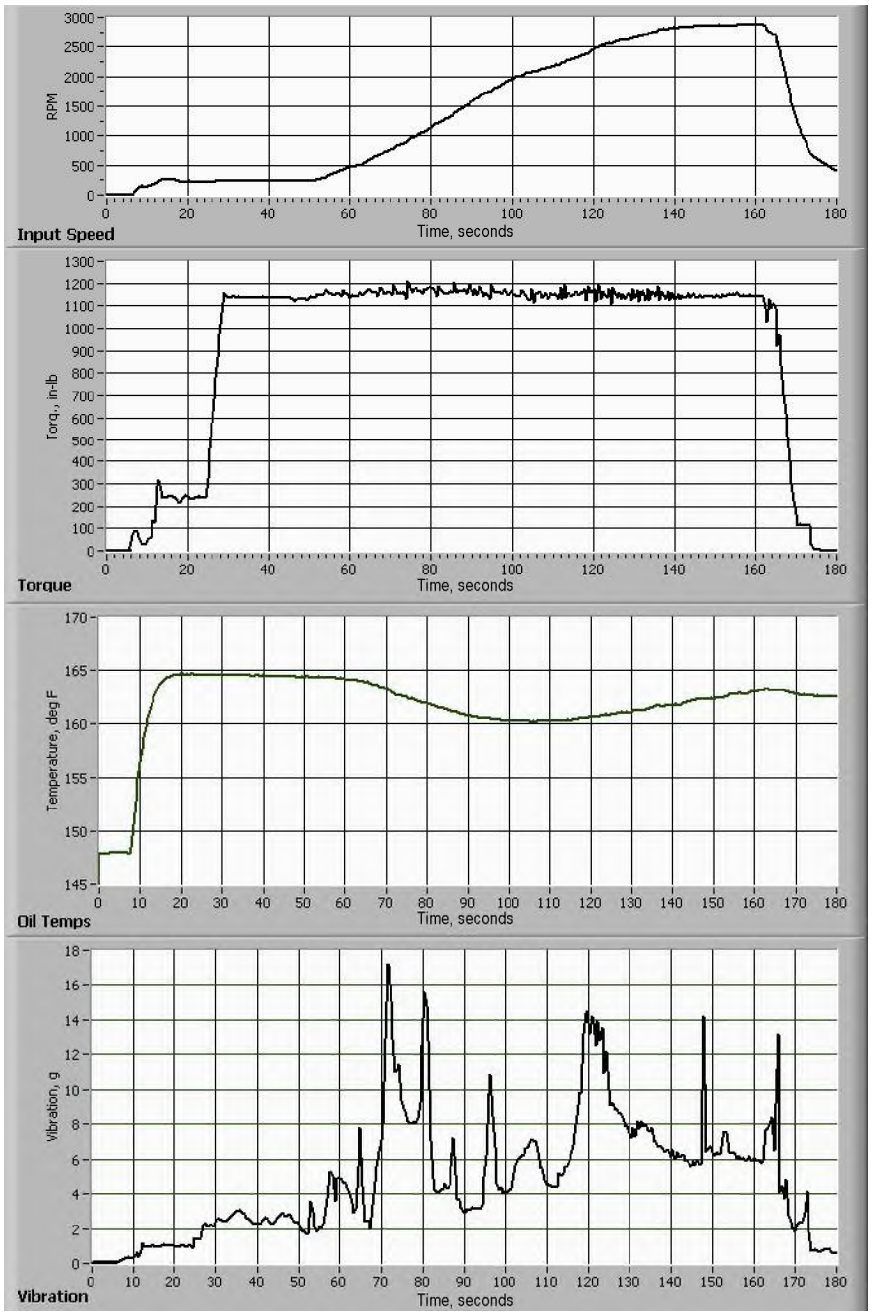

Figure 3.17.—Time histories of input ring gear speed and torque, oil fling temperature and pinion rms vibration level for Score-1 test on side-2, build-1.

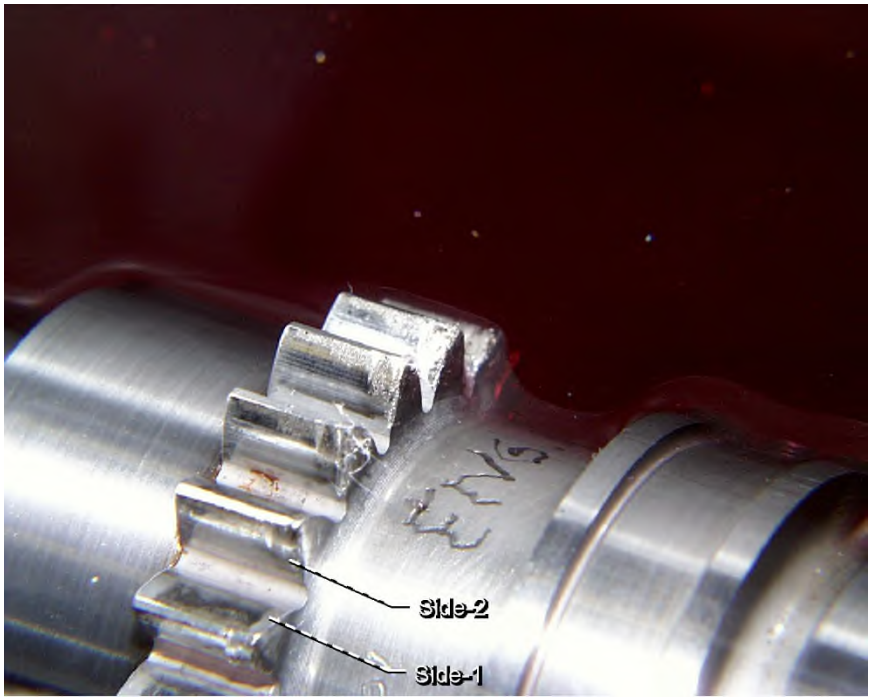

Figure 3.18.—Damaged teeth of pinion gear after disengagement at 14,000 rpm pinion speed during the Score-2 test on side-2, build-1. White cloth fibers are caught on teeth from wiping oil.

Figure 3.19.—Damaged teeth of ring gear after disengagement at 14,000 rpm pinion speed during the score-2 test on side-2, build-1. White cloth fibers are caught on teeth from wiping oil.

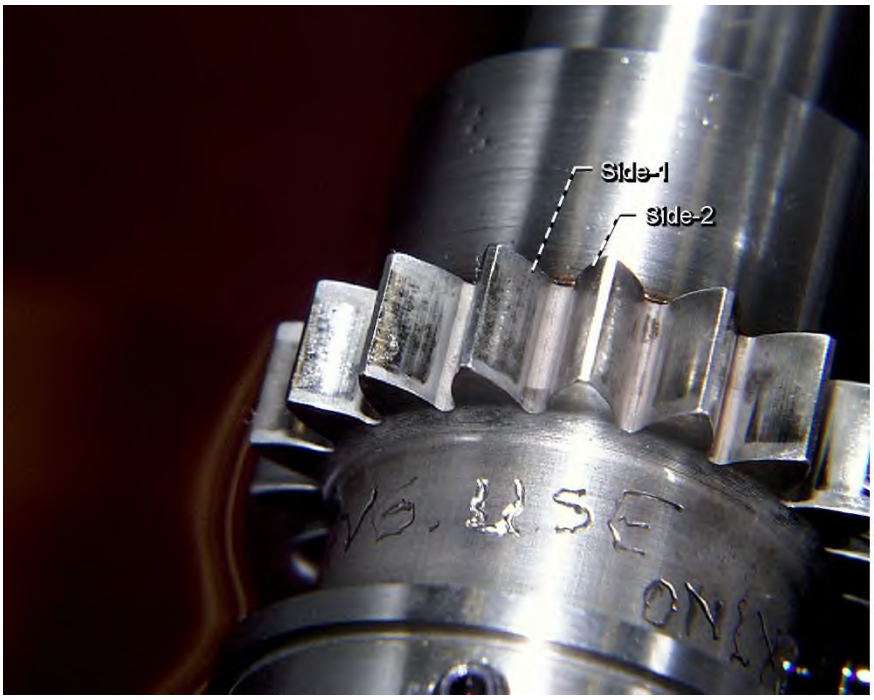

Figure 3.20.—Driven side of pinion gear teeth after the test Final-5 are still in good condition.

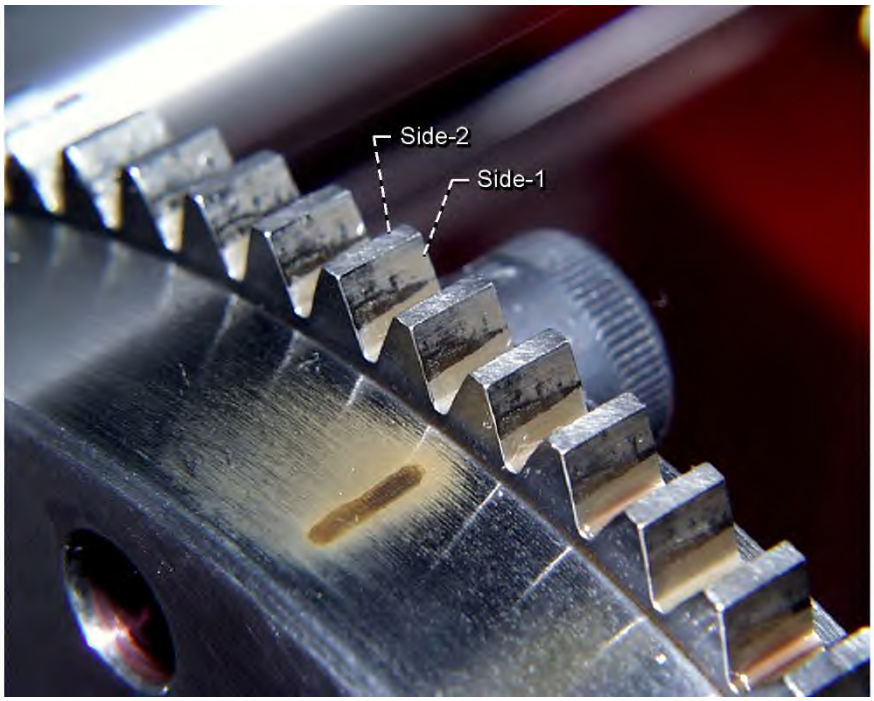

Figure 3.21.—Driving side of ring gear teeth after the Final-5 are still in good condition.

Chapter 4: Wear of Spur Gears Having a Dithering Motion and Lubricated With a Perfluorinated Polyether Grease

Timothy Krantz
U.S. Army Research Laboratory
Glenn Research Center
Cleveland, Ohio 44135

Fred Oswald
National Aeronautics and Space Administration
Glenn Research Center
Cleveland, Ohio 44135

Robert Handschuh
U.S. Army Research Laboratory
Glenn Research Center
Cleveland, Ohio 44135

Abstract

Gear contact surface wear is one of the important failure modes for gear systems. Dedicated experiments are required to enable precise evaluations of gear wear for a particular application. The application of interest for this study required evaluation of wear of gears lubricated with a grade 2 perfluorinated polyether grease and having a dithering (rotation reversal) motion. Experiments were conducted using spur gears made from AISI 9310 steel. Wear was measured using a profilometer at test intervals encompassing 10,000 to 80,000 cycles of dithering motion. The test load level was 1.1 GPa maximum Hertz contact stress at the pitch line. The trend of total wear as a function of test cycles was linear, and the wear depth rate was approximately 1.2 nm maximum wear depth per gear dithering cycle. The observed wear rate was about 600 times greater than the wear rate for the same gears operated at high speed and lubricated with oil.

Introduction

Gear contact surface wear is one of the important failure modes in gear systems. Wear and the associated material loss can lead to structural failure (gear tooth fracture). Wear can also lead to changes in vibration and noise behavior (Ref. 4.1 to 4.3). In addition, wear can change the patterns of gear contact such that the altered load distributions and contact stresses will accelerate the occurrence of other failure modes such as pitting and scoring (Ref. 4.4). Gear wear debris can also be detrimental to the performance of bearings or other components of a drive system (Ref. 4.5).

The study of wear is becoming one of the emerging areas of gear research. A number of recent wear modeling efforts (Refs. 4.6 to 4.10) form a solid foundation for studying gear wear. The common thread to these studies is that all use the well-known Archard's wear model (Ref. 4.11) in conjunction with a gear contact model and relative sliding calculations. Archard's wear equation can be expressed for a local point on one of the contacting gear surfaces as $dh/ds = kP$ where k is an experimentally determined wear coefficient, h is the wear depth accumulated, P is the contact pressure, and s is the sliding distance between the mating surfaces at the point of interest. From this equation, to calculate the wear depth h, the contact pressure P and the sliding distance s must be determined. Flodin and Andersson (Refs. 4.6 to 4.8) and Bajpai et al. (Ref. 4.9) proposed wear models for spur and helical gears, and the focus was to determine P and s. The tooth contact pressures P were computed in these models using either simplified Hertzian contact (Refs. 4.6 to 4.8) or boundary element (Ref. 4.9) formulations under quasi-static

conditions. Sliding distance *s* calculations were determined from gearing kinematics, and Archard's wear model (Ref. 4.11) was used with an empirical wear coefficient to compute the surface wear distribution.

Perhaps the most significant shortcoming of the gear wear prediction models discussed above is that they consider wear depth to be a function of only two parameters, contact pressure *P* and sliding distance *s*. All other influences, such as surface material, surface roughness, and lubrication at the contact interface, are all accounted for by the wear coefficient *k* (Ref. 4.12). When all of the parameters including lubricant type, temperature, flow rate, gear material composition, surface topography, and surface hardness are consistent, then it is possible to define K using a small number of controlled experiments (Ref. 4.9). However, if all of the stated properties are not consistent, then determining a wear rate coefficient is a challenging task. In addition, the influence of such parameters on wear cannot be described by these models. As such, dedicated experiments are often required to enable accurate predictions of gear wear for a particular application.

Perfluorinated polyether greases are commonly used for space mechanisms. Discussions in support of mechanism maintenance (Ref. 4.13) have highlighted the need for data to better understand the wear and behavior of mechanical components operated using such grease. Some qualitative results of gear wear experiments were previously reported (Ref. 4.14). To quantify wear rates for gears lubricated with perfluorinated polyether grade 2 grease, spur gear experiments were completed.

Test Methodology

Test Rig

The experiments were conducted using the NASA Glenn Research Center Spur Gear Fatigue Test Rigs. These test rigs have been used for more than 30 years to test oil-lubricated spur gears, with emphasis on studying contact fatigue (spalling, pitting, and micropitting). The test rig, as shown in Figure 4.1(a), uses the four-square (torque-regenerative) principle of applying test loads, and thus the motor needs to overcome only the frictional losses in the system. The test rig is belt driven using a variable speed electric motor. A schematic of the loading apparatus is shown in Figure 4.1(b). Hydraulic oil pressure and leakage replacement flow is supplied to the load vanes through a shaft seal. As the oil pressure is increased on the load vanes located inside one of the slave gears, torque is applied to its shaft. This torque is transmitted through the test gears and back to the slave gears. In this way power is circulated, and the desired load and corresponding stress level on the test gear teeth may be obtained by adjusting the hydraulic pressure.

Figure 4.1 depicts the spur gear rig as it has been used for tests operated at 10,000 rpm for the purpose of evaluating the fatigue lives of oil-lubricated gears. The test setup as used for the grease tests reported herein differed from the depiction of Figure 4.1 in two important ways. Figure 4.1 illustrates the test gears operating with faces offset. The face-offset condition is used to concentrate the Hertz contact stress as is desired for accelerated life testing of high cycle fatigue. For the grease-lubricated gear testing, the gears were operated with zero offset (full faces in contact with each other). Also, Figure 4.1 depicts pressurized labyrinth seals on the two shafts. For the grease testing reported herein, lip seals were used on the two shafts to prevent leakage of the slave gear lubricating oil to the grease-lubricated test gear section. The lip seals have been used with much success on these rigs to maintain zero-leakage even for speeds of 10,000 rpm.

For some applications, gear teeth will operate both as a driving and as a driven member depending on the motions and torques applied to the machine at any given instant. Hall et al. (Ref. 4.13) provide an example of an actuator that operated in a dithering mode whereby a gear rotated with a back and forth motion with a nominally constant torque (Fig. 4.2). For such operation, the gears can create wear debris on an approach path and then entrain the debris into the gear contact on the return path. For the subject experiments, the gear test rig was operated in such a dithering mode. To create the dithering motion, a four-bar linkage mechanism was attached to the drive shaft of the test rig (Fig. 4.3). The four-bar linkage was designed to allow for adjustments to the range of motion. For the tests reported herein a full rotation

of the electric motor rotated the gears through ±28° of rotation. This range of motion ensured that one tooth pair would operate for a full gear tooth engagement cycle for each forward and return stroke of the mechanism. The frequency of motion was 4 Hz (4 dithering cycles per second).

Test Gears and Lubricant

The test gears used for this work were manufactured from a single lot of consumable-electrode vacuum-melted (CVM) AISI 9310 steel. The nominal chemical composition of the AISI 9310 material is given in Table 4.1. The gears were case carburized and heat treated according to Table 4.2. The nominal properties of the carburized gears were a case hardness of Rockwell C60, a case depth of 0.97 mm (0.038 in.), and a core hardness of Rockwell C38. The dimensions for the test gears are given in Table 4.3. The gear pitch diameter was 89 mm (3.5 in.), and the tooth form was a 20° involute profile modified to provide a tip relief of 0.013 mm (0.0005 in.) starting at the highest point of single-tooth contact. The gears have zero lead crowning but do have a nominal 0.13-mm- (0.005-in.-) radius edge break at the tips and sides of the teeth. The gear tooth surface finish after final grinding was specified as a maximum of 0.406 μm (16 μin.) rms. Tolerances for the gear geometries were specified to meet AGMA (American Gear Manufacturers Association) quality-level class 11. Gears were lubricated using a single container of grade 2 perfluorinated polyether grease. The grease is qualified for use on space mechanisms.

Test Procedure

The test gears were cleaned to remove a rust-preventative preservative, assembled on the test rig, and grease was applied. The gears were tested with the tooth faces fully engaged (the faces were not offset as depicted in Fig. 4.1). Tests were run at a frequency of 4 full dither cycles per second. All tests were conducted with a hydraulic pressure of 1.72 MPa (250 psi) applied to the loading device. The torque produced for such a hydraulic pressure was verified both before and after testing to be 68 N-m (51 ft-lb). The applied torque resulted in a contact condition of 1.1 GPa (160 ksi) maximum Hertz contact stress at the pitch line. The Hertz stress just stated is an idealized stress index assuming static equilibrium, gears meshing at the pitch-point position, perfectly smooth surfaces, and an even load distribution across the measured active face width.

The active face width was measured using a profilometer tracing in the lead direction. The profile trace was used to determine the effect of the edge break radius on the active face width. Three pairs of gear teeth were tested. For each tooth pair, the testing was stopped three times to make tooth profile measurements. The test matrix of running times (dithering cycles) is listed in Table 4.4. Prior to measuring the tooth profiles, grease and wear debris were removed from the teeth using soft-tipped tools. Chemicals were not used to assist the removal of the grease and wear debris to avoid contamination of the tooth surface that was to undergo additional testing.

Measurement of Wear

Wear was determined by measuring the gear tooth profiles prior to testing, then again measuring the tooth profiles after testing, and comparing the data. The teeth were measured using a stylus profilometer with a small-bore diamond-tipped stylus having a 2 μm 90° tip. Three traces were obtained for each gear for each test condition, the three traces at nominally equal spacing across the face width. The profilometery data were not filtered (other than the mechanical filtering inherent to the stylus-type measurement technique). The profiles measured were of 7.2 mm length, tracing from below the true involute form radius in the root area of the gear to beyond the tip and across the topland of the tooth. The concept of the wear measurement procedure involved overlaying traces of the new gear and worn gear, with any differences attributed to wear. To assist with the overlaying procedure, the gears were mounted on the measuring machine using a fixture employing a gear rack (Fig. 4.4). The fixture was used to fix the orientation of the gear relative to the measuring machine coordinate axes. With such a fixture, profiles

could be overlaid after translation of one trace relative to the other. Rotations of coordinate systems were not necessary. A typical set of raw data plots for a gear tooth, before and after testing, is provided in Figure 4.5(a).

To determine wear from profilometer traces, it was necessary to first overlay the two traces and then subtract one from the other. The overlaying of traces was done using a semi-automated procedure. The first step was to visually translate the data for profile of the "worn" tooth until the plots of the two profiles were closely matched in the root and topland parts of the profiles (that is, those locations with no contact and no wear). After this initial manual operation of overlaying was completed, a computer algorithm was then used to optimize the translation of the trace. The optimization was done to minimize the sum of the squares of the distances between the nearest-neighbor data points on the two traces in the regions of the root and topland that were not in contact. A typical data plot for two traces after optimizing the translation of the worn trace is provided in Figure 4.5(b). Subtracting the "new" profile data from the "worn" profile data point by point yielded the wear of the tooth as a function of position along the tooth (Fig. 4.5(c)).

Wear amounts were characterized and summarized as follows. For each wear profile the maximum depth of wear and the area under the wear curve (by numerical integration) were determined. The wear area can be considered as a measure of the volume of material removed per unit face width of the gear tooth. The wear depth and wear area data were fit to regression models. To complete the regression and accompanying statistical analysis, the data were first transformed as $X = (\text{number of dithering cycles})^{1/2}$ and $Y = (\text{wear})^{1/2}$. Such a transformation was found to provide a regression model having X proportional to Y and having residuals with normal distributions and equal variance for all tested values of X. Two-sided point-by-point 95 percent tolerance intervals at 95 percent statistical confidence were determined using the method of Hahn and Meeker (Ref. 4.15).

Test Results

To quantify wear rates for gears lubricated with perfluorinated polyether grade 2 grease a set of spur gear experiments were completed. The wear amounts were characterized by (a) the maximum depth of wear and (b) the total volume of material removed per unit face width (termed wear area). Wear profiles for all test conditions are provided in Reference 4.13. The gear teeth developed unique wear patterns. That is, there were significant differences in wear profile amount and shapes from one tooth to another. It is speculated that the wear patterns are determined by the detailed geometry and conditions of the mating teeth including all of form, waviness, roughness features, and hardness.

A photograph showing the typical condition of a worn tooth is provided in Figure 4.6. The visual appearance of the tested surface differed from tip to root, likely depending on the amounts of relative sliding. In areas of high relative sliding (toward the tip), the surface is relatively smooth. For areas of low to moderate sliding, the surface appears to have some plastic flow (rippling) and evidence of abrasive wear. Note that some wear products remained on the surface after the mild mechanical cleaning that was done prior to measurements. The visual appearance of the teeth surfaces were similar for all tests ranging from 20,000 to 80,000 total dithering cycles.

The wear profiles were characterized by the maximum wear depth and by the wear areas, and the data were fit to a regression model. The wear depth data and regression results are provided in Figure 4.7 and the wear area data and regression results are provided in Figure 4.8. The wear rate was approximately 1.2 nm maximum wear depth per gear dithering cycle. The rate of wear area removal was approximately 5×10^{-6} mm^2 per gear dithering cycle. Both the wear depth data and wear area data show a linear trend of wear accumulation for the full range of test cycles that were investigated. The data also shows a significant range of results for a given number of cycles. To characterize the data, two-sided point-by-point 95 percent tolerance intervals at 95 percent statistical confidence were calculated. The statistical intervals quantify the range of data one could expect for a large population of tests conducted in identical fashion. By plotting the sorted residuals of the regression models, it was verified that the assumption of a normal distribution of the residuals in the transformed domain was a reasonable assumption. The tolerance intervals are provided on the data plots of Figures 4.7 and 4.8.

Discussion

The experiments and test results characterized the wear of 8-pitch spur gears having a dithering type motion, a 1.1 GPa (160 ksi) maximum Hertz contact stress at the pitch line, and lubricated with a perfluorinated polyether grade 2 grease. For such test conditions the gears operate in the boundary lubrication regime, and this produced high wear rates relative to the wear rates of high-speed, oil-lubricated gearing. Comparing the rate of wear depth accumulation of the present experiments to the experiments of Krantz and Kahraman (Ref. 4.10) that made use of gears having the same material and geometry, the wear rate for the grease-lubricated gears of this study was on the order of 600 times greater than for oil-lubricated gears operating in the mixed elastohydrodynamic lubrication regime. If such wear rates for the grease-lubricated gears would not meet the application requirements, then it would be necessary to investigate component redesign, surface engineering, an improved lubricant, and/or improved anti-wear additives to provide the desired performance.

A significant finding was to discover that the trend of total wear was a linear function of test cycles. For the application of this data to validate inspection and reuse criteria, it would be reasonable to project continued linear trends of field data so long as the maximum wear depths and relative percentage of case depth loss were bounded by the data of the present investigation.

Summary

Discussions in support of space mechanism maintenance have highlighted the need for data to better understand the wear and behavior of mechanical components operated using perfluorinated polyether grease. To quantify wear rates for gears lubricated with such grease, a set of spur gear experiments were completed. The following results were obtained.

(1) The visual appearance of the tested surface differed from tip to root, likely depending on the amounts of relative sliding and surface geometry details.
(2) The visual appearance of the teeth surfaces were similar for all tests ranging from 20,000 to 80,000 total dithering cycles.
(3) The wear rate was approximately 1.2 nm maximum wear depth per gear dithering cycle.
(4) The wear rate for the grease-lubricated gears of this study was on the order of 600 times greater than referenced data for oil-lubricated gears operating in the mixed elastohydrodynamic lubrication regime.
(5) Both the wear depth data and wear area data show a linear trend of wear accumulation for the full range of test cycles that were investigated.
(6) The data showed a significant range of wear results for a given number of cycles. Statistical intervals were calculated to quantify the range of data one could expect for a large population of tests conducted in identical fashion.

References

4.1. Choy, F.K., et al.: Analysis of the Effects of Surface Pitting and Wear on the Vibration of a Gear Transmission System. Tribol. Int., vol. 29, 1996, pp. 77–83.

4.2. Mackaldener, M.; Flodin, A.; and Andersson, S.: Robust Noise Characteristics of Gears Due to Their Application, Manufacturing Errors and Wear (Gear Dynamics and Noise). JSME International Conference on Motion and Power Transmission, Fukuoka, Japan, 2001, pp. 21–26.

4.3. Kuang, J.H.; and Lin, A.D.: The Effect of Tooth Wear on the Vibration Spectrum of a Spur Gear Pair. J. Vib. Acoust., vol. 123, 2001, pp. 311–317.

4.4. Chen, Yong; and Matubara, Masami: Effect of Automatic Transmission Fluid on Pitting Fatigue Strength of Carburized Gears. JSME International Conference on Motion and Power Transmission, Fukuoka, Japan, 2001, pp. 151–156.

4.5. Shifeng, Wu; and Cheng, H.S.: Sliding Wear Calculation in Spur Gears. J. Tribol., vol. 115, 1993, pp. 493–503.
4.6. Flodin, Anders; and Andersson, S.: Simulation of Mild Wear in Spur Gears. Wear, vol. 207, 1997, pp. 16–23.
4.7. Flodin, Anders; and Andersson, Soren: Simulation of Mild Wear in Helical Gears. Wear, vol. 241, 2000, pp. 123–128.
4.8. Flodin, Anders; and Andersson, Soren: A Simplified Model for Wear Prediction in Helical Gears. Wear, vol. 249, 2001, pp. 285–292.
4.9. Bajpai, P.; Kahraman, A.; and Anderson, N.E.: A Surface Wear Prediction Methodology for Parallel-Axis Gear Pairs. J. Tribol., vol. 126, 2004, pp. 597–605.
4.10. Krantz, T.L.; and Kahraman, A.: An Experimental Investigation of the Influence of the Lubricant Viscosity and Additives on Gear Wear. Tribol. T., vol. 47, 2004, pp. 138–148.
4.11. Archard, J.F.: Contact of Rubbing Flat Surfaces. J. Appl. Phys., vol. 24, no. 8, 1953, pp. 981–988.
4.12. Challen, J.M.; Oxley, P.L.B.; and Hockenhull, B.S.: Prediction of Archard's Wear Coefficient for Sliding Metallic Sliding Friction Assuming Low Cycle Fatigue Wear Mechanism. Wear, vol. 111, 1986, pp. 275–288.
4.13. Munafo, Paul, et al.: Orbiter Rudder/Speed Brake (R/SB) Gear Margins Technical Assessment Report. NASA/TM—2009-215727, 2005. http://ntrs.nasa.gov
4.14. Krantz, T.; and Handschuh, R.: A Study of Spur Gears Lubricated With Grease—Observations from Seven Experiments. Proceedings of the 58th Meeting of the Society for Machinery Failure Prevention Technology, Virginia Beach, VA, 2004.
4.15. Hahn, Gerald J.; and Meeker, William Q.: Statistical Intervals: A Guide for Practitioners. John Wiley & Sons, Inc., New York, NY, 1991.

TABLE 4.1.—NOMINAL CHEMICAL COMPOSITION
OF AISI 9310 GEAR MATERIAL

Element	wt%
Carbon	0.10
Nickel	3.22
Chromium	1.21
Molybdenum	0.12
Copper	0.13
Manganese	0.63
Silicon	0.27
Sulfur	0.005
Phosphorous	0.005
Iron	balance

TABLE 4.2.—HEAT TREATMENT FOR AISI 9310 GEARS

Step	Process	Temperature		Time, hr
		K	ºF	
1	Preheat in air	—	—	—
2	Carburize	1,172	1,650	8
3	Air cool to room temperature	—	—	—
4	Copper plate all over	—	—	—
5	Reheat	922	1,200	2.5
6	Air cool to room temperature	—	—	—
7	Austentize	1,117	1,550	2.5
8	Oil quench	—	—	—
9	Subzero cool	180	-120	3.5
10	Double temper	450	350	2 each
11	Finish grind	—	—	—
12	Stress relieve	450	350	2

TABLE 4.3.—SPUR GEAR DATA
[Gear tolerance per AGMS class 11]

Number of teeth	28
Module, mm	3.175
Diametral pitch	8
Circular pitch, mm (in.)	9.975 (0.3927)
Whole depth, mm (in.)	7.62 (0.300)
Addendum, mm (in.)	3.18 (.125)
Chordal tooth thickness reference, mm (in.)	4.85 (0.191)
Tooth width, mm (in.)	6.35 (0.25)
Pressure angle, deg.	20
Pitch diameter, mm (in.)	88.90 (3.500)
Outside diameter, mm (in.)	95.25 (3.750)
Root fillet, mm (in.)	1.02 to 1.52 (0.04 to 0.06)
Measurement over pins, mm (in.)	96.03 to 96.30 (3.7807 to 3.7915)
Pin diameter, mm (in.)	5.49 (0.216)
Backlash reference, mm (in.)	0.254 (0.010)
Tip relief, mm (in.)	0.010 to 0.015 (0.0004 to 0.0006)

TABLE 4.4.—TEST MATRIX FOR SPUR GEAR WEAR TESTING SHOWING CYCLE COUNT WHERE TESTING WAS STOPPED FOR WEAR MEASUREMENTS

Tooth Pair	Accumulated Number of Dithering Cycles
B	5,000
B	10,000
C	10,000
A	20,000
C	20,000
A	40,000
B	40,000
A	80,000
C	80,000

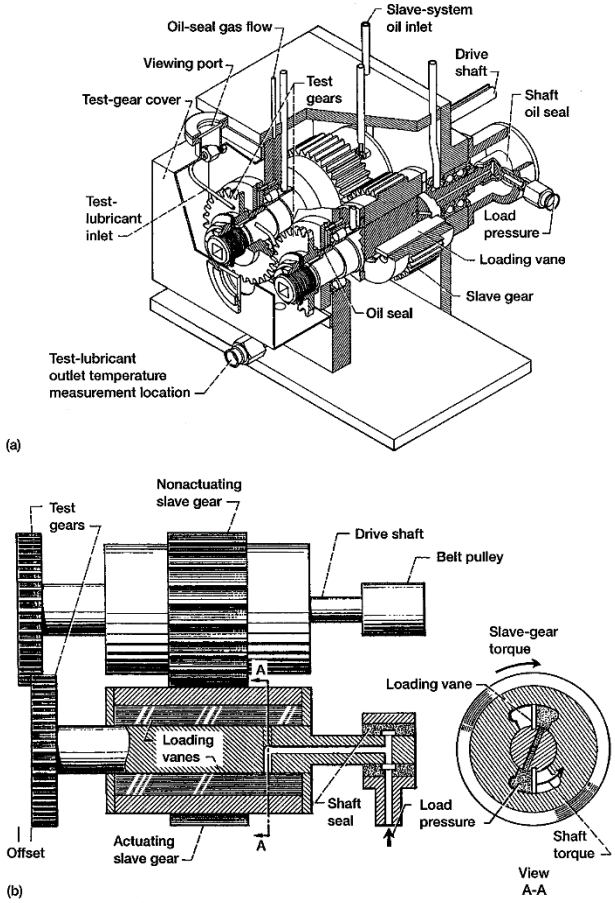

Figure 4.1.—NASA Glenn Research Center gear fatigue test apparatus. (a) Cutaway view. (b) Schematic view.

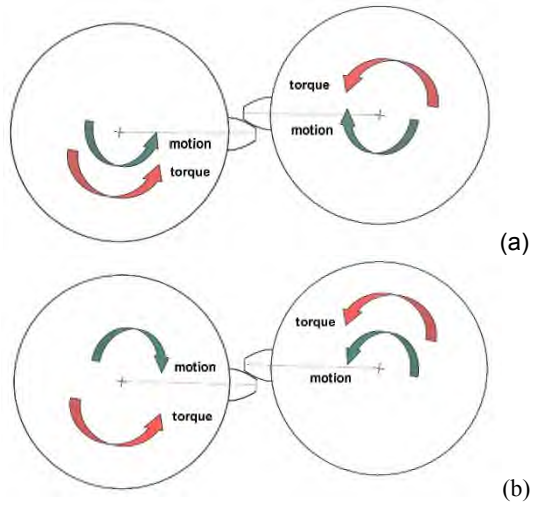

Figure 4.2.—Illustration of the reversal of motion and constant direction of torque used for wear testing. (a) Forward stroke of dithering motion. (b) Reverse stroke of dithering motion.

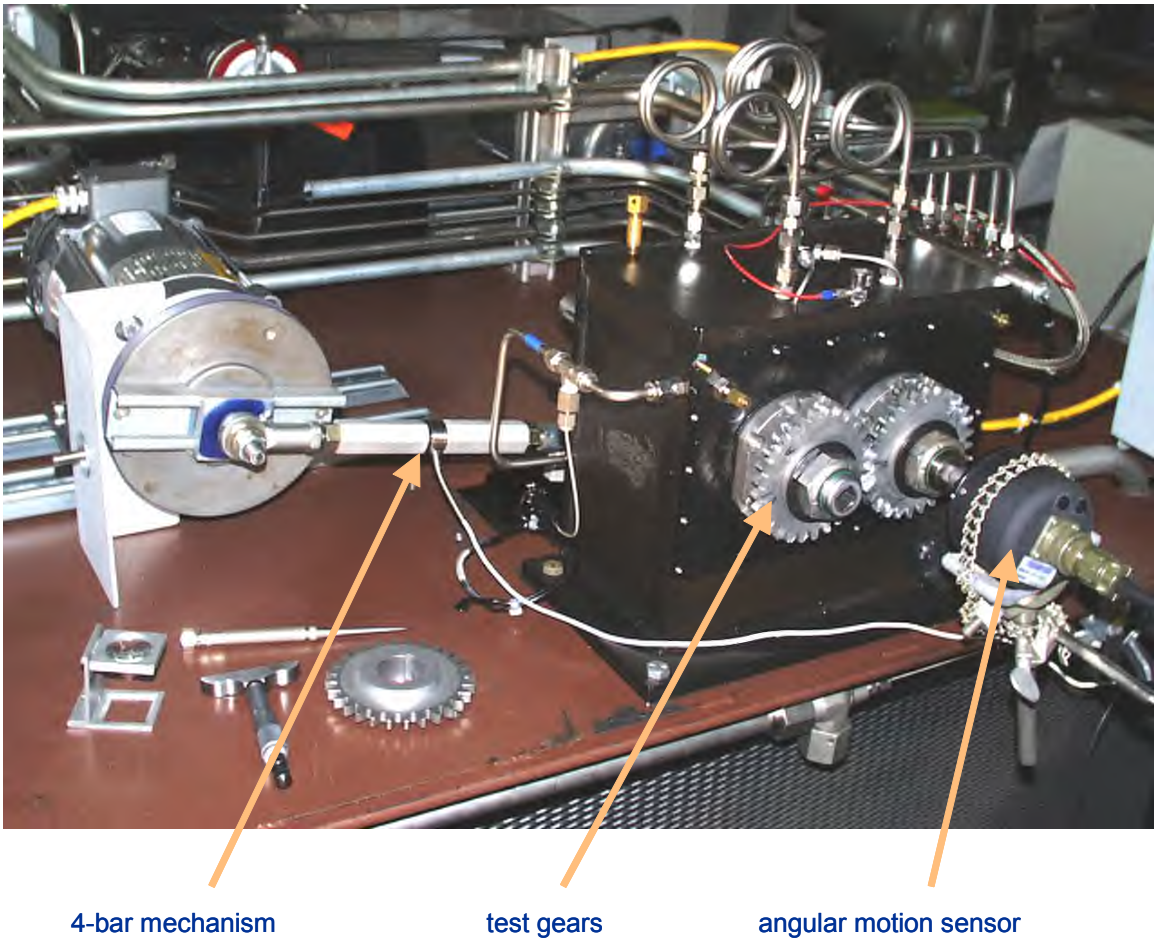

Figure 4.3.—Spur gear test rig configured for grease-lubricated testing using a dithering motion.

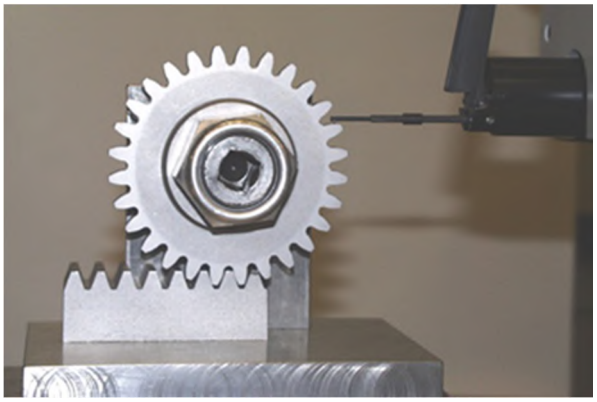

Figure 4.4.—Gear mounted on a profilometer using a gear rack to locate and orient the tooth.

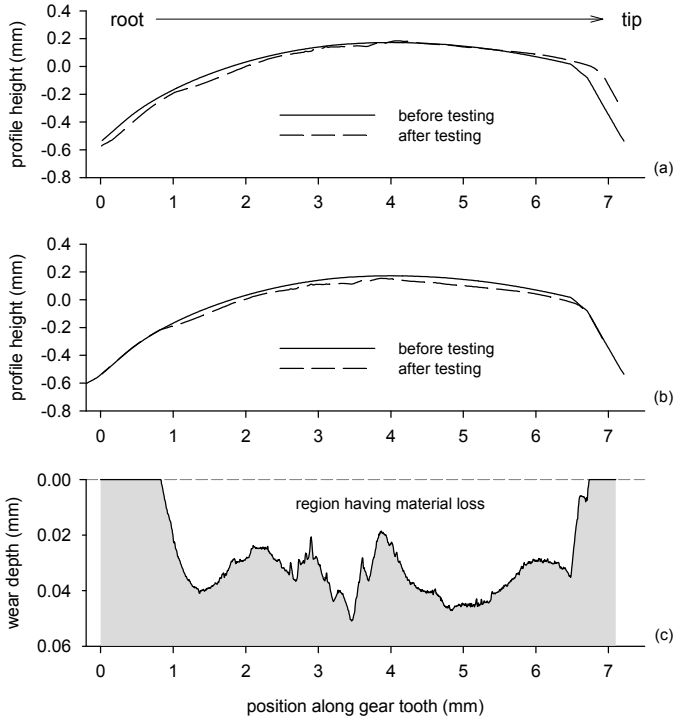

Figure 4.5.—Method for determining wear from profilometer data. (a) Raw traces of the profilometer data. (b) Profilometer data after X and Y translations of the second trace to match up profiles in the tooth root and topland regions. (c) Wear depths as obtained by the difference of the two traces of plot (b).

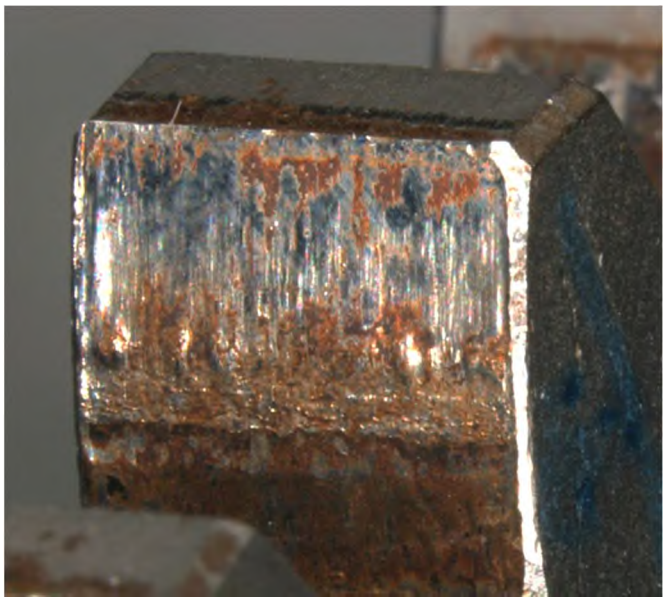

Figure 4.6.—Typical condition of the worn gear teeth.

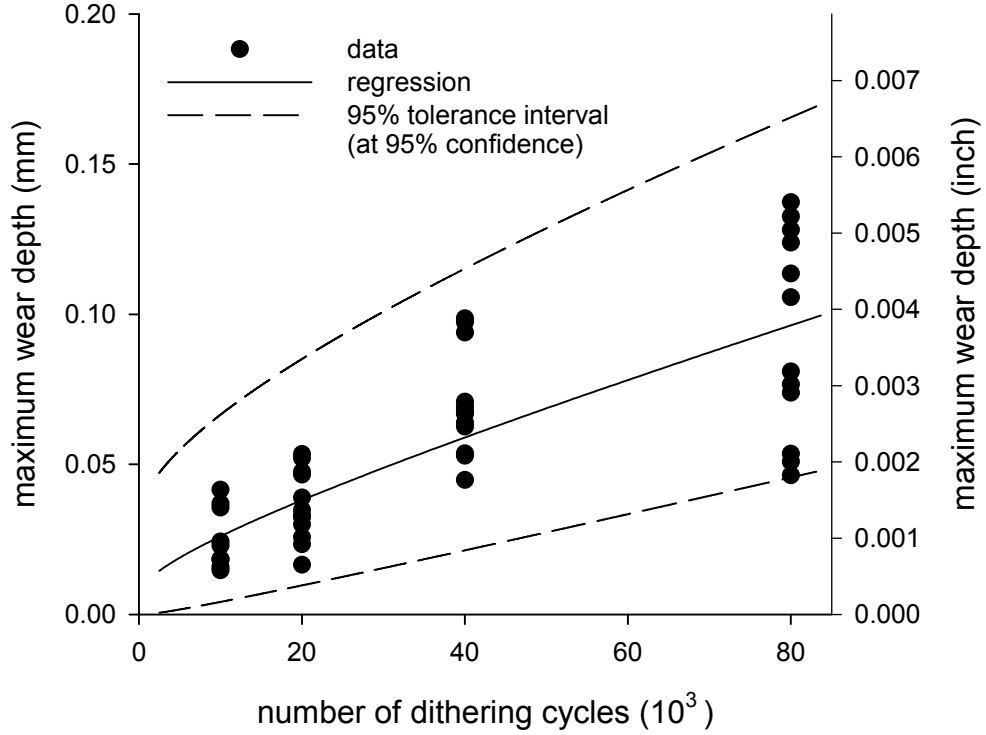

Figure 4.7.—Summary of maximum wear depths as a function of number of dithering cycles showing data points, regression model, and tolerance intervals.

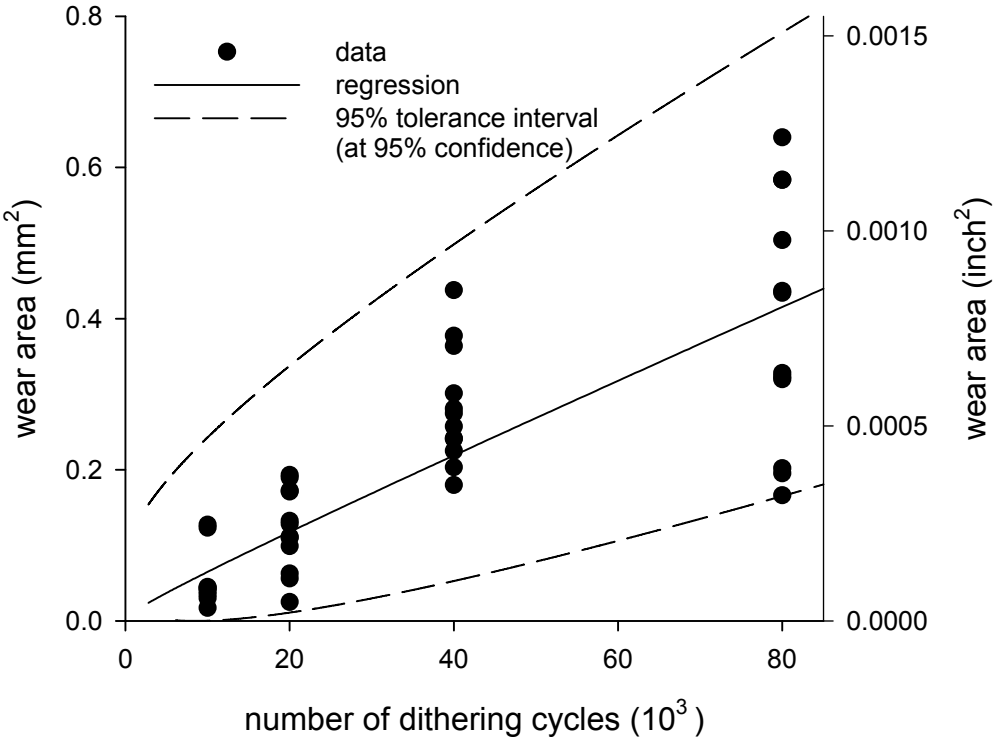

Figure 4.8.—Summary of wear area (or wear volume per unit face width) as a function of number of dithering cycles showing data points, regression model, and tolerance intervals.

Chapter 5: Probabilistic Analysis of Space Shuttle Body Flap Actuator Ball Bearings

Fred B. Oswald
National Aeronautics and Space Administration
Glenn Research Center
Cleveland, Ohio 44135

Timothy R. Jett
National Aeronautics and Space Administration
Marshall Space Flight Center
Marshall Space Flight Center, Alabama 35812

Roamer E. Predmore
Swales Aerospace
Greenbelt, Maryland 20771

Erwin V. Zaretsky
National Aeronautics and Space Administration
Glenn Research Center
Cleveland, Ohio 44135

Abstract

A probabilistic analysis, using the two-parameter Weibull-Johnson method, was performed on experimental life test data from space shuttle actuator bearings. Experiments were performed on a test rig under simulated conditions to determine the life and failure mechanism of the grease-lubricated bearings that support the input shaft of the space shuttle body flap actuators. The failure mechanism was wear that can cause loss of bearing preload. These tests established life and reliability data for both shuttle flight and ground operation. Test data were used to estimate the failure rate and reliability as a function of the number of shuttle missions flown. The Weibull analysis of the test data for the four actuators on one shuttle, each with a two-bearing shaft assembly, established a reliability level of 96.9 percent for a life of 12 missions. A probabilistic system analysis for four shuttles, each of which has four actuators, predicts a single bearing failure in one actuator of one shuttle after 22 missions (a total of 88 missions for a four-shuttle fleet). This prediction is comparable with actual shuttle flight history in which a single actuator bearing was found to have failed by wear at 20 missions.

Nomenclature

e	Weibull slope
F	probability of failure, fraction or percent
h	lubricant film thickness, m (in.)
i	failure number
L	life, hr, revolutions, missions, etc.
L_{mis}	mission life based on mission spectrum, missions
L_n	life at operating condition n, hr, revolutions, missions, etc.
L_{sys_n}	system life based on operation condition n, missions
L_β	characteristic life or life at which 63.2 percent of population fails, hr, revolutions, missions, etc.
L_{10}	10-percent life or life at which 90 percent of a population survives, hr, revolutions, missions, etc.

L_1 1-percent life or life at which 99 percent of a population survives, hr, revolutions, missions, etc.
$L_{0.1}$ 0.1-percent life or life at which 99.9 percent of a population survives, hr, revolutions, missions, etc.
n number of components (samples)
S probability of survival (reliability), fraction or percent
S_{sys} probability of survival or reliability of a system of components, fraction or percent
X_n time fraction spent at operating condition n, fraction or percent

Introduction

Spacecraft have many components whose surfaces either oscillate or rotate slowly. Typical applications involve rolling-element bearings that support scanning mirrors, extendable booms, and the mechanical actuators for control surfaces on some reentering spacecraft. Oscillatory motion is motion in which the shaft turns in one angular direction and then returns in the same arc on either a periodic or intermittent basis. For boom oscillation, the angular velocities are generally low (<6°/s) and equal in both directions. For scanning mirrors the rotation in one direction is usually extremely slow (2°/s) followed by a rapid return (>60°/s) (Ref. 5.1). The body flap actuators (BFAs) used in the space shuttle operate at input speeds to 80 rpm against rapid deflections caused by transient aerodynamic loads during reentry.

The lubrication of spacecraft bearings is as varied as their space applications. The purpose of lubrication is to separate the surfaces in relative motion by a material that has a low resistance to shear so that the surfaces do not sustain significant damage. This low resistance material may comprise a variety of materials (e.g., adsorbed gases, liquids, films, chemical reaction products, or solid lubricants) (Ref. 5.1).

Depending on the type of intervening film and its thickness, a number of lubrication regimes can be identified (Ref. 5.1). These regimes are called hydrodynamic, elastohydrodynamic, mixed, and boundary. The regimes can be defined by the approximate thickness (h) of the separating film.

In the hydrodynamic lubrication regime, the surfaces are completely separated by the film, $h>10^{-7}$ m (10^{-5} in.). The hydrodynamic regime blends into the elastohydrodynamic lubrication regime, where loads cause elastic deformation of the surfaces of the mechanism and affect the viscosity of the fluid film, $10^{-8}\leq h\leq 10^{-6}$ m ($10^{-6}\leq h\leq 10^{-4}$ in.).

As the film becomes progressively thinner, surface interactions start taking place. This regime of increasing friction, which combines asperity interactions and fluid film effects, is the mixed lubrication regime, $10^{-9}\leq h\leq 10^{-8}$ m ($10^{-7}\leq h\leq 10^{-6}$ in.). The transition between full film and mixed lubrication depends not only on film thickness but also on the roughness of the bearing surfaces. The following surface finishes (arithmetic averages) are typically specified for gas turbine engine bearings (Ref. 5.2):

Balls, μm, (μin.)	<0.025 (<1)
Ball races, μm, (μin.)	<0.125 (<5)
Rollers, μm, (μin.)	<0.100 (<4)
Roller races, μm, (μin.)	<0.125 (<5)

Finally, in the boundary lubrication regime, oxide films and other impurities are needed to prevent welding of the contacting surfaces $h\leq 10^{-9}$ m (10^{-7} in.). Most space mechanisms operate in the boundary lubrication regime.

In the boundary lubrication regime, the degree of metal-to-metal contact and the wear rate increase as the load increases. Noncorrosive lubricants allow adhesive wear under boundary and mixed lubrication conditions. Under moderate loads, wear is generally mild. However, very high loads create severe adhesion and surface distress (scoring). Lubricants that contain corrosive (extreme pressure and antiwear) additives can extend the boundary regime before boundary film failure begins. At this point, total surface failure occurs, followed by seizure. Besides the load, other operating variables that will affect lubricant film performance include speed, temperature, and the environment, including the ambient atmosphere (Ref. 5.1).

A search of the literature reveals a large amount of qualitative wear data that has been generated on an assortment of laboratory testers over a period of decades. Equations and analysis exist together with friction and wear data to allow for calculating lubricant film thickness, lubrication operating regime, and the qualitative severity of the wear (Refs. 5.3 to 5.5). However, there is no definitive analysis that allows an engineer to predict, with any degree of engineering certainty, the quantity of wear that can occur in a specific application. Quantitative results need to be obtained experimentally for specific applications. These resulting wear data are not deterministic, but rather, statistical (distributive).

Bearing life and reliability calculations are usually based on rolling element (contact) fatigue of the running surfaces. In some applications, particularly where lubrication is marginal, the failure mechanism may become adhesive or abrasive wear rather than fatigue of the rolling elements and races of the bearings. Reference 5.6 compares tests in a vacuum spiral orbit tribometer with full-scale rig tests of instrument scanner bearings that continuously operate in dither motion. Reference 5.7 discusses accelerated wear testing of the bearings on small electric motors. Reference 5.8 covers wear phenomena. However, its coverage of life modeling deals with fatigue failure, which becomes a source of wear debris, rather than wear itself as a failure mechanism. Most of the other reports in the literature that deal with wear life and reliability of bearings, concern the beneficial effect from filtration of liquid lubricants. Such filtration is not feasible with grease lubrication.

The U.S. space shuttle was originally intended to have a life of 100 flights for each vehicle without scheduled maintenance or inspection. Each shuttle has four BFAs (two on each wing) on a common segmented shaft. These actuators control the position of the large body flap that controls the attitude of the shuttle. During actuator refurbishment and inspection, the grease-lubricated ball bearings in these actuators exhibited various degrees of wear. Given the observed wear, the question arises regarding the timing for removal of the actuators for refurbishing. To put it concisely, how many space shuttle flights should be allowed before the actuators are removed and refurbished because of wear of the actuator bearings?

Based on the above discussion, the objectives of the work reported herein were to (a) experimentally duplicate the operating conditions of the space shuttle BFA input shaft ball bearings; (b) generate, under these simulated conditions, a statistical data base codifying bearing wear; (c) determine the usable life of the actuator bearings based on a two-parameter Weibull distribution function for the bearings using strict-series system reliability; and (d) compare these results to field data from the space shuttle fleet.

Apparatus, Specimens, and Procedure

Body Flap Actuator Bearings

Each of the four BFAs (shown in cross section in Fig. 5.1) is a two-stage, differential planetary gearbox with a speed reduction ratio of 162:1. The actuator input shaft acts as a tension rod to clamp the actuator housing together. The actuator components were greased “for life” and sealed. They were not intended to be reopened nor inspected during the operational life of the space shuttles.

The shaft is supported by two angular-contact ball bearings that carry a heavy axial (thrust) preload of 16 kN (3500 lb). The smaller shaft bearing is a full complement, 106-size (30-mm bore) deep-groove ball bearing containing 18 balls of 7.14 mm (0.281 in.) diameter. The larger bearing is a full complement, 108-size (40-mm bore) deep-groove ball bearing containing 21 balls of 7.94 mm (0.3125 in.) diameter. These bearings are made from carbon vacuum degassed (CVD) AISI 52100 steel.

When the transient aerodynamic load is added, the total bearing load can reach 22 kN (5000 lb). Because of these high loads, the contact stress is very high—up to 3.41 GPa (495 ksi) on the smaller 106-size bearing and 3.03 GPa (440 ksi) on the 108-size bearing. With this high load, the ball running track extends nearly to the shoulder of the bearing inner race.

The actuator performs oscillatory motion during reentry from body flap actuation against transient aerodynamic loads with input speeds as high as 80 rpm.

Lubricant

The mechanical actuators used on the space shuttle are lubricated by a space-rated, grade 2 grease containing a perfluorinated polyether base oil with small polytetrafluoroethylene (PTFE) particles as a thickener, and sodium nitrite and dimethyloctyldecylbenzyl ammonium bentonite as rust and corrosion inhibitors. The grease has a wide operating temperature range: –80 to 200 °C (–112 to 400 °F). The viscosity of the lubricant base oil at the three temperatures used for this test program (24, 60, and 74 °C (75, 140, and 165 °F)) is approximately 4,750, 128, and 77 cSt, respectively. The grease does not contain reactive extreme pressure additives that are typically added to hydrocarbon grease because these additives will not dissolve in the base oil (Ref. 5.9).

Test Apparatus and Procedure

Tests were conducted at the NASA Marshall Space Flight Center on angular-contact ball bearings representative of the smaller (106-size) bearings used on the input shaft of the space shuttle BFAs (Ref. 5.11). The tests were conducted in air under axial loads between 16 and 22 kN, at ambient temperatures of 24 °C (75 °F) to 74 °C (165 °F), and at speeds between 50 and 80 rpm.

The bearing life test rig (shown in Fig. 5.2) uses an electric motor and cog belt drive to rotate the bearing shaft. The bearing housings are axially guided on parallel shafts to hold close alignment. The axial preload acting on the bearings was manually set with a mechanical screw actuator. The axial load was measured by a load cell and monitored by a computer, which automatically terminated the test if the load dropped by 1.3 kN. The drive belt creates a small radial load on the bearings, about 10 percent of the axial load. The loading conditions are similar to those in the actuator under flight conditions.

The bearing housing temperature was controlled by circulating ethylene glycol through passages in the bearing test housings to raise the test bearing temperature to 60 or 74 °C (140 or 165 °F) for the elevated temperature tests. Thermocouples on the outer races monitored the bearing temperatures.

Test bearings include three used flight bearings that had been removed from flight actuators. These were supplemented with 106-size commercial bearings modified to be similar to the full complement bearings used in flight actuators. The original flight bearings were manufactured to RBEC–3 specifications. The commercial test bearings were RBEC–7. The measured surface finish (arithmetic average) in unworn parts of the inner race of the flight bearings was 0.28 μm (11 μin.) compared to 0.06 μm (2 μin.) for the commercial bearings. The bearings were lubricated by perfluorinated polyether oil-based grease as is used in the space shuttle actuators.

A bearing test spectrum, based on the original actuator life mission spectrum, was developed to demonstrate that worn shuttle bearings could operate for 48 flight missions after cleaning and relubrication. This would indicate a life of 12 missions with a 4X safety factor. The life mission spectrum was based on a compressed version of the shuttle loads analysis. Table 5.1 shows the run time, speed, load, and calculated inner race Hertz stress for each condition of the test spectrum. Stresses were calculated by the SHABERTH bearing analysis program (Ref. 5.11). In the initial bearing life testing, the test spectrum was repeated 48 times in a 24 hr period for a total of 112,800 revolutions per test.

The test program produced a total of 18 bearing failures out of 38 bearings tested, where failure was defined by loss of preload (of 1.3 kN). The failures occurred in nearly equal numbers from the 2 bearing mounts on the test device (see Fig. 5.2), 8 failures near the load application side, and 10 at the load reaction side (near the load cell).

Later reexamination of the shuttle mission time line by the NASA Engineering and Safety Center (NESC) established the actual operation time to be only 13.1 min per mission at the normal speed of 80 rpm (1048 rev/mission). This was allocated as 35 sec of flight operation at 60 °C (140 °F) temperature and 12.5 min of ground operations (24 °C (75 °F)). The bearing life and reliability results reported here have been adjusted to be consistent with the revised mission time.

Statistical Analysis

Weibull Analysis

In 1939, Weibull (Refs. 5.12 to 5.14) developed a method and equation for statistically evaluating the fracture strength of materials. He also applied the method and equation to fatigue data based upon small sample (population) sizes, where the two-parameter expression relating life, L, characteristic life, L_β and probability of survival, S is

$$\ln\ln\left(\frac{1}{S}\right) = e\ln\left(\frac{L}{L_\beta}\right) \quad \text{where} \quad 0 < L < \infty;\ 0 < S < 1 \tag{5.1}$$

When plotting the ln ln [1/S] as the ordinate against the ln L as the abscissa, fatigue data are assumed to plot as a straight line (Fig. 5.3). The ordinate ln ln [1/S] is graduated in statistical percent of components failed or removed for cause as a function of ln L, the log of the time or cycles to failure. The tangent of the line is designated the Weibull slope e, which is indicative of the shape of the cumulative distribution or the amount of scatter of the data. The method of using the Weibull distribution function for data analysis for determining component life and reliability was later developed and refined by Johnson (Refs. 5.15 and 5.16).

The Johnson-Weibull method has been in continual use by NASA for over 50 years to statistically analyze cumulative failure data such as occurs in bearings and gears for which an extensive data base now exists in the open literature. The method allows for reasonable engineering estimates and comparisons of cumulative life distributions with small sample sizes or populations.

The Weibull slope of the resultant Weibull plot approximates the statistical distribution of the data. As an example, a Weibull slope of 1 approximates an exponential distribution. A Weibull slope of 2 approximates a Raleigh distribution. A Weibull slope of 3.57 approximates a Gaussian or normal distribution. The resulting values of life compare reasonably well with other statistical distributions such as log normal. However, the ease of use and consistency of results offers an advantage of the Johnson-Weibull method over these other distribution functions. For this reason, the Johnson-Weibull method was used to analyze the wear data reported herein.

System Life Prediction

The reliability (or probability of survival), S and the probability of failure, F are related by $F = (1\text{-}S)$. For a given time or life, the reliability S_{sys} of a system is the product of the reliabilities S_i $(i = 1, 2, ..., n)$ of the components in the system, as shown in equation (2):

$$S_{sys} = S_1 \times S_2 \times \cdots \times S_n \tag{5.2}$$

If all components have the same reliability S_n (as is assumed here), then equation (2) reduces to

$$S_{sys} = S_n^n \tag{5.3}$$

Each actuator has two input bearings and each shuttle has four actuators for a total of eight bearings. Thus, for one shuttle, equation (3) can be written as

$$S_{sys} = S_n^8 \tag{5.4}$$

From equation (1), the lives of each of the bearings at a specified reliability can be combined to determine the calculated system L_{sys} life using the two-parameter Weibull distribution function (eq. (1)) for the bearings comprising the system and strict-series system reliability (Refs. 5.17 to 5.19) as follows:

$$\frac{1}{L_{sys}^{e}} = \left(\frac{1}{L_1^{e_1}} + \frac{1}{L_2^{e_2}} + \cdots \frac{1}{L_n^{e_n}} \right) \tag{5.5}$$

In this work, the two shaft bearings are assumed to have the same life—the life of the smaller (size 106) bearing. In addition, the four actuators are assumed to have equal lives. This means that each of the bearings will have the same life at a specified reliability, where $L_1 = L_2 = \ldots L_n$ and $e_1 = e_2 = \ldots e_n$. Accordingly, equation (5) can be written for the eight bearings in four actuators as

$$\frac{1}{L_{sys}^{e}} = \left(\frac{8}{L^{e_n}} \right) \tag{5.6}$$

The calculated system life is dependent on the resultant value of the system Weibull slope e. For wear data, this value is normally not known with certainty, but a reasonable value can be assumed from the Weibull plots of the resultant wear data.

The bearing system life of the actuators is calculated for each operating condition of their mission profile. In order to obtain the mission life of the actuators, the resulting system lives for each of the operating conditions are combined in equation (7) using the linear damage (Palmgren-Langer-Miner) rule (Refs. 5.17 to 5.19) where $L_{sys\ n}$ is the life for condition n and X_n is the time fraction spent at condition n,(n = 1, 2, …).

$$\frac{1}{L_{mis}} = \frac{X_1}{L_{sys_1}} + \frac{X_2}{L_{sys_2}} + \cdots \frac{X_n}{L_{sys_n}} \tag{5.7}$$

Results and Discussion

During actuator refurbishment and inspection, the grease-lubricated ball bearings in these actuators exhibited various degrees of wear. While a bearing exhibiting significant wear may continue to function over an extended time period, it is considered no longer fit for its intended application and, hence, failed.

As the bearing preload continues to decline due to increasing wear, the actuator can eventually be rendered inoperable. In the absence of a viable lubricating film, the worn contacting surfaces can experience adhesive wear, possibly leading to seizure of the mating bearing surfaces. Based upon these observations, an issue arises regarding the time to removal of the actuators for refurbishing and replacement of the bearings.

There have been 116 shuttle flights in the history of the program from 1981 to 2006. Actual space shuttle maintenance history shows that one BFA bearing has been replaced due to excessive wear during the history of shuttle flights. A portion of the inner race of this failed flight bearing is shown in Figure 5.4. The failure was found after 20 missions on the affected vehicle. In addition, another actuator bearing was removed after 20 flights due to formation of a black iron oxide coating, apparently caused by decomposition of the lubricant. However, this bearing had only minor wear.

In an effort to determine the life and failure mechanism of the grease-lubricated bearings that support the input shaft of the BFAs, life tests were performed on a test rig under simulated flight and ground operations conditions. The damage to the inner race of one of the failed test bearings is shown in Figure 5.5. The damage appears similar to that of the failed flight bearing shown in Figure 5.4. Both bearings show minor cracking of the raceway, in addition to the severe wear. The wear tracks of the flight and test bearings as measured by a profilometer were similar in width: 2.74 and 2.97 mm (0.108 and 0.117 in.), respectively.

A probabilistic analysis using the two-parameter Weibull-Johnson method was performed on the life test data generated by these experiments. The tests and analysis established life and reliability data for both shuttle flight and ground operation as a function of the number of shuttle missions flown.

The bearing lives were calculated using the two-parameter Weibull-Johnson method for reliabilities of 99.9, 99.0, and 90 percent. In the test series presented below, we combined results of tests that gave similar lives in order to present larger data sets, even though some tests were run under somewhat different conditions.

Tables 5.2 to 5.6 summarize the results from four series of tests described below in terms of lives $L_{10,}$ $L_{1,}$ and $L_{0.1}$. The L_{10} life is the time (in terms of the number of bearing revolutions) at which 10 percent of a population of bearings can be expected to fail (or 90 percent not to fail). Likewise, L_1 represents the time to fail 1 percent and $L_{0.1}$ is the time to failure for 0.1 percent.

The life is also given in terms of missions, assuming the revised NESC mission length of 1048 shaft revolutions (13.1 min). The reliability for the entire system will be the product of the reliabilities in all components comprising the system, including the other six bearings in the actuator not considered here. The system reliability will always be less than the reliability of the lowest-lived component of the system.

The air pressure inside the actuator housing during flight is unknown. While the housings have vitron seals, it is assumed that the air trapped within the housing will leak away during the several days that the shuttle spends in space. On reentry into the atmosphere it is further assumed that the housing will repressurize it is not known how rapidly this can occur. However, analysis of the shuttle operation records shows that less than 5 percent of the actuator operating time occurred during flight and thus in possible vacuum. The balance of the operating time was ground operation where the bearings operate in air. Accordingly, the tests reported herein were conducted in air at atmospheric conditions.

Bearing wear data were obtained for four series of operating conditions. The test series are described below.

Test Series 1, Mission Spectrum at 60 °C

These tests used the original, simplified, shuttle program 30-min mission spectrum shown in Table 5.1. The mission spectrum was intended to represent the actual loads and speeds the actuator experiences during flight and ground operations. In this series, the bearings were heated to an ambient temperature of 60 °C (140 °F) to simulate the flight environment at shuttle reentry.

Test articles included three used flight bearings plus three commercial bearings modified to be similar to the flight bearings. All six bearings completed 48 simulated missions (112,800 revolutions) with no failures (i.e., six runouts). The individual test duration (inner race revolutions) data are shown in Table 5.2. Since there were no failures, Weibull analysis cannot be performed on these data.

Test Series 2, Mission Spectrum at 24 °C

These tests used the same mission spectrum as above except the bearings were not heated (ambient temperature of 24 °C (75 °F)). Only modified commercial bearings were used because no more used flight bearings were available. These tests were run until one of the bearings in the rig failed, thus producing three failures out of six bearings tested. Although the data points for the nonfailed (suspended tests) are not shown in the figure, they were statistically weighted in the analysis using the method of Johnson (Ref. 5.16).

The Weibull analysis of Test Series 2 gives an L_{10} (90 percent reliability) life of 62,000 revolutions. Raw data are shown in Table 5.3A and results are shown in Table 5.3B and Figure 5.6. Based on these data and using the revised mission time (13.1 min or 1048 revolutions), the reliability of one bearing for a life of 12 shuttle missions is 99.8 percent. For the eight input shaft bearings (assumed to have identical lives) in four actuators on one shuttle, the risk of failure would be 1.4 percent (reliability 98.6 percent).

The Weibull plots in Figures 5.6 to 5.9 include 90 percent confidence bands for the data. If a large number of similar tests were performed, one would expect that 90 percent of the data would lie within these confidence bands.

Combination of Test Series 1 and 2

In actual shuttle operation, approximately 4.5 percent of the operating time would be simulated by Test Series 1 (flight) and 95.5 percent by Test Series 2 (ground operations). Using equation (7) to combine Test Series 1 and 2, and for the purpose of calculation, assuming infinite life for Test Series 1 and an L_{10} (90 percent reliability) life of 62,000 revolutions for Test Series 2, the combined L_{10} life for the system equals 64,900 revolutions.

The mission life and reliability for the 13.1 min (1048 revolutions), combined operation time were predicted by combining the results of the tests summarized in Series 1 and 2 above in proportion to the operation time (ground and flight), according to the linear damage rule of equation (7) where L is the life,

$$\frac{1}{L} = \frac{X_1}{L_1} + \frac{X_2}{L_2} \tag{5.8}$$

X_1 and X_2 are the time fractions ($X_1 + X_2 = 1.00$) that occur at conditions 1 and 2, and L_1 and L_2 are the lives for these conditions. Using the data for 90 percent reliability from Series 1 and 2, equation (8) becomes

$$\frac{1}{L} = \frac{0.045}{\infty} + \frac{0.955}{62{,}000} = \frac{1}{64{,}900}\text{, thus } L = 64{,}900 \tag{5.9}$$

For purposes of comparison only, the data from both series above were combined to produce a Weibull plot that represents all of the mission spectrum tests at both elevated and room temperatures (12 bearings tested with three failures). The Weibull analysis on this combined set gives an L_{10} (90 percent reliability) life of 80,000 revolutions. The results, shown in Table 5.4 and Figure 5.7, show higher life than would be anticipated based on the weighted results from equation (7) above. (Runout tests were included in the analysis but are not shown in the figure.)

The analysis on the combined dataset shows the reliability of one bearing for a life of 12 missions is 99.99 percent. For the eight input shaft bearings (assumed to have identical lives) in four actuators on one shuttle, the risk of failure would be 0.07 percent (reliability 99.93 percent).

Test Series 3, Speed 50 and 80 rpm, Temperature 24 °C, Thrust Loads 16, 20, and 24 kN

Tests were conducted at room temperature (24 °C (75 °F)) with thrust loads of 16, 20, or 22 kN (3500, 4500, or 5000 lb) and speeds of 50 or 80 rpm. The differences in speeds and loads had little effect on the lives for the limited range tested; hence, smaller data sets were combined together. Raw data are shown in Table 5.5A and results are shown in Table 5.5B and Figure 5.8.

Some tests of this series were restarted after a failure by replacing the failed bearing and continuing the test with the surviving bearing. In one test, both bearings failed at approximately the same time. Twenty bearings were tested with 12 failures.

Based on these data, the reliability of one bearing for a life of 12 missions is 99.6 percent. For the eight input shaft bearings (assumed to have identical lives) in four actuators on one shuttle, the risk of failure would be 3.4 percent (reliability 96.6 percent).

Test Series 4, Speed 50 and 80 rpm, Elevated Temperature 60 and 74 °C, Thrust Load 16 kN

Three bearing failure tests (with three runout tests of the bearings at the other end of the shaft) were conducted at elevated temperature (two at 60 °C (140 °F) and one at 74 °C (165 °F)). The tests were run at constant speed (50 or 80 rpm) and an axial load of 16 kN (3500 lb). As in series 3 above, there was little difference in lives found between these two temperatures and two speeds; therefore, results were combined. Raw data are shown in Table 5.6A and results are shown in Table 5.6B and Figure 5.9.

Based on these data, the reliability of one bearing for a life of 12 missions is 99.9 percent. For the eight input shaft bearings (assumed to have identical lives) in four actuators on one shuttle, the risk of failure would be 0.5 percent (reliability 99.5 percent).

Bearing Wear

In general, the test temperature was found to have the greatest effect on the lives of the bearings, with lower temperature (room temperature) tests giving shorter life. This result of lower life at lower test temperatures was not expected. It may have been caused by lubricant starvation, because the cooler oil flowed back into the contact area at a slower rate after ball passage.

One method to determine bearing wear is to accurately weigh cleaned bearings before and after a test and subtract the two readings. This method suffers from the limitation that it does not detect material transferred from one surface to another in addition to the problem of subtracting two nearly equal numbers.

The bearings tested here were not weighed prior to testing. Cleaned failed bearings were weighed and compared with cleaned new bearings of the same type. These indicate an average loss of about 180 mg or about 0.16 percent. However, the new bearings showed a much greater variation in weight from heaviest to lightest (0.60 percent) than the variation between new and failed bearings.

Bearing failure during tests was marked by a transition from stable bearing temperature and load to increasing temperature and declining preload. These failures were caused by the normal wear under boundary lubrication shifting to accelerated wear induced by lubricant breakdown. One test (at 50 rpm) was continued for four additional hours after the onset of severe wear. (This represents 11.5 additional missions at 1048 inner race revolutions each). The extended run created severe wear damage in which about 75 percent of the preload was lost due to wear.

After the onset of severe wear, these bearings would no longer be fit for their intended use. However, the very gradual onset of this failure mode indicates that imminent seizure is unlikely. Thus, bearing failure should not cause a failure of the actuator that would endanger the space shuttle as long as a reasonable inspection schedule is followed.

Estimated System Life and Reliability

The mission life of these bearings under combined ground and flight operation was predicted by combining the results of Series 3 (representing ground operation temperature) and Series 4 (representing flight) according to the linear damage rule (eq. (7)). NESC Analysis of the records of the shuttle fleet has established an average operation time of 13.1 min per mission. This consists of 35 sec of flight operation at an assumed temperature of 60 °C (140 °F) and 12.5 min of ground operations at 24 °C (75 °F). Assuming a normal operation speed of 80 rpm, there will be 1048 revolutions per mission. The 13.1 min operation time is less than half the 30 min initially assumed by the NESC.

The mission life and reliability for the 13.1 min combined operation time were predicted by combining the results of the tests summarized in Series 3 and 4 above in proportion to the operation time (ground and flight), according to the linear damage rule of equation (8). Using the data for 90 percent reliability from Series 3 and 4, equation (8) becomes

$$\frac{1}{L} = \frac{0.045}{110} + \frac{0.955}{39} = \frac{1}{40}, \text{ thus } L = 40 \tag{5.10}$$

The predicted L_{10} and $L_{0.1}$ lives for combined 24 and 60 °C (75 and 140 °F) operations is 40 and 7 missions, respectively. The reliability of a single bearing for a life of 12 missions is 99.6 percent. Each actuator has two input bearings and each shuttle has four actuators, thus, from equation (3), based on four actuators and eight bearings of equal life, per shuttle,

$$S_{sys} = S_n^n = (0.996)^8 = 0.969 \text{ or } 96.9 \text{ percent} \tag{5.11}$$

Therefore, the risk of an input shaft bearing failure would be 3.1 percent (reliability 96.9 percent) for 12 missions of one shuttle (assuming all input shaft bearings have identical reliability). The relation between reliability, number of bearings involved, and number of missions is shown in Figure 5.10.

Predicted Failure Rate for Actuator Input Shaft Bearings

As a final way to present BFA input shaft bearing test data, we relate the bearing reliability found from this test program to the expected failure rate as a function of the number of missions for the space shuttle fleet.

We used the reliability level for eight bearings presented in the previous section (96.9 percent). This reliability is for 12 shuttle missions using the combined mission profile discussed above (35 sec of flight and 12.5 min ground operation). We assumed the Weibull slope (2.739) as found for the 24 °C (75 °F) tests and, using equation (1), computed the characteristic life to be 42.4 missions for one bearing failure in one vehicle of the fleet. The characteristic life is the time by which 63.2 percent of a large population of identical vehicles would have a failure.

We assumed the following scenario: The fleet starts out with four new shuttle vehicles. These are each flown in turn until a bearing failure occurs. (No other failures are considered, only in BFA input shaft bearings.) Then the shuttle with a failed bearing is retired and the remaining shuttles continue to fly until an input bearing has failed in each of the four shuttles. In this calculation, the reliability, *S(t)* was estimated from the median rank of the failures, according to equation (12) (Ref. 5.20), where *i* is the failure number and *n* is the number of samples (in this case, $n = 4$):

$$F \approx \frac{i - 0.3}{n + 0.4} \tag{5.12}$$

The predicted number of shuttle missions until failure based on the scenario described above was calculated from equations (1) and (12) and is shown in Table 5.7. We predict that the first failure will occur at about the 22nd mission of the shuttle vehicle involved. If all four vehicles at that time have the same number of missions, the total number of missions will be 88. Then we assume the remaining three vehicles continue to fly until the second failure occurs at flight 33 on another shuttle. At that time, the fleet will have 121 missions [22+(3×33)]. Likewise, failure number three occurs at flight 42 or fleet mission 139 [22+33+(2×42)] and the final failure at flight 53, or fleet mission 150 (22+33+42+53).

Actual space shuttle maintenance history shows that one BFA bearing has been replaced due to excessive wear during the history of shuttle flights through 2006. The failure was found after 20 missions on the affected vehicle. In addition, another actuator bearing was removed after 20 missions due to a

black iron oxide coating, apparently caused by decomposition of the lubricant. However, there was only minor wear associated with the bearing having the blackened ball.

The one historical failure due to wear at 20 missions is consistent with the results of Table 5.7, which predicts the first failure at 22 missions. Since there have been 116 flights in the history of the program through 2006, the analysis indicates another failure might have been expected soon in the absence of inspection and bearing replacement.

Summary of Results

The U.S. space shuttle has four body flap actuators (BFAs) (two on each wing) on a common segmented shaft to control the position of the large body flap on the space shuttle. During actuator refurbishment and inspection, the grease-lubricated ball bearings in these actuators exhibited various degrees of wear. Bearing tests were performed to experimentally duplicate the operating conditions of the space shuttle actuator ball bearings and to generate a statistical data base to codify the wear in these bearings. The usable life and reliability of these actuator bearings were determined based on a two-parameter Weibull distribution function using strict-series system reliability for both shuttle flight and ground operation as a function of the number of shuttle missions flown. These experimental results were compared to field data from the space shuttle fleet. The following results and conclusions were obtained:

1. The actuator bearing failure mechanism was severe wear that created the onset of bearing preload loss. After the onset of severe wear, the bearings would no longer be fit for their intended use. However, the very gradual onset of this failure mode indicates that imminent seizure is unlikely. Thus, bearing failure should not cause a failure of the actuator and endanger the space shuttle as long as a reasonable inspection schedule is followed.
2. The Weibull analysis of the test data for the four actuators on one shuttle, each with a 2-bearing shaft assembly, established a reliability level of 96.9 percent for a life of 12 missions.
3. A reasonable inspection and maintenance program of the BFAs should be implemented to enable safe operation of the shuttle orbiter fleet. This interval should not be more than 12 missions for any shuttle vehicle.
4. A probabilistic system analysis for four shuttles, each of which has four actuators, predicts a single bearing failure in one actuator of one shuttle after 22 missions. (This means a total of 88 missions for a four-shuttle fleet.) This prediction is comparable with actual shuttle flight history in which a single actuator bearing was found to have failed by wear at 20 missions. Since there have been 116 flights in the history of the program through 2006, the analysis indicates another failure might have been expected soon in the absence of inspection and bearing replacement.

References

5.1. Zaretsky, Erwin V., ed.: Tribology for Aerospace Applications. STLE SP–37, Society of Tribologists and Lubrication Engineers, Park Ridge, IL, 1997, pp. 51–53.
5.2. Zaretsky, Erwin V., ed.: STLE Life Factors for Rolling Bearings. Second Ed., STLE SP–34, Society of Tribologists and Lubrication Engineers, Park Ridge, IL, 1999, p. 41.
5.3. Bhushan, Bharat, ed.: Modern Tribology Handbook, Vol. 1, CRC Press, Boca Raton, FL, 2000.
5.4. MacGregor, Charles W.: Handbook of Analytical Design for Wear. Plenum Press, New York, NY, 1964.
5.5. Booser, E. Richard, ed.: CRC Handbook of Lubrication: Theory and Practice of Tribology. Volume II: Theory and Design, CRC Press, Boca Raton, FL, 1983.
5.6. Jansen, Mark J., et al.: Relative Lifetimes of Several Space Liquid Lubricants Using a Vacuum Spiral Orbit Tribometer (SOT). NASA/TM—2001-210966, 2001. http://ntrs.nasa.gov

5.7. Wang, W.; and Dragomir-Daescu, D.: Reliability Quantification of Induction Motors-Accelerated Degradation Testing Approach. Proceedings of the Reliability and Maintainability Symposium, Seattle, WA, 2002.
5.8. Roylance, B.J.; Williams, J.A.; and Dwyer-Joyce, R.: Wear Debris and Associated Wear Phenomena—Fundamental Research and Practice. Proceedings of the Institution of Mechanical Engineers, Part J, Journal of Engineering Tribology, vol. 24, no. 1, 2000, pp. 79–105.
5.9 Carre, David J.: The Performance of Perfluoropolyalkylether Oils Under Boundary Lubrication Conditions. Trib. Trans., vol. 31, no. 4, 1988, pp. 437–441.
5.10. Jett, Timothy R., et al.: Space Shuttle Body Flap Actuator Bearing Testing for NASA Return to Flight. NASA/CP—2006-214290, 2006, pp. 253–268. http://ntrs.nasa.gov
5.11. Hadden, G.B., et al.: Research Report: User's Manual for Computer Program AT81y003 SHABERTH. NASA CR–165365, 1981. http://ntrs.nasa.gov
5.12. Weibull, Waloddi: A Statistical Theory of the Strength of Materials. Ingeniorsvetanskapsakad. Handl., no. 151, 1939.
5.13. Weibull, Waloddi: The Phenomenon of Rupture in Solids. Ingeniorsvetanskapsakad. Handl., no. 153, 1939.
5.14. Weibull, Waloddi: A Statistical Distribution Function of Wide Applicability. J. Appl. Mech., no. 18, 1951, pp. 293–297.
5.15. Johnson, L.G.: The Median Ranks of Sample Values in Their Population With an Application to Certain Fatigue Studies. Ind. Math., vol. 2, 1951, pp. 1–9.
5.16. Johnson, Leonard Gustave: The Statistical Treatment of Fatigue Experiments. Elsevier Publishing Co., Amsterdam, 1964.
5.17. Palmgren, A.: The Service Life of Ball Bearings. Zectsckrift des Vereines Deutscher Ingenieure, vol. 68, no. 14, 1924, pp. 339–341.
5.18. Langer, B.F.: Fatigue Failure From Stress Cycles of Varying Amplitude. J. Appl. Mech., vol 4, no. 4, 1937, pp. A160–A162.
5.19. Miner, Milton A.: Cumulative Damage in Fatigue. J. Appl. Mech., vol. 12, no. 3, 1945, pp. A159–A164.
5.20. NIST/SEMATECH e-Handbook of Statistical Methods. 2006. http://www.itl.nist.gov/div898/handbook/ Accessed Jan. 10, 2017.

TABLE 5.1.—BEARING TEST MISSION SPECTRUM

Time, min	Speed, rpm	Axial load, kN, (lb)	Inner race Hertz stress, GPa, (ksi)
27	80	16 (3500)	3.13 (452)
1.5	70	18 (4100)	3.27 (473)
1.0	60	20 (4500)	3.37 (486)
0.5	50	22 (5000)	3.41 (495)

TABLE 5.2.—TEST SERIES 1, MISSION SPECTRUM TESTS AT 60 °C

Bearing no.	Status	Life, Revolutions
1	survived	112800
2	survived	112800
3	survived	112800
4	survived	112800
5	survived	112800
6	survived	112800

TABLE 5.3A.—TEST SERIES 2, MISSION SPECTRUM TESTS AT 24 °C

Bearing no.	Status	Life, Revolutions
1	failed	105125
2	survived	105125
3	failed	62771
4	survived	62771
5	failed	129890
6	survived	129890

TABLE 5.3B.—TEST SERIES 2, MISSION SPECTRUM TESTS AT 24 °C
WEIBULL SLOPE, e = 2.556, CHARACTERISTIC LIFE, L_β = 148,693 rev

Life	Reliability, %	Revolutions	Missions
L_{10}	90	62,000	59
L_1	99	25,000	23
$L_{0.1}$	99.9	10,000	10

TABLE 5.4.—TEST SERIES 1 AND 2 (COMBINED), MISSION SPECTRUM TESTS AT 60 °C AND 24 °C WEIBULL SLOPE,
e = 2.931, CHARACTERISTIC LIFE, L_β = 172,866 rev

Life	Reliability, %	Revolutions	Missions
L_{10}	90	80,000	77
L_1	99	36,000	34
$L_{0.1}$	99.9	16,000	16

TABLE 5.5A.—TEST SERIES 3, CONSTANT SPEED AND LOAD TESTS AT 24 °C, 16-24 kN, 50 AND 80 rpm

Bearing no.	Status	Life, Revolutions	Test conditions
1	failed	35310	50 rpm, 16 kN, 24 °C
2	failed	56850	50 rpm, 16 kN, 24 °C
3	failed	79000	50 rpm, 16 kN, 24 °C
4	survived	13170	50 rpm, 16 kN, 24 °C
5	failed	50640	50 rpm, 22 kN, 24 °C
6	failed	50640	50 rpm, 22 kN, 24 °C
7	failed	38400	50 rpm, 24 kN, 24 °C
8	survived	38400	50 rpm, 24 kN, 24 °C
9	failed	96480	80 rpm, 16 kN, 24 °C
10	survived	96480	80 rpm, 16 kN, 24 °C
11	failed	65040	80 rpm, 16 kN, 24 °C
12	survived	65040	80 rpm, 16 kN, 24 °C
13	failed	51024	80 rpm, 16 kN, 24 °C
14	survived	51024	80 rpm, 16 kN, 24 °C
15	failed	114240	80 rpm, 16 kN, 24 °C
16	survived	114240	80 rpm, 16 kN, 24 °C
17	failed	102240	80 rpm, 16 kN, 24 °C
18	survived	102240	80 rpm, 16 kN, 24 °C
19	failed	61440	80 rpm, 16 kN, 24 °C
20	survived	61440	80 rpm, 16 kN, 24 °C

TABLE 5.5B.—TEST SERIES 3, CONSTANT SPEED AND LOAD TESTS AT 24 °C, 16-24 kN, 50 AND 80 rpm
WEIBULL SLOPE, e = 2.739, CHARACTERISTIC LIFE, L_β = 91,798 rev

Life	Reliability, %	Revolutions	Missions
L_{10}	90	40,000	39
L_1	99	17,000	16
$L_{0.1}$	99.9	7,400	7

TABLE 5.6A.—TEST SERIES 4, ELEVATED TEMPERATURE TESTS AT 16 kN LOAD, 50 AND 80 rpm

Bearing No.	Status	Life, Revolutions	Test conditions
1	failed	196050	50 rpm, 16 kN, 60 °C
2	survived	196050	50 rpm, 16 kN, 60 °C
3	failed	118950	50 rpm, 16 kN, 60 °C
4	survived	118950	50 rpm, 16 kN, 60 °C
5	failed	270336	80 rpm, 16 kN, 74 °C
6	survived	270336	80 rpm, 16 kN, 74 °C

TABLE 5.6B.—TEST SERIES 4, ELEVATED TEMPERATURE TESTS AT 16 kN LOAD, 50 AND 80 rpm
WEIBULL SLOPE, e = 2.334, CHARACTERISTIC LIFE, L_β = 301,729 rev.

Life	Reliability, %	Revolutions	Missions
L_{10}	90	115,000	110
L_1	99	42,000	40
$L_{0.1}$	99.9	16,000	15

TABLE 5.7.—PREDICTED FAILURE RATE FOR ACTUATOR INPUT SHAFT BEARINGS

Failure no.	Mission no. on failed shuttle	Cumulative fleet missions
1	22	88
2	33	121
3	42	139
4	53	150

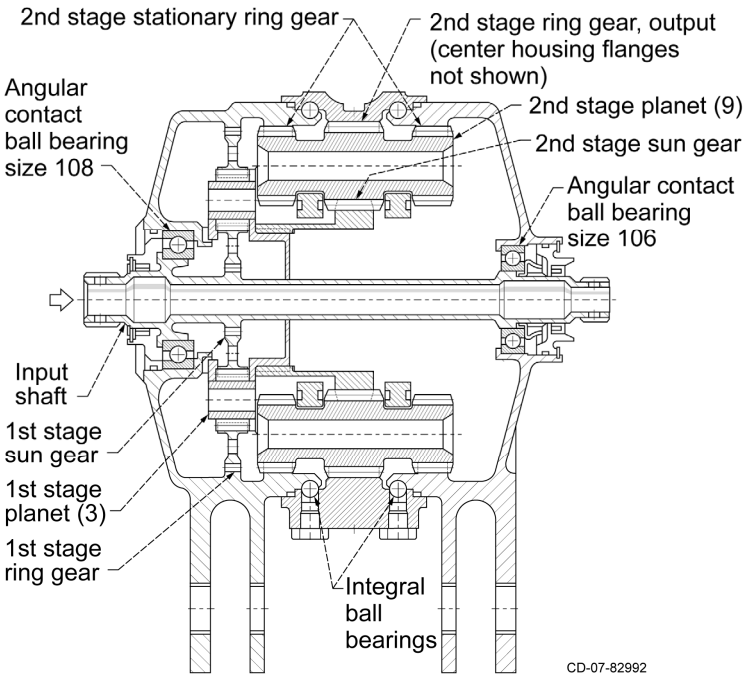

Figure 5.1.—Body flap actuator cross section showing input shaft bearings.

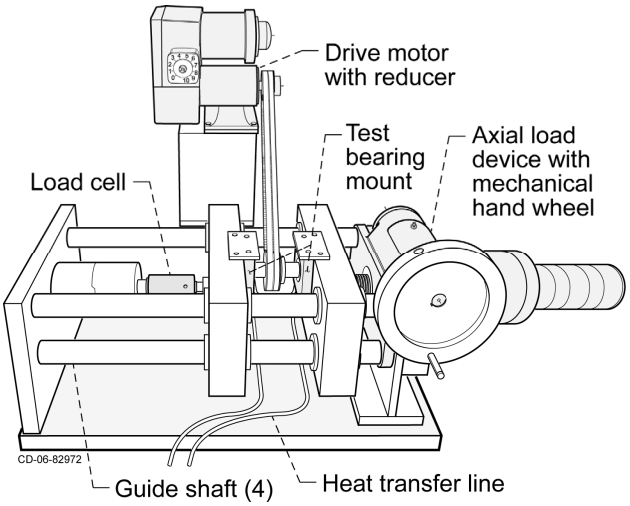

Figure 5.2.—Bearing test apparatus.

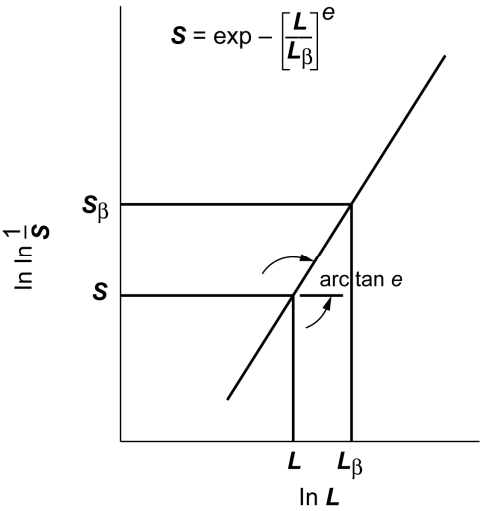

Figure 5.3.—Weibull plot where (Weibull) slope of tangent of line is *e*; probability of survival, S_{β}, is 36.8 percent at which $L = L_{\beta}$ or $L/L_{\beta} = 1$.

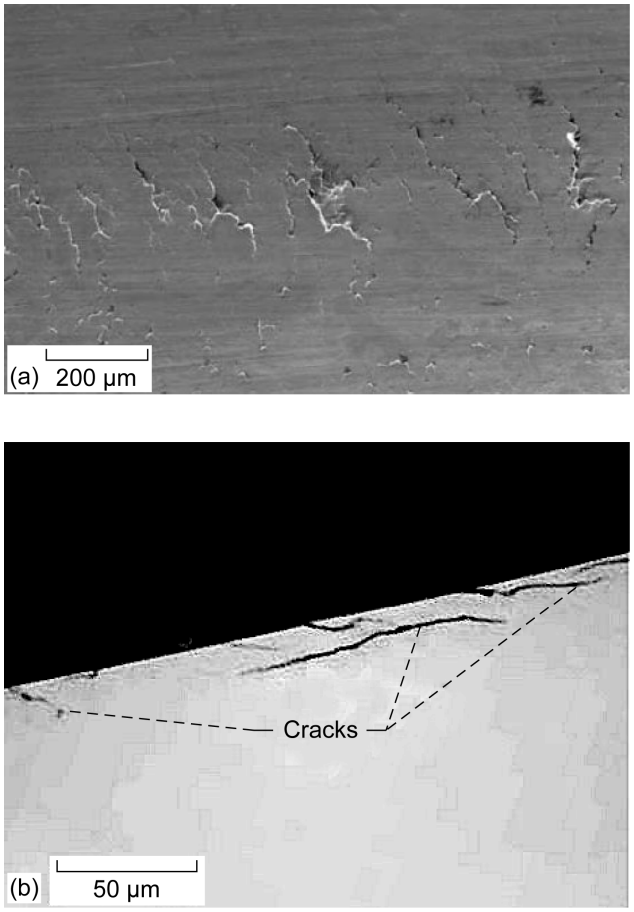

Figure 5.4.—Damage to shuttle body flap actuator bearing inner race after 20 flights. (a) SEM view of wear band in race. (b) Cross section showing cracks below surface.

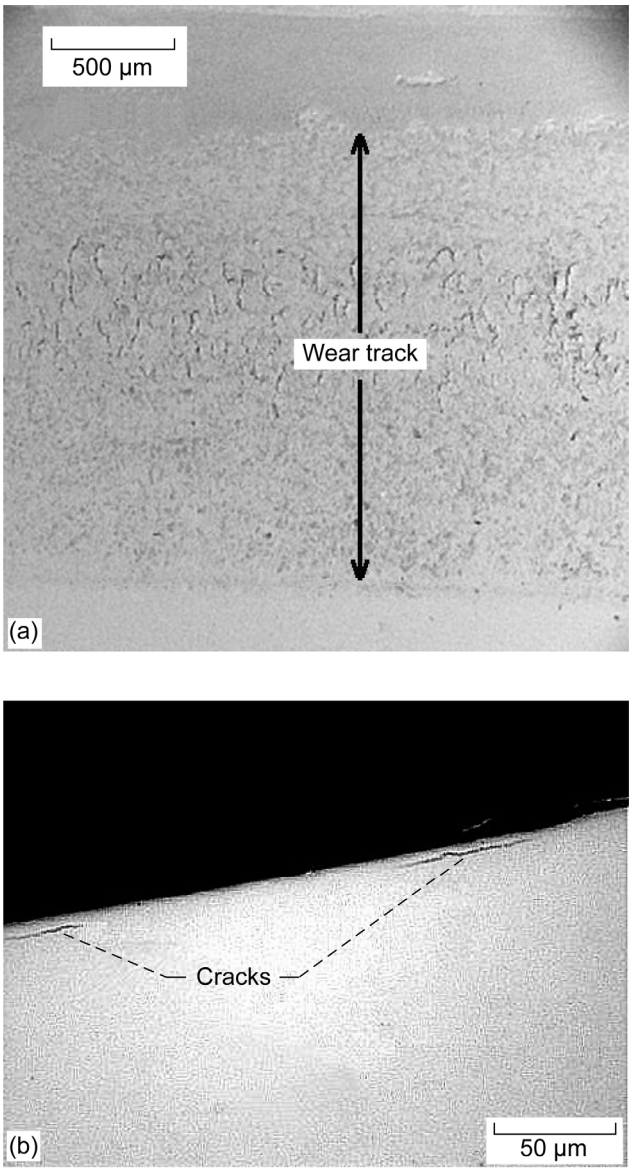

Figure 5.5.—Damage to test bearing at failure. (a) SEM view of wear band in race. (b) Cross section showing cracks below surface.

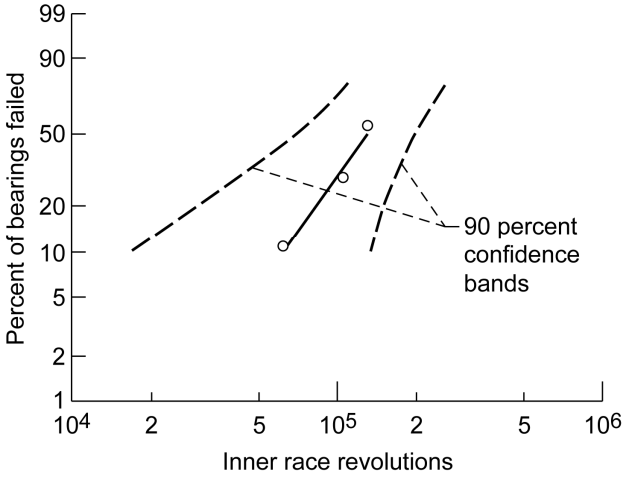

Figure 5.6.—Weibull plot of Series 2 mission spectrum tests at 24 °C. Failure index 3/6.

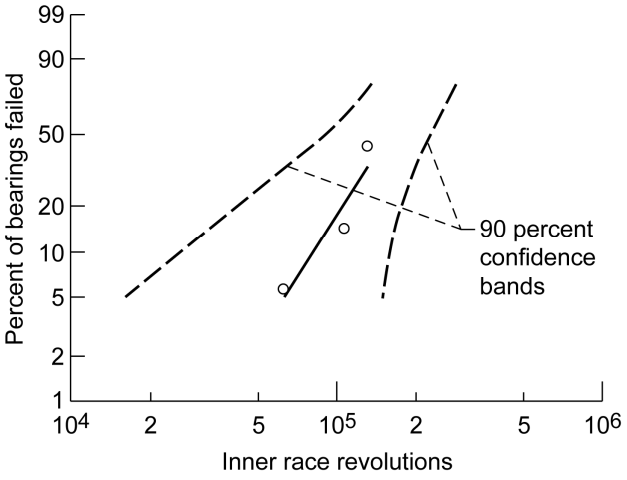

Figure 5.7.—Weibull plot of Series 1 and 2 mission spectrum tests at 60 and 24 °C. Failure index 3/12.

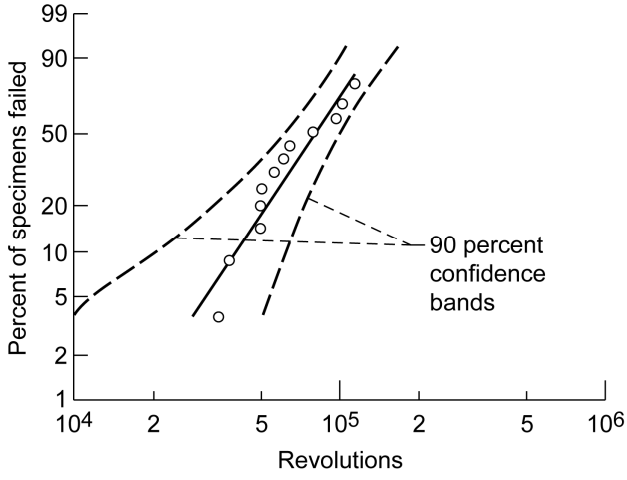

Figure 5.8.—Weibull plot of Series 3 tests at 24 °C, 16-24 kN; 50 and 80 rpm. Failure index 12/20.

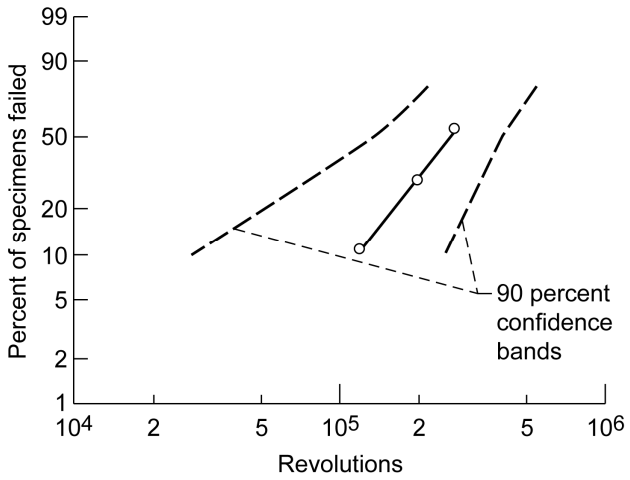

Figure 5.9.—Weibull plot of Series 4 elevated temperature tests at 16 kN load, 50 and 80 rpm. Failure index 3/6.

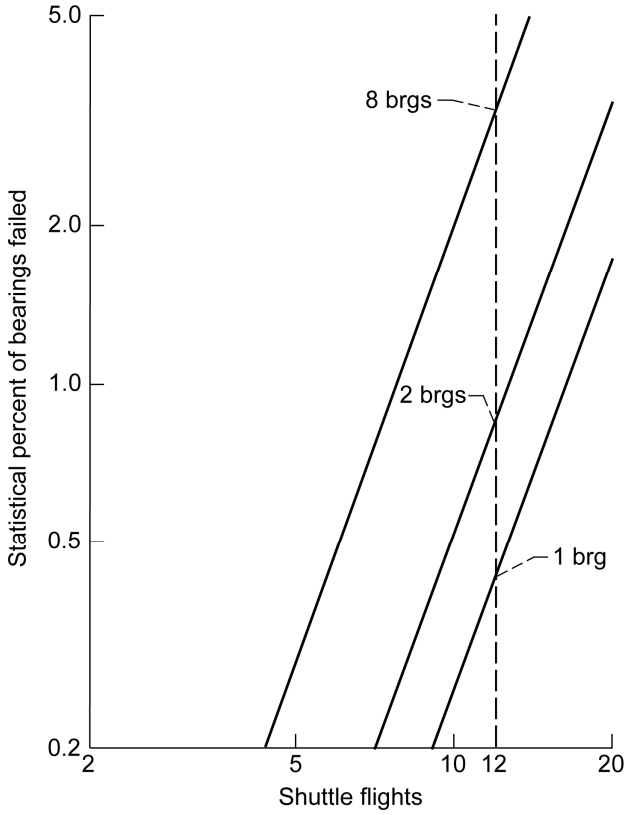

Figure 5.10.—Estimated life and reliability of input shaft bearings.

Chapter 6: Engagement of Metal Debris Into a Gear Mesh

Robert F. Handschuh and Timothy L. Krantz
National Aeronautics and Space Administration
Glenn Research Center
Cleveland, Ohio 44135

Abstract

A series of bench-top experiments was conducted to determine the effects of metallic debris being dragged through meshing gear teeth. A test rig that is typically used to conduct contact fatigue experiments was used for these tests. Several sizes of drill material, shim stock, and pieces of gear teeth were introduced and then driven through the meshing region. The level of torque required to drive the "chip" through the gear mesh was measured. From the data gathered, chip size sufficient to jam the mechanism can be determined.

Introduction

In some space mechanisms the loading can be so high that there is some possibility that a gear chip might be liberated while in operation of the mechanism (Refs. 6.1 to 6.5). Also, due to the closely packed nature of some space mechanisms and the fact that a space grease is used for lubrication, chips that are released can then be introduced to other gear meshes within this mechanism. In this instance, it is desirable to know the consequences of a gear chip entering in between meshing gear teeth. To help provide some understanding, a series of bench-top experiments was conducted to engage chips of simulated and gear material fragments into a meshing gear pair. One purpose of the experiments was to determine the relationship of chip size to the torque required to rotate the gear set through the mesh cycle. The second purpose was to determine the condition of the gear chip material after engagement by the meshing gears, primarily to determine if the chip would break into pieces and to observe the motion of the chip as the engagement was completed. This document also presents preliminary testing done with metal "debris" other than chips from gears, namely steel shim stock and drill bits of various sizes and diameters.

Test Equipment

The gear testing was done using a NASA Glenn Research Center Spur Gear Fatigue test rig. This rig uses two identical spur gears engaged with one another. The shaft mounting is an overhung arrangement for the test gears, and the nearby bearings are roller bearings. The overhung distance from the bearing supports is approximately 32 mm (1.25 in.). Because the test machine was designed for experiments of gear fatigue, the shaft and bearing supports are relatively large and stiff. Figure 6.1 shows the test gearbox with a pair of test gears mounted.

Test Gears, Test "Debris" and Chips, and Procedure

The gears used for this study were case-carburized and ground, and were manufactured from the steel alloy AISI 9310. The gears design information is shown in Table 6.1. The gears were shot-peened after hardening and before final grinding. The gears were representative of gears utilized in a space mechanism that was being simulated.

The gear design specifications and the actual mounted center distance determine the root clearance and backlash of a pair of gears. The backlash and root clearances were determined for the first pair of test gear mounted on the test fixture. The backlash was measured as 0.15 mm (0.006 in.) using a standard measurement setup (Fig. 6.2). The root clearance was measured as 0.94 mm (0.037 in.). The root clearance was determined by running a piece of soft material (solder) through the mesh and measuring the deformed material with a caliper.

Three types of "debris" were placed into the meshing gear teeth for testing, namely steel shim stock, drill bit shanks, and pieces or "chips" from gear teeth. The shim stock materials used were steel and stainless steel. The shim thickness ranged from 0.13 to 1.88 mm (0.005 to 0.074 in.). The shims were cut to a length of approximately 2.5 to 3.8 mm (0.100 to 0.150 in.), representing approximately half of the tooth height. The shim lengths were wider than the faces of the gears and were placed to engage the full-face width of the gear teeth (Fig. 6.3). The drill bit shanks used for these experiments had shank diameters ranging from 1.07 to 1.96 mm (0.042 to 0.077 in.).

The gear chip pieces used in this work were liberated from a spare test gear (case-carburized and ground AISI 9310 steel). Ten gear chips were used for testing. Eight of the ten chips were created by scoring a mark on the gear tooth using a small rotating cutting wheel and then striking the score-line with a cold chisel. This created chips with irregular shapes and the chips were of varying sizes (mass). Two of the gear chips were made by cutting the gear tooth using a metals-lab cutting wheels. These two chips have a more regular shape and (as compared to chips made by striking) relatively smooth edges. To quantify the sizes of the chips, the mass of each chip was determined (see Table 6.2). The figures that follow show at least one image with a scale marker for each chip used for testing.

Testing using the shims and drill bits were done with no lubrication on the gear teeth. For tests done with gear chips, a generous amount of a Teflon-based, space-qualified grease was applied with a brush to the teeth prior to testing. During testing, one of the gear shafts (the driven gear) was free to rotate. That is, there was no resistive torque applied. The driving gear was rotated with a torque wrench by hand in a very deliberate manner. The peak torque reading recorded by the torque wrench was recorded as the engaged debris was rolled through the mesh.

Test Results

The results for the shim stock and drill bit testing will be discussed first. To relate the peak torque required to roll the object through the gear mesh to the size of the object, the volume of the object was calculated assuming the full-face width of the gear was engaged and using a nominal height of 3.18 mm (0.125 in.) for the shim objects. The resulting relationship of peak torque to the object volume is provided in Figure 6.4. For the smallest shims tested, only a very small nominal drag torque of the rig setup was required to rotate the shim through mesh. The drill bit shanks required a significantly greater peak torque for an equivalent volume of shim stock material. This can be explained by the higher hardness of the drill bit shank relative to shim stock, thereby requiring larger peak torque before any plastic deformation (or shaft deflection) of the bit shank or gear teeth takes place.

For the drill bit test data a straight line can be passed through the data. In the data for the much softer shim stock, there initially appears to be a linear relation up top a certain volume. Then a region of this data is nearly nonvarying and only increasing torque slightly as the volume was increased. Finally for this data, a rather large increase in torque was recorded as the shim volume was in excess of 35 mm^3.

A plausible explanation for this can be stated as follows. Initially the shim stock plastically compresses and an increase in volume causes a proportional change in torque. As the volume is increased, enough of the tooth tip—root clearance is still available to plastically compress the shim material resulting in little increase in the torque needed. Finally as the volume of the tooth tip to root clearance is used up the torque require to "extrude" the shim increases substantially.

For the case of the shim stock material, the main effect was elastic deformation of the support structure (shaft and bearings) and plastic deformation of the shim stock. Essentially the shim stock was extruded. The shim stock took the shape of the root-fillet region of the driven gear with intrusion by the

tip of the driving gear (Fig. 6.5). The peak torque was roughly a linear function of the engaged shim volume. By visual examination, it was judged that the gear teeth were not damaged by engagement of the shim stock. For the case of the drill bit shanks, the main effect was elastic deformation of the supporting structure and some plastic deformation of the teeth. The drill bit shanks permanently deformed and damaged the tooth tip that made contact with the bit shank during the meshing process (Fig. 6.6).

Next, the results of testing with the gear chips will be discussed. The peak torque required to rotate the gears was, to a good approximation, a linear function of the mass of the engaged chip (Fig. 6.7). For chip #2 of Table 6.2, the peak torque exceed the measuring capacity of the torque wrench, and since the peak torque was not know precisely the data point was not included in the plot of Figure 6.7. A larger capacity torque wrench was used for subsequent testing.

It was noted that immediately after testing the disengaged chips were hot, indicative of the tremendous friction forces and plastic deforming work being done during the meshing process. Some of the smaller chips tended to remain in the root of the gear after the engagement. Larger chips were forced out of the mesh and were found on the tabletop just below the gear mesh. The gear on the left had been rotated clockwise with the torque wrench (the input torque direction), so the motion tended to throw and/or allow the chip to drop to the tabletop. For the two largest chips (chips #6 and #7 of Table 6.2), the engaged gear teeth were deformed and damaged significantly enough that the gears could no longer be rotated with hand torque past the damaged tooth. An image of such damage is provided in Figure 6.8.

Images of the chips both before and after engagement testing are provided in Figures 6.9 to 6.18. The images show that the main effects on the chips were deformation of the chips to conform to the available tooth root spaces. In general, the chips remained intact. For the case of chips #5 and #8, small pieces were liberated from the main piece as can be seen in the figures. Chip #10 especially shows that the case-carburized material, even though generally described as brittle, can be significantly deformed and exhibit some toughness. Although the chip experienced some “tearing,” the chip did not “shatter” or otherwise exhibit extreme brittleness.

Finally all the data generated is shown in Figure 6.19. The drill bit and shim stock mass data was found using the data from Figure 6.4. The drill bit data was very comparable to the tooth chip data following the same trend. The shim stock data had a lower torque level over all the data taken. This must be an artifact of the nominal material hardness. The scatter in the tooth chip data is possibly due to nonsymmetric shapes in comparison to the symmetry of the drill bit data.

Summary and Conclusions

A series of bench-top experiments was conducted to provide an understanding of the engagement of metal debris into a gear mesh. The gears used for testing were case-carburized 12-pitch spur gears made from the steel alloy AISI 9310. The metal debris that was engaged into the pair of meshing test gears was shim stock, drill bit shanks, and chips of gears liberated from a test gear.

It was found that the peak torque required to rotate the gears with the object engaged was proportional to the size (mass) of the engaged object. Engaging objects of higher hardness required a significantly greater peak torque relative to an equivalent-sized object of lesser hardness.

For the largest chips sizes tested, sufficient deformation occurred to the gear teeth to prevent smooth motions of the gear when the damaged tooth is engaged.

During this study, no new chips and no obvious tooth fracture occurred.

Even though case-carburized steel hardened in the manner of the aerospace gears is generally described as “brittle,” the chips exhibited significant deformation and exhibited some toughness. Chips did not “shatter” or otherwise exhibit extreme brittle behavior.

Although large chips caused significant damage to the test gear teeth, the data generated in this study could be used for minimum power needed to drive a chip of a certain mass through mesh.

References

6.1. Krantz, Timothy L.; and Handschuh, R.: A Study of Spur Gears Lubricated With Grease—Observations From Seven Experiments. NASA/TM—2005-213957 (ARL-TR-3159), 2005. http://ntrs.nasa.gov

6.2. Proctor, Margaret P.; Oswald, Fred B.; and Krantz, Timothy L.: Shuttle Rudder/Speed Brake Power Drive Unit (PDU) Gear Scuffing Tests With Flight Gears. NASA/TM—2005-214092, 2005. http://ntrs.nasa.gov

6.3. Handschuh, Robert F., et al.: Investigation of Low-Cycle Bending Fatigue of AISI 9310 Steel Spur Gears. NASA/TM—2007-214914 (ARL–TR–4100), 2007. http://ntrs.nasa.gov

6.4. Krantz, Timothy; and Tufts, Brian: Pitting and Bending Fatigue Evaluations of a New Case-Carburized Gear Steel. NASA/TM—2007-215009 (ARL–TR–4123), 2007. http://ntrs.nasa.gov

6.5. Krantz, T.; Oswald, F.; and Handschuh, R.: Wear of Spur Gears Having a Dithering Motion and Lubricated With a Perfluorinated Polyether Grease. NASA/TM—2007-215008 (ARL–TR–4124), 2007. http://ntrs.nasa.gov

TABLE 6.1.—BASIC GEAR DIMENSIONS

Number of Teeth	42
Module, (Diametral Pitch); mm (1/in.)	2.12 (12)
Circular Pitch, mm (in.)	6.65 (0.2618)
Whole Depth, mm (in.)	4.98 (0.196)
Addendum, mm (in.)	2.11 (0.083)
Chordal Tooth Thickness mm (in.)	3.25 (0.1279)
Helix Angle (degrees)	0
Pressure Angle (degrees)	25
Pitch Diameter, mm (in.)	88.9 (3.50)
Outside Diameter, mm (in.)	93.14 (3.667)
Root Fillet, mm (in.)	1.02 (0.04)
Measurement over pins, mm (in.)	93.87 (3.6956)
Pin Diameter, mm (in.)	3.66 (0.144)
Backlash, mm (in.)	0.15 (0.006)
Tip relief, mm (in.)	0.015 (0.0006)

TABLE 6.2.—MASS OF THE TEST GEAR CHIPS

Chip Identification number	Mass (grams)
1	0.090
2	0.100
3	0.106
4	0.116
5	0.139
6	0.252
7	0.342
8	0.045
9	0.096
10	0.032

Figure 6.1.—Bench setup for gear chip engagement testing using the NASA Glenn Research Center Fatigue Rig.

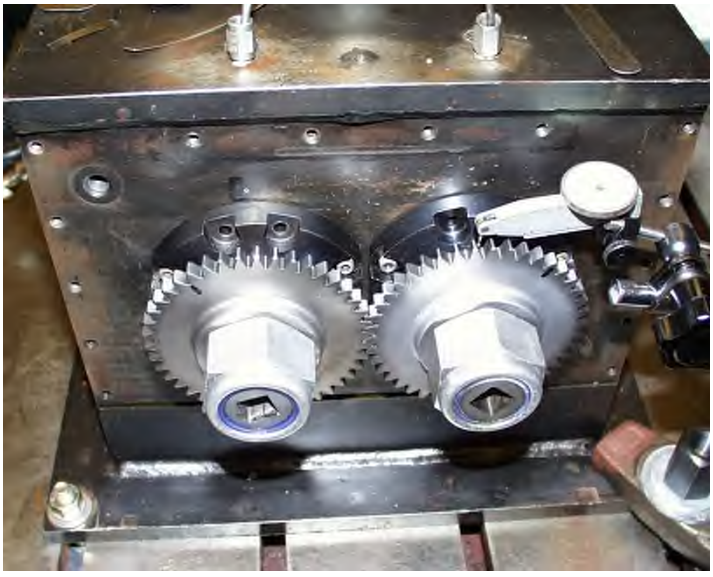

Figure 6.2.—Setup for backlash measurement using dial indicator.

Figure 6.3.—Example of shim and placement used for engagement testing.

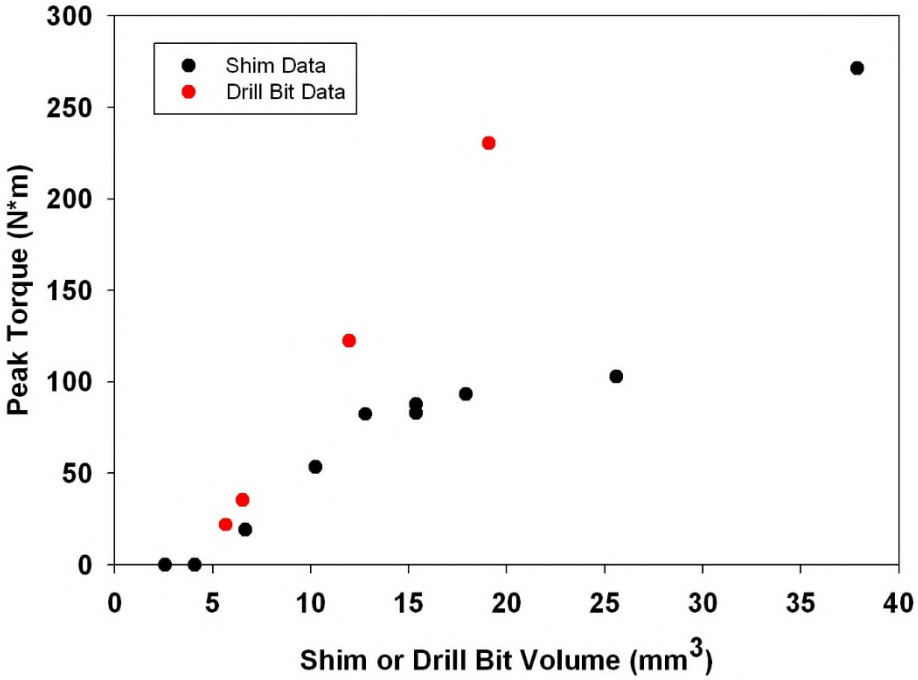

Figure 6.4.—Relationship of volume of engaged object to the peak torque required to rotate the gears for the NASA Glenn Research Center spur gear rig using 12-pitch case-carburized steel gears.

Figure 6.5.—Example of deformed shim stock after engagement of meshing gear teeth.

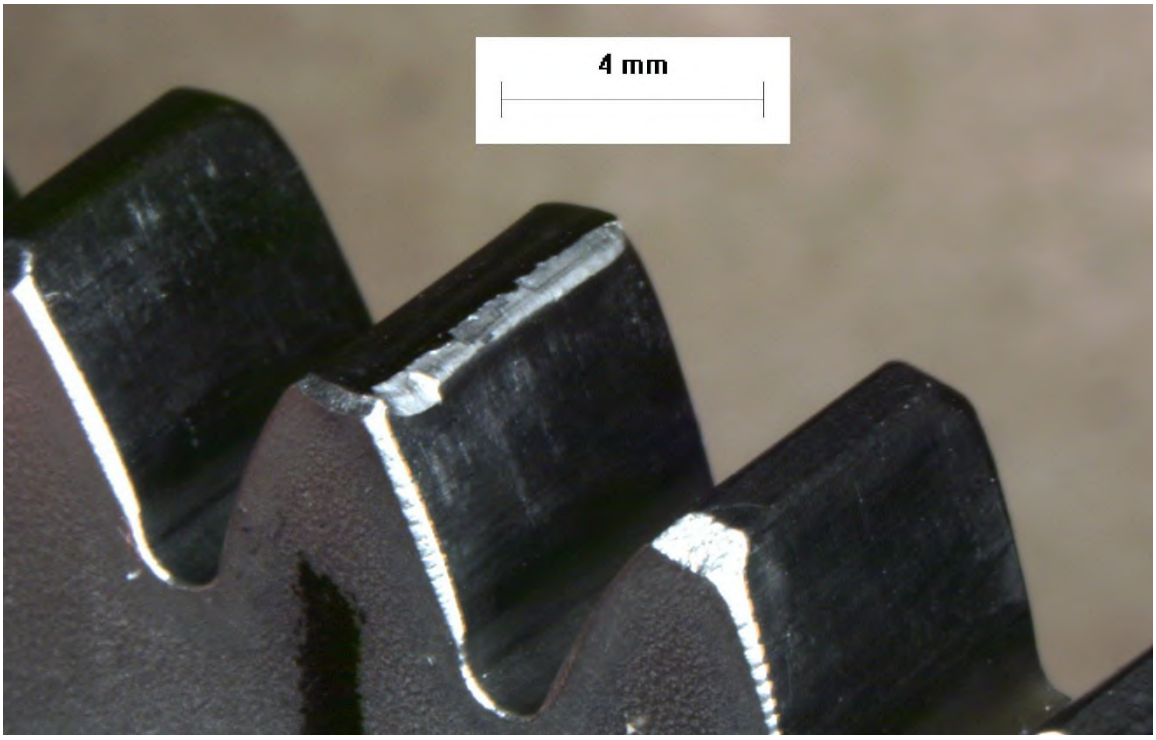

Figure 6.6.—Example of damaged tooth tip after engagement of 1.96-mm- (0.077-in.-) diameter drill bit shank.

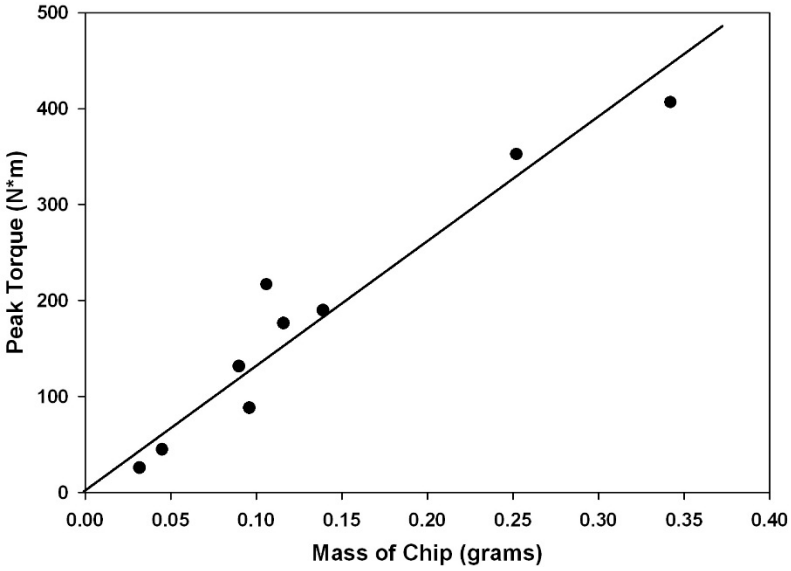

Figure 6.7.—Peak torque recorded during gear chip engagement testing on NASA Glenn Research Center bench test setup as a function of the mass of the engaged chip. The line is a linear regression of the data.

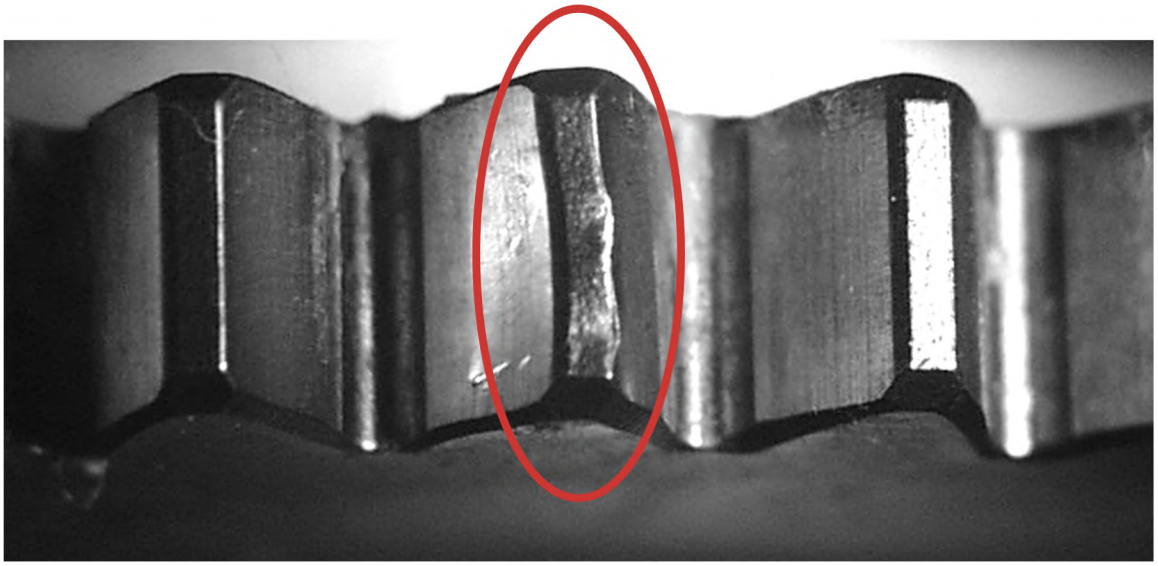

Figure 6.8.—Severely deformed gear tooth as result of engagement with largest chip tested, chip #7 having mass of 0.342 grams. The gears can no longer be rotated to engage and pass through this tooth using hand torque.

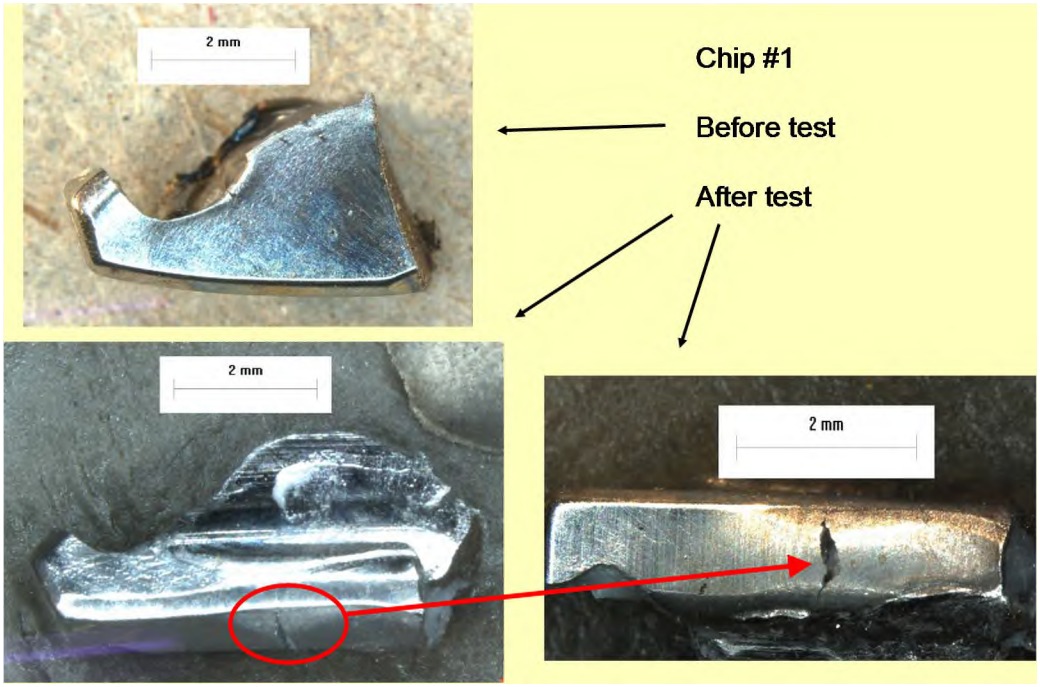

Figure 6.9.—Chip #1, mass of chip 0.090 grams.

Figure 6.10.—Chip #2, mass of chip 0.100 grams.

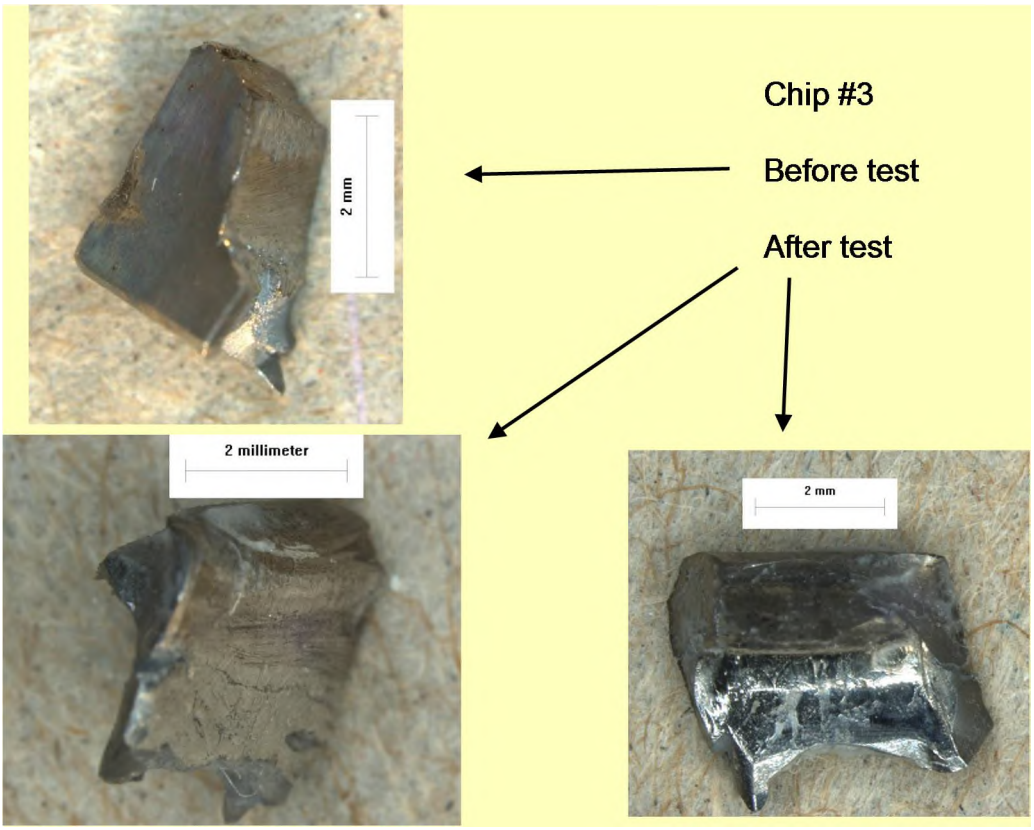

Figure 6.11.—Chip #3, mass of chip 0.106 grams.

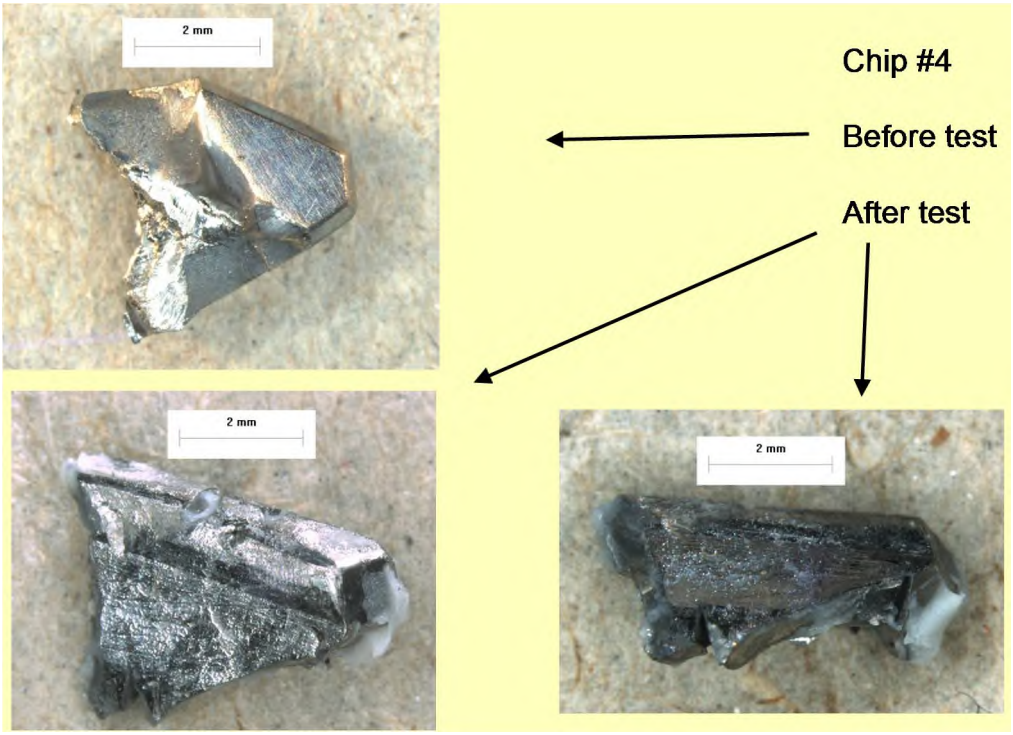

Figure 6.12.—Chip #4, mass of chip 0.116 grams.

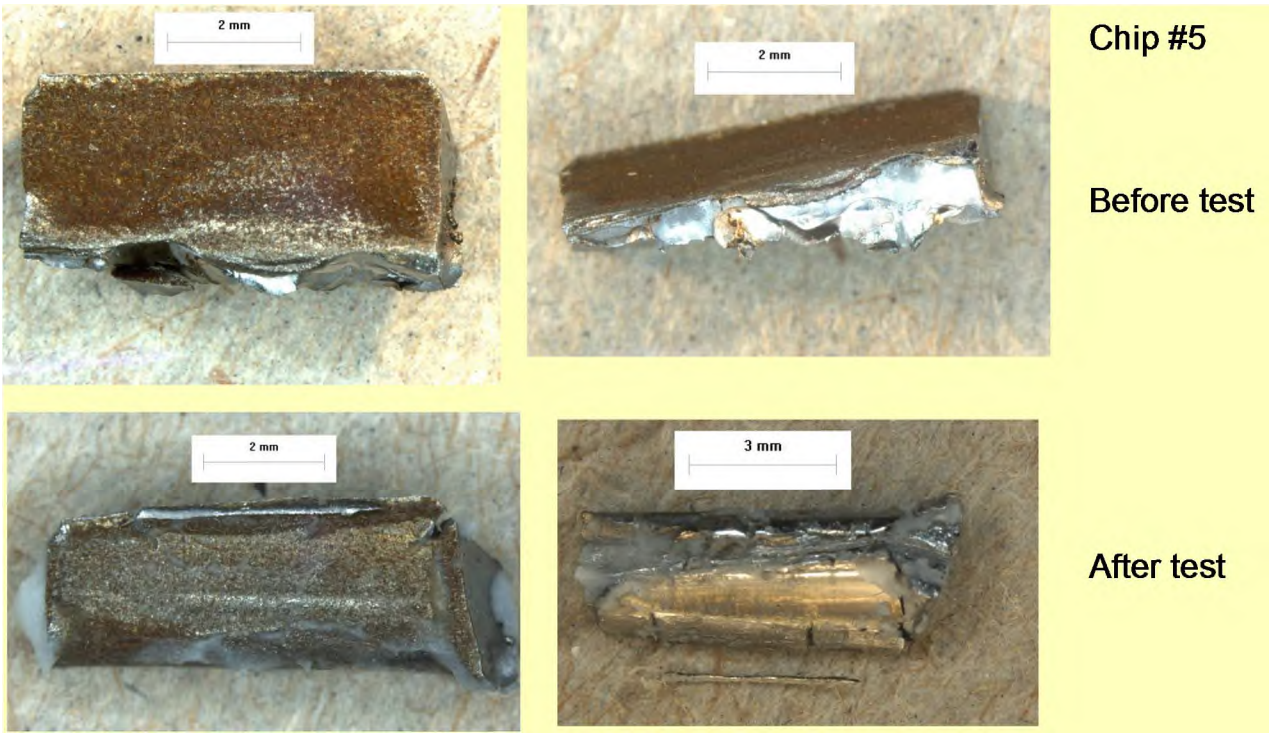

Figure 6.13.—Chip #5, mass of chip 0.139 grams.

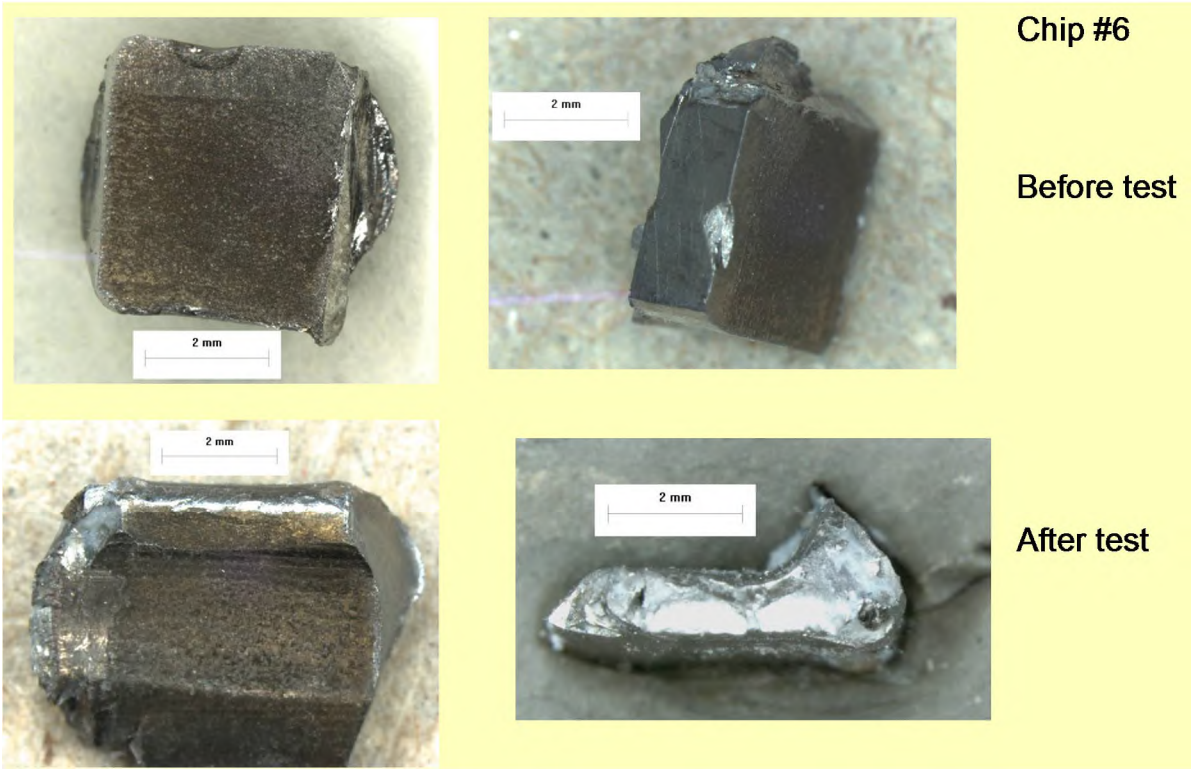

Figure 6.14.—Chip #6, mass of chip 0.252 grams.

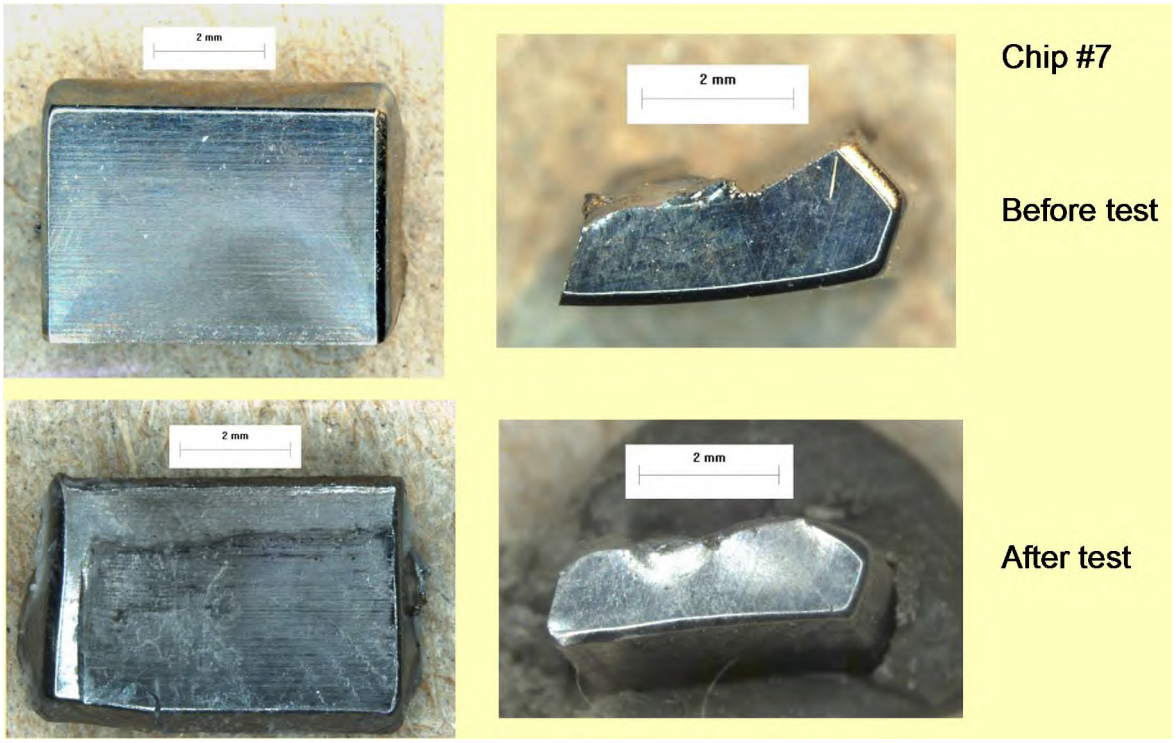

Figure 6.15.—Chip #7, mass of chip 0.342 grams.

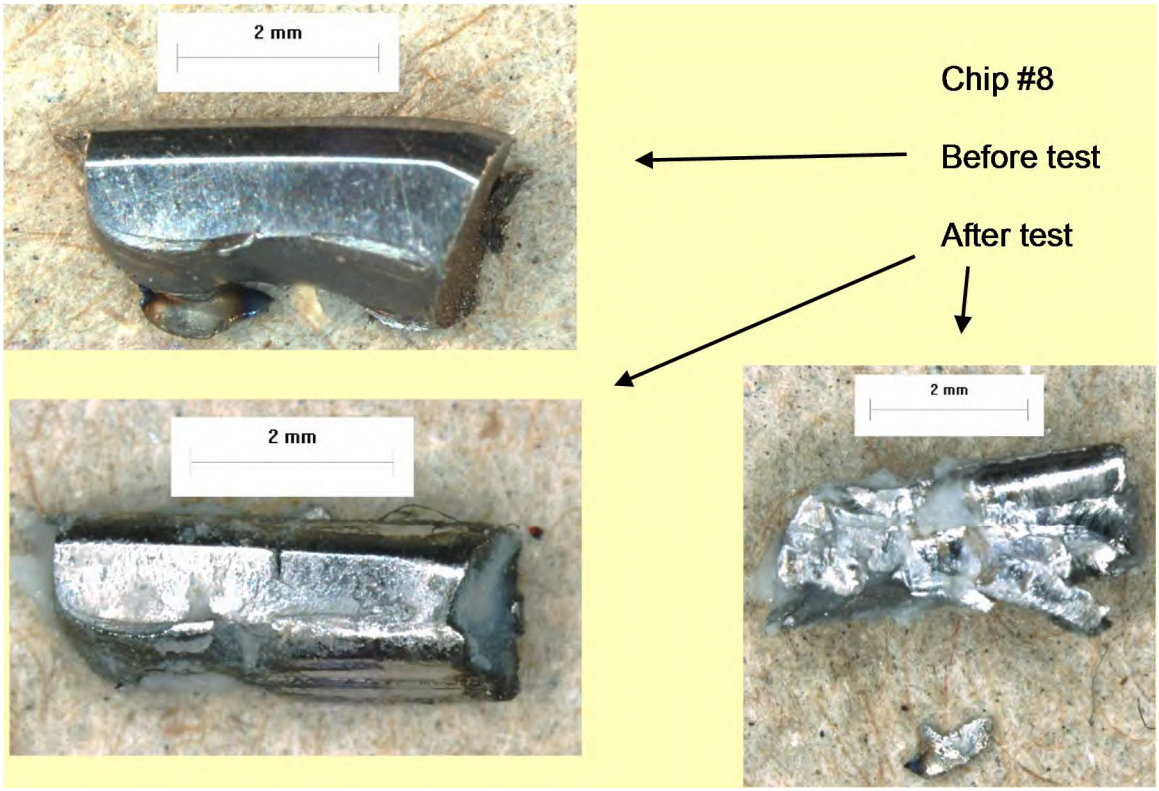

Figure 6.16.—Chip #8, mass of chip 0.045 grams.

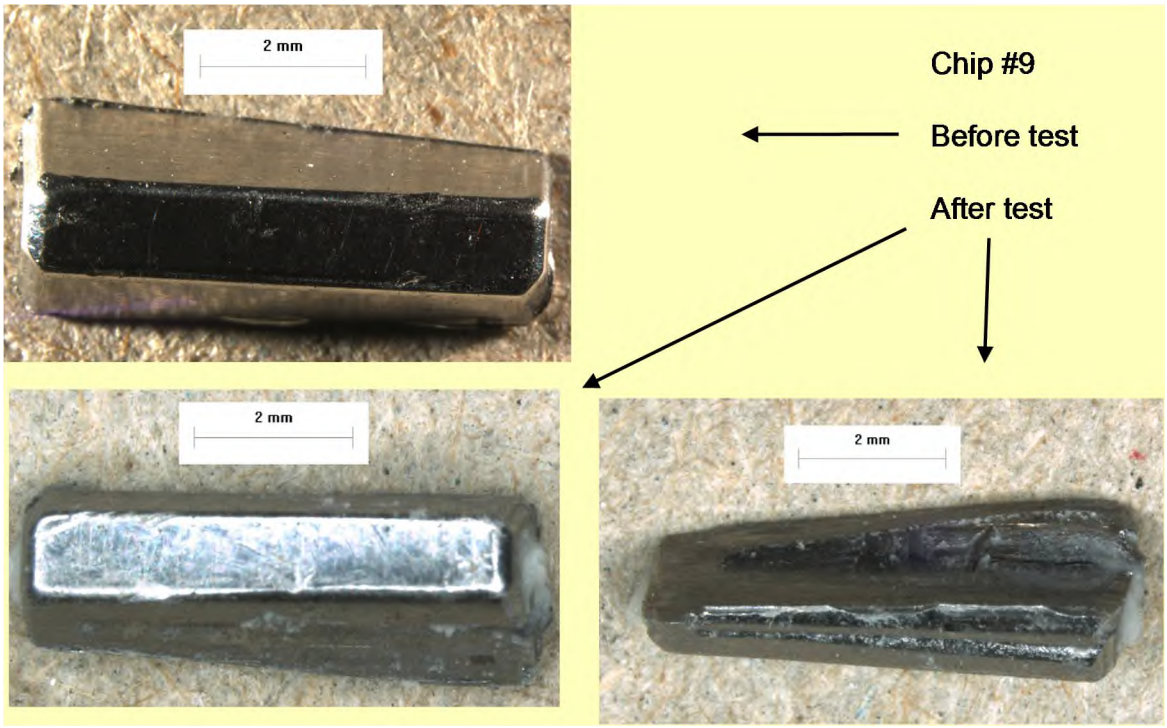

Figure 6.17.—Chip #9, mass of chip 0.096 grams.

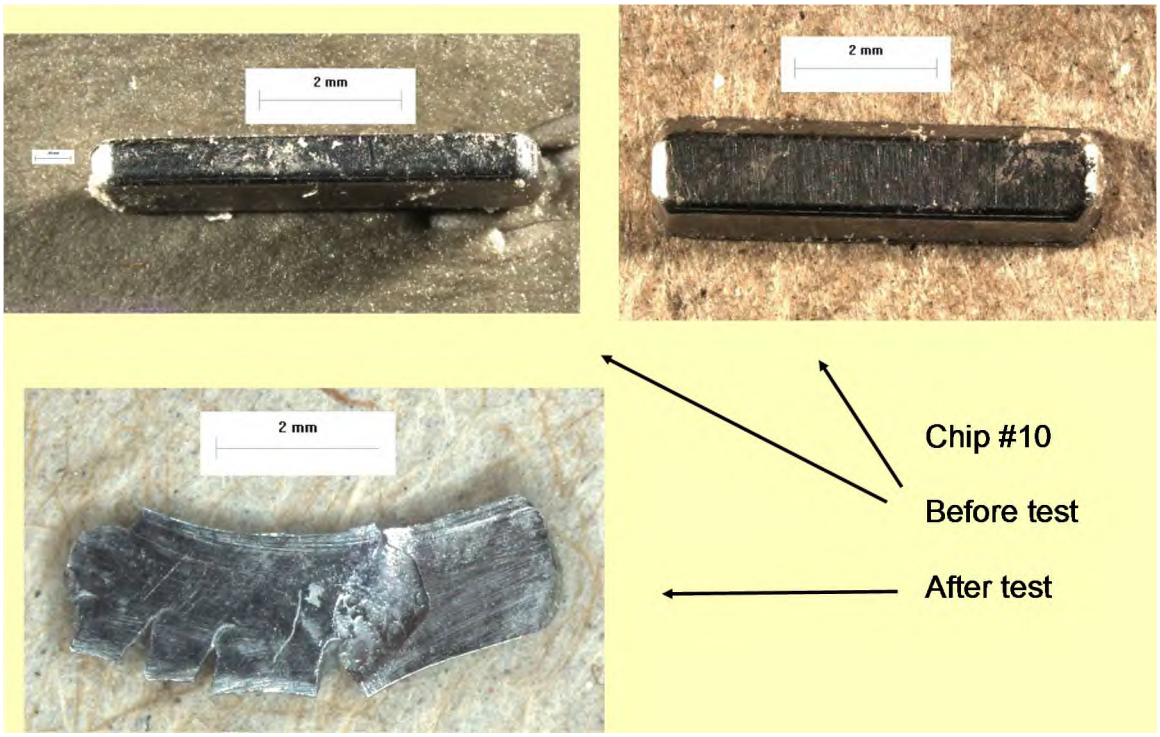

Figure 6.18.—Chip #10, mass of chip 0.032 grams.

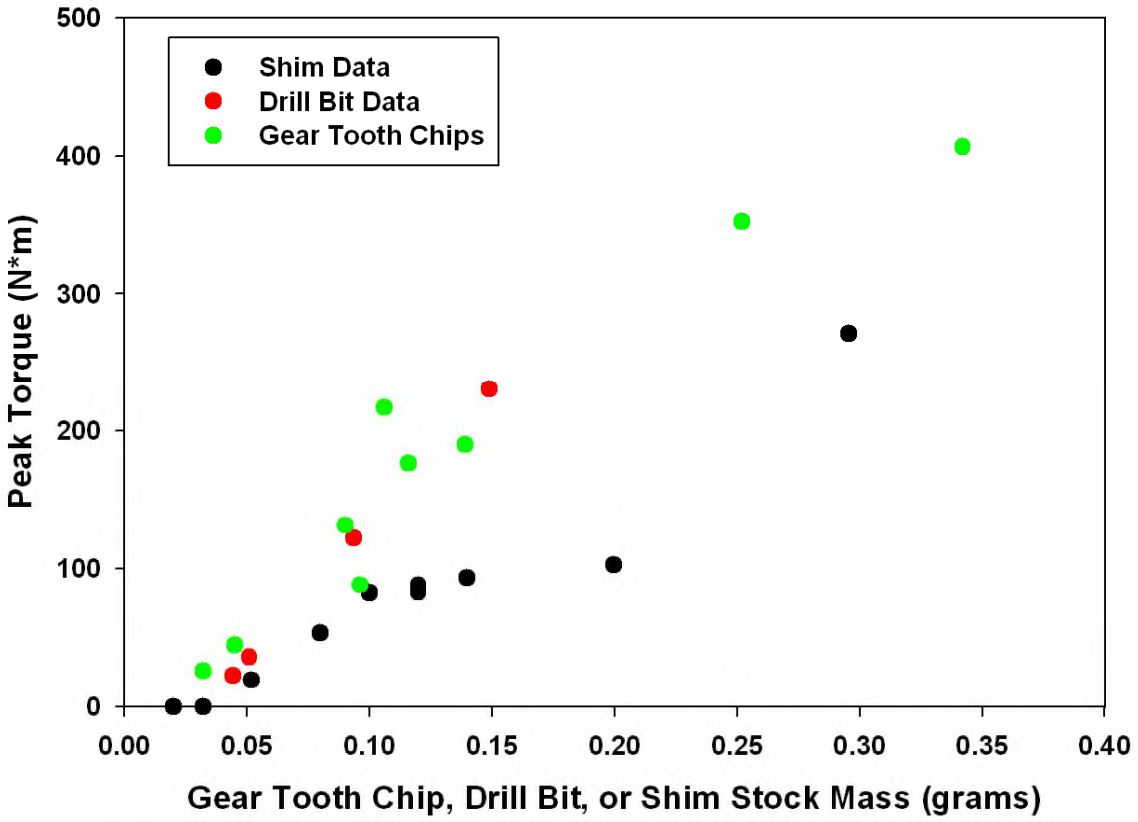

Figure 6.19.—Debris mass versus peak torque required to rotate the gear mesh.

Chapter 7: Performance and Analysis of Perfluoropolyalkyl Ether Grease Used on Space Shuttle Actuators—A Case Study

Wilfredo Morales, Kenneth W. Street, Jr., and Erwin V. Zaretsky
National Aeronautics and Space Administration
Glenn Research Center
Cleveland, Ohio 44135

Abstract

Actuators used on the U.S. space shuttle fleet are lubricated with unspecified amounts of Braycote 601 (Castrol Braycote) grease consisting of a perfluoropolyalkyl ether (PFPAE) base oil thickened with a polytetrafluoroethylene (PTFE) filler. Each shuttle has four body flap actuators (BFAs) (two on each wing) on a common segmented shaft and four rudder/ speed brake (RSB) actuators. The actuators were designed to operate for 10 years and 100 flights without periodic relubrication. Visible inspection of two partially disassembled RSB actuators in continuous use for 19 years raised concerns over possible grease degradation due to discoloration of the grease on several places on the surfaces of the gears. Inspection revealed fretting, micropitting, wear, and corrosion of the bearings and gears. A small amount of oil dripped from the disassembled actuators. Whereas new grease is beige in appearance, the discolored grease consisted of both grey and reddish colors. Grease samples taken from the actuators together with representative off-the-shelf new and unused grease samples were analyzed by gravimetry for oil content; by inductively coupled plasma spectroscopy (ICP) for metals content; Fourier transform infrared (FTIR) spectroscopy for base oil decomposition; and by size exclusion chromatography (SEC) for determination of the molecular weight distributions of the grease oil. The Braycote 601 grease was stable after 19 years of continuous use in the sealed RSB actuators and was fit for its intended purpose. There were no significant chemical differences between the used grease samples and new and unused samples. Base oil separation was not significant within the sealed actuators. No corrosive effect in the form of iron fluoride was detected. The grey color of grease samples was due to metallic iron. The red color was due to oxidation of the metallic wear particles from the gears and the bearings comprising the actuators.

Introduction

The U.S. space shuttle fleet was originally intended to have a life of 100 flights for each vehicle, over a 10 year period, with minimum scheduled maintenance or inspection. The first space shuttle flight was that of the Space Shuttle *Columbia* launched April 12, 1981. The disaster that destroyed the *Columbia* occurred on its 28th flight, February 1, 2003, nearly 22 years after first being launched. At that time as well as today, the Space Shuttle *Discovery* had the most flights. The 30th flight of the *Discovery* occurred August 10, 2001. This was approximately 17 years after its first flight launched August 30, 1984. As a result of the *Columbia* accident, concern was raised in July 2003 over possible grease degradation and wear of body flap actuators (BFAs) and rudder/speed brake (RSB) actuators rolling-element bearings made from AISI 52100 steel and gears made from AISI 9310. Visible inspection of the partially disassembled *Discovery* RSB actuators was made September 16, 2003.

Each shuttle has four BFAs (two on each wing) on a common segmented shaft and four RSB actuators. The BFA comprises a single planetary gear set. The RSB comprises two planetary gear sets. The BFAs control the position of the large body flap that controls the attitude of the shuttle. The RSB actuators act to extend the sides of the rudder to slow the shuttle on descent into the Earth's atmosphere. The sealed actuators are lubricated with space-qualified grade 2 perfluoropolyalkyl ether (PFPAE) grease and were designed to operate for life without periodic relubrication and maintenance (Ref. 7.1).

Many of these actuators were without maintenance in excess of 20 years. During actuator refurbishment and inspection, there were external signs of corrosion on one of the RSB actuators. Pitted gears and discolored grease were observed inside. The grease-lubricated ball bearings and gears making up the actuators exhibited various degrees of wear. Both the bearings and gears operated under a dithering (rotation reversal) motion in the actuators when these systems were powered during ground operations (Ref. 7.1). Grease samples taken from the disassembled actuators ranged in color from beige taken from one actuator to grey and red taken from the second actuator. Beige is the original grease color. In addition, a small amount of oil dripped from one of the disassembled actuators.

Two studies were conducted by Oswald et al. (Ref. 7.1) and Krantz et al. (Ref. 7.2) to experimentally duplicate the operating conditions of the space shuttle actuator gears and input shaft ball bearings and determine their usable life. The results were compared to field data from the space shuttle fleet to establish actuator life and reliability.

The disassembled actuators presented a unique opportunity to assess the condition of the grade 2 PFPAE grease that had been in use for at least 20 years lubricating the bearings and gears inside these actuators. One primary area of concern was the extent of base oil separation from the grease thickener leading to less than adequate lubrication. The other area of concern was base oil degradation and its effect on the condition of the grease and its ability to provide effective lubrication.

A search of the literature reveals a large amount of qualitative wear data that has been generated on an assortment of laboratory testers over a period of decades. Equations and analysis exist together with friction and wear data to allow for calculating lubricant film thickness, lubrication operating regime, and the qualitative severity of the wear (Refs. 7.3 to 7.5). However, there is no definitive analysis that allows an engineer to predict, with any degree of engineering certainty, the quantity of wear or the applicable usable life of a specific lubricant (grease) that can occur in a specific application. Quantitative results need to be obtained experimentally for specific applications (Ref. 7.1).

Ohno et al. (Ref. 7.6) tested two greases used for space applications and their respective base oils. All tests were done under ambient laboratory temperature and air atmosphere. One of the greases was the same or similar PFPAE grease to that used for the space shuttle actuators. Tests were performed in order to characterize the rheological base oil behavior of each grease versus pressure and temperature. Longer ball bearing fatigue life was obtained with the PFPAE grease than with the PFPAE base oil (Ref. 7.6).

Analysis showed that the viscosity of the PFPAE base oil, containing perfluoromethyl- and perfluoroethyl- ether groups (-(CF_2)O-) and (-$(CF_2)_2$O-), was lowered by the high shear rates in the elastohydrodynamic (EHD) Hertzian contact. Ohno et al. (Ref. 7.6) concluded that the PFPAE base oil decomposes, generating acid fluoride, which then hydrolyzes to hydrogen fluoride by reacting with water moisture. As a result, the formation of the hydrogen fluoride shortens bearing life by forming metal fluorides when run with only the base oil. However, for the PFPAE grease, viscosity loss of the base oil did not occur (i.e., no base oil decomposition) resulting in longer bearing life (Ref. 7.6).

In a continuation of the research reported in Reference 7.6, Ohno et al. (Ref. 7.7) performed bearing fatigue tests of the PFPAE base (815Z) oil and multiply alkylated cyclopentane (MAC 2001A) base oil in air and vacuum environments. The test oils were analyzed to determine whether changes occurred as a result of operating in air and in a vacuum. In vacuum, the PFPAE base (815Z) oil had a longer fatigue life than the MAC 2001A oil. However, in an air environment, the MAC 2001A had a longer fatigue life than the PFPAE base (815Z) oil.

In the study by Krantz et al. (Ref. 7.2), spur gear pairs made from AISI 9310 steel, the same material used for the actuator gears without surface coatings, were lubricated with the grade 2 PFPAE grease. The gear pairs were loaded to a maximum Hertz stress of 1.1 GPa (160 ksi) and operated under a dithering motion at ambient (room) temperature and atmosphere. The gears were run from 20,000 to 80,000 total dithering cycles. The wear rate for these spur gears “was on the order of 600 times greater than referenced data for oil-lubricated gears” using six different polyol esters and one polyalkylene glycol based oil (Ref. 7.2). In a related study, Krantz et al. (Ref. 7.8) lubricated spur gear pairs with PFPAE grease and ran them under different atmospheres. The tests conducted under ambient air or dry air produced reddish

colored debris in the PFPAE grease, whereas tests conducted in dry nitrogen (N_2) produced grey colored debris in the grease. Neither the reddish nor the grey colored debris were chemically identified.

In view of the aforementioned, the objectives of the work reported herein were to (a) determine long-term stability of grade 2 PFPAE grease in the space shuttle actuators; (b) quantify base oil separation from the actuator grease samples; (c) identify base oil degradation in order to assess actuator grease performance; and (d) identify the grey and reddish colored materials in the grease samples taken from the actuators.

Apparatus, Specimens, and Procedure

Rudder/Speed Brake (RSB) Actuator

The RSB actuator system is contained in the space shuttle orbiter tail section shown in Figure 7.1. The RSB actuator system comprises a Power Drive Unit (PDU) and four RSB actuators. The system controls the rudder/speed brake panels through the four actuators that are driven by the single PDU.

A schematic of the RSB actuator is shown in Figure 7.2. The actuators are designed to provide both rudder and speed brake (S/B) functions by a split design in the vertical tail section shown in Figure 7.1 in which two input shafts enter the actuator – one at each end. By rotating the shafts in the same direction, the panels are moved concurrently for rudder function. When the input shafts rotate in opposite directions, the panels move apart for S/B function. Both rudder and S/B functions can be used simultaneously.

The gears comprising the actuators were manufactured from AISI 9310 steel. Typical chemical content for the AISI 9310 steel is as follows: 3.0 to 3.5 percent Ni; 0.45 to 0.65 percent Mn; 1.0 to 1.4 percent Cr; 0.08 to 0.15 percent Mo; and the balance, Fe. Most, if not all, of the AISI 9310 gears were coated with manganese phosphate.

Manganese phosphate coatings were introduced in the 1940s as an anti-rust process. It forms a crystalline coating on the steel surface by taking advantage of the surface pH while etching the steel surface (Ref. 7.9). Recently, it was reported by Chen et al. (Ref. 7.9) that the coating decreases wear and increases the contact fatigue life of steel gears.

The actuators' rolling-element bearings were manufactured from AISI 52100 steel. Typical chemical content for AISI 52100 steel is 0.95 to 1.1 percent C; 0.2 to 0.5 percent Mn; ≤ 0.35 percent Si; ≤ 0.025 percent S; nil Ni; 1.3 to 1.6 percent Cr; and the balance, Fe. Coatings were not applied to the AISI 52100 rolling-element bearings.

Lubricant

The mechanical actuators used on the space shuttle are lubricated by Braycote 601, a space-rated, grade 2 grease containing a perfluoropolyalkyl ether (PFPAE) base oil, a Z-type fluid, with small polytetrafluoroethylene (PTFE) particles as a thickener, and sodium nitrite and dimethyloctyldecylbenzyl ammonium bentonite as rust and corrosion inhibitors. It is formulated to a buttery smooth consistency of grade 2 grease, hence the ratio of oil to PTFE thickener may vary slightly from lot-to-lot due to the thickening ability of the variations in PTFE. The grease manufacturer does not have data on the particle size range or shape of the PTFE telomeres used for thickening.

The PFPAE base oil itself is a low molecular weight polymeric liquid having an average molecular weight of 9400 atomic mass units (amu). The grease has a wide operating temperature range: –80 to 200 °C (–112 to 400 °F). The viscosity of the lubricant base oil at the three temperatures used for this test program, 24, 60, and 74 °C (75, 140, and 165 °F), is approximately 4750, 128, and 77 cSt, respectively. Gschwender and Snyder (Ref. 7.10) provide an excellent overview of the properties of this and other PFPAE base oils. The grease does not contain reactive extreme pressure additives that are typically added to hydrocarbon grease because these additives will not dissolve in the base oil (Ref. 7.11). Although

considerable advances in PFPAE-soluble additives have been made since the grease in question was formulated in the early 1980's, none are in use to date.

New (unused) grease has a beige color. Grease samples removed from two of the four disassembled actuators ranged in color from beige to grey (taken from RSB–403), and red (taken from RSB–405). In addition, a small amount of oil dripped from the disassembled actuators. These samples of grease along with representative virgin grease samples were analyzed for base oil content, for metals content, and for signs of base oil decomposition.

Gravimetric Analysis

Gravimetric analysis was performed on various grease samples to determine the amount of base oil and solid filler material in the grease samples. A fluorinated solvent, 1,1,2-trichlorotrifluoroethane (TCTF), was used to dissolve and extract the base oil from pre-weighed grease samples leaving behind solid residue. The solid residue was dried and weighed and this weight was then subtracted from the original grease weight resulting in the weight of the base oil. Both the residue (for the grey and reddish greases, the residue weight was corrected for the wear metal content as described later) and base oil weights were converted to percentages. This procedure was performed on used grease samples taken from the shuttle actuators as well as unused PFPAE grease samples manufactured in the years 1987, 1988, 1994, and 2004.

Insoluble Fraction Analysis

The weighed residue from the fluorinated solvent extraction was transferred to a PTFE beaker. This residue was then heated to just below boiling with 3 ml of 6 molar hydrochloric acid, followed by 3 ml of 6 molar nitric acid and finally with 3 ml of 6 molar hydrofluoric acid. The solutions were not boiled to prevent loss of volatiles such as SiF_4. The sample was then filtered through a pre-weighed PTFE filter. The filter was dried and weighed to obtain the acid soluble content by difference in the weight. The acid soluble sample filtrate was then subjected to Inductively Coupled Plasma (ICP) analysis for the metals contained in AISI 9310 gear steel, sodium (from sodium nitrite additive in the grease formulation), aluminum and silicon (from the bentonite additive in the grease formulation), and phosphorus from the manganese phosphate coatings on the AISI 9310 gears.

Fourier Transform Infrared (FTIR) Spectroscopy Analysis

Infrared spectra were collected with a FTIR spectrometer equipped with a standard deuteratedtriglycine sulfate (DTGS) detector. Spectra were acquired over the range of 650 to 4000 cm^{-1} at 4 cm^{-1} wavenumber resolution in transmittance mode through samples of neat grease pressed between potassium chloride (KCl) windows to the appropriate thickness. Typically, between 100 and 250 scans were averaged, converted from transmittance to absorbance and corrected to remove baseline curvature and water vapor and carbon dioxide absorption bands where necessary.

Size Exclusion Chromatography Analysis

Size exclusion chromatography (SEC), a molecular separation technique, was performed on both unused and used grease samples. A weighed amount of grease, 10 mg, was added to 3 ml of TCTF in a 5 ml sample bottle with a PTFE lined cap. After shaking the bottle until all the grease disintegrated, the contents were filtered through a 0.5 μm PTFE filter, collected and a 100 μl aliquot was injected in the SEC unit. The SEC unit utilized the fluorinated solvent as the mobile phase running at 1.0 ml per min through one 500 Å and one 100 Å size exclusion columns in series and then through a refractive index detector where the separated molecules were detected and recorded as peaks.

Results and Discussion

The U.S. space shuttle fleet was originally intended to have a life of 100 flights for each vehicle, over a 10 year period, with minimum scheduled maintenance or inspection. The first space shuttle flight was that of the Space Shuttle *Columbia* launched April 12, 1981. The disaster that destroyed the *Columbia* occurred on its 28th flight, February 1, 2003, nearly 22 years after first being launched. At that time as well as today, the Space Shuttle *Discovery* had the most flights. The 30th flight of the *Discovery* occurred August 10, 2001. This was approximately 17 years after its first flight launched August 30, 1984.

Each shuttle has four BFAs (two on each wing) on a common segmented shaft and four RSB actuators shown in Figures 1 and 2. The actuators are lubricated with Braycote 601 grease consisting of perfluoropolyalkyl ether (PFPAE) base oil thickened with a polytetrafluoroethylene (PTFE) filler. The actuators were designed to operate for their design life (10 years) without periodic relubrication. However, some had been in continuous use for over 20 years without inspection and relubrication. This was in contrast to commercial aircraft actuators that are refurbished every 2 1/2 to 3 years. Even for light duty, it is good engineering practice to replenish the grease in a system on a periodic basis and not for a period longer than 5 years. This is because, with time, the liquid (oil) separates from the grease (thickener). When approximately 50 percent of the liquid is lost, the grease is referred to as “dead grease” and is generally no longer effective in providing reliable lubrication (Ref. 7.12).

In July 2003, as a result of the *Columbia* accident, concern was raised over possible grease degradation and wear of *Discovery* RSB actuators. Inspection of the actuators revealed fretting, micropitting, wear, and corrosion of the bearings and gears. The condition of these components suggested the need to replace the *Discovery* RSB actuators before its return to flight.

For the remaining actuators in the space shuttle fleet, work performed under simulated operating conditions by Oswald et al. (Ref. 7.1) and Krantz et al. (Ref. 7.2) established with reasonable engineering and statistical certainty the life and reliability of the space shuttle actuator gears and input shaft ball bearings. However, concerns remained over possible grease degradation due to discoloration of the grease on several places on the surfaces of the gears. New (unused) grease has a beige color. Grease samples removed from two of the four disassembled actuators ranged in color from beige to grey taken from one actuator, and red taken from the second actuator. In addition, a small amount of oil dripped from the disassembled actuators. How long can the Braycote 601 grease remain in situ in the actuators and still be fit for its intended purpose? The answer to this question would, together with the results from References 7.1 and 7.2, determine whether some or all of the actuators on the remaining space shuttles would be replaced and/or refurbished before being returned to space.

In order to answer the question regarding the long-term viability of the grease, grease samples were taken from the *Discovery* actuators, a Hamilton Sundstrand qualification unit, and representative off-the-shelf virgin grease. These samples were analyzed by gravimetry for oil content; inductively coupled plasma spectroscopy (ICP) for metals content; Fourier transform infrared (FTIR) spectroscopy for signatures of base oil decomposition; and SEC for determination of the molecular weight distributions of the grease oil.

Gravimetric Analysis

A gravimetric analysis of the unused grease samples was performed and is summarized in Table 7.1. Referring to Table 7.1, the weight percent oil for the unused grease samples ranged from 70.7 to 77.3 percent. Duplicate analysis of the 1994 grease sample yielded good precision for this analysis. This suggests that the variation in the results for these unused greases is correct and that the variation is likely associated with the grease formulation. The grease manufacturer indicated that the grease formulation process has not changed over the years; however, the oil to thickener ratio may vary slightly as discussed previously. The only used beige grease falling outside this range was from the HS Qual Unit with unknown history. The RSB–403 grey samples fell within this range although the grey and red samples from RSB–405 did not as these results are skewed by the presence of large amounts of metal (especially iron) in the residue detected by ICP metal analysis described and discussed below.

Taking the metal content for the RSB–405 reddish grease into account from Table 7.2 (Cr, Fe (calculated as Fe or Fe_2O_3—see below), Mn, and Ni), all components of 9310 steel as well as P (calculated as PO_4) from the phosphating revises the total residue weight from 20.3 mg to possibly as low as 6.1 mg (based on Fe as Fe_2O_3) or 9.9 mg (based on Fe as elemental Fe). The Cu is not part of the 9310 or 52100 steel but is also not a component of the virgin grease, hence it too was subtracted from the TCTF insoluble residue weight. This would revise the oil content to 89 or 84 percent base oil, respectively. These high percentage oil numbers are perhaps the result of only a small sample being available for analysis, but from this we can conclude that calculations of the amount (percentage) of oil loss by determining filler content can lead to potentially large errors in the direction of oil loss if not corrected for wear metal content. No information was available to determine if correction should be based on Fe as the metal or as oxide other than color. Small amounts of the oxide may have colored over the grey, which would have been present if some of the Fe was as metal. The grey grease is an unambiguously elemental Fe contaminant and when a similar correction is applied, the grey grease oil content from RSB–403 becomes 82 and 84 percent, which would be in line with the red grease if most of the Fe in it was as elemental Fe. For reference, if we apply a similar correction to the unused greases that also have normal iron contaminant, it raises their oil content by a percent or two as well. Removal of the Fe from the unused grease is incorrect since virgin grease also contains iron, thus begging the question "exactly how much of the Fe in the used colored greases is original grease contaminant and how much is wear metal?" The amount of Fe in the grey and red grease clearly requires correction but because there is no way of telling the Fe sources apart, the corrections applied above are overcompensations on the order of a few percent more oil. To provide perspective, for a grease initially containing 75 percent oil to be "dead" as previously defined, the percent insoluble fraction from the grease alone would be 40 percent plus any content from wear metals. The results of gravimetric tests for red or grey grease show that base oil depletion through tribological destruction was not significant for over two decades of use. Further, separation of oil from the beige actuator grease was not significant after two decades within the sealed actuators.

ICP Metal Analysis

Unused PFPAE grease was analyzed for metal content and is summarized in Table 7.2. The analysis yielded several percent of the original TCTF insoluble residue as acid soluble (Table 7.2). Very small amounts of iron were found, which may be a contaminant of another component in the grease such as the bentonite mineral. The majority of the residuals were sodium (from the sodium nitrite) and aluminum and silicon from the bentonite, $Al_2Si_4O_{12}H_2 \cdot xH_2O$ (Ref. 7.13).

The analysis of the grey grease sample (Table 7.2) contained substantial amounts of Na, Al, and Si as compared to iron. This would suggest that a small amount of wear metal contamination relative to the grease additive materials is in this grey grease sample supporting the above discussion. The red grease sample (Table 7.2) contained significant amounts of iron plus traces of other components of AISI 9310 steel, including Ni, indicating that a large fraction of the acid soluble material contained wear metal. The

52100 steel used in the bearings has negligible Ni content implying that the metallic debris is gear material. The amounts of Na, Al, and Si were considerably lower than the amount of iron in this sample although Na, Al, and Si were still in the same relative ratio with respect to each other as in the unused grease residue and the grey grease residue, again supporting the gravimetric analysis discussion. Analysis of the undissolved solids from RSB–403 (beige) and the HS Qual Unit (beige) showed negligible iron (1.8 and 1.3 percent, respectively, of the residue weight) and amounts of Na, Al, and Si similar to the unused grease samples.

The virgin grease, used as a comparative baseline, had Na, Al, and Si, the last two being in correct additive ratios. The grey and brown colored grease from the actuators in addition to Na, Al, and Si, had around 8 to 10 percent Fe, 5.3 percent Mn, and 4.1 percent P. In this grease the Fe and Mn are not in correct ratio for 9310 steel but are more likely attributed to the gear phosphating process leaving a surface manganese phosphate rich layer, which was removed prior to disintegration of the gear metal. The actuators with the red grease in addition to Na, Al, and Si, had 43 percent Fe, 2 percent Ni, 3.7 percent Mn, and 3 percent P, which are explained similarly to the grey grease above. Nickel is not a component of AISI 52100 steel although it cannot be concluded that all the wear debris came from the AISI 9310 gears.

It was concluded that the grey color in the grease sample was due to metallic iron and that the red color was due to oxidation of the wear particles from the gears and the bearings comprising the actuators. Small amounts of the wear metals were submitted to x-ray diffraction to see if metal oxides or fluorides could be detected. Some iron oxides and no metal fluorides were detected although the samples were too small for rigorous analysis.

FTIR Spectroscopy

Figure 7.3 is the FTIR spectra of virgin and used grease. In these spectra we examine the regions between 1900 to 1700 cm^{-1} and between 3700 and 3400 cm^{-1}. The peak in the 1800 cm^{-1} range would be indicative of the carbonyl band formation due to oxidation of a carbon backbone in a lubricant or the formation of acid fluorides, both degradation products associated with the PFPAE based greases. The peaks found between 3700 to 3400 cm^{-1} would be indicative of the acid fluoride formation. While the acid fluorides are quite volatile, they are also quite reactive to both water and metals. Direct attack of the acid fluorides with metals in the absence of water would yield less volatile organo-metallic compounds readily observable in the 1550 to 1650 cm^{-1} and near 1400 cm^{-1} regions of the IR (Refs. 7.14 and 7.15).

No difference was observed between the used and unused greases in these locations of the IR spectra, suggesting little or no degradation by these pathways was observed over the decades of operation in the actuators. Unfortunately, these compounds may not have survived in the grease if the grease was exposed to vacuum prior to reaction with metals so degradation still could have occurred. As previously stated, no evidence of the more stable metal fluorides was found. If there was degradation of the grease, it would have occurred in the Hertzian contact areas of the bearings and gears. Unfortunately, we were not able to retrieve grease samples from these contact areas.

Size Exclusion Chromatography (SEC)

In SEC analysis, various substances dissolved in the mobile phase solvent are physically separated from each other based on their molecular size (or weight). Larger molecules are eluted first from the separatory column followed by medium and then smaller molecules. The set of columns used in this study were capable of separating six different standard substances ranging in molecular weight from >2 million to 92 amu.

SEC analysis has been successfully used to show PFPAE base oil decomposition. Figure 7.4 shows the results of a study (Ref. 7.16) where a new PFPAE base oil sample was catalytically decomposed by aluminum oxide at elevated temperatures. The changing patterns in the chromatograms indicate decomposition of the PFPAE base oil to smaller molecular weight products. The x axis (retention time in minutes) is approximately related to the logarithm (base 10) of the molecular weight, with higher

molecular weight compounds having shorter retention times. The y-axis (refractive index, RI, units) indicates the approximate concentration of the compound. In other words, the SEC plot reveals the molecular weight distribution and concentration of individual polymer components comprising the sample material as all chromatograms were run on the same RI scale.

Figure 7.5 shows the SEC chromatograms of the oil from the actuator RSB–403 grey and RSB–405 red grease samples in addition to a PFPAE control sample, 2004 unused Braycote grease. All three chromatograms, when normalized to the chromatographic peak, completely overlap at all locations. No noticeable degradation of the base oil occurred in the samples analyzed. Lighter degradation fragments from end group cleavage (Ref. 7.10) may have volatilized off during vacuum exposure leaving slightly lower molecular weight fragments having very low volatility. The remarkable correspondence in these chromatograms gives great confidence that no degradation occurred. Degradation would have skewed these chromatograms toward slightly lower molecular weights resulting from the end group cleavage pathway, which would not have volatilized and would be readily apparent in the chromatographic overlays.

Summary of Results

The U.S. space shuttle fleet was originally intended to have a life of 100 flights for each vehicle, over a 10 year period, with minimum scheduled maintenance or inspection. Each shuttle has four body flap actuators (BFAs) (two on each wing) on a common segmented shaft and four rudder/speed brake (RSB) actuators. The actuators are lubricated with Braycote 601 grease consisting of perfluoropolyalkyl ether (PFPAE) base oil thickened with a polytetrafluoroethylene (PTFE) filler. The actuators were designed to operate for their design life of 10 years and 100 flights without periodic relubrication or inspection. Some actuators had been in continuous use for over 20 years. Visible inspection of two partially disassembled RSB actuators, however, raised concerns over possible grease degradation due to discoloration of the grease on several places on the surfaces of the gears. Inspection also revealed fretting, micropitting, wear, and corrosion of the bearings and gears. The objectives of the work reported were to determine long-term stability of grade 2 PFPAE grease in the space shuttle actuators; quantify base oil separation from the actuator grease samples; identify base oil degradation in order to assess actuator grease performance; and identify the grey and reddish colored materials in the grease samples taken from the actuators. The following results and conclusions were obtained:

(1) The Braycote 601 grease consisting of perfluoropolyalkyl ether (PFPAE) base oil thickened with a polytetrafluoroethylene (PTFE) filler was stable after 19 years in the sealed RSB actuators and was fit for its intended purpose.

(2) Both FTIR and SEC analyses show no significant chemical differences between the used grease samples taken from the sealed RSB actuators after 19 years of use and new, unused samples of the same grease.

(3) Gravimetric tests from the actuator PFPAE grease show that neither base oil consumption nor separation was significant within the sealed actuators.

(4) The grey color of grease samples taken from the shuttle actuators was due to metallic iron. The red color was due to oxidation of the metallic wear particles from the gears and the bearings comprising the actuators.

References

7.1 Oswald, Fred B., et al.: Probabilistic Analysis of Space Shuttle Body Flap Actuator Ball Bearings. Trib. Trans., vol. 51, no. 2, 2008, pp. 193–203.

7.2 Krantz, Timothy; Oswald, Fred; and Handschuh, Robert: Wear of Spur Gears Having a Dithering Motion and Lubricated With a Perfluorinated Polyether Grease. NASA/TM—2007-215008, 2007. http://ntrs.nasa.gov

7.3 Bhushan, B., ed.: Modern Tribology Handbook. Vol. 1, CRC Press, Boca Raton, FL, 2000.

7.4 MacGregor, Charles Winters: Handbook of Analytical Design for Wear. Plenum Press, NY, 1964.

7.5 Booser, E.R., ed.: CRC Handbook of Lubrication: Theory and Practice of Tribology, Volume II: Theory and Design. CRC Press, Boca Raton, FL, 1983.

7.6 Ohno, N., et al.: Bearing Fatigue Life Tests in Advanced Base Oil and Grease for Space Applications. Proceedings of STLE 62nd Annual Meeting & Exhibition, Philadelphia, PA, 2007.

7.7 Ohno, Nobuyoshi, et al.: Bearing Fatigue Life Tests of Two Advanced Base Oils for Space Applications Under Vacuum and Atmospheric Environments. Tribol. T., vol. 54, no. 6, 2011, pp. 859–866.

7.8 Krantz, Timothy L.; and Handschuh, Robert F.: A Study of Spur Gears Lubricated With Grease—Observations From Seven Experiments. NASA/TM—2005-213957 (ARL TR–3159), 2005. http://ntrs.nasa.gov

7.9 Chen, Y.; Yamamoto, A.; and Omori, K.: Improvement of Contact Fatigue Strength of Gears by Tooth Surface Modification Processing. Proceedings of the 12th World Congress in Mechanism and Machine Science, Besancon, France, 2007.

7.10 Gschwender, Lois J.; and Snyder, Carl E., Jr.: U.S. Air Force Perfluoropolyalkylether Experiences. Trib. Trans., vol. 52, no. 2, 2009, pp. 165–170.

7.11 Carre, David J.: The Performance of Perfluoropolyalkylether Oils Under Boundary Lubrication Conditions. Trib. Trans., vol. 31, no. 4, 1988, pp. 437–441.

7.12 Lonsdale, C.P.; and Lutz, M.L.: Locomotive Traction Motor Armature Bearing Life Study. Lubrication Engineering, J. STLE, vol. 53, no. 8, 1997, pp. 12–19.

7.13 Mason, B.; and Berry, L.G.: Elements of Mineralogy. J. Gilluly and A.O. Woodford, eds., W.H. Freeman and Co., London, 1968, pp. 446–447.

7.14 Nakamoto, K.: Infrared and Raman Spectroscopy of Inorganic and Coordination Compounds. Part B, Fifth ed., John Wiley & Sons, New York, NY, 1997.

7.15 Tackett, James: FT–IR Characterization of Metal Acetates in Aqueous Solution. Appl. Spect., vol. 43, no. 3, 1989, pp. 483–489.

7.16 Morales, Wilfredo: Decomposition of a Commercial Perfluoropolyalkylether on Alpha and Gamma Catalytic Aluminas. Trib. Trans., vol. 39, no. 1, 1996, pp. 148–156.

TABLE 7.1.—GRAVIMETRIC DETERMINATION OF SOLIDS IN USED AND UNUSED PFPAE GREASE TAKEN FROM SPACE SHUTTLE ACTUATORS

Grease	2004 unused	1994 unused	1994 unused	1988 unused	1987 unused	(Beige)	(Brown)	(Beige)	(Grey)	(Grey)	(Beige)	(Grey)	(Red)
Description	Braycote	Braycote	Braycote	Braycote	Braycote	HS Qual Unit	HS Qual Unit	RSB–403	RSB–403	RSB–403	RSB–405	RSB–405	RSB–405
Sample		Sample A	Sample B			Sample A	Sample B	Sample A	Sample B	Sample C	Sample A	Sample B	Sample C
Wt grease, (g)	1.0428	0.3088	0.3154	0.3224	0.3022	0.3208	0.1772	0.5089	0.4091	0.1088	0.5966	0.3033	0.0713
Total Wt residue, (g)	0.3052	0.0721	0.0716	0.0802	0.0710	0.0665	0.0375	0.1215	0.0874	0.0213	0.1536	0.0789	0.0203
Wt% residue, (%)	29.3	23.3	22.7	24.9	23.5	20.7	21.2	23.9	21.4	19.6	25.7	26.0	28.5
Wt acid solubles, (mg)	19.7	6.2	6.7	7.6	6.4	5.0	4.2	14.4	9.9	2.1	---------	----------	6.8
Wt% acid solubles, (%)	1.9	2.0	2.1	2.4	2.1	1.6	2.4	2.8	2.4	1.9			9.5
Wt% oil, (%)	70.7	76.7	77.3	75.1	76.5	79.3	78.8	76.1	78.6	80.4	74.3	74.0	71.5

TABLE 7.2.—INDUCTIVELY COUPLED PLASMA EMISSION SPECTROSCOPIC ANALYSIS OF ACID SOLUBLES FROM EXTRACT RESIDUE

Sample	2004 unused	199 unused	1994 unused	1988 unused	1987 unused	(Beige)	(Brown)	(Beige)	(Gray)	(Gray)	(Red)
Description	Braycote	Braycote	Braycote	Braycote	Braycote	HS Qual Unit	HS Qual Unit	RSB–403	RSB–403	RSB–403	RSB–405
		Sample A	Sample B			Sample A	Sample B	Sample A	Sample B	Sample C	Sample C
Element	Wt% of Acid Soluble Materials[a]										
	AISI 9310 and 52100 metal elements (Iron, a contaminant of Braycote, is included here as the major element of steels)										
Fe	1.73	2.1	2.2	1.8	1.6	1.3	8.8	1.8	10	8.2	43
Cr	-----	-----	-----	-----	-----	-----	0.21		0.7	1.0	1.1
Ni	-----	0.10	-----	-----	0.40	-----	0.42	0.10	0.70	1.0	2.0
Cu	-----	-----	-----	-----	-----	-----	-----	-----	0.12	0.18	0.15
	Grease component elements										
Al	6.11	5.7	5.3	5.9	5.4	3.9	2.4	4.5	3.3	4.7	1.0
Si	18.3	20	21	18	17	12	7.7	14.9	13	15	3.2
Na	12.1	12	12	10	11	11	4.0	9.5	7.7	9.2	1.9
	Phosphating elements (Manganese, a component of 9310 and 52100 steel is included here as the high amounts are likely from phosphating)										
P	-----	-----	-----	-----	-----	-----	-----	-----	4.1	4.0	3.0
Mn	-----	-----	-----	-----	-----	-----	-----	-----	5.2	2.8	3.7
	Miscellaneous uncharacterized elements										
Mo						0.02	0.04	0.01	0.05	0.06	0.09
Mg	0.80	0.68	0.51	0.83	0.76	0.41	0.23	0.46	0.44	0.78	0.20
Zn	-----	-----	1.3	0.14	-----	0.18	-----	-----	0.11	0.17	0.23

[a]Any values not listed are <0.1 percent.

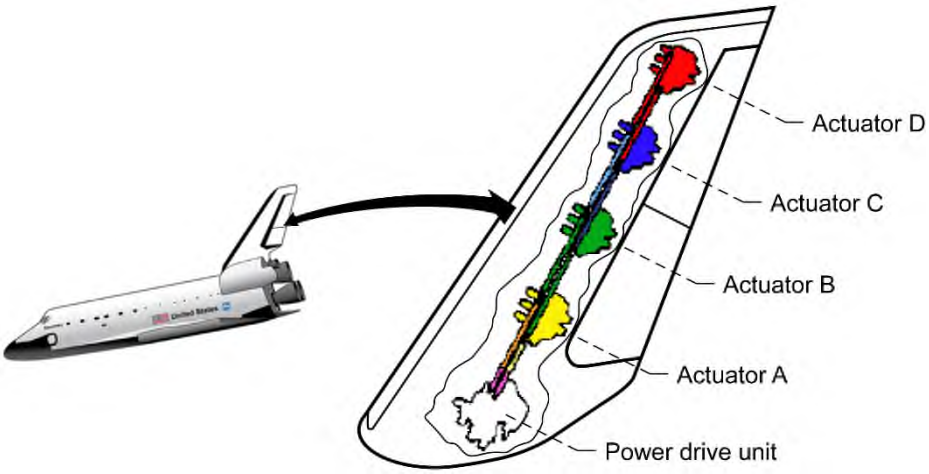

Figure 7.1.—Rudder/Speed Brake actuation components.

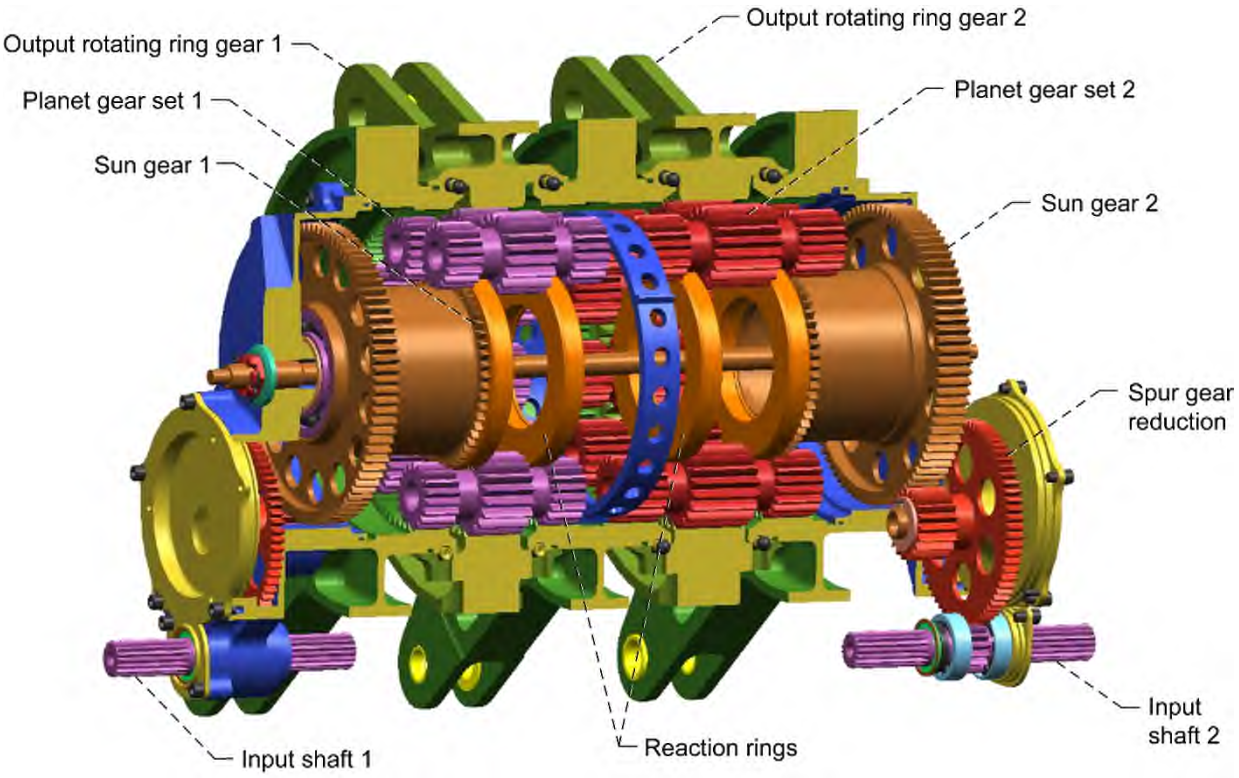

Figure 7.2.—Schematic of space shuttle Rudder Speed/Brake (RSB) actuator.

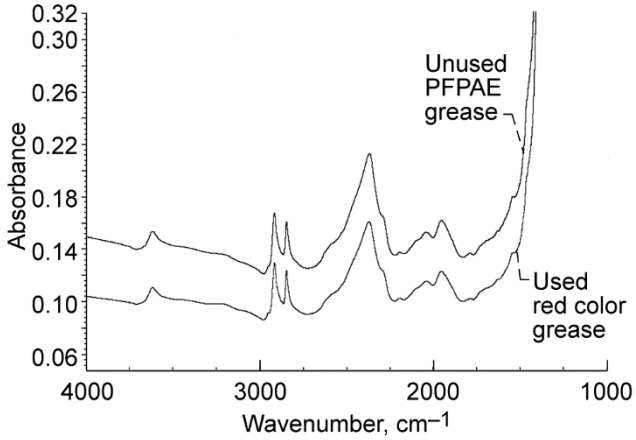

Figure 7.3.—Fourier Transform Infared (FTIR) spectra of unused PFPAE grease and used red colored PFPAE grease removed from space shuttle actuator.

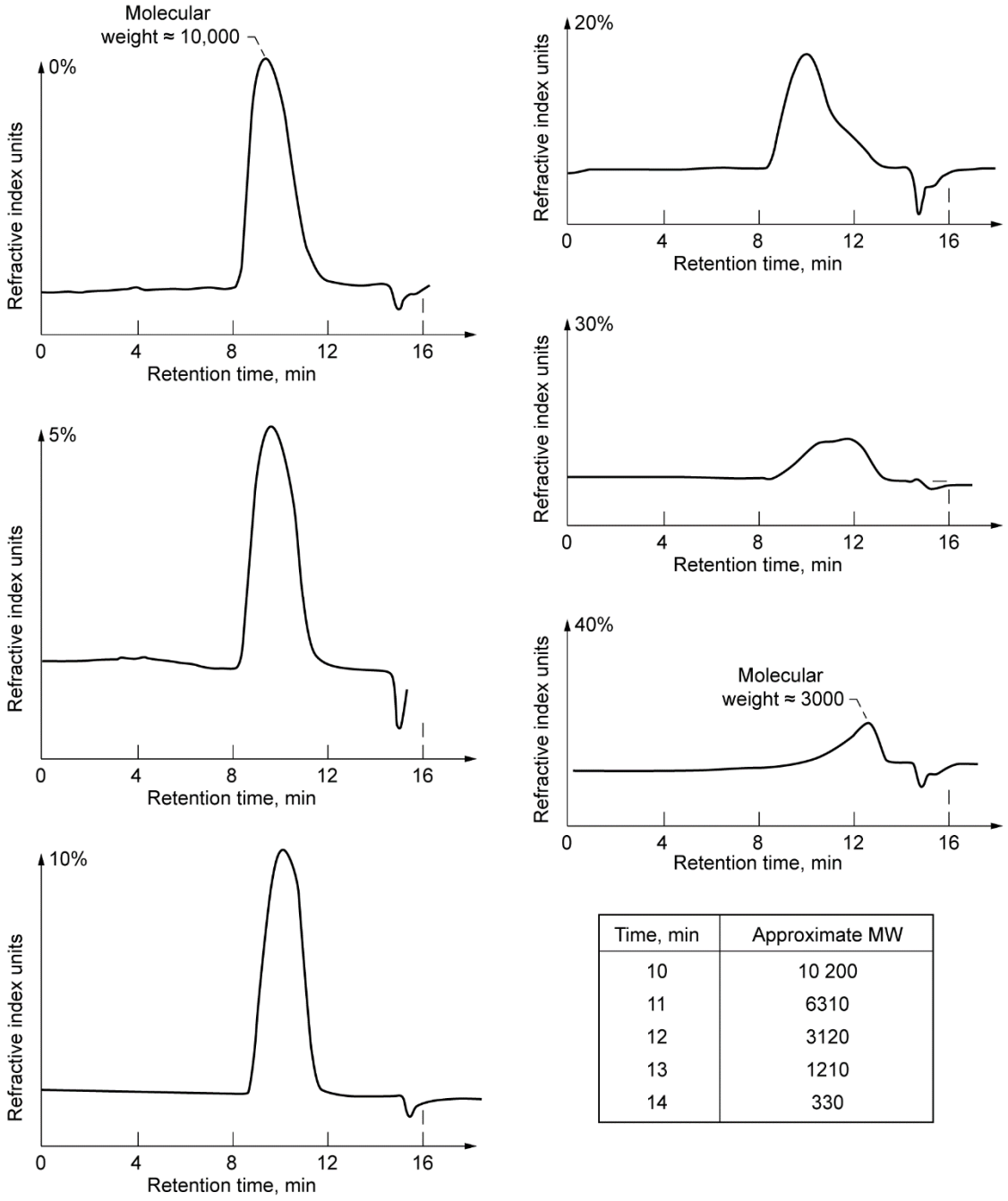

Time, min	Approximate MW
10	10 200
11	6310
12	3120
13	1210
14	330

Figure 7.4.—SEC chromatograms of 0, 5, 10, 20, 30, and 40 percent PFPAE Z-type fluid decomposition on gamma alumina.

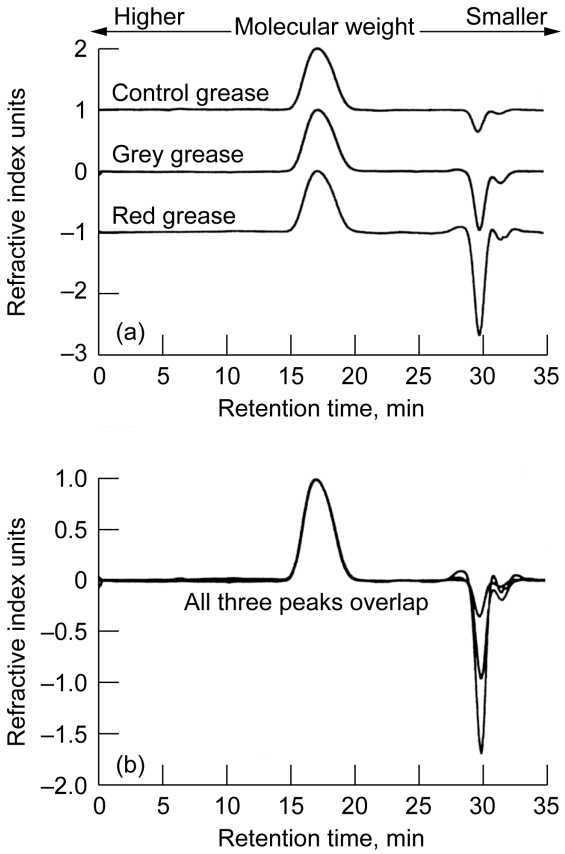

Figure 7.5.—SEC analysis of oil degradation in shuttle grease samples. (a) Individual offset chromatograms. (b) Chromatograms from (a) overlapped.

Chapter 8: Space Shuttle Rudder/Speed Brake Actuator—A Case Study Probabilistic Fatigue Life and Reliability Analysis

Fred B. Oswald*
National Aeronautics and Space Administration
Glenn Research Center
Cleveland, Ohio 44135

Michael Savage
University of Akron
Akron, Ohio 44325

Erwin V. Zaretsky†
National Aeronautics and Space Administration
Glenn Research Center
Cleveland, Ohio 44135

Abstract

The U.S. space shuttle fleet was originally intended to have a life of 100 flights for each vehicle, lasting over a 10-year period, with minimal scheduled maintenance or inspection. The first space shuttle flight was that of the Space Shuttle *Columbia* (OV–102), launched April 12, 1981. The disaster that destroyed *Columbia* occurred on its 28th flight, February 1, 2003, nearly 22 years after its first launch. In order to minimize risk of losing another space shuttle, a probabilistic life and reliability analysis was conducted for the space shuttle rudder/speed brake (RSB) actuators to determine the number of flights the actuators could sustain. A life and reliability assessment of the actuator gears was performed in two stages: a contact stress fatigue model and a gear tooth bending fatigue model. For the contact stress analysis, the Lundberg-Palmgren bearing life theory was expanded to include gear-surface pitting for the actuator as a system. The mission spectrum of the space shuttle RSB actuator was combined into equivalent effective hinge moment loads including an actuator input preload for the contact stress fatigue and tooth bending fatigue models. Gear system reliabilities are reported for both models and their combination. Reliability of the actuator bearings was analyzed separately, based on data provided by the actuator manufacturer. As a result of the analysis, the reliability of one-half of a single actuator was calculated to be 98.6 percent for 12 flights. Accordingly, each actuator was subsequently limited to 12 flights before removal from service in the space shuttle.

Introduction

The U.S. space shuttle fleet was originally intended to have a life of 100 flights for each vehicle, lasting over a 10-year period, with minimal scheduled maintenance or inspection. The first space shuttle flight was that of the Space Shuttle *Columbia* (OV-102), launched April 12, 1981. The disaster that destroyed *Columbia* occurred on its 28th flight, February 1, 2003, nearly 22 years after its first launch.

The space shuttle actuators are lubricated with space-qualified National Lubricating Grease Institute grade 2 perfluoropolyalkyl ether (PFPAE) grease and were intended to operate for life without periodic re-lubrication and maintenance (Refs. 8.1 and 8.2). Many of these actuators were operated without maintenance in excess of 20 years.

*Retired.
†Distinguished Research Associate.

During space shuttle actuator inspection and refurbishment after the *Columbia* space shuttle disaster, there were external signs of corrosion on one of the space shuttle rudder/speed brake (RSB) actuators. Visible inspection of two partially disassembled RSB actuators from the Space Shuttle *Discovery* was made on September 16, 2003. Pitted gears and discolored grease were observed inside. The grease-lubricated ball bearings and gears making up the actuators exhibited various degrees of wear. In some cases the wear was severe. Both the bearings and gears operated under a dithering (rotation reversal) motion when these systems were powered during ground operations (Ref. 8.2).

The observations summarized above led to several research efforts to determine the causes of the grease degradation, damage and wear to estimate the future life and reliability of the shuttle actuators, and to investigate design improvements for future heavily loaded space mechanisms. These works included Morales, et al. (Ref. 8.1), which analyzed the condition of the grease in two actuators after 39 flights, Oswald, et al. (Ref. 8.2), which describes a probabilistic analysis of the life and reliability of Body Flap Actuator (BSA) bearings, Krantz, et al. (Ref. 8.3) and Krantz and Handschuh (Ref. 8.4), which examined wear of spur gears lubricated by PFPAE grease, Proctor, et al. (Ref. 8.5), which describes experiments to characterize gear scuffing damage observed on one gear of the power drive unit (PDU) that operates the RSB actuators, and Handschuh, and Krantz (Ref. 8.6), which investigated a concern that a tooth might break off from a planet gear, potentially jamming the mechanism.

In order to minimize the risk of losing another space shuttle, Oswald, et al. (Ref. 8.2) performed experiments on a test rig under simulated conditions to determine the life and failure mechanism of the grease-lubricated space shuttle BFA bearings that support the input shaft of the space shuttle BFAs. The failure mechanism was wear that can cause loss of bearing preload. These experimental life data were analyzed using the two-parameter Weibull-Johnson method (Refs. 8.7 and 8.8) on experimental life test data from bearings. These tests established life and reliability data for both shuttle flight and ground operation. Test data were used to estimate the failure rate and reliability as a function of the number of shuttle missions flown. The Weibull analysis of the test data for the four actuators on one shuttle, each with a two-bearing shaft assembly, established a reliability level of 96.9 percent for a life of 12 missions. A probabilistic system analysis for four shuttles, each of which has four actuators, predicts a single bearing failure in one actuator of one shuttle after 22 missions (a total of 88 missions for a four-shuttle fleet). This prediction is comparable with actual shuttle flight history in which a single actuator bearing was found to have failed by wear at 20 missions.

The work of Oswald et al. (Ref. 8.2) was extended to perform a probabilistic life and reliability analysis of the space shuttle RSB actuators to determine the number of flights and/or the probability of failure that the actuators could sustain based on rolling-element (contact) fatigue of the rolling-element bearings and gears and tooth bending fatigue for a minimum of 12 space shuttle missions. (The 12 mission life requirement was based on the test data for the space shuttle BFA bearings discussed above.) Accordingly, the objectives of the work reported were to (1) determine the life and reliability of each of the gears and bearings in a RSB actuator and (2) extend the analysis to the four RSB actuators on each shuttle vehicle to estimate the system reliability.

Nomenclature

a	major semiaxis of contact ellipse, m (in.)
a_1	life adjustment factor for reliability
a_2	life adjustment factor for materials and processing
a_3	life adjustment factor for operating conditions including lubrication
B	gear material constant, $N/m^{1.979}$ ($lbf/in.^{1.979}$)
C_D	basic dynamic capacity of a ball or roller bearing, N (lbf)
C_t	basic dynamic capacity of gear tooth, N (lbf)
d	diameter of rolling element, m (in.)

F_t normal tooth load, N (lbf)
f tooth face width, m (in.)
f_{cm} bearing geometry and material coefficient
i number of rows of rolling elements
J AGMA gear tooth form factor
K AGMA bending stress adjustment factor
k gear tooth stress cycles per input shaft revolution
L life, hr, stress cycles, or revolutions
L_β characteristic life or life at which 63.2 percent of population fails, hr, stress cycles, or revolutions
L_{10} 10-percent life or life at which 90 percent of a population survives, hr, stress cycles, or revolutions
l length of stressed track, m (in.) or roller length, m (in.)
m Weibull slope; exponent or gear tooth module, mm
N number of gear teeth
n life, stress cycles
P diametral pitch, 1.0/in.
P_{eq} equivalent bearing load, m (in.)
P_t normal tooth load, N (lbf)
p load-life exponent
R reliability for bending fracture, fractional percent
r pitch circle radius of gear, m (in.)
S probability of survival, fractional percent or material strength MPa (ksi)
V stressed volume, m^3 where $V = alz$
X_n fraction of time spent at load-speed condition n
Z number of rolling elements per row
z depth beneath the surface of maximum orthogonal or maximum shear stress, m (in.)

α contact angle, deg
η_{10t} L_{10} life of single gear tooth, stress cycles
Λ lubricant film parameter
ρ curvature sum, m^{-1} ($in.^{-1}$)
σ gear tooth bending stress
σ_1, σ_2 surface roughness of bodies 1 and 2, rms, m (in.)
τ maximum orthogonal or maximum shear stress, MPa (ksi)
φ gear pressure angle, deg

Subscripts:

1, 2 bodies 1 or 2; load-life condition 1, 2, etc.
B bearing
G gear
g gear reliability
i individual gear
n body n or load-life condition n

ref reference
s, *sys* system
t tooth

Rudder/Speed Brake (RSB) Actuator System

The space shuttle RSB actuator system is contained in the space shuttle orbiter tail section shown in Figure 8.1. The actuator system comprises a PDU and four actuators. Each actuator contains two complete gear trains, designated left and right. The system controls the RSB panels through the four actuators that are driven by a single PDU.

A schematic of an RSB actuator is shown in Figure 8.2. The actuators are designed to provide both rudder and speed brake functions by a split design in the vertical tail section shown in Figure 8.1 in which two input shafts enter the actuator. By rotating the shafts in the same direction, the panels are moved concurrently for the rudder function. When the input shafts rotate in opposite directions, the panels move apart for the speed brake function. Both functions can be used simultaneously.

The 1L (left) RSB gearbox shown in Figure 8.2 (designated Actuator A in Fig. 8.1) is composed of a 19.75:1 offset compound spur reduction followed by a differential planetary with a 24:1 speed ratio. The overall speed ratio is 474:1. The input shafts are shown in the lower right and left corners of the figure. A series of two spur reductions bring the input power to the shaft of a sun gear, which drives a nine-planet differential planetary with two ring gears, one of which is fixed. In this arrangement, the fixed ring gear is split into two parts that straddle the output ring gear. The sun gear has a small face width and drives the rightmost planet set that meshes with the fixed ring gear. It is placed near the center of the planet spools. The geometric properties of the gears in both the compound spur reduction and the differential planetary reduction are given in Table 8.1.

In Table 8.1, the gear face widths were reduced to estimate the gear tooth contact stresses more closely since the analyses only deals with a constant stress across the gear face. In the planetary, the actual diametral pitch and pressure angles of the gears differ from the nominal values because the gears operate at nonstandard center distances.

The compound spur gear input stage has an offset configuration with a 155° angle between the two gear centerlines connecting its three shafts. The input shaft is supported by two symmetrically placed cylindrical roller bearings. The intermediate shaft is supported by a quill of four; one-half-inch-wide rows of 0.125-in.-diameter rollers. This quill is modeled as two half-inch-long roller bearings at its ends with increased capacity. The sun gear shaft is supported by a single ball bearing in the plane of the spur output gear. An axial thrust bearing is placed between the sun gear and the nearest of the two planet support rings.

The two support rings carry the radial loads applied to the nine planets by the fixed and output ring gears. Finally, there are two ball bearings placed between the output ring and the housing. These bearings carry the radial load associated with the hinge moment of the output arm. They also carry the axial preload applied to the rudder speed brake actuator by a rod through its center.

The gears comprising the actuators were manufactured from case carburized AISI 9310 steel. Most of the rolling-element bearing rings were manufactured from AISI 9310 steel. Two bearing rings were made from through-hardened AISI 52100 steel. The rolling elements were made from AISI 52100 steel except the balls for the bearings that connect the fixed and movable ring gears were made from AMS 6491 steel.

Analytic Procedure

For the contact stress analysis, the Lundberg-Palmgren bearing life theory (Ref. 8.9) was expanded to include gear-surface pitting for the actuator as a system. The mission spectrum of the space shuttle RSB actuator was combined into equivalent effective hinge moment loads including an actuator input preload for the contact stress fatigue and tooth bending fatigue models.

The reliabilities from the contact stress and tooth bending analyses were calculated for a series of estimated loads and load cycles for 100 missions of the shuttle. The loads considered were the output hinge moments on the gearbox. The analyses were performed for the applied loads and for a combination of the applied loads with a pre-load due to assembly of 50 lb-in. Once the reliabilities of the separate analyses were obtained for each loading condition, they were combined to determine an overall reliability for the gearbox for the analyzed loading conditions and cycle counts. This analysis was performed for the left half of the first actuator, with the assumption that the life and reliability of the right half were identical. The life and reliability for the four actuators on each space shuttle was assumed equal as well. The results were extended to the system of four full actuators on a single shuttle.

The life and reliability assessment of the gears was performed in two stages: a contact stress fatigue model and a gear tooth bending fatigue model. The actuator manufacturer provided L_{10} life data for the actuator bearings, assuming a Weibull slope of 1.11. These bearing life data are shown in Table 8.2. The analyses do not consider the probable reduction in life and reliability caused by boundary lubrication, wear, and grease degradation.

The original intent of the space shuttle design was for a life of 100 flights with minimal maintenance. During the Return to Flight program, post 2003 Columbia disaster, this goal was initially reduced to 20 flights. The reliability analysis for the gear tooth bending, gear tooth surface fatigue, and bearing fatigue were calculated separately along with the total system reliability for 1, 12, 20, and 100 space shuttle flights. The reliability values did not consider other modes of failure, such as wear or lubricant degradation.

Enabling Equations and Analysis

TLIFE: Transmission Life and Reliability Modeling

The method of probabilistic design was applied to the space shuttle RSB left half actuator gearbox number 1L (designated Actuator A in Fig. 8.1). A fatigue life and reliability assessment of the gearbox was performed in two stages: a contact stress fatigue life and reliability model and a gear tooth bending fatigue life and reliability model. The initial effort to determine the fatigue life and reliability of the 1L rudder speed brake actuator gearbox was focused on adapting the program TLIFE (Ref. 8.10) to analyze this gearbox. This program performs life and reliability analysis in three stages:

(1) It determines the loads and load cycles on the components of the gearbox based on the overall load and speed of the gearbox.
(2) It then determines the lives and reliabilities of the individual components based on these loads and load cycles.
(3) It combines these lives and reliabilities to determine the life and reliability of the gearbox system.

This program did not initially include an analysis for the differential planetary described above. It did have an analysis for the compound spur gear reduction that precedes the differential planetary. The analysis for the differential planetary based on the analysis of the preceding section was added as part of this effort.

The loading for this analysis was obtained from two Shuttle Program Office tables. The first three columns of Table 8.3 are a list of shuttle events, the corresponding rudder speed brake applied moment and its duration in minutes. For a flight of 7.604 hr, 7.25 hr are for the ferry from the landing site to the launch site. In the original table, specific moments and times are given but no load cycle counts.

The second table, Table 8.4, lists load ranges for given cycle counts. The total cycle count in this table is 35,297,798. However, 91,500 of these cycles are for reversed loading (negative moments) at lower moment ranges. These loads are applied to the opposite sides of the teeth and do not add to the positive moment fatigue damage. Removing these cycles from the total gives 35,188,298 positive load cycles for this analysis. Multiplying this total by the percent times of duration gives the estimates of the cycles for each applied moment, which are presented in the last column of Table 8.3. These loads and cycles are the basis of this analysis. The loading condition analyzed represents a median load for the

conditions considered. It should be noted that a 57,827 N (13,000 lb) axial pre-load is included in the loading on the output ring support ball bearings.

The two-parameter Weibull distribution function was used to model the statistical variations in life and strength for both models. For the contact stress analysis, the Lundberg-Palmgren bearing life theory (Ref. 8.9) has been expanded to include gear-surface pitting and the gearbox as a system (Ref. 8.11). The mission spectrum of the space shuttle rudder speed brake unit 1L gearbox has been combined into a single equivalent hinge moment effective load based on the contact stress fatigue model using the Linear Damage Rule also referred to as "the Palmgren-Langer-Miner Rule" (Refs. 8.12 and 8.13). This load was also used for the bending fatigue analysis.

Weibull Analysis

In 1939, Weibull (Refs. 8.16 and 8.17) developed a method and equation for statistically evaluating the fracture strength of materials. He also applied the method and equation to fatigue data based upon small sample (population) sizes, where

$$\ln\ln\left(\frac{1}{S}\right) = m\ln\left(\frac{L-L_\mu}{L_\beta - L_\mu}\right) \quad \text{where} 0 < L < \infty; 0 < S < 1 \tag{8.1a}$$

The location parameter L_μ is the time or life at or below, which no failures are expected to occur or they will be 100 percent probability of survival. Equation (1a) is referred to as the three-parameter Weibull equation relating life and probability of survival. If $L_\mu = 0$, the expression is referred to as "the two-parameter Weibull equation" and is written as follows:

$$\ln\ln\left(\frac{1}{S}\right) = m\ln\left(\frac{L}{L_\beta}\right) \quad \text{where} 0 < L < \infty; 0 < S < 1 \tag{8.1b}$$

When plotting the ln ln [1/S] as the ordinate against the ln L as the abscissa, fatigue data are assumed to plot as a straight line (Fig. 8.3). The ordinate ln ln [1/S] is graduated in statistical percent of components failed or removed for cause as a function of ln L, the log of the time or cycles to failure. The tangent of the line is designated the Weibull slope m, which is indicative of the shape of the cumulative distribution or the amount of scatter of the data (Refs. 8.7 and 8.15).

The method of using the Weibull distribution function for data analysis to determine component life and reliability was later developed and refined by Johnson (Ref. 8.17).

Rolling-Element Bearing Life Analysis

Lundberg and Palmgren (Refs. 8.9 and 8.18) extended the theoretical work of Weibull (Refs. 8.16 and 8.17) and showed that the probability of survival S could be expressed as a power function of maximum orthogonal shear stress τ, life n, depth of maximum orthogonal shear stress z, and stressed volume V:

$$\ln\frac{1}{S} \sim \frac{\tau^c n^m}{z^h} V \tag{8.2}$$

$$\ln\frac{1}{S} \sim \frac{\tau^c n^m a l}{z^{h-1}} \tag{8.3}$$

By substituting the bearing geometry and the Hertzian contact stresses for a given load into Equation (3), the bearing basic dynamic load capacity C_D can be calculated (Ref. 8.9). The basic dynamic load capacity C_D is defined as the load that a bearing can carry for a life of one-million inner-race revolutions with a 90-percent probability of survival (L_{10} life). Lundberg and Palmgren (Ref. 8.9) obtained the following additional relation:

$$L_{10} = \left(\frac{C_D}{P_{eq}} \right)^p \tag{8.4}$$

where P_{eq} is the equivalent bearing load and p is the load-life exponent (Ref. 8.9).

Formulas for the basic dynamic load ratings derived by Lundberg and Palmgren (Refs. 8.9 and 8.18) and incorporated in the ANSI/ABMA and ISO standards (Refs. 8.19 to 8.21) are as follows:

Radial ball bearings with $d \leq 25.4$ mm:

$$C_D = f_{cm} \left(i \cos \alpha \right)^{0.7} Z^{2/3} d^{1.8} \tag{8.5}$$

Radial ball bearings with $d > 25.4$ mm:

$$C_D = 3.647 \, f_{cm} \left(i \cos \alpha \right)^{0.7} Z^{2/3} d^{1.4} \tag{8.6}$$

Radial roller bearings:

$$C_D = f_{cm} \left(i \ell \cos \alpha \right)^{7/9} Z^{3/4} d^{29/27} \tag{8.7}$$

Equation (4) can be modified using life factors based on reliability a_1, materials and processing a_2, and operating conditions such as lubrication a_3 (Refs. 8.22 and 8.23) where

$$L = a_1 a_2 a_3 L_{10} \tag{8.8}$$

For the boundary lubrication under which the rolling-element bearings in the actuator operate, the lubricant film parameter, Λ can be used as an indicator of rolling-element bearing performance and life. For $\Lambda < 1$, surface smearing or deformation, accompanied by wear will occur on the rolling surfaces and the factor a_3 in Equation (8) can vary from 0.2 to 0.5 (Ref. 8.22). If the effect of boundary lubrication had not been considered by the actuator manufacturer, the bearing lives summarized in Table 8.2 would be as much as 80 percent less than those shown.

Gear Life Analysis

Between 1975 and 1981, Coy, Townsend, and Zaretsky (Refs. 8.24 to 8.26) published a series of papers developing a methodology for calculating the life of spur and helical gears based upon the Lundberg-Palmgren theory and methodology for rolling-element bearings. Coy, Townsend, and Zaretsky (Ref. 8.27) reported that for AISI 9310 spur gears, the Weibull slope m_G is 2.5. Based on Equation (2), for all gears except a planet gear, the gear life can be written as

$$L_{10_G} = \frac{N^{-1/m_G} \eta_{10_t}}{k} \tag{8.9}$$

For a planet gear, the life is

$$L_{10_G} = \frac{N^{-1/e_G}\left(\eta_{10_{t1}}^{-m_G} + \eta_{10_{t2}}^{-m_G}\right)^{-1/m_G}}{k} \tag{8.10}$$

The L_{10} life of a single gear tooth can be written as

$$\eta_{10_t} = a_2 a_3 \left(\frac{C_t}{F_t}\right)^{p_G} \tag{8.11}$$

where

$$C_t = Bf^{0.907}\rho^{-1.165}l^{-0.093} \tag{8.12}$$

and

$$\rho = \left(\frac{1}{r_1} + \frac{1}{r_2}\right)\frac{1}{\sin\varphi} \tag{8.13}$$

and η_{10_t} is the L_{10} life in millions of stress cycles for one particular gear tooth. This number can be determined by using Equation (11), where C_t is the basic load capacity of the gear tooth; F_t is the normal tooth load; p_G is the load-life exponent (usually taken as 4.3 for gears based on experimental data for AISI 9310 steel); and a_2 and a_3 are life adjustment factors similar to that for rolling-element bearings. Life factors a_2 for materials and processing are determined experimentally. The value for C_t can be determined by using Equation (12), where B is a material constant that is based on experimental data and is approximately equal to 1.39×10^8 when calculating C_t in SI units (Newtons and meters) and 21 800 in English units (pounds and inches) for AISI 9310 steel spur gears; f is the tooth width; and ρ is the curvature sum at the start of single-tooth contact.

The L_{10_G} life of the gear (all teeth) in millions of output shaft load cycles at which 90 percent will survive can be determined from Equations (9) or (10) where N is the total number of teeth on the gear; m_G is the Weibull slope for the gear and was taken to be 2.5 (Ref. 8.28); and k is the number of load (stress) cycles on a gear tooth per output shaft load cycle.

For all gears except the planet gears, each tooth will see load on only one side of its face for a given direction of input shaft rotation. However, each tooth on a planet gear will see contact on both sides of its face for a given direction of input shaft rotation. One side of its face will contact a tooth on the sun gear, and the other side of its face will contact a tooth on the ring gear. Equation (10) takes this into account, where $\eta_{10_{t1}}$ is the L_{10} life in millions of stress cycles of a planet tooth meshing with the sun gear, and $\eta_{10_{t2}}$ is the L_{10} life in millions of stress cycles of a planet tooth meshing with the ring gear.

Equations (9) to (13) are for gears in a single mesh only. For the case of collector gears such as parallel reduction, planetary gear trains, and idler gears, the damage accumulates differently. As the load count will be different for these gears, the equations must be modified to account for this variable loading. In planets and idler gears each tooth is loaded on both faces in one rotation. Since the surface fatigue damage accumulates separately on the faces, the gear faces are treated as separate gears in their own mesh in this simulation. The load count factor, $\boldsymbol{l_c}$, is used in other cases. This has units of load cycles per output load cycle.

For gears, this analysis used values for the Weibull slope, $m = 2.5$, gearing load-life exponent, $p = 4$ and dynamic capacity surface strength, S_{ac}, 500 ksi. Based on a mission duration of 7.604 hr, the reliability (probability of survival) of the gears based on contact (surface) fatigue is given in Table 8.5 for 12, 20, and 100 shuttle flights.

Gear Bending Life Analysis

Gear tooth bending stresses are calculated using the AGMA bending stress adaptation of the Lewis bending stress calculation (Ref. 8.29). This adaptation included the Dolan and Broghammer stress concentration factor (Ref. 8.30). The maximum bending stress on each tooth is used for the life and reliability calculations. For both the pinion and the gear, this stress, σ, is the bending stress at the root of the tooth caused by the full mesh load F_t, applied at the highest point of single-tooth contact on that tooth.

$$\sigma = \frac{F_t}{fmJ} K(MPa) = \frac{F_t P}{fJ} K(\text{ksi}) \tag{8.14}$$

The first part of the equation is the metric form, with the tooth size in Equation (14) defined by the gear tooth module, m. The second part of the equation is the English version with the tooth size defined by the diametral pitch, P. The symbol J is the AGMA tooth form factor and the symbol K is for the AGMA stress adjustment factors.

This stress is compared to the maximum allowable corresponding fatigue strength, S, in MPa (ksi) for AISI 9310 carburized gear steel (Ref. 8.31). Using a Goodman diagram, one can determine the corresponding alternate strength S_e, where the ultimate strength, S_u is 1889 MPa (274 ksi) where:

$$\frac{1}{S} = \frac{0.5}{S_u} + \frac{0.5}{S_e} \tag{8.15}$$

It is very unusual to have the full alternating strength available in an in-service device and since there is the presence of a corrosive environment after a period of time, this alternating strength will be de-rated to 80 percent of its full value. The reciprocal of Equation (15) including this de-rating factor gives the zero to maximum fatigue strength:

$$S = \frac{2}{\frac{1}{S_u} + \frac{1}{0.8S_e}} = \frac{2}{\frac{1}{1889} + \frac{1}{752}} = 1076 \text{ MPa} \tag{8.16a}$$

$$S = \frac{2}{\frac{1}{S_u} + \frac{1}{0.8S_e}} = \frac{2}{\frac{1}{274} + \frac{1}{109}} = 150 \text{ ksi} \tag{8.16b}$$

Using Equations (14) to (16), a bending stress analysis of the gears can be performed to determine their life and reliability in terms of the maximum fatigue strength S, load-life factor p and Weibull slope m.

The bending stress is directly proportional to the load. Accordingly,

$$L \sim (1/P_t)^p \sim (1/S)^p \tag{8.17a}$$

The load-life factor can be determined from the slope of the S-N curve in the region between one-thousand cycles to failure and one-million cycles to failure. For AISI 9310 carburized gear steel, $S = 1076$ MPa (156 ksi). Due to insufficient statistical tooth bending stress life data, a value of $m = 2.5$ is estimated for the bending stress-life Weibull slope. This is the same Weibull slope as used for the gear tooth contact-stress life slope. It is higher than that used for the bearing contact stress life slope. With the 90-percent reliability fatigue strength equal to 0.9 S_u at 10^3 cycles and the endurance strength equal to S at 10^6 cycles, the load-life factor p becomes

$$p = \frac{\ln L_2 - \ln L_1}{\ln S_1 - \ln S_2} = \frac{\ln 10^6 - \ln 10^3}{\ln(0.9S_u) - \ln S} = \frac{\ln 10^6 - \ln 10^3}{\ln(0.9(1889)) - \ln(1076)} = 11.6 \tag{8.17b}$$

The maximum bending stress on each tooth is used for the life and reliability calculations. For both the pinion and the gear, this stress is the bending stress at the root of the tooth caused by the full mesh load at the highest point of single-tooth contact on that tooth. The load-life relationship for bending fatigue is

$$L_{10,g} = \left(\frac{S}{\sigma}\right)^p \tag{8.18}$$

where $L_{10,g}$ is the 90-percent reliability life of the gear for the applied stress, σ. In terms of this life, the gear reliability R_g for a given life, L, is given by

$$\ln\left(\frac{1}{R_g}\right) = \ln\left(\frac{1}{0.9}\right)\left(\frac{L}{L_{10,g}}\right)^m \tag{8.19}$$

With the life and reliability of the gears in a single mesh established, the next step is to combine the analyses for all the meshes. For this analysis, the system bending reliability is the product of all the individual bending reliabilities:

$$R_s = \prod R_i \tag{8.20}$$

The pinion torque for each gear mesh is determined as a ratio to the output hinge moment on the rudder speed brake. The number of teeth in engagement in each mesh for a single output ring gear tooth engagement is counted.

The load cycles throughout the gearbox for every output ring motion of one tooth engagement, which equals 1/81 of a revolution or 4.444° were counted. Since there are nine planets, the fixed and movable ring gears each see nine tooth load cycles. Although each of the nine planets that mesh with the ring gears see only one load cycle, collectively they see nine. Each planet-sun mesh sees four load cycles for each planet-ring cycle (four teeth mesh at the sun for each tooth at the ring), thus the count for the sun with its planets is 36.

The two meshes in the compound spur reduction are a little different. The spur-sun mesh sees 26 load cycles. However, the intermediate gear that meshes with this gear has only 19 teeth. Thus, seven of its teeth see two load cycles and 12 teeth see only one load cycle. The input mesh sees the most load cycles with 14 of the teeth on the input spur seeing six load cycles for the one tooth rotation of the output.

The overall reliability for all the meshes taken together is the product of all the calculated reliabilities in the analysis. By calculating this analysis with different loads for one-million cycles, the dynamic capacity of the gearbox in bending is determined. It is the load that produces a reliability of 90 percent for one-million stress cycles.

System Life Prediction

The L_{10} lives of the individual bearings and gears that make up a rotating machine are calculated for each condition of their operating profiles. For each component, the resulting lives from each of the operating conditions are combined using the linear damage (Palmgren-Langer-Miner) rule (Refs. 8.12 to 8.15) where

$$\frac{1}{L} = \frac{X_1}{L_1} + \frac{X_2}{L_2} + \cdots \frac{X_n}{L_n} \tag{8.21}$$

The Lundberg-Palmgren bearing life theory was expanded to include gear-surface pitting for the gearbox as a system. A second fatigue life and reliability analysis was also conducted for the bending fatigue lives of the gear teeth in the actuator. Gear and bearing system reliabilities were calculated and combined using strict series reliability where

$$S = S_1 \cdot S_2 \cdot S_3 \cdot \ldots S_n \tag{8.22}$$

At a specified reliability, the cumulative lives of each of the machine components are combined to determine the calculated machine system L_{10} life using the Lundberg-Palmgren formula (Ref. 8.9):

$$\frac{1}{L_{sys}^m} = \left(\frac{1}{L_{B_1}^{m_B}} + \frac{1}{L_{B_2}^{m_B}} + \cdots \frac{1}{L_{B_n}^{m_B}} \right) + \left(\frac{1}{L_{G_1}^{m_G}} + \frac{1}{L_{G_2}^{m_G}} + \cdots \frac{1}{L_{G_n}^{m_G}} \right) \tag{8.23}$$

Unfortunately, Equation (23) is only an approximation since the system Weibull slope varies with load. In a balanced life transmission, the system Weibull slope will be somewhere between the highest and the lowest of the components' Weibull slopes. A form of this equation can be solved numerically for system reliability as a function of life and plotted on Weibull coordinates (Ref. 8.32). The resulting graph can be fitted with a straight line to determine the system Weibull slope and the system L_{10} life. In the event of an unbalanced life transmission, the lowest lived component will dominate the transmission failures and thus can serve as a good approximation for the system Weibull properties. However, at a given reliability, the system life will always be lower than the lowest lived component because other components can also fail.

Based upon the Lundberg-Palmgren equation, the L_{10} life for the actuator as a system can be calculated where

$$L_{10} = \left[\frac{C}{T} \right]^p \tag{8.24}$$

C is the theoretical load that produces a life of one million cycles (designated the dynamic capacity), T is the equivalent output torque and p is the load-life exponent. Using the Linear Damage Rule, where X_n is the time and T_n is the torque at condition n:

$$T = \frac{X_1 T_1^p + X_2 T_2^p + X_3 T_3^p + ... + X_n T_n^p}{X_1 + X_2 + X_3 + ... + X_n} \tag{8.25}$$

A mission spectrum for the actuator as supplied by the NASA Shuttle Program Office was used to compute effective hinge moment loads for both gear tooth contact stress and tooth bending stress using the Palmgren-Langer-Miner linear damage rule.

A gear contact stress fatigue model established the output hinge moment dynamic capacity for the actuator as 44 860 N-m (397 050 in.-lb) with a Weibull slope of 2.5 and load-life exponent of 3.64. A similar analysis for tooth bending fatigue produced a dynamic capacity of 25 280 N-m (223 740 in.-lb) with Weibull slope of 2.5 and load-life exponent of 11.6.

A loading spectrum for 100 missions consisting of 35, 188, and 292 load cycles was assumed for the gearbox. Output hinge moment loads varied from 1700 to 27,100 N-m (15,000 to 240,000 in.-lb). An input preload of 5.6 Nm (50 in.-lb) added 2010 Nm (17,800 in.-lb) to the external hinge moment for the analysis.

Results and Discussion

Rudder/Speed Brake (RSB) Actuator Loading

The RSB actuator was designed and manufactured in the 1970's for an expected life of 100 missions over a period of 10 years with no definitive plans for relubrication, maintenance, and refurbishment. At that time and during the course of the operation of the space shuttle fleet and until the time of the Columbia disaster, it was assumed by the Shuttle Program Office that no maintenance would be required of the actuators and/or that no failure should be anticipated. In other words, there would be a 100 percent probability of survival for the designated 100 missions. As a result, design loads were not available for the analysis reported by us.

The Shuttle Program Office did provide two simplified load versus time and load cycle tables shown in Tables 8.3 and 8.4. These tables give load ranges for an operation in output load cycles. It was assumed that the frequency of loading was constant for all missions and that the full cycle count of 35 188 298 positive load cycles was the total for the 100 missions. On this basis, the cycles were totaled, each time was converted to a percent time and this percent was multiplied by the 35 188 298 cycles to obtain the number of cycles at each listed load. The average mission duration operating time was given as 7.604 hr.

Rolling-Element Bearing Life

The L_{10} lives of the bearings, (the rolling-element fatigue life at a 90-percent probability of survival) were calculated by the actuator manufacture for the left half of actuator number 2 and were not recalculated by us. Based on Equation (1a), for each of the bearings, the location parameter L_μ is the time below which no failures would be expected (100 percent probability of survival) where $L_\mu = 0.053 L_{10}$ (Ref. 8.23). These results are shown in Table 8.2. However, as previously discussed, the analyses reported do not consider the negative effects of grease degradation, boundary lubrication, and resultant wear on the life and reliability of the bearings and gears.

The lowest lived bearing in the system dictates the time below which no bearing failure should occur. From Table 8.2 this time is 58 hr. Based on an average mission duration operating time of 7.604 hr and using the two-parameter Weibull equation (Eq. (1b)), the probability of survival for each bearing was calculated for 1, 12, 20, and 100 missions. The product of the reliabilities of the individual bearings represents the reliability of the system of bearings in one-half actuator.

These results are shown in Table 8.5 for 12, 20, and 100 shuttle flights. Based on the results reported for bearing 6b (Table 8.2) having a life of 58 hr below, which no failure should occur, it can be reasonably concluded that the bearings as a system will operate with no failure for about 8 missions (58 hr/7.604 hr per mission).

Gear Contact Fatigue Life

Gear tooth failures can be similar to failures of bearing elements. However, there are a few differences due to the complex shape of the gear tooth. Most differences result in sudden tooth breakage in a poorly lubricated, overloaded mesh. For our analysis we did not consider this as a failure mode.

For the gear analysis the values for the Weibull slope, $m = 2.5$, gearing load-life exponent, $p = 4$ and dynamic capacity surface strength, $S_{ac} = 3450$ MPa (500 ksi). Based on a mission duration of 7.604 hr, the reliability (probability of survival) of the gears based on contact (surface) fatigue is given in Table 8.5 for 12, 20, and 100 shuttle flights.

Gear Bending Fatigue Life

A bending stress analysis of the gears was performed to determine their life and reliability in terms of the maximum fatigue strength S, load-life factor p, and Weibull slope m that have been determined. These values are: $S = 1076$ MPa (156 ksi), $p = 11.6$, and $m = 2.5$, respectively.

The maximum bending stress on each tooth was used for the life and reliability calculations. For both the pinion and the gear, this stress is the bending stress at the root of the tooth caused by the full mesh load at the highest point of single-tooth contact on that tooth.

The result of this analysis is a dynamic capacity of 25,279 N-m (223,741 in.-lb). Coupled with the load-life factor of 11.6 and the Weibull slope of 2.5, this dynamic capacity enabled the bending stress life and reliability to be calculated along with the life and reliability for contact stress. The resulting reliabilities based on tooth bending fatigue are summarized in Table 8.5 for 12, 20, and 100 shuttle flights.

Rudder/Speed Brake (RSB) System Reliability

The reliabilities for the gears and bearings are summarized for a single half actuator (the 1L (left) RSB gearbox shown in Fig. 8.2) and for four full actuators as a system in Table 8.5 for 12, 20, and 100 flights. The bearing reliabilities are summarized under the column “Actual Bearing Reliability” in Table 8.5. The reliability of the gears as a system is summarized under “Gear Reliability for each failure mode in Table 8.5. The column showing “Combined Bending and Surface” reliability is the product of the reliabilities for “Tooth Bending Fatigue” and “Tooth Surface Fatigue.” The Total System Reliability shown under the column “Total System Reliability” in Table 8.5 is the product of the reliabilities shown in each line for the “Combined Bending and Surface Reliability” for the gears and the “Actuator Bearing Reliability.”

There are four full actuators on each shuttle. The failure of a single actuator can result in the loss of a shuttle. When considering the probability of survival of four actuators together these numbers become 89.0, 81.1, and 21.3 percent for 12, 20, and 100 flights, respectively. For 20 flights the probability of a gear failure in one of four actuators is less than 0.6 percent. However, for 100 flights the probability of a gear failure in any one of four actuators increases to 28.3 percent where bending fatigue failure becomes the predominant mode of gear failure. This is an unacceptable risk.

The reliability of the bearings was determined separately from those of the gears. Combining the bearing and gear statistical analysis for eight missions results in a 100 percent probability of survival for all four actuators as a system. The reliability of the gears in the actuators for both surface and bending fatigue is higher than the reliability of the bearings. This means the reliability of this system is dominated by the reliability of its bearings.

The Weibull plots of Figure 8.4 illustrate this. They are for the subsystems and full system of Rudder Speed Brake 1L. The gear surfaces subsystem, shown to the far right as a dashed line is by far the strongest with the highest reliabilities. The gear teeth bending subsystem is somewhat less reliable and weaker and dominates the gear system reliability. Finally, the bearings are the weakest system, which dominates the full system reliability at high reliabilities or low percent of failures.

These life and reliability data for a single half actuator were assumed to apply to all four full rudder speed brake actuators used in the space shuttle. Based on four RSB actuators per shuttle, the probability of survival or the actuators as a system is the probability of survival of a single half actuator at a designated number of flights to the 8th power or S^8. The Weibull plots of Figure 8.5 show the comparison of the reliabilities of the 1L gearbox and the full system of four gearboxes with their higher statistical percent of failures and lower reliabilities.

The above analysis does not include wear as a failure mode. Wear, as fatigue, is probabilistic and not deterministic. We know that wear occurred in the RSB actuators. However, without an experimental data base and predefined acceptable wear criterion for critical components, wear as a failure mode could not be analytically predicted.

General Comments

From Table 8.5, the 81.1 percent system reliability for 20 flights was deemed an unacceptable risk for the space shuttle. As a result, the number of future flights per actuator was limited to 12. The reliability for 12 flights on a single half actuator was calculated to be 98.6 percent. The reliability of the four full actuators as a system in a single space shuttle was calculated to be 89.0 percent for 12 flights. This means the probability of fatigue failure of the bearings or gears in the system of four full RSB actuators on a single shuttle is 11 percent over a life of 12 flights.

Because of time constraints, a life and reliability analysis was not performed by us on the space shuttle BFA gears and bearings. However, Oswald et al. (Ref. 8.2) performed experiments on a test rig under simulated conditions to determine the life and failure mechanism of the grease-lubricated space shuttle BFAs bearings that support the input shaft of the space shuttle BFAs. The Weibull analysis of the test data for the four space shuttle BFAs on one shuttle, each with a two-bearing shaft assembly, established a reliability level of 96.9 percent for a life of 12 missions. For the purpose of our analysis, it was assumed by us that this reliability is that for the entire BFA assembly. If this reliability is for the entire BFA assembly, then the combined reliability with the RSB assembly for 12 missions on a single space shuttle was 86.2 percent [(0.969 × 0.890) × 100]. This yields a 13.8 percent probability that a bearing and/or gear failure will occur on either a BFA or RSB actuator.

In the 1970's when the space shuttle RSB actuator was designed and manufactured, a sophisticated gearbox life probabilistic life and reliability analysis of the type presented in this article was not available. The RSB actuator was designed for a life of 100 missions over a period of 10 years with no definitive plans for relubrication, maintenance, and refurbishment. However, a bearing life and reliability analysis was performed by the manufacturer of the actuators. The bearing analysis performed by us and reported herein was an extension of the one performed by the manufacturer. Previous related studies (Refs. 8.1 to 8.6) reported the effects of boundary lubrication, grease degradation, and wear on BFA and RSB actuators' life and reliability. For this fatigue study, we did not consider the negative effects of boundary lubrication, wear, and grease degradation on bearing and gear life and reliability.

The risk of a rudder speed brake actuator bearing failure (not including the risk of gear failures) that could result in the loss of a space shuttle at 100 missions was 70.2 percent. For 20 missions that risk was reduced to 18.4 percent. However, it appears that the NASA Program Office did not examine or extend the bearing analysis to reflect the reliability and/or consider that an actuator bearing failure could be a probable cause for loss of a space shuttle. This omission was further compounded by a failure to provide for a scheduled maintenance program to remove, examine, repair, replace, and/or refurbish these actuators based on time and missions flown.

Summary of Results

A probabilistic life analysis was applied to the space shuttle rudder/speed brake (RSB) actuator 1L. A contact stress fatigue model and a gear tooth bending fatigue model were used for a life and reliability assessment of the gears. Life and reliability of the bearings in the actuator were analyzed separately, based on data provided by the actuator manufacturer using the Lundberg-Palmgren life model. The life and reliability results for the gears and bearings in a single half actuator were combined using strict series reliability. The life and reliability of each of the four full actuators was assumed equal and the results extended to the four actuators on each shuttle as a single system. Although the analyses do not consider the probable reduction in life and reliability caused by boundary lubrication, wear, and grease degradation, the recommendation to limit actuators to 12 flights before refurbishment addresses this concern. The following results were obtained.

(1) Based on the analysis, the space shuttle RSB actuators were limited to 12 flights each in order to maintain a reliability of 98.6 percent for any half actuator and 89.0 percent for the system of four full actuators on one shuttle.
(2) The life and reliability of the actuator gears as a system for both surface and bending fatigue is higher than the life and reliability of the bearings as a system. Thus, the life and reliability of the actuator system is dominated by that of the bearings.
(3) Based on the original design requirement of the space shuttle, the rudder/speed brake actuator system, comprising four actuators on each shuttle, has a calculated reliability of 81.1 percent for a life of 20 flights and a reliability of 21.3 percent for a life of 100 flights.

References

8.1. Morales, W.; Street, K.W.; and Zaretsky, E.V.: Performance and Analysis of Perfluorinated Grease used on Space Shuttle Actuators-A Case Study. Tribology T., vol. 55, no. 1, 2011, pp. 77-85.
8.2. Oswald, F.B., et al.: Probabilistic Analysis of Space Shuttle Body Flap Actuator Ball Bearings. Tribology T., vol. 51, no. 2, 2008, pp. 193–202.
8.3. Krantz, T.L.; Oswald, F.B.; and Handschuh, R.F.: Wear of Spur Gears Having Dithering Motion and Lubricated With a Perfluorinated Polyether Grease. ASME Paper No. DETC2007–34089, 2007.
8.4. Krantz, Timothy L.; and Handschuh, Robert F.: A Study of Spur Gears Lubricated With Grease—Observations From Seven Experiments. NASA/TM—2005-213957 (ARL TR–3159), 2005. http://ntrs.nasa.gov
8.5. Proctor, Margaret; Oswald, Fred B.; and Krantz, Timothy L.: Shuttle Rudder/Speed Brake Power Drive Unit (PDU) Gear Scuffing Tests With Flight Gears. NASA/TM—2005-214092, 2005. http://ntrs.nasa.gov
8.6. Handschuh, Robert F.; and Krantz, Timothy L.: Engagement of Metal Debris Into a Gear Mesh. NASA/TM—2010-216759, 2010. http://ntrs.nasa.gov
8.7. Johnson, L.G.: The Statistical Treatment of Fatigue Experiments. Elsevier Publishing Co., Amsterdam, Netherlands, 1964.
8.8. Vlcek, B.L.; and Zaretsky, E.V.: Rolling-Element Fatigue Testing and Data Analysis—A Tutorial. Tribology T., vol. 54, no. 4, 2011, pp. 523–541.
8.9. Lundberg, G.; and Palmgren, A.: Dynamic Capacity of Rolling Bearings. Acta Polytechnica Mechanical Engineering Series, vol. 1, no. 3, Stockholm, Sweden, 1947.
8.10. Savage, M.; Prasanna, M.G.; and Rubadeux, K.L.: TLIFE: A Program for Spur, Helical and Spiral Bevel Transmission Life and Reliability Modeling. NASA CR–4622 (ARL–TR–506), 1994. http://ntrs.nasa.gov

8.11. Savage, M., et al.: Spur, Helical, and Spiral Bevel Transmission Life Modeling. J. Propul. Power, vol. 12, no. 2, 1996, pp. 283–288.
8.12. Palmgren, A.: The Service Life of Ball Bearings. NASA–TT–F–13460, 1971 (Translation from Z. Ver. Devut. Ingr., vol. 68, no. 14, 1924, pp. 339–341). http://ntrs.nasa.gov
8.13. Langer, B.F: Fatigue Failure From Stress Cycles of Varying Amplitude. J. App. Mech., vol 4, no. 4, 1937, pp. A–160—A–162.
8.14. Miner, M.A.: Cumulative Damage in Fatigue. J. Appl. Mech., vol. 12, no. 3, 1945, pp. A–159—A–164.
8.15. Nikas, G.K., ed.: Recent Developments in Wear, Friction and Lubrication Research. Rolling Bearing Life Prediction, Theory, and Application, E.V. Zaretsky, 2010, pp. 45–36.
8.16. Weibull, W.: A Statistical Theory of the Strength of Materials. Proceedings of the Royal Swedish Institute of Engineering Research (Ingenioersvetenskapsakad. Handl.) vol. 151, 1939, pp. 5–55.
8.17. Weibull, W.: The Phenomenon of Rupture in Solids. Proceedings of the Royal Swedish Institute of Engineering Research (Ingeniorsvetenskapsakad. Handl.), vol. 153, 1939, pp. 1–55.
8.18. Lundberg, G.; and Palmgren, A.: Dynamic Capacity of Roller Bearings. Acta Polytechnica Mechanical Engineering Series, vol. 2, no. 4, Stockholm, Sweden, 1952.
8.19. International Organization for Standardization: Rolling Bearings—Dynamic Load Ratings and Rating Life. First ed., ISO 281, 1990.
8.20. Load Ratings and Fatigue Life for Ball Bearings. ANSI/ABMA–9, 1990.
8.21. Load Ratings and Fatigue Life for Roller Bearings. ANSI/ABMA–11, 1990.
8.22. Zaretsky, Erwin V., ed.: Tribology for Aerospace Applications. STLE SP–37, Society of Tribologists and Lubrication Engineers, Park Ridge, IL, 1997.
8.23. Zaretsky, Erwin V., ed.: STLE Life Factors for Rolling Bearings. STLE SP–34, Society of Tribologists and Lubrication Engineers, Park Ridge, IL, 1992.
8.24. Coy, J.J.; Townsend, D.P.; and Zaretsky, E.V.: Dynamic Capacity and Surface Fatigue Life for Spur and Helical Gears. J. Lubric. Tech.-T ASME, vol. 98, no. 2, 1976, pp. 267–274.
8.25. Coy, John J.; Townsend, Dennis P.; and Zaretsky, Erwin V.: Analysis of Dynamic Capacity of Low-Contact-Ratio Spur Gears Using Lundberg-Palmgren Theory. NASA TN D–8029, 1975. http://ntrs.nasa.gov
8.26. Coy, John J.; and Zaretsky, Erwin V.: Life Analysis of Helical Gear Sets Using Lundberg-Palmgren Theory. NASA TN D–8045, 1975. http://ntrs.nasa.gov
8.27. Coy, J.J.; Townsend, D.P.; and Zaretsky, E.V.: An Update on the Life Analysis of Spur Gears. Advanced Power Transmission Technology, G.K. Fischer, ed., NASA CP–2210, 1983, pp. 421–434. http://ntrs.nasa.gov
8.28. Townsend, D.P.; Coy, J.J.; and Zaretsky, E.V.: Experimental and Analytical Load-Life Relation for AISI 9310 Steel Spur Gears. J. Mech. Des., vol. 100, no. 1, 1978, pp. 54–60.
8.29. Fundamental Rating Factors and Calculation Methods for Involute Spur and Helical Gear Teeth. ANSI/AGMA 2001–D04, 2001.
8.30. Dolan, T.J.; and Broghamer, E.L.: A Photoelastic Study of Stresses in Gear Tooth Fillets. University of Illinois, Engineering Experimental Station Bulletin 335, 1942.
8.31. McIntire, W.; and Malott, R.: Advancement of Spur Gear Design Technology. USAAVLABS Technical Report 66–85, U.S. Army Aviation Materiel Laboratories, Ft. Eustis, VA, 1966.
8.32. Savage, M., et al.: Computational Life and Reliability Modeling for Turboprop Transmissions. J. Propul. Power, vol. 5, no. 5, 1996, pp. 610–614.

TABLE 8.1.—GEAR GEOMETRIC PROPERTIES IN COMPOUND SPUR REDUCTION AND DIFFERENTIAL PLANETARY REDUCTION

Gear	No. of teeth	Face width, mm (in.)	Nominal tooth size,[a] module-mm dia. pitch (1.0/in.)	Nominal pressure angle, deg.	Working Tooth size[a], Module-mm dia. pitch (1.0/in.)	Working Pressure angle, deg.
Input (1)	16	10.85 (0.427)	1.814 (14)	25	1.814 (14)	25.0
Intermediate (2)	69	10.85 (0.427)	1.814 (14)	25	1.814 (14)	25.0
Intermediate (3)	19	23.75 (0935)	2.117 (12)	25	2.117 (12)	25.0
Spur Output (4)	87	23.75 (0935)	2.117 (12)	25	2.117 (12)	25.0
Sun (5)	54	3.18 (0.125)	2.117 (12)	25	2.169 (11.708)	27.839
Planet on Sun (6a)	18	3.18 (0.125)	2.117 (12)	25	2.169 (11.708)	27.839
Planet on fixed ring (6b)	18	52.20 (2.055)	2.117 (12)	25	2.169 (11.708)	27.839
Fixed ring (7)	90	52.20 (2.055)	2.117 (12)	25	2.169 (11.708)	27.839
Output planet (8)	18	37.34 (1.470)	2.54 (10)	25	2.479 (10.245)	21.797
Output ring (9)	81	37.34 (1.470)	2.54 (10)	25	2.479 (10.245)	21.797

[a]The tooth size standards in metric and in English units are different. The metric module is the pitch diameter divided by the number of teeth. The English Diametral Pitch is the number of teeth divided by the pitch diameter.

TABLE 8.2.—SUMMARY OF ROLLING-ELEMENT BEARING LIVES FOR RUDDER SPEED BRAKE ACTUATOR

Bearing no.	1a	1b	2	3a	3b	4	6a	6b
Bearing type	Roller	Roller	Roller	Roller	Roller	Ball	Ball	Ball
L_{10} life (hr)	647,000	647,000	15,823	4,875	4,875	54,973	1,509	1,089
$L_{0.1}$ life (hr)	9,747	9,747	238	73	73	828	23	16
Min life (hr)	34,291	34,291	839	258	258	2,914	80	58

TABLE 8.3.—EVENT DURATION

Event	Moment, (N-m) lb-in.	Duration, min	Cycles calculated
Ferry	(1,693) 15,000	420	32,392,514
Ferry	(23,953) 212,000	0.25	19,281
Ascent	(9,039) 80,000	0.2	15,425
Ascent	(5,197) 46,000	1.7	131,113
Ascent	(11,073) 98,000	0.1	7,713
Descent	(15,818) 140,000	33	2,545,126
Descent	(27,116) 240,000	1	77,125

TABLE 8.4.—INITIAL APPLIED LOADING INFORMATION

Load range, N-m (in.-lb)		Cycles
–50,814 to –39,545	(–450,000 to –350,000)	0
–39,545 to –28,246	(–350,000 to –250,000)	0
–28,246 to –16,948	(–250,000 to –150,000)	2,939
–16,948 to –5,649	(–150,000 to –50,000)	88,561
–5,649 to 5,649	(–50,000 to 50,000)	34,369,892
5,649 to 11,298	(50,000 to 100,000)	20,768
11,298 to 16,948	(100,000 to 150,000)	67,044
16,948 to 22,597	(150,000 to 200,000)	439,135
22,597 to 28,246	(200,000 to 250,000)	291,459
28,246 to 33,895	(250,000 to 300,000)	0
33,895 to 39,545	(300,000 to 350,000)	0
39,545 to 45,194	(350,000 to 400,000)	0
>45,194	(> 400,000)	0
Total cycles		35,297,798

TABLE 8.5.—RUDDER SPEED BRAKE ACTUATOR PROBABILITY OF SURVIVAL

Number of flights	Number of actuators	Gear reliability, percent			Actuator bearing reliability, percent	Total system reliability, percent
		Tooth bending fatigue	Tooth surface fatigue	Combined bending and surface		
100	1/2	95.943	99.978	95.922	85.950	82.4
100	4	71.793	99.822	71.666	29.782	21.3
20	1/2	99.926	99.999+	99.926	97.495	97.4
20	4	99.409	99.997	99.406	81.632	81.1
12	1/2	99.979	99.999+	99.979	98.571	98.6
12	4	99.835	99.999	99.834	89.126	89.0

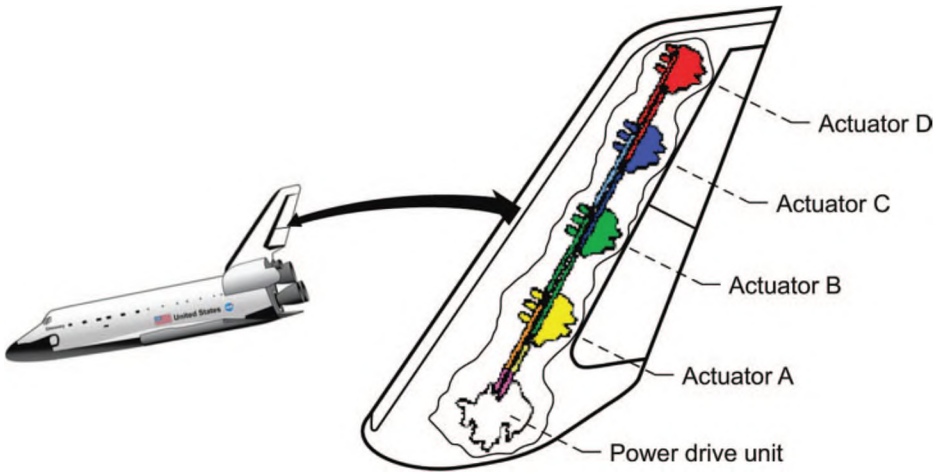

Figure 8.1.—Rudder/speed brake actuating components.

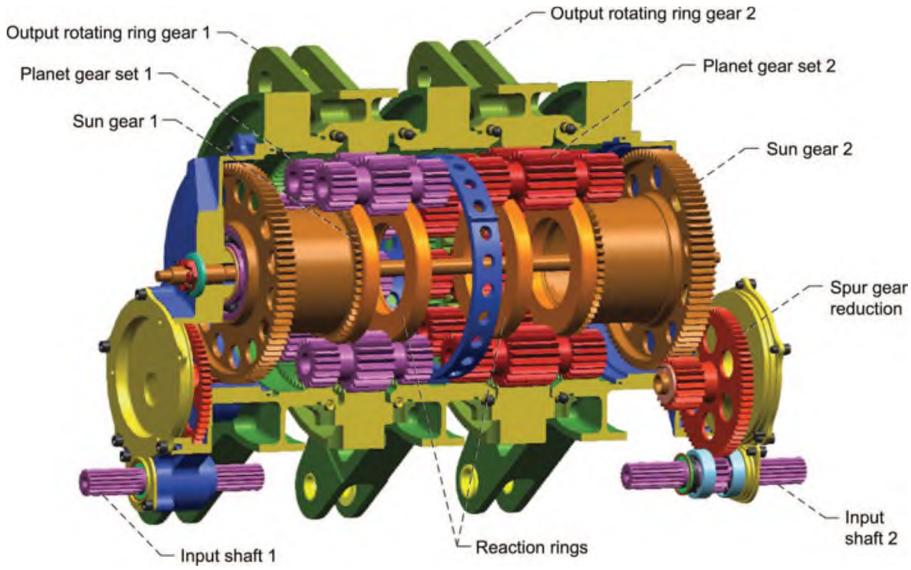

Figure 8.2.—Schematic of space shuttle rudder/speed brake (RSB) actuator.

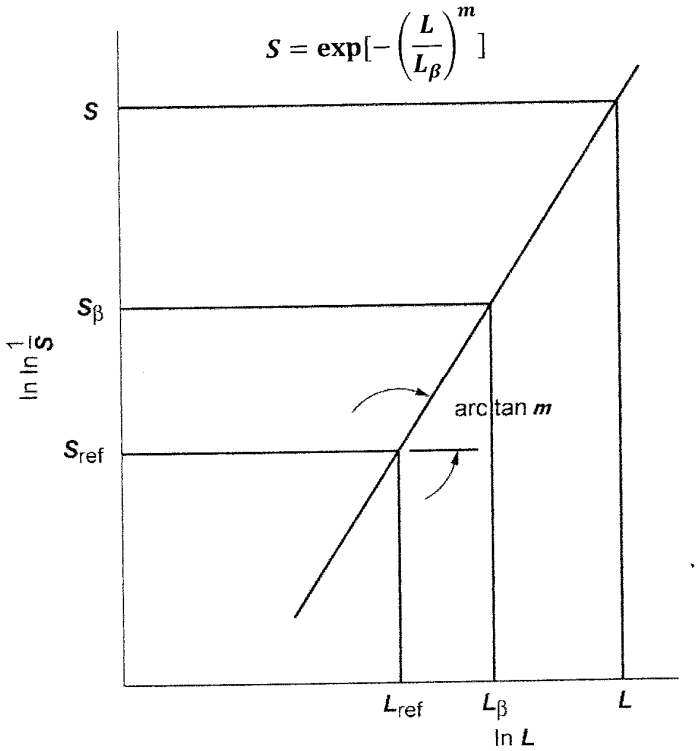

Figure 8.3.—Weibull plot where (Weibull) Slope of tangent or line is *m*. Probability of survival S_β of 36.8 percent at which $L = L_\beta$ or $L/L_\beta = 1$.

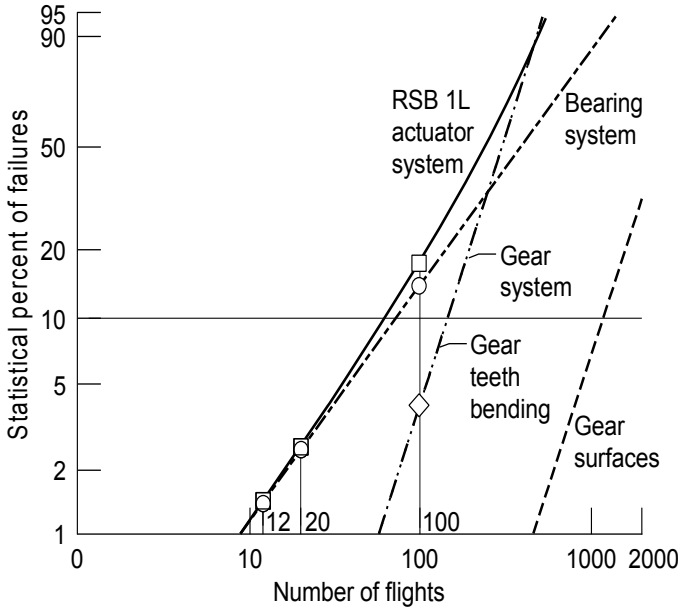

Figure 8.4.—Rudder speed brake 1L actuator component and system Weibull plots.

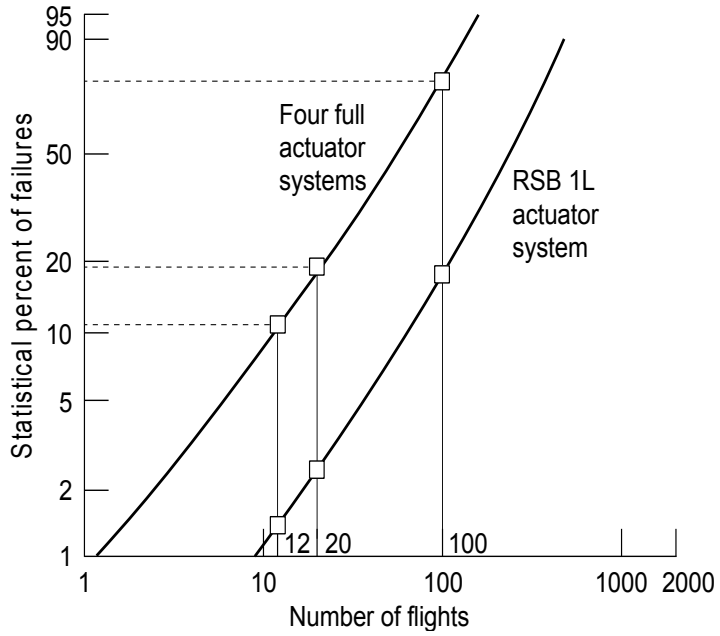

Figure 8.5.—System Weibull plot for 1L actuator and four full actuators.

Attachment A: Letter to NASA JSC Regarding OV104 Body Flap Actuator

National Aeronautics and
Space Administration

John H. Glenn Research Center
Lewis Field
Cleveland, OH 44135-3191

Reply to Attn 5900

July 17, 2003

Memorandum

To: JSC-ES4/Jay E. Bennett
NASA Johnson Space Center

From: 5900/Chief Engineer
Structures and Acoustics
NASA Glenn Research Center

Subject: OV104 body flap actuator

Reference is made to our two telephone conversations of July 7 and 8, 2003 and your three emails of July 7, 2003. NASA examined one outboard and two inboard body flap actuators from the Space Shuttle fleet. The body flap actuators are a planetary gear mechanism. I reviewed the schematic of the body flap actuator and the photographs of the gear component that you sent. According to my examination of the schematic, the photographs appear to be that of a male gear spline of the shaft of the sun gear. There are two gear splines on each end of the sun gear shaft. The gear spline appears to be counter bored with a hole through the side of the gear perpendicular to its centerline. This component, in practice, should mate with a female gear coupling or connector not shown in the schematic. A pin would be placed though the gear coupling it into position and securing the mating components.

According to the description that you relayed in our verbal conversation, it is my understanding that the actuator is used to control the movements of the Space Shuttle's flaps on reentry and landing. Significant corrosion was found in outboard body flap actuator taken from OV104 and is visible in the photographs of the gear spline teeth. No corrosion was reported on the remaining two actuators examined from the OV104. There was no examination of the bearings on any of the actuators. I do not have photographs of the sun and planetary gears. It is my understanding that Sundstrand Corporation manufactured the component.

The actuator had a design life of "10 years." However, you had no information at the time of our conversation on how the 10-year life estimate was determined. All of the mechanisms on all of the Space Shuttles have been in service continuously for "20 years" or more, during which time they have never been serviced nor inspected except for the three mentioned above. You had no information on the number of bearings or type in the system nor the resultant loading that the system and its components experience over the flight operation envelope. The gears were manufactured from AISI 9310 steel. The entire actuator mechanism is lubricated by Braycote grease. Except for the initial grease in the mechanism, there has been no grease added nor have any of the actuators been regreased during their 20 years of operation.

Examination of the photographs sent to me by email confirmed the presence of corrosion products and cracking of the gear component. It appears that the gear may have been cleaned before being photographed since there were no visible signs of grease being present. There was cracking, pitting, and chipping of one or more of the AISI 9310 steel gear teeth as well as significant corrosion present. There was a pit on what appears from the schematic to be the mating surface for contacting seals of the one-piece machined integral sun gear shaft.

Attachment A (Concluded):

I discussed use of the Braycote grease and the corrosion with Dr. Wilfredo Morales who is a resident expert here at GRC on this type lubricant. Braycote greases are composed of Flomblin PFPE and a PTFE thickener. All initial greases produced contain no additives due to the fact that no soluble additives could be made. Dr. Morales informed me, and I believe that you also mentioned that Dupont has started selling PFPE grease containing a rust inhibitor. However, he stated that whether this grease works under "actual" boundary-lubricating conditions is still an opened question.

The PFPE liquid in the Braycote grease will eventually react with the ferrous surfaces that result in the formation of iron fluoride. The iron fluoride will then catalyze the decomposition of PFPE further resulting in formation of iron fluoride. If there is moisture present, the iron fluoride will have a small solubility in water and breakdown the PFPE. The breakdown products of PFPE are highly reaction species and can also react with moisture leading to the formation of highly corrosive HF. This probably explains the observed corrosion on the gear. I would also expect the same phenomena on the bearings.

You informed me that Sundstrand refurbishes their commercial aircraft actuators every $2^1/_2$ to 3 years. Even for light duty, it is good engineering practice to replenish the grease in a system on a periodic basis and not more than 5 years. This is because that with time, the liquid (oil) separates from its thickener. When approximately 20% of the liquid is lost, the grease is referred to as "dead grease" and it is no longer effective in providing lubrication. This can result in gross wear of the components and failure of the rolling-element bearings. This may have occurred in one or more of the actuators now in service considering the length of time that the actuators were operated without regreasing.

While I realize that it is difficult and expensive to access and inspect the actuators now in service in the Shuttle fleet, it is my opinion that there is a high probability that one or more of the actuators can experience a seizure with the current lubrication condition and corrosion being present. I would recommend that all actuators now in service be cleaned, inspected and regreased, and, if necessary, be refurbished. Depending on the condition of the remaining actuators, a substitute grease should be considered.

Erwin V. Zaretsky, P.E.

cc: 0100/D. J. Campbell
0500/V. W. Wessel
5000/W. Whitlow
5900/D. L. Huff
5950/J. J. Zakrajsek
5950/W. Morales
JSC-NA/Y. Y. Marshall

Attachment B: Memorandum to NESC regarding OV-105 Rudder Speed Brake Actuator Components

National Aeronautics and
Space Administration
John H. Glenn Research Center
Lewis Field
Cleveland, OH 44135-3191

July 5, 2005

Reply to Attn of: RSM

TO: NESC

FROM: NASA Glenn Research Center Shuttle Actuator Team

SUBJECT: Update to June 18, 2004 memo from GRC Shuttle Actuator Team regarding OV-105 Rudder Speed Brake Actuator Components

Background

The GRC Shuttle Actuator Team released a memo on June 18, 2004 in response to the Shuttle Program Offices decision to reuse Rudder Speed Brake (RSB) Actuator components from orbiter OV-105 for orbiter OV-104. Prior to the reuse decision, a planned course of action was in place for RSB actuators to be used on OV-104 that would employ new parts as much as possible by making use of (by parts count) 94 percent new hardware and 6 percent hardware that had been previously flown. The new course of action proposed to the Orbiter Configuration Control Board on June 10, 2004 assumed that all of the components from the OV-105 actuators (less seals and o-rings) will, upon some inspection, likely be judged as fit for re-use and will be installed on OV-104.

The GRC Shuttle Actuator Team objected to the new plan and thus drafted the June 18, 2004 memo stating their position, rationale, issues and recommendations. A copy of this memo is attached, with appropriate comments / updates in red, as it relates to the current position. The June 18, 2004 position, as stated in the memo, is as follows:

The NASA Glenn Research Center Shuttle Actuator Team recommends that the appropriate course of action is to abandon the plan to reuse the OV-105 hardware as a shipset on OV-104. The GRC team's strong recommendation is that the program continue with the earlier plan to assemble and install on OV-104 a Rudder Speed Brake actuator shipset that consists of 94 percent new hardware and 6 percent previously flown hardware. The GRC team also strongly recommends a critical assessment of the reuse criteria for previously flown Rudder Speed Brake Actuator hardware.

The main issues and questions in the June 18, 2004 memo, grouped into two main categories, are as follows:

Attachment B (Continued):

Inspection process, & re-use criteria:

- The procedures and criteria for part re-use (as of June 8, 2004) is subjective and may lead to erroneous conclusions – no data or analysis used as basis
- What criteria for component and actuator removal should be used
- What inspection processes should be used
- What is considered acceptable levels of wear, & what is this criteria based on

Design & life prediction methodologies of actuator components

- Defining the life of an actuator as equal to the lowest lived component in the actuator is incorrect. The life of a system at a given probability of survival is less than the lowest lived component in the system. The combined life of each component in the system defines the life of the actuator. With a total of 4 actuators, the reliability of the 4 actuator system is the fractional reliability of a single actuator to the fourth power.
- The load, speed and number of cycles that were used in the original 100 mission life estimate was not adequately specified, nor the level of reliability used in the analysis.

July 5, 2005 Position and Recommendation:

New Actuators

- The GRC Shuttle Actuators Team concurs with the 12 flights or 6 years (whichever comes first) initial inspection interval for new actuators. (Note: The 12 flight 6 year initial inspection interval for new actuators was agreed to on May 18, 2005, during the NESC telecon)

Inspection process, & re-use criteria:

- A significant volume of work has been completed in the last year to validate the proposed reuse criteria. Based on experimental data from GRC and MSFC, the GRC Shuttle Actuator Team concurs with Hamilton Sundstrand Re-use criteria. (Removal of components with Level 3 or worse damage)
- A reasonable inspection interval for actuators with re-used components still needs to be defined, based on condition of components and load history. However, the number of intermediate flights should not be more than the inspection interval assigned to new actuators (12 flights or 6 years)
- The inspection process to categorize components based on Hamilton Sundstrand defined levels of damage needs to be codified and adopted as standard practice in the Shuttle maintenance program.

Design & life prediction methodologies of actuator components

- The GRC Team understands that Hamilton Sundstrand is using NASA Requirements that are "A-Basis" (99% reliability @ 95% confidence) for

Attachment B (Continued):

ultimate/yield strength, and "B–Basis" (90% reliability @ 4 x life @ 95% confidence) for fatigue. GRC agrees with this method. However the material property allowables and stress concentration factor effects are still under examination.

- The GRC Team continues to recommend using probabilistic analysis of the whole actuator system to determine projected life and reliability of the system. GRC conducted a probability analysis of the RSB Actuators using a load and cycle spectrum provided by Boeing - Huntington Beach based on a 7.6 hour mission cycle. With new actuators, the probability of survival for a single actuator based upon gear life only, was found to be 99.9% (including the 50 in-lb rigging load), for a life of 20 missions. For 4 actuators, the reliability is reduced to 99.7% for the same 20 missions. The bearing reliability based upon contact fatigue for a single actuator is 97.5% and 90.1% for 4 actuators. Combining both gear and bearing reliabilities, the single actuator reliability is 97.4% and for 4 actuators – 90.1%. (Failure is defined as crack initiation of a gear tooth and/or spall initiation of a gear tooth or bearing surface. Based upon GRC testing and experience, the bearings and gears will continue to operate for a time after either one of these failure modes occur.)

Recommendations specific to the orbiters:

- OV-103 (Discovery) – all new RSB Actuators have been installed. These actuators were in controlled storage at KSC for 17 years. GRC accepts flying these actuators until the next maintenance interval (12 flights or 6 years whichever comes first, per consensus arrived at on May 18, 2005 NESC Shuttle Actuator Telecon).
- OV-104 (Atlantis) – Although GRC accepts the re-use criteria based on inspection results, a reasonable inspection interval needs to be defined for used components. The GRC Team concurs with the NESC's recommendation to conduct the full system fatigue test. Providing that test results are satisfactory, the GRC Team further recommends that the rudder speed brake actuators on OV-104 be disassembled and inspected at the next OV-104 Orbiter maintenance interval. Based on the current Shuttle manifest, OV-104 is scheduled for OMM after 5 flights.
- OV-105 (Endeavor) – All new RSB Actuators are currently being manufactured by Hamilton Sundstrand and their subcontractors. Same recommendation as given for OV-103.

In summary, the GRC Shuttle Actuators Team concurs with the re-use of used actuator components on the condition that proper inspection procedures are used, and a strict inspection and maintenance interval is defined and followed. The GRC Team does not, however, concur with further extensions of service life beyond that agreed upon herein without additional experimental data verification.

Attachment B (Concluded):

S/	S/
Dr. Phillip Abel	Fred B. Oswald
S/	S/
Dr. Robert F. Handschuh	Dr. Kenneth Street
S/	S/
Dr. Timothy L. Krantz	Erwin V. Zaretsky
S/	S/
Dr. Wilfredo Morales	James J. Zakrajsek

Enclosure

cc:
R/T. Keith
R/J. Lei
RS/Division File
PO/A. Otero
PO/C. Quinn
NESC/D. Cheston